
JSCSEN 79(9)1051–1198(2014)

ISSN 1820-7421(Online)

Journal of the Serbian Chemical Society

e
Version
electronic

VOLUME 79

No 9

BELGRADE 2014

Available on line at



www.shd.org.rs/JSCS/

The full search of JSCS

is available through

DOAJ DIRECTORY OF

OPEN ACCESS

JOURNALS

www.doaj.org



Journal of the Serbian Chemical Society

JSCS-info@shd.org.rs • www.shd.org.rs/JSCS

J. Serb. Chem. Soc. Vol. 79, No. 9 (2014)

CONTENTS

Organic Chemistry

- K. Kundu and S. K. Nayak: Camphor-10-sulfonic acid catalyzed condensation of 2-naphthol with aromatic/aliphatic aldehydes to 14-aryl/alkyl-14H-dibenzo[*a,j*]xanthenes... 1051
M. A. Salem, M. I. Marzouk and N. F. Mahmoud: Synthesis of various fused pyrimidine rings and their pharmacological and antimicrobial evaluation..... 1059

Biochemistry and Biotechnology

- M. N. Filimon, S. O. Voia, R. Popescu, D.-M. Bordean, D. L. Vladoiu, M. Mituletu and V. Ostafe: The effect of chlorsulfuron and MCPB-Na on the enzymatic activity of microorganisms..... 1075
D. Dekanski, N. Mihailović-Stanojević, J. Grujić Milanović, D. Jovović and Z. Miloradović: Effects of high dose olive leaf extract on the hemodynamic and oxidative stress parameters in normotensive and spontaneously hypertensive rats 1085

Inorganic Chemistry

- M. A. Rezvani, A. F. Shojaei and F. M. Zonozi: Anatase titania–vanadium polyphosphomolybdate as an efficient and reusable nano catalyst for the desulphurization of gas oil 1099

Theoretical Chemistry

- D.-D. Wang, L.-L. Feng, G.-Y. He and H.-Q. Chen: QSAR studies for assessing the acute toxicity of nitrobenzenes to *Tetrahymena pyriformis* 1111

Physical Chemistry

- A. J. Albrbar, A. Bjeljac, V. Djokić, J. Miladinović, Dj. Janaćković and R. Petrović: Photocatalytic efficiency of titania photocatalysts in saline waters 1127
S. Zeljković, T. Ivas, S. Vaucher, D. Jelić and L. J. Gauckler: The changes of Ba_{0.5}Sr_{0.8}Co_{0.8}Fe_{0.2}O_{3-δ} perovskite oxide on heating in oxygen and carbon dioxide atmospheres 1141

Materials

- N. Jović, M. P. Calatayud, B. Sanz, A. Montone and G. F. Goya: *Ex situ* integration of iron oxide nanoparticles onto exfoliated expanded graphite flakes in aqueous suspension..... 1155

Environmental

- M. D. Antonijević, M. Arsović, J. Časlavský, V. Cvetković, P. Dabić, M. Franko, G. Ilić, M. Ivanović, N. Ivanović, M. Kosovac, D. Medić, S. Najdanović, M. Nikolić, J. Novaković, T. Radovanović, D. Ranić, B. Šajatović, G. Spiljunović, I. Stankov, J. Tošović, P. Trebše, O. Vasiljević and J. Schwarzbauer: Actual contamination of the Danube and Sava Rivers at Belgrade (2013)..... 1169

Geochemistry

- D. D. Vicić, M. M. Stoilković, J. M. Ninkov, N. Č. Bojat, M. S. Sabovljević and B. M. Stevanović: *Ex situ* integration of iron oxide nanoparticles onto exfoliated expanded graphite flakes in aqueous suspension 1185

Published by the Serbian Chemical Society
Karnegijeva 4/III, P. O. Box 36, 11120 Belgrade 35, Serbia
Printed by the Faculty of Technology and Metallurgy
Karnegijeva 4, P. O. Box 35-03, 11120 Belgrade, Serbia

Available online at: www.shd.org.rs/jscs/

(C) 2014 SCS. All rights reserved.





Camphor-10-sulfonic acid catalyzed condensation of 2-naphthol with aromatic/aliphatic aldehydes to 14-aryl/alkyl-14H-dibenzo[*a,j*]xanthenes

KSHAMA KUNDU and SANDIP K. NAYAK*

Bioorganic Division, Bhabha Atomic Research Centre, Mumbai – 400085, India

(Received 5 August, revised 3 October 2013, accepted 12 March 2014)

Abstract: The (\pm)-camphor-10-sulfonic acid (CSA) catalyzed condensation of 2-naphthol with both aliphatic/aromatic aldehydes at 80 °C yielded 14-alkyl/aryldibenzoxanthenes as the sole products in high yields. However, the same condensation with benzaldehyde at 25 °C afforded a mixture of the intermediate 1,1-bis-(2-hydroxynaphthyl)phenylmethane and 14-phenyldibenzoxanthene, while the condensation with aliphatic aldehydes at 25 °C furnished the corresponding 14-alkyldibenzoxanthenes as the sole products. Moreover, the condensation of 2-naphthol with aromatic/aliphatic aldehydes with low catalyst loading (2 mol %) was greatly accelerated under microwave irradiation to afford the corresponding 14-aryl/alkyldibenzoxanthenes as the sole products in high yields.

Keywords: dibenzoxanthenes; β -naphthol; (\pm)-camphor-10-sulfonic acid; microwave irradiation.

INTRODUCTION

Xanthenes and benzoxanthenes are important biologically active heterocycles as they possess several important bioactivities including antiviral,¹ anti-inflammatory,² and antibacterial activities.³ Furthermore, these heterocycles are used as sensitizers in photodynamic therapy,⁴ leuco dyes in laser technology,⁵ antagonists of the paralyzing action of zoxazolamine (2-amino-5-chlorobenzoxazole)⁶ and pH-sensitive fluorescent materials for the visualization of biomolecules.⁷ Therefore, the synthesis of various xanthene derivatives is of great synthetic importance. Several methods have been reported for the synthesis of xanthenes and benzoxanthenes, which include trapping of benzenes with phenols,⁸ cyclodehydration,⁹ cyclocondensation of 2-hydroxyaromatic aldehydes with 2-tetralone¹⁰ and intramolecular phenyl carbonyl coupling reactions of benzaldehydes

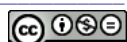
*Corresponding author. E-mail: sknayak@barc.gov.in
doi: 10.2298/JSC130805021K

and acetophenones.¹¹ In addition, 14-aryl-14*H*-dibenzo[*a,j*]xanthenes and related compounds have been synthesized from the reaction of 2-naphthol with formamide,¹² 1-(hydroxymethyl)naphthalen-2-ol¹³ and carbon monoxide.¹⁴ Moreover, various catalysts, including TaCl₅,¹⁵ Sr(OTf)₂,¹⁶ Yb(OTf)₃,¹⁷ sulfamic acid,¹⁸ iodine,¹⁹ Amberlyst-15,²⁰ cyanuric chloride,²¹ ceric ammonium nitrate (CAN),²² BF₃:SiO₂,²³ P₂O₅ or InCl₃,²⁴ Sc[N(SO₂C₈F₁₇)₂]₃,²⁵ RuCl₃·nH₂O,²⁶ poly(ethylene glycol)-SO₃H (PEG)-SO₃H,²⁷ an ionic liquid,²⁸ dodecylphosphonic acid (DPA) or dodecylsulfamic acid (DSA),²⁹ nano-silica phosphoric acid (nano-SPA),³⁰ nano-SnCl₄·SiO₂,³¹ 4-dodecylbenzenesulfonic acid (DBSA),³² tungstophosphoric acid³³ and a functionalized mesoporous material³⁴ were found to catalyze condensation reactions of 2-naphthol with different aldehydes to afford 14-substituted-14*H*-dibenzo[*a,j*]xanthenes. However, many of the reported methodologies suffered from one or more disadvantages, such as long reaction time, use of toxic and expensive catalysts, harsh reaction conditions, etc. Bearing this in mind, as well as the increasing importance of benzoxanthenes in the pharmaceutical industry, there is still a necessity for the development of an efficient, environmentally benign and inexpensive catalyst for their synthesis. Herein, a convenient microwave-assisted synthesis of 14-aryl/alkyl-14*H*-dibenzo[*a,j*]xanthenes from 2-naphthol and aromatic/aliphatic aldehydes using (\pm)-camphor-10-sulfonic acid as a catalyst is reported.

RESULTS AND DISCUSSION

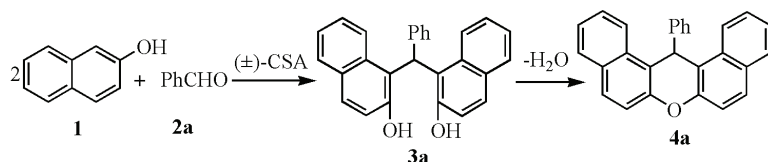
Camphor-10-sulfonic acid (CSA) is an inexpensive and easy to handle organo-catalyst that has been used in various organic transformations. Recently, it was observed that CSA is a highly efficient catalyst for the activation of imines in the Mannich type reaction of enolizable ketones.³⁵ As an extension to this work, it was considered of interest to explore its catalytic potential for the activation of aldehydes in the condensation of 2-naphthol with aldehydes to afford dibenzoxanthenes. In a preliminary study, the reaction of 2-naphthol (**1**) with benzaldehyde (**2a**, 0.55 equiv.) was performed at ambient temperature (25 °C) with (\pm)-CSA (5 mol. %) under solvent-free conditions. The reaction was found to be very sluggish as both the intermediate bis-(2-hydroxy-1-naphthyl)phenylmethane (**3a**) as well as 14-phenyl-14*H*-dibenzo[*a,j*]xanthene (**4a**) were isolated in 55 and 10 % yields, respectively, along with unreacted **1** (\approx 18 %) and **2a** (\approx 10 %) after stirring for 24 h (Table I, entry 1). Compounds **3a** and **4a** were characterized by physical and spectroscopic (IR, ¹H-NMR, ¹³C-NMR and MS) data. Increasing the catalyst loading (10 mol %) (25 °C, 24 h) led to marginal improvements in the yields of both **3a** and **4a**, although small amounts of the respective starting materials were still recovered (Table I, entry 2).

However, with 20 mol % catalyst, both starting compounds were consumed while **3a** and **4a** were isolated in 75 and 21 % yields, respectively (Table I, entry



3). In order to improve the yield and selectivity of the desired product **4a**, the above reaction was performed at an elevated temperature (80 °C) with 10 mol % CSA as the catalyst. Gratifyingly, both the starting materials **1** and **2a** were consumed and **4a** was isolated as a sole product in 81 % yield, while the intermediate **3a** was found to be absent (Table I, entry 4). Further increase in catalyst loading (15 mol %) led to completion of the reaction within 2 h at 80 °C to yield **4a** as the sole product in 89 % yield (Table I, entry 5).

TABLE I. Optimization of the reaction conditions for the (\pm)-CSA-catalyzed condensation of 2-naphthol (**1**) with benzaldehyde (**2a**)



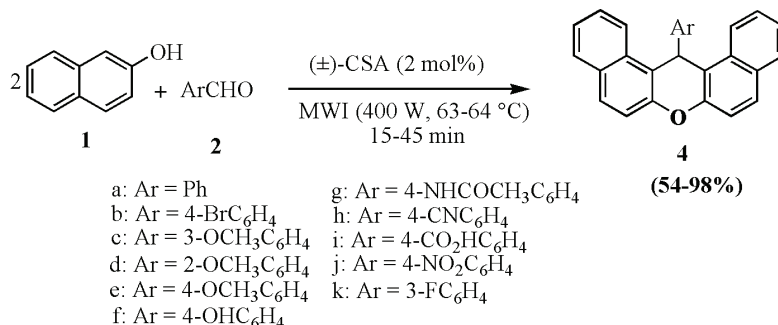
| Entry | Reaction conditions ^a | (\pm)-CSA, mol. % | Time, h | Yield, % ^b | |
|-------|----------------------------------|-----------------------|---------|-----------------------|-----------|
| | | | | 3a | 4a |
| 1 | 25 °C | 5 | 24.0 | 55 | 10 |
| 2 | 25 °C | 10 | 24.0 | 63 | 14 |
| 3 | 25 °C | 20 | 16.0 | 75 | 21 |
| 4 | 80 °C | 10 | 8.0 | — | 81 |
| 5 | 80 °C | 15 | 2.0 | — | 89 |
| 6 | MWI, 63–64 °C | 10 | 0.25 | — | 89 |
| 7 | MWI, 63–64 °C | 5 | 0.25 | — | 88 |
| 8 | MWI, 63–64 °C | 2 | 0.25 | — | 88 |
| 9 | MWI, 63–64 °C | 0 | 0.50 | — | 0 |

^a2-Naphthol was reacted with benzaldehyde (0.55 equiv.) under solvent-free conditions; ^bisolated yields

Microwave irradiation (MWI) is known to be an important tool in organic synthesis to improve the selectivity, rate enhancement and reduction of thermal degradative byproducts.³⁶ To reduce the catalyst loading as well as the reaction time required for the condensation at high temperature, reaction of **1** with **2a** (0.55 equiv.) was performed without solvent using a varied amount of (\pm)-CSA (2–10 mol %) under MWI (400 W, 63–64 °C) when **4a** was obtained as the sole product in 88–89 % yields (Table I, entries 6–8). The reaction without using CSA as catalyst did not yield any product **4a** and both the starting compounds were recovered. (Table I, entry 9). As evidenced from Table I, optimal catalyst loading for the microwave-assisted condensation was found to be 2 mol %, affording **4a** in 88 % yield and therefore the same conditions were used for all subsequent reactions.

To see the scope and generality of this microwave-assisted protocol, CSA catalyzed condensation of 2-naphthol with a variety of aromatic aldehydes (**2b–k**) was investigated under MWI. In all the cases, the desired dibenzoxan-

thenes were obtained (Scheme 1) in good to high yields and the results are summarized in Table II. In the case of solid aromatic aldehydes, such as 4-cyanobenzaldehyde (**2h**), acetonitrile (0.25 ml mmol⁻¹) was used as solvent to make a uniform slurry, when the corresponding cyano dibenzoxanthene **4h** was isolated in 86 % yield. Solvent optimization of this reaction with other microwave-active solvents, *viz.* H₂O and DMF without changing catalyst loading was also investigated. To this end, the use of H₂O led to the formation of **4h**, albeit in poor yield (32 %), while no product was detected using DMF as solvent, when both starting compounds were recovered.



Scheme 1. Reaction scheme with structures of reactants **2b–k** and products **4b–k**.

TABLE II. Microwave assisted, (±)-CSA catalyzed condensation of 2-naphthol (**1**) with aromatic aldehydes (ArCHO) to 14-aryl-14H-dibenzo[*a,j*]xanthene (**4b–k**); reaction conditions: 2-naphthol, aldehydes (0.55 equiv.) and (±)-CSA (0.02 equiv.) were irradiated in a microwave reactor at 400 W, 63–64 °C for 15–45 min

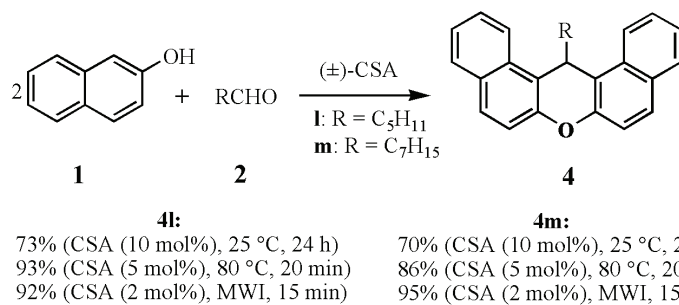
| Entry | Aldehydes | Product | Time, min | Yield, % ^a | Melting point, °C | |
|----------------|-----------|-----------|-----------|-----------------------|-------------------|----------|
| | | | | | Found | Reported |
| 1 | 2b | 4b | 30 | 82 | 293–294 | 295–296 |
| 2 | 2c | 4c | 15 | 98 | 177–178 | 179–180 |
| 3 | 2d | 4d | 45 | 54 | 258–259 | 258–260 |
| 4 | 2e | 4e | 15 | 88 | 207–208 | 205–206 |
| 5 ^b | 2f | 4f | 45 | 61 | 138–139 | 138–140 |
| 6 ^b | 2g | 4g | 45 | 86 | 153–154 | – |
| 7 ^b | 2h | 4h | 30 | 86 | 294–295 | 291–292 |
| 8 ^b | 2i | 4i | 30 | 85 | >300 | – |
| 9 ^b | 2j | 4j | 30 | 84 | >300 | 310–311 |
| 10 | 2k | 4k | 30 | 95 | 256–257 | 259 |

^aIsolated yields; ^bacetonitrile (0.25 mL mmol⁻¹) was used to make a uniform reaction mixture

The electronic effect of the substituents in the aromatic aldehydes was found to have a minimal effect, as evidenced by the high yield of the corresponding dibenzoxanthenes in almost all the cases (**4b–k**) (Table II, entries 1–10). However, the moderate yield of **4d** derived from 2-methoxybenzaldehyde (**2d**) could

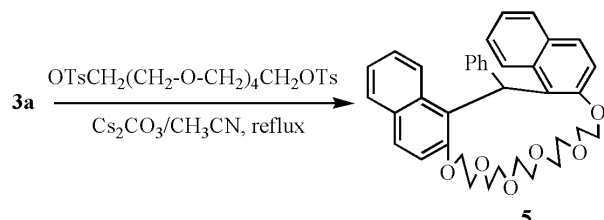
be explained by the large steric strain (resulting from the bulky methoxy group) involved during the cyclodehydration step to dibenzoxanthene (Table II, entry 3).

To explore the generality of the catalyst, CSA catalyzed condensation of 2-naphthol (**1**) with aliphatic aldehydes was also investigated. In contrast to benzaldehyde, the CSA catalyzed (10 mol %) condensation of **1** with hexanal (**2l**) at 25 °C without solvent (24 h) led to complete consumption of starting materials and 14-pentyldibenzoxanthene (**4l**) was obtained as the sole product in 73 % yield; no trace of 1,1-bis(2-hydroxynaphthyl)hexane was detected (Scheme 2). Similarly, the reaction with octanal (**2m**) led to the formation of 14-heptyldibenzoxanthene (**4m**) as the only product. However, at a higher temperature (80 °C), both the reactions (with hexanal and octanal) were completed within 20 min using a lower catalyst loading (5 mol %) to afford the corresponding dibenzoxanthenes in 93 and 86 % yields, respectively (Scheme 2). Moreover, the above reactions under MWI were completed in 15 min with a lower catalyst loading (2 mol %), as compared to the high temperature reactions, affording the corresponding dibenzoxanthenes (**4l** and **4m**) in 92 and 95 % yields, respectively (Scheme 2). Most catalysts^{24–26,29} reported so far for the condensation of **1** with aliphatic aldehydes furnished the corresponding dibenzoxanthenes in longer reaction times and in moderate yields. Therefore, CSA displayed its catalytic efficiency in the faster condensation of **1** with both aliphatic and aromatic aldehydes to afford corresponding alkyl/aryl substituted dibenzoxanthenes in high yields. Incidentally, the catalytic potential of CSA in terms of reaction time and yield was found to be superior/similar to most of the hitherto reported catalysts.



Scheme 2. (±)-CSA-catalyzed condensation of 2-naphthol (**1**) with aliphatic aldehydes (RCHO) to 14-alkyl-14*H*-dibenzo[*a,j*]xanthene (**4l,m**).

Compound **3a**, obtained from the condensation of **1** and **2a** at ambient temperature, belongs to the important class of tethered bis(2-naphthol)s, which in principle could be exploited further for the synthesis of a variety of macrocycles, including crown ethers. To this end, reaction of **3a** with pentaethyleneglycol ditosylate and K₂CO₃ in acetonitrile yielded the corresponding crown ether **5** in good yield (Scheme 3).

Scheme 3. Synthesis of *bis*-naphthalenocrown-6.

EXPERIMENTAL

Microwave irradiation (MWI) was performed with an Anton Paar microwave reactor (model SYNTHOS 3000). The melting points were determined using a Fisher–Johns melting point apparatus and are uncorrected. The IR spectra were scanned with a Jasco FT IR 4100 spectrophotometer. The ^1H - and ^{13}C -NMR spectra were recorded with a Bruker AC 200/300 MHz spectrometer. Spectra were referenced to the residual chloroform (δ 7.25 ppm, ^1H ; 77.0 ppm, ^{13}C). The low-resolution mass spectra were recorded on a Varian 500 mass spectrometer (ESI/APCI) and a Shimadzu GC-MS 2010 mass spectrometer (EI 70 eV). The high-resolution mass spectra were recorded on a Q-TOF (YA-105) micromass spectrometer (ESI, Ar) and a Bruker maXis impact mass spectrometer (ESI). The microanalyses were realized using a Vario Micro elemental analyzer. (\pm)-Camphor-10-sulfonic acid (CSA) was purchased from Aldrich, USA, and was used as received. The spectral data of the known compounds were in accordance with those reported in the literature, while the unknown compounds were characterized by IR, NMR, HRMS and microanalytical data, which are given as Supplementary Material to this paper.

Typical procedure for the solvent-free condensation of 2-naphthol (1) with benzaldehyde (2a) to the dibenzoxanthene 4a

A mixture of 2-naphthol (1.44 g, 10.0 mmol), benzaldehyde (0.584 g, 5.50 mmol) and (\pm)-CSA (0.192 g, 15.0 mol. %) was heated at 80 °C without any solvent. After completion of the reaction (monitored by TLC), the formed pinkish solid was quenched with water, filtered, washed with water and air-dried. The crude solid was recrystallized with hexane–ethyl acetate, 9:1, to afford pure **4a** (1.60 g, 89 %).

Typical procedure for the solvent-free condensation of 2-naphthol (1) with benzaldehyde (2a) to the dibenzoxanthene 4a under microwave irradiation

A mixture of 2-naphthol (1.44 g, 10.0 mmol), benzaldehyde (0.584 g, 5.50 mmol) and (\pm)-CSA (0.026 g, 2.0 mol. %) was placed in a microwave vessel and irradiated (400 W, 63–64 °C). After 15 min, TLC showed complete consumption of both the starting materials and the formation of **4a** as the only product. The thus formed solid was quenched with water, filtered, washed with water and air-dried. The crude solid was recrystallized with hexane–ethyl acetate, 9:1, to afford pure **4a** (1.59 g, 88 %).

Typical procedure for the synthesis of bis-naphthocrown-6 (5) from 3a

A mixture of bis-(2-naphthol) **3a** (0.790 g, 2.10 mmol), pentaethyleneglycol ditosylate (1.26 g, 2.30 mmol, 1.1 equiv.) and Cs_2CO_3 (1.73 g, 5.30 mmol, 2.5 equiv.) in dry acetonitrile (30 mL) was refluxed for 8 h when TLC showed the absence of both **3a** and the ditosylate. The solvent was removed under *vacuo*, cooled, quenched with 1 M HCl and extracted with ethyl acetate. The organic layer was washed with water and brine, and dried (Na_2SO_4). Remo-

val of solvent afforded a thick mass which was purified by silica gel column chromatography (using CHCl_3 as the eluant) to afford pure **5** (0.948 g, 78 %).

CONCLUSIONS

In conclusion, a simple, efficient and microwave-assisted (15–45 min) protocol for the CSA-catalyzed condensation of 2-naphthol with aromatic/aliphatic aldehydes to 14-aryl/alkyl-14*H*-dibenzo[*a,j*]xanthenes was developed. In contrast to the poor yields of 14-alkyl-dibenzo[*a,j*]xanthenes from aliphatic aldehydes with most of the reported catalysts, CSA was found to be a superior catalyst to yield the corresponding dibenzoxanthenes in high yields. Shorter reaction time, simple work-up procedure and easy isolation of the products in high yields are some of the salient features of this new protocol. The intermediate bis(2-naphthol) derived from the condensation of 2-naphthol and benzaldehyde at ambient temperature was used in the synthesis of a novel class of crown ethers.

SUPPLEMENTARY MATERIAL

The physical, analytic and spectral data for the prepared compounds as well as their ^1H - and ^{13}C -NMR spectra are available electronically from <http://www.shd.org.rs/JSCS/>, or from the corresponding author on request.

ИЗВОД

КОНДЕНЗАЦИЈА 2-НАФТОЛА СА АРОМАТИЧНИМ/АЛИФАТИЧНИМ АЛДЕХИДИМА У СИНТЕЗИ 14-АРИЛ/АЛКИЛ-14Н-ДИБЕНЗО[*a,j*]КСАНТЕНА КАТАЛИЗОВАНА КАМФОР-10-СУЛФОНСКОМ КИСЕЛИНОМ

KSHAMA KUNDU и SANDIP K. NAYAK

Bio-Organic Division, Bhabha Atomic Research Centre, Mumbai – 400085, India

(\pm)-Камфор-10-сулфонска киселина (CSA) катализује кондензацију 2-нафтола са ароматичним/алифатичним алдехидима, на 80 °C у синтези 14-арил/алкил-14*H*-дibenzo[*a,j*]ксантена као јединих производа, у високом приносу. У реакција кондензације са бензалдехидом на 25 °C добија се смеша интермедијера бис(2-хидроксиафтил)-фенилметана и производа 14-фенил-дibenзоксантена, док кондензацијом са алифатичним алдехидима на 25 °C настају 14-алкил-дibenзоксантени као једини производи. Даље, кондензацијом 2-нафтола са ароматичним/алифатичним алдехидима у присуству малих количина катализатора (2 mol %), под условима озрачивања микроталасима, реакција се брже одвија и настају одговарајући 14-арил/алкилдibenзоксантени као једини производи.

(Примљено 5. августа, ревидирано 3. октобра 2013, прихваћено 12. марта 2014)

REFERENCES

1. R. W. Lambert, J. A. Martin, J. H. Merrett, K. E. B. Parkes, G. J. Thomas, PCT Int. Appl. WO 9706178 (1997) (*CA* **126** P212377y)
2. J. P. Poujelin, G. Saint-Rut, O. Foussard-Blanpin, G. Narcisse, G. Uchida-Ernouf, R. Lacroix, *Eur. J. Med. Chem.* **13** (1978) 67
3. T. Hideo, Jpn. Tokyo Koho JP 56004580 (1981) (*CA* **95** 80922b)
4. R. M. Ion, A. Planner, K. Wiktorowicz, D. Frackowiak, *Acta Biochim. Pol.* **45** (1998) 833



5. S. De, S. Das, A. Girigoswami, *Spectrochim. Acta, A* **61** (2005) 1821
6. G. Saint-Ruf, H.-T.-Hieu, J.-P. Poupelein, *Naturwissenschaften* **62** (1975) 584
7. C. G. Knight, T. Stephenes, *Biochem. J.* **258** (1989) 683
8. D. W. Knight, P. B. Little, *J. Chem. Soc. Perkin Trans I* **15** (2001) 1771
9. C. A. Buehler, D. E. Cooper, E. O. Scrudder, *J. Org. Chem.* **8** (1943) 316
10. A. Jha, J. Beal, *Tetrahedron Lett.* **45** (2004) 8999
11. C.-W. Kuo, J.-M. Fang, *Synth. Commun.* **31** (2001) 877
12. J. A. V. Allan, D. D. Giannini, T. H. Whitesides, *J. Org. Chem.* **47** (1982) 820
13. R. N. Sen, N. Sarkar, *J. Am. Chem. Soc.* **47** (1925) 1079
14. K. Ota, T. Kito, *Bull. Chem. Soc. Jpn.* **49** (1976) 1167
15. A. K. Bhattacharya, K. C. Rana, M. Mujahid, I. Sehar, A. K. Saxena, *Bioorg. Med. Chem.* **19** (2009) 5590
16. J. Li, W. Tang, L. Lu, W. Su, *Tetrahedron Lett.* **49** (2008) 7117
17. W. Su, D. Yang, C. Jin, B. Zhang, *Tetrahedron Lett.* **49** (2008) 3391
18. B. Rajitha, B. Sunil Kumar, Y. Thirupathi Reddy, P. Narsimha Reddy, N. Sreenivasulu, *Tetrahedron Lett.* **46** (2005) 8691
19. M. A. Pasha, V. P. Jayashankara, *Bioorg. Med. Chem. Lett.* **17** (2007) 621
20. S. Ko, C.-F. Yao, *Tetrahedron Lett.* **47** (2006) 8827
21. M. A. Bigdeli, M. M. Heravi, G. Hossein Mahdavinia, *Catal. Commun.* **8** (2007) 1595
22. A. Kumar, S. Sharma, R. A. Maurya, J. Sarkar, *J. Comb. Chem.* **12** (2010) 20
23. B. B. F. Mirjalili, A. Bamoniri, A. Akbari, *Tetrahedron Lett.* **49** (2008) 6454
24. R. Kumar, G. C. Nandi, R. K. Verma, M. S. Singh, *Tetrahedron Lett.* **51** (2010) 442
25. M. Hong, C. Cai, *J. Fluorine Chem.* **130** (2009) 989
26. K. Tabatabaeian, A. Khorshidi, M. Mamaghani, A. Dadashi, *Synth. Commun.* **41** (2011) 1427
27. D. Prasad, M. Nath, *Catal. Sci. Technol.* **2** (2012) 93
28. M. A. Zolfigol, V. Khakyzadeh, A. R. Moosavi-Zare, A. Zare, S. B. Azimi, Z. Asgari, A. Hasaninejad, *C. R. Chim.* **15** (2012) 719
29. S. Ghassamipour, A. R. Sardarian, *J. Heterocycl. Chem.* **49** (2012) 669
30. A. Bamoniri, B. F. Mirjalili, S. Nazemian, *Curr. Chem. Lett.* **2** (2013) 27
31. B. F. Mirjalili, A. Bamoniri, M. A. Mirhoseini, *Chem. Heterocycl. Compd.* **48** (2012) 856
32. D. Prasad, A. Preetam, M. Nath, *C. R. Chim.* **15** (2012) 675
33. T. S. Rivera, M. N. Blanco, L. R. Pizzio, G. P. Romanelli, *Green Chem. Lett. Rev.* **5** (2012) 433
34. J. Mondal, M. Nandi, A. Modak, A. Bhaumik, *J. Mol. Catal., A* **363–364** (2012) 254
35. K. Kundu, S. K. Nayak, *RSC Adv.* **2** (2012) 480
36. a) S. Caddick, *Tetrahedron* **51** (1995) 10403; b) A. Lopuy, A. Petit, J. Hamelin, F. Texier-Bouleau, P. Jacquault, D. Mathe, *Synthesis* (1998) 1213.





SUPPLEMENTARY MATERIAL TO
**Camphor-10-sulfonic acid catalyzed condensation of
2-naphthol with aromatic/aliphatic aldehydes to
14-aryl/alkyl-14H-dibenzo[a,j]xanthenes**

KSHAMA KUNDU and SANDIP K. NAYAK*

Bioorganic Division, Bhabha Atomic Research Centre, Mumbai – 400085, India

J. Serb. Chem. Soc. 79 (9) (2014) 1051–1058

PHYSICAL AND SPECTRAL DATA OF THE PRODUCTS (3a, 4a–m AND 5)

*Bis-(2-hydroxy-1-naphthyl)phenylmethane (3a).*¹ Pink solid; m.p.: 195–196 °C; IR (CHCl₃, cm⁻¹): 3471, 3423, 3019, 1618, 1597, 1513, 1491, 1468, 1390, 1253, 1046, 877; ¹H-NMR (200 MHz, CD₃COCD₃, δ / ppm): 7.13–7.38 (12H, *m*, ArCHAr, ArH), 7.74–7.84 (4H, *m*, ArH), 8.12 (2H, *d*, *J* = 8.3 Hz, ArH); ¹³C-NMR (50 MHz, CD₃COCD₃, δ / ppm): 43.0, 120.1, 120.4, 123.6, 123.7, 126.8, 127.5, 128.8, 129.1, 129.7, 130.0, 130.5, 135.2, 143.3, 154.0; ESI-MS (*m/z*, (relative abundance, %)): 376 (M, 25), 375 (M–H, 95), 353 (8), 349 (11), 339 (16), 337 (10), 325 (10), 321 (100), 311 (11), 309 (16), 293 (22), 283 (9), 265 (16), 231 (58), 143 (39); HRMS: *m/z* calcd. for C₂₇H₂₀O₂Na (M+Na): 399.1361; found: 399.1365.

*14-Phenyl-14H-dibenzo[a,j]xanthene (4a).*² Colorless solid; m.p.: 187–188 °C (lit. 186–187 °C); IR (CHCl₃, cm⁻¹): 3061, 3017, 2924, 1592, 1456, 1401, 1251, 1215, 962, 808; ¹H-NMR (200 MHz, CDCl₃, δ / ppm): 6.50 (1H, *s*, ArCHAr), 6.96–7.03 (1H, *m*, ArH), 7.16 (2H, *t*, *J* = 7.5 Hz, ArH), 7.38–7.63 (8H, *m*, ArH), 7.82 (4H, *t*, *J* = 7.8 Hz, ArH), 8.41 (2H, *d*, *J* = 8.5 Hz, ArH); ¹³C-NMR (50 MHz, CDCl₃, δ / ppm): 38.0, 117.3, 117.9, 122.6, 124.1, 126.3, 126.6, 128.2, 128.4, 128.6, 128.7, 131.0, 131.4, 145.0, 148.7; EI-MS (*m/z*, (relative abundance, %)) = 358 (M, 20), 281 (100), 252 (13), 250 (8).

*14-(4-Bromophenyl)-14H-dibenzo[a,j]xanthene (4b).*³ Colorless solid; m.p.: 293–294 °C (lit. 295–296 °C); IR (CHCl₃, cm⁻¹): 3019, 2906, 1633, 1482, 1214; ¹H-NMR (200 MHz, CDCl₃, δ / ppm): 6.45 (1H, *s*, ArCHAr), 7.23–7.27 (2H, *m*, ArH), 7.37–7.50 (6H, *m*, ArH), 7.54–7.62 (2H, *m*, ArH), 7.82 (4H, *t*, *J* = 7.7 Hz, ArH), 8.31 (2H, *d*, *J* = 8.4 Hz, ArH); ¹³C-NMR (50 MHz, CDCl₃, δ / ppm): 37.4, 116.7, 118.0, 120.2, 122.4, 124.3, 126.9, 128.9, 129.1, 129.8, 131.1, 131.2,

*Corresponding author. E-mail: sknayak@barc.gov.in

131.5, 143.9, 148.7; HRMS: *m/z* calcd. for C₂₇H₁₈BrO (M+H): 437.0536; Found: 437.0533.

14-(3-Methoxyphenyl)-14H-dibenzo[a,j]xanthene (4c).² Colorless solid; m.p.: 177–178 °C (lit. 179–180 °C); IR (CHCl₃, cm⁻¹): 3018, 2938, 1593, 1486, 1457, 1432, 1400, 1215; ¹H-NMR (200 MHz, CDCl₃, δ / ppm): 3.63 (3H, *s*, OCH₃), 6.46 (1H, *s*, ArCHAR), 6.50–6.56 (1H, *m*, ArH), 7.03–7.19 (3H, *m*, ArH), 7.37–7.50 (4H, *m*, ArH), 7.59 (2H, *td*, *J* = 7.7, 1.3 Hz, ArH), 7.81 (4H, *t*, *J* = 8.3 Hz, ArH), 8.40 (2H, *d*, *J* = 8.4 Hz, ArH); ¹³C-NMR (50 MHz, CDCl₃, δ / ppm): 37.9, 54.9, 110.9, 114.9, 117.1, 117.9, 120.7, 122.7, 124.1, 126.7, 128.7, 128.8, 129.2, 131.0, 131.4, 146.5, 148.7, 159.6; ESI-MS (*m/z*, (relative abundance, %)): 389 (M+H, 13), 388 (M, 14), 387 (M–H, 10), 363 (8), 297 (9), 282 (40), 281 (100).

14-(2-Methoxyphenyl)-14H-dibenzo[a,j]xanthene (4d).³ Colorless solid; m.p.: 258–259 °C (lit. 258–260 °C); IR (CHCl₃, cm⁻¹): 3019, 1641, 1459, 1404, 1243, 1215; ¹H-NMR (200 MHz, CDCl₃, δ / ppm): 4.27 (3H, *s*, OCH₃), 6.60–6.67 (1H, *m*, ArCHAR), 6.84–7.00 (3H, *m*, ArH), 7.19 (1H, *dd*, *J* = 7.6, 1.6 Hz, ArH), 7.35–7.57 (6H, *m*, ArH), 7.78 (4H, *t*, *J* = 8.0 Hz, ArH), 8.58 (2H, *d*, *J* = 8.4 Hz, ArH); ¹³C-NMR (50 MHz, CDCl₃, δ / ppm): 30.3, 55.6, 110.6, 117.9, 118.5, 121.7, 123.3, 124.1, 126.6, 127.5, 128.4, 130.7, 130.8, 132.1, 134.6, 148.8, 153.8; APCI-MS (*m/z*, (relative abundance, %)): 389 (M+H, 100), 388 (M, 9), 282 (32), 281 (79), 246 (12).

14-(4-Methoxyphenyl)-14H-dibenzo[a,j]xanthene (4e).² Colorless solid; m.p.: 207–208 °C (lit. 205–206 °C); IR (CHCl₃, cm⁻¹): 3017, 2955, 2399, 1607, 1509, 1432, 1215; ¹H-NMR (200 MHz, CDCl₃, δ / ppm): 3.61 (3H, *s*, OCH₃), 6.45 (1H, *s*, ArCHAR), 6.67 (2H, *d*, *J* = 8.7 Hz, ArH), 7.37–7.62 (8H, *m*, ArH), 7.80 (4H, *t*, *J* = 8.8 Hz, ArH), 8.38 (2H, *d*, *J* = 8.5 Hz, ArH); ¹³C-NMR (50 MHz, CDCl₃, δ / ppm): 37.1, 55.0, 113.8, 117.5, 117.9, 122.7, 124.1, 126.7, 128.6, 128.7, 129.1, 131.1, 131.4, 137.3, 148.7, 157.9; EI-MS (*m/z*, (relative abundance, %)): 388 (M, 22), 281 (100), 252 (20), 250 (11), 92 (13), 77 (14), 64 (6).

4-(14H-Dibenzo[a,j]xanthen-14-yl)phenol (4f).⁴ Pink solid; m.p.: 138–139 °C (lit. 138–140 °C); IR (CHCl₃, cm⁻¹): 3535, 3402, 3070, 3019, 2926, 1609, 1592, 1509, 1458, 1431, 1401, 1241, 1214, 1173; ¹H-NMR (200 MHz, CDCl₃, δ / ppm): 6.43 (1H, *s*, ArCHAR), 6.58 (2H, *d*, *J* = 8.5 Hz, ArH), 7.34–7.49 (6H, *m*, ArH), 7.58 (2H, *td*, *J* = 7.6, 1.2 Hz, ArH), 7.80 (4H, *t*, *J* = 8.6 Hz, ArH), 8.36 (2H, *d*, *J* = 8.4 Hz, ArH); ¹³C-NMR (50 MHz, CDCl₃, δ / ppm): 37.1, 115.3, 117.5, 117.9, 122.7, 124.1, 126.7, 128.6, 128.7, 129.3, 131.1, 131.4, 148.7, 153.9; EI-MS (*m/z*, (relative abundance, %)): 374 (M, 20), 281 (100), 252 (15), 250 (6), 178 (6).

N-[4-(14H-Dibenzo[a,j]xanthen-14-yl)phenyl]acetamide (4g). Colorless solid; m.p.: 153–154 °C; Anal. Calcd. for C₂₉H₂₁NO₂: C, 83.83; H, 5.09; N, 3.37 %. Found: C, 83.58; H, 5.44; N 3.08 %; IR (CHCl₃, cm⁻¹): 3436, 3019, 1634,



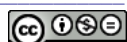
1513, 1410, 1320, 1240, 1215; $^1\text{H-NMR}$ (200 MHz, CDCl_3 , δ / ppm): 1.99 (3H, *s*, NHCOCCH_3), 6.45 (1H, *s*, ArCHAr), 7.02 (1H, *br*, NH), 7.21–7.26 (3H, *m*, ArH), 7.36–7.49 (5H, *m*, ArH), 7.56 (2H, *t*, J = 7.6 Hz, ArH), 7.80 (4H, *t*, J = 7.9 Hz, ArH), 8.34 (2H, *d*, J = 8.5 Hz, ArH); $^{13}\text{C-NMR}$ (50 MHz, CDCl_3 , δ / ppm): 24.0, 37.3, 117.0, 117.8, 119.9, 122.5, 124.2, 126.7, 128.6, 128.7, 128.8, 130.9, 131.3, 136.0, 141.0, 148.5, 168.4; ESI-MS (*m/z*, (relative abundance, %)): 438 (M+Na, 100), 416 (M+H, 60), 281 (10), 175 (19), 164 (8), 151 (16), 139 (26), 131 (18), 122 (26); HRMS: *m/z* calcd. for $\text{C}_{29}\text{H}_{22}\text{NO}_2$ (M+H): 416.1651. Found: 416.1653.

*4-(14H-Dibenzo[a,j]xanthen-14-yl)benzonitrile (4h).*¹⁷ Colorless solid; m.p.: 294–295 °C (lit. 291–292 °C); IR (CHCl_3 , cm^{-1}): 3019, 2930, 2400, 2225, 1633, 1414, 1237, 1215; $^1\text{H-NMR}$ (200 MHz, CDCl_3 , δ / ppm): 6.55 (1H, *s*, ArCHAr), 7.40–7.51 (6H, *m*, ArH), 7.55–7.64 (4H, *m*, ArH), 7.81–7.87 (4H, *m*, ArH), 8.27 (2H, *d*, J = 8.4 Hz, ArH); $^{13}\text{C-NMR}$ (75 MHz, CDCl_3 , δ / ppm): 38.0, 115.9, 118.0, 118.6, 122.1, 124.6, 127.1, 128.9, 129.0, 129.5, 131.0, 131.1, 132.1, 132.4, 148.8, 150.0; EI-MS (*m/z*, (relative abundance, %)): 383 (M, 18), 281 (100), 252 (17), 250 (10), 192 (9), 141 (10), 126 (6), 102 (13), 75 (8).

4-(14H-Dibenzo[a,j]xanthen-14-yl)benzoic acid (4i). Colorless solid; m.p.: >300 °C; Anal. Calcd. for $\text{C}_{28}\text{H}_{18}\text{O}_3$: C, 83.57; H, 4.51 %. Found: C, 83.36; H, 4.73 %; IR (CHCl_3 , cm^{-1}): 3428, 3019, 1679, 1604, 1421, 1214, 1080, 1018; $^1\text{H-NMR}$ (200 MHz, CDCl_3 , δ / ppm): 6.55 (1H, *s*, ArCHAr), 7.37–7.53 (4H, *m*, ArH), 7.58–7.62 (4H, *m*, ArH), 7.78–7.86 (6H, *m*, ArH), 8.32 (2H, *d*, J = 8.4 Hz, ArH); $^{13}\text{C-NMR}$ (75 MHz, CDCl_3 , δ / ppm): 38.1, 116.3, 118.0, 122.3, 124.4, 127.0, 128.4, 128.9, 129.3, 130.5, 130.7, 131.0, 131.3, 148.7, 150.8, 170.9; ESI-MS (*m/z*, (relative abundance, %)): 403 (M+H, 9), 402 (M, 25), 401 (M–H, 100), 397 (25), 369 (13), 358 (7), 340 (8), 326 (5), 281 (5), 277 (19), 259 (8), 215 (9); HRMS: *m/z* calcd. for $\text{C}_{28}\text{H}_{19}\text{O}_3$ (M+H): 403.1334. Found: 403.1352.

*14-(4-Nitrophenyl)-14H-dibenzo[a,j]xanthene (4j).*³ Yellow solid; m.p.: >300 °C (lit. 310–311 °C); IR (CHCl_3 , cm^{-1}): 3019, 1634, 1516, 1340, 1250, 1239, 1106, 1014; $^1\text{H-NMR}$ (200 MHz, CDCl_3 , δ / ppm): 6.60 (1H, *s*, ArCHAr), 7.40–7.69 (8H, *m*, ArH), 7.81–7.86 (4H, *m*, ArH), 7.97–8.01 (2H, *m*, ArH), 8.28 (2H, *d*, J = 8.5 Hz, Ar); $^{13}\text{C-NMR}$ (50 MHz, CDCl_3 , δ / ppm): 37.8, 115.8, 118.0, 122.0, 123.8, 124.6, 127.2, 128.9, 129.0, 129.6, 131.1, 146.3, 148.8, 151.9; HRMS: *m/z* calcd. for $\text{C}_{27}\text{H}_{17}\text{NNaO}_3$ (M+Na): 426.1101. Found: 426.1100.

*14-(3-Fluorophenyl)-14H-dibenzo[a,j]xanthene (4k).*⁵ Colorless solid; m.p.: 256–257 °C (lit. 259 °C); IR (CHCl_3 , cm^{-1}): 3019, 2926, 2854, 2399, 2347, 1592, 1458, 1401, 1249, 1215; $^1\text{H-NMR}$ (200 MHz, CDCl_3 , δ / ppm): 6.48 (1H, *s*, ArCHAr), 6.65–6.73 (1H, *m*, ArH), 7.05–7.18 (2H, *m*, ArH), 7.33–7.51 (5H, *m*, ArH), 7.59 (2H, *t*, J = 7.3 Hz, ArH), 7.82 (4H, *t*, J = 7.7 Hz, ArH), 8.34 (2H, *d*, J = 8.5 Hz, ArH); $^{13}\text{C-NMR}$ (50 MHz, CDCl_3 , δ / ppm): 37.6, 113.2, 113.6, 115.0, 115.5, 116.7, 118.0, 122.4, 123.7, 123.8, 124.3, 126.9, 128.8, 129.1,



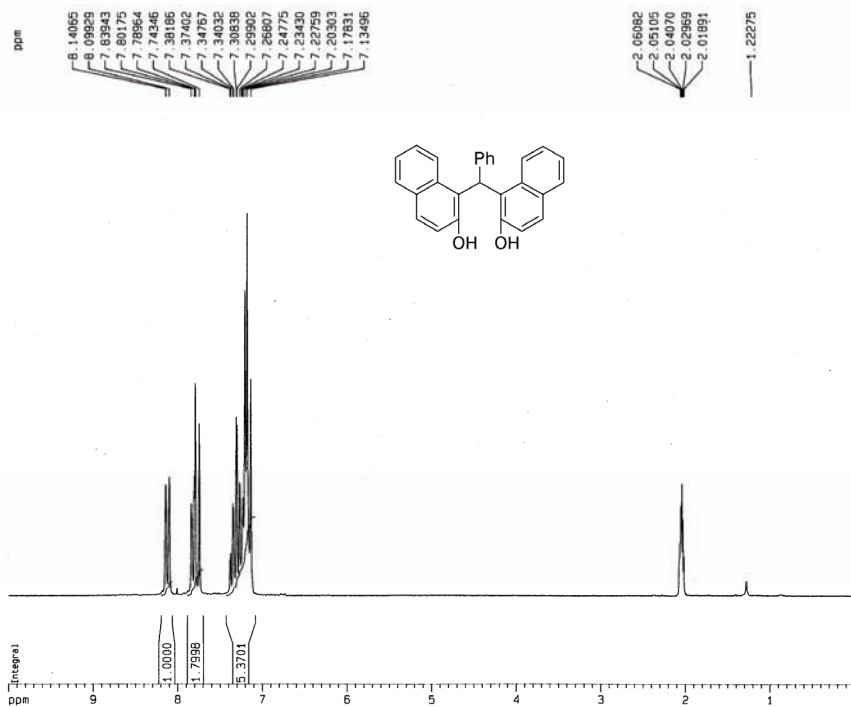
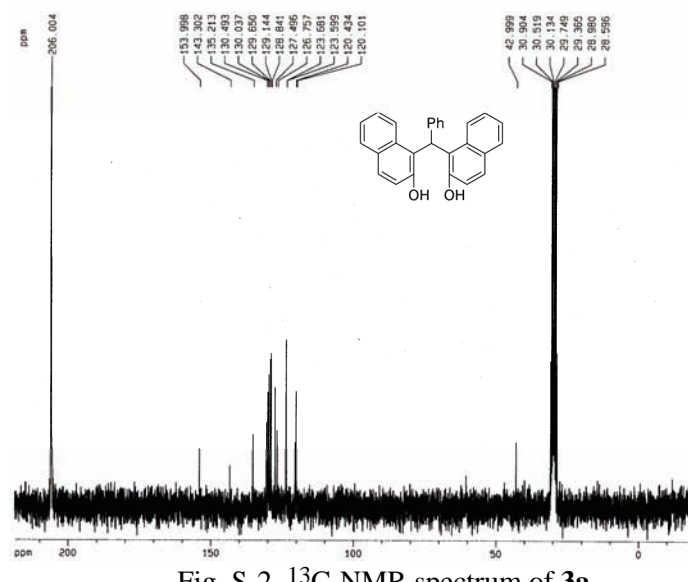
129.6, 129.8, 131.0, 131.3, 147.3, 147.4, 148.8, 160.5, 165.4; EI-MS (*m/z*, (relative abundance, %)): 376 (M, 8), 281 (100), 252 (14), 250 (8), 141 (6).

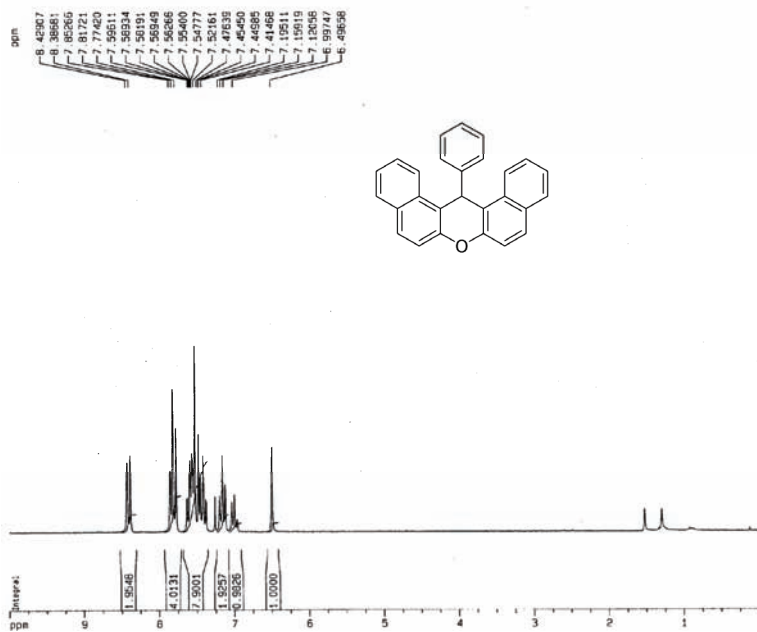
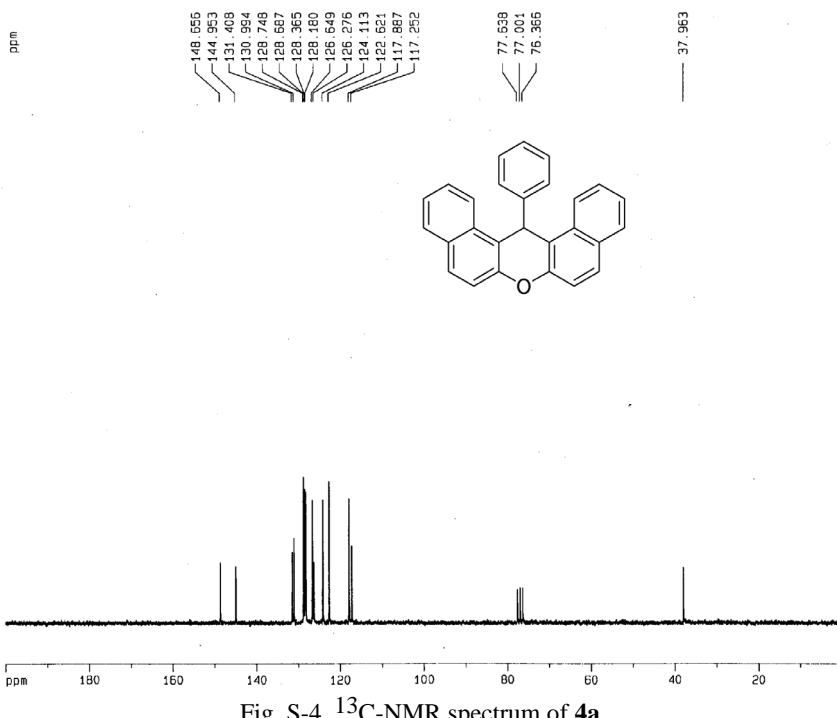
14-Pentyl-14H-dibenzo[a,j]xanthene (4l). Colorless solid; m.p.: 94–95 °C; Anal. Calcd. for C₂₆H₂₄O: C, 88.60; H, 6.86 %. Found: C, 88.28; H, 6.63 %; IR (CHCl₃, cm⁻¹): 3070, 2956, 2932, 2857, 1622, 1591, 1516, 1457, 1435, 1400, 1254, 1240, 956, 907, 815; ¹H-NMR (300 MHz, CDCl₃, δ / ppm): 0.63 (3H, *t*, *J* = 6.5 Hz, C₄H₈CH₃), 0.97 (6H, *m*, CH₂C₃H₆CH₃), 2.05 (2H, *m*, ArCHCH₂), 5.57 (1H, *t*, *J* = 4.3 Hz, ArCHAr), 7.39 (2H, *d*, *J* = 9.0 Hz, ArH), 7.47 (2H, *t*, *J* = 7.7 Hz, ArH), 7.63 (2H, *dd*, *J* = 7.5, 1.2 Hz, ArH), 7.78 (2H, *d*, *J* = 8.7 Hz, ArH), 7.89 (2H, *d*, *J* = 8.1 Hz, ArH), 8.27 (2H, *d*, *J* = 8.4 Hz, ArH); ¹³C-NMR (75 MHz, CDCl₃, δ / ppm): 13.9, 22.4, 24.4, 30.9, 31.9, 35.8, 116.5, 117.5, 122.4, 124.0, 126.5, 128.1, 128.8, 130.9, 131.4, 149.9; EI-MS (*m/z*, (relative abundance, %)): 352 (M, 2), 281 (100), 140 (14), 126 (4); HRMS: *m/z* calcd. for C₂₆H₂₅O (M+H): 353.1905. Found: 353.1912.

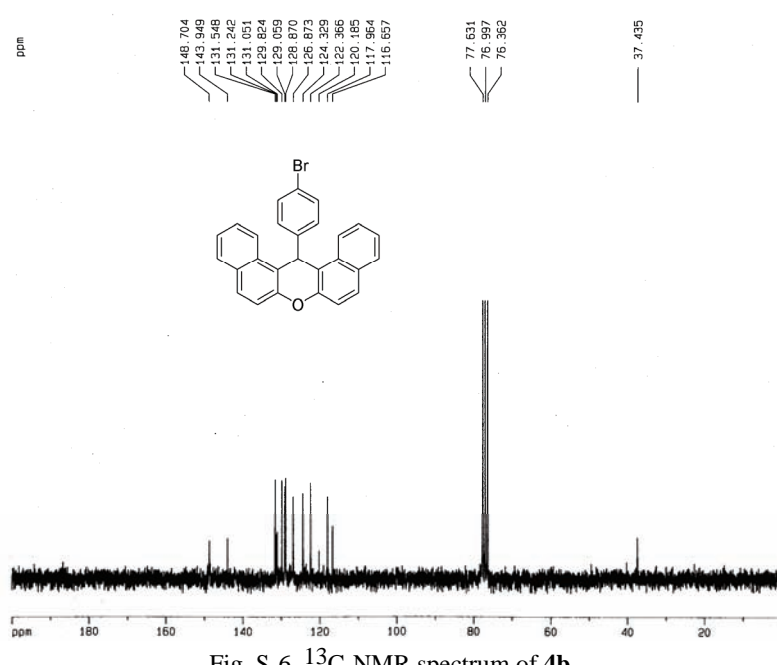
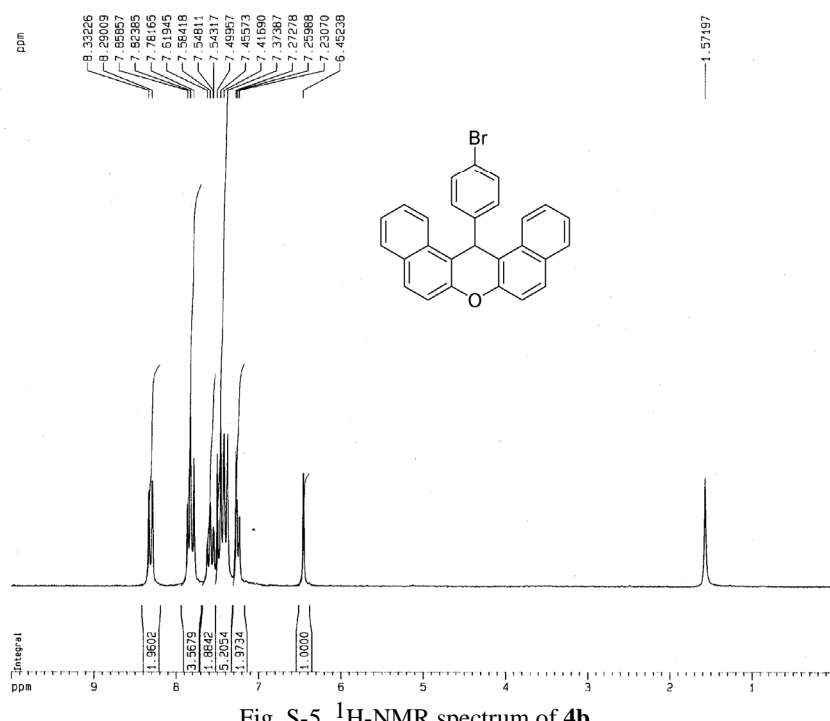
14-Heptyl-14H-dibenzo[a,j]xanthene (4m). Viscous liquid; Anal. Calcd. for C₂₈H₂₈O: C, 88.38; H, 7.42 %. Found: C, 87.95; H, 7.87 %; IR (CHCl₃, cm⁻¹): 3067, 2928, 2854, 1622, 1591, 1515, 1457, 1434, 1400, 1240, 1157, 1140, 960, 861, 813; ¹H-NMR (200 MHz, CDCl₃, δ / ppm): 0.77 (3H, *t*, *J* = 7.1 Hz, C₆H₁₂CH₃), 1.02–1.36 (10H, *m*, C₅H₁₀CH₃), 2.10–2.11 (2H, *m*, ArCHCH₂), 5.59 (1H, *t*, *J* = 4.3 Hz, ArCHAr), 7.36–7.53 (4H, *m*, ArH), 7.66 (2H, *t*, *J* = 7.7 Hz, ArH), 7.80 (2H, *d*, *J* = 8.9 Hz, ArH), 7.91 (2H, *d*, *J* = 8.1 Hz, ArH), 8.30 (2H, *d*, *J* = 8.5 Hz, ArH); ¹³C-NMR (50 MHz, CDCl₃, δ / ppm): 13.9, 22.4, 24.8, 28.9, 29.6, 30.9, 31.6, 35.9, 116.6, 117.4, 122.3, 123.9, 126.4, 128.0, 128.7, 131.0, 131.4, 149.9; HRMS: *m/z* calcd. for C₂₈H₂₉O (M+H): 381.2218. Found: 381.2212.

2,3,5,6,8,9,11,12,14,15-Decahydro-23-phenyl-23H-dinaphtho[2,1,q:1'2't]-1,4,7,10,13,16-hexaoxacycloheicosin (5). Light yellow solid; m.p.: 155–156 °C; Anal. Calcd. for C₃₇H₃₈O₆: C, 76.79; H, 6.62 %. Found: C, 76.96; H, 6.51 %; IR (CHCl₃, cm⁻¹): 3058, 3016, 2874, 1622, 1598, 1511, 1492, 1451, 1451, 1295, 1259, 1243, 1215, 1176, 928, 806, 697; ¹H-NMR (200 MHz, CDCl₃, δ / ppm): 2.88–2.98 (2H, *m*, OCH₂CH₂O), 3.10–3.21 (2H, *m*, OCH₂CH₂O), 3.31–3.35 (4H, *m*, 2×OCH₂CH₂O), 3.45–3.48 (8H, *m*, 4×OCH₂CH₂O), 3.69–3.71 (2H, *m*, OCH₂CH₂O), 3.77–3.83 (2H, *m*, OCH₂CH₂O), 7.03–7.14 (6H, *m*, ArCHAr, ArH), 7.23–7.30 (6H, *m*, ArH), 7.73–7.81 (6H, *m*, ArH); ¹³C-NMR (50 MHz, CDCl₃, δ / ppm): 43.9, 68.4, 68.9, 70.3, 116.1, 122.7, 124.0, 124.8, 125.2, 125.8, 127.5, 128.1, 128.2, 128.7, 129.4, 133.4, 144.9, 155.2; APCI-MS (*m/z*, (relative abundance, %)): 579 (M+H, 70), 578 (M, 100), 577 (M-H, 43), 259 (35), 171 (31), 169 (25); HRMS: *m/z* calcd. for C₃₇H₃₉O₆ (M+H): 579.2747. Found: 579.2731.

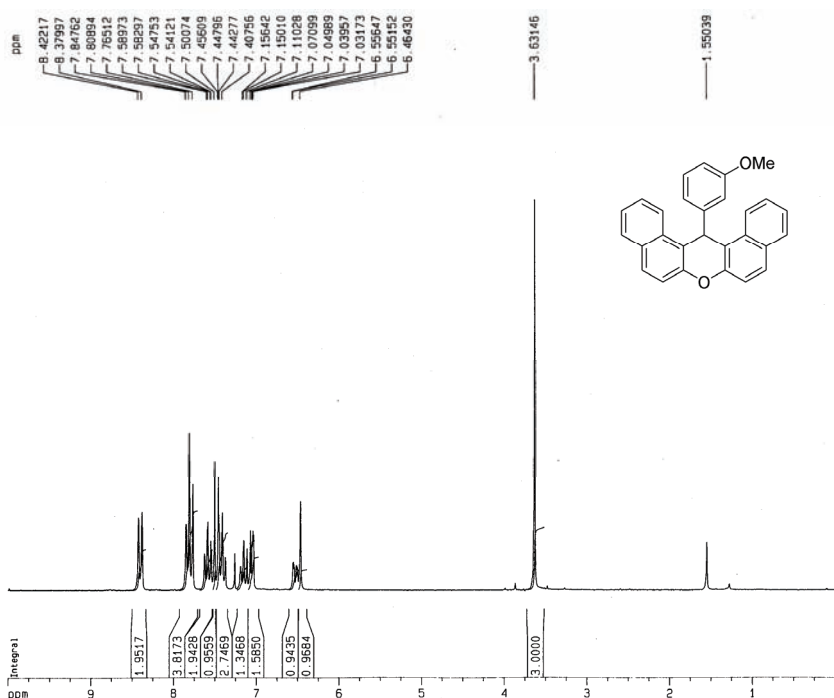
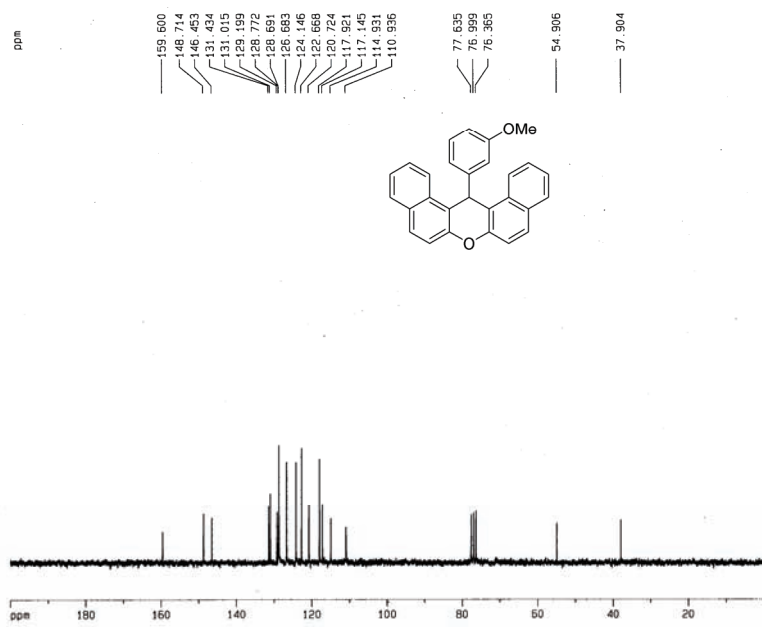


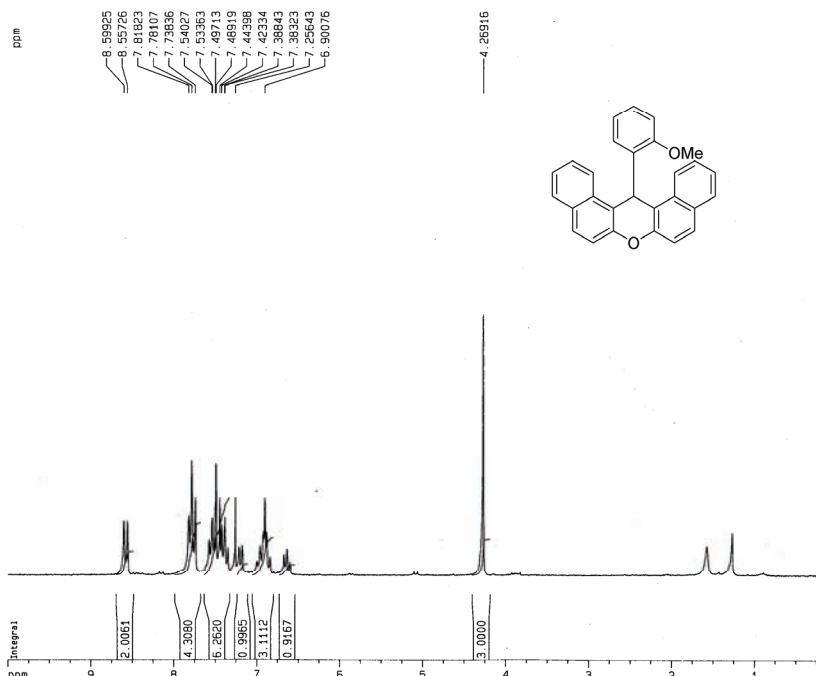
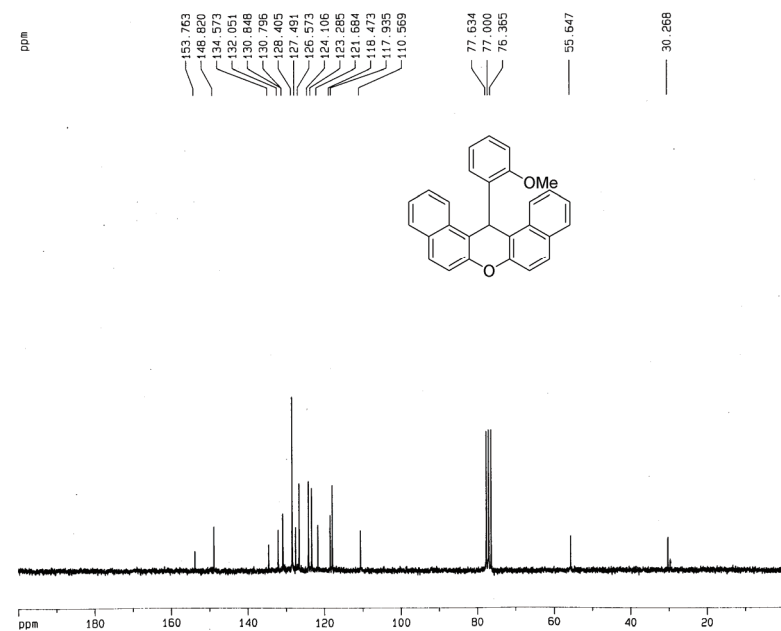
¹H- AND ¹³C-NMR SPECTRA FOR COMPOUNDS 3a, 4a-4m AND 5Fig. S-1. ¹H-NMR spectrum of 3a.Fig. S-2. ¹³C-NMR spectrum of 3a.

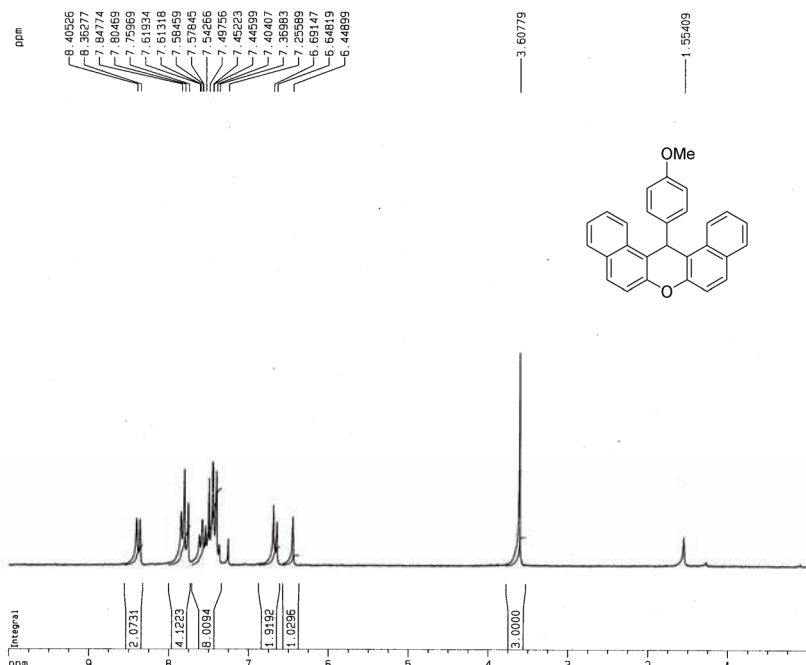
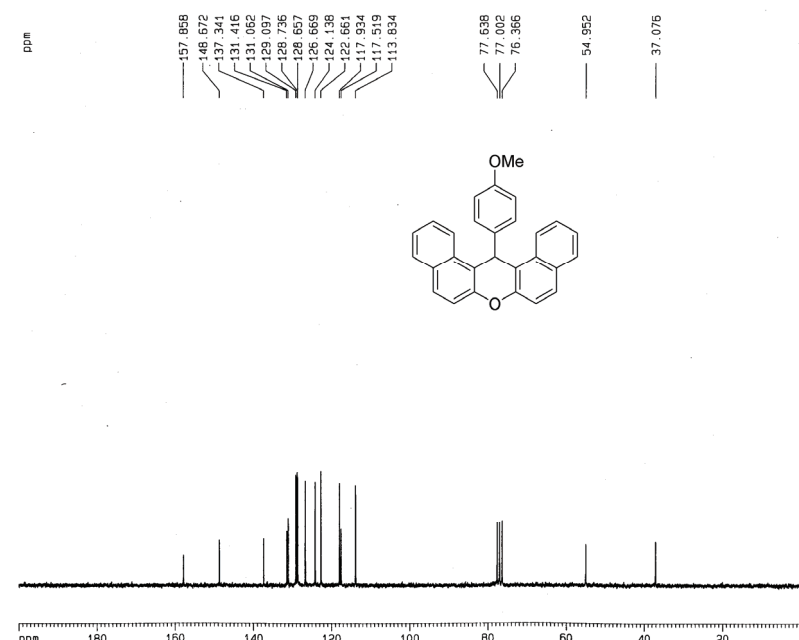
Fig. S-3. ¹H-NMR spectrum of 4a.Fig. S-4. ¹³C-NMR spectrum of 4a.

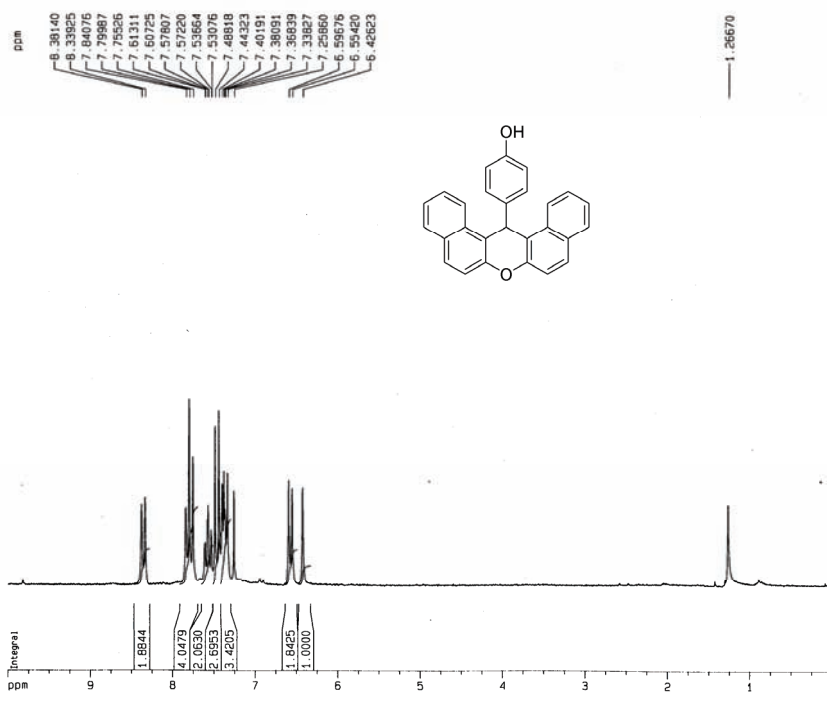
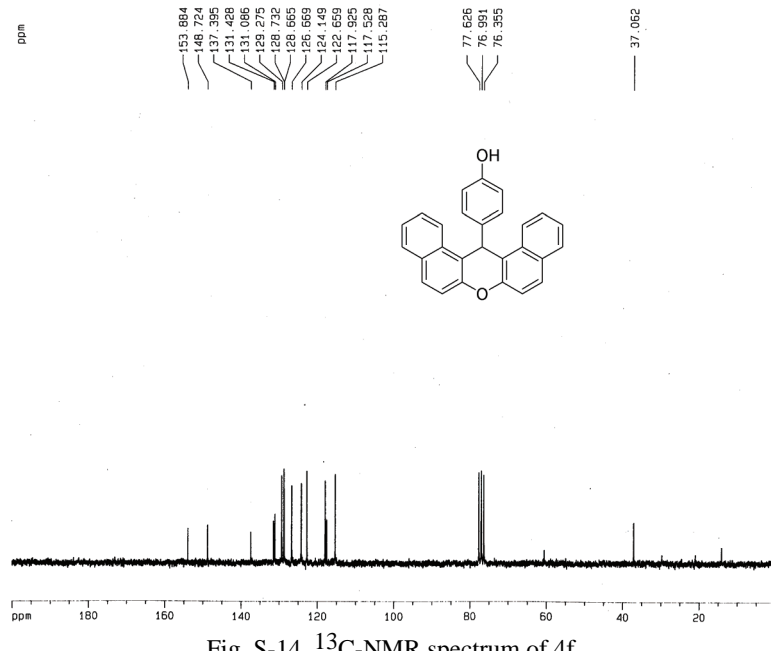


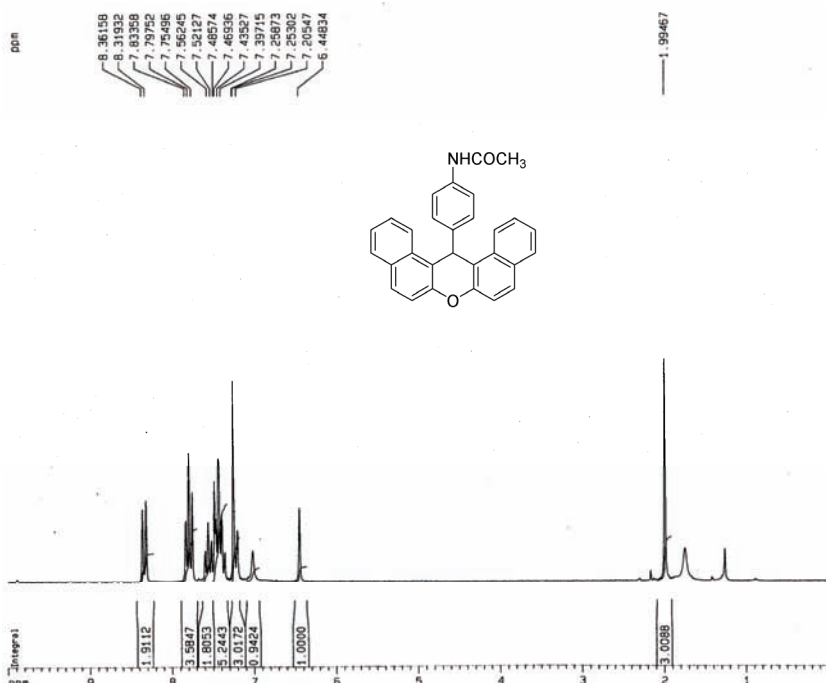
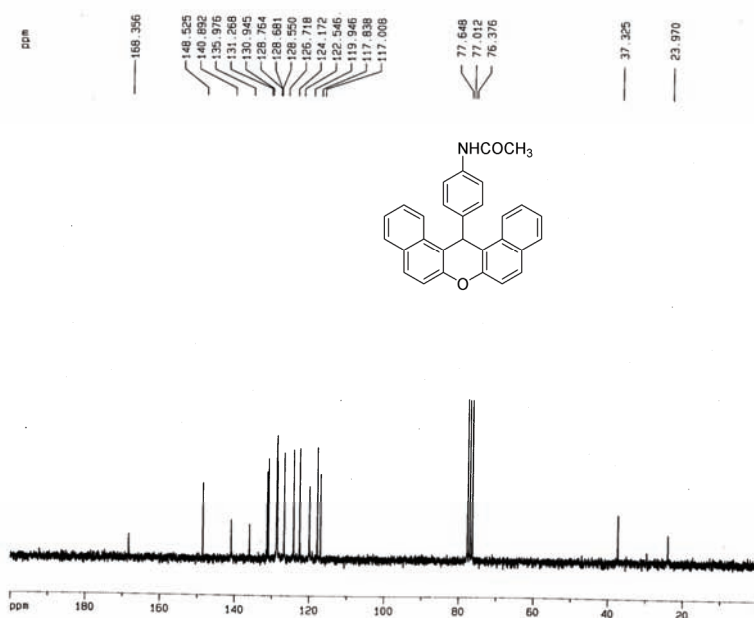
SUPPLEMENTARY MATERIAL

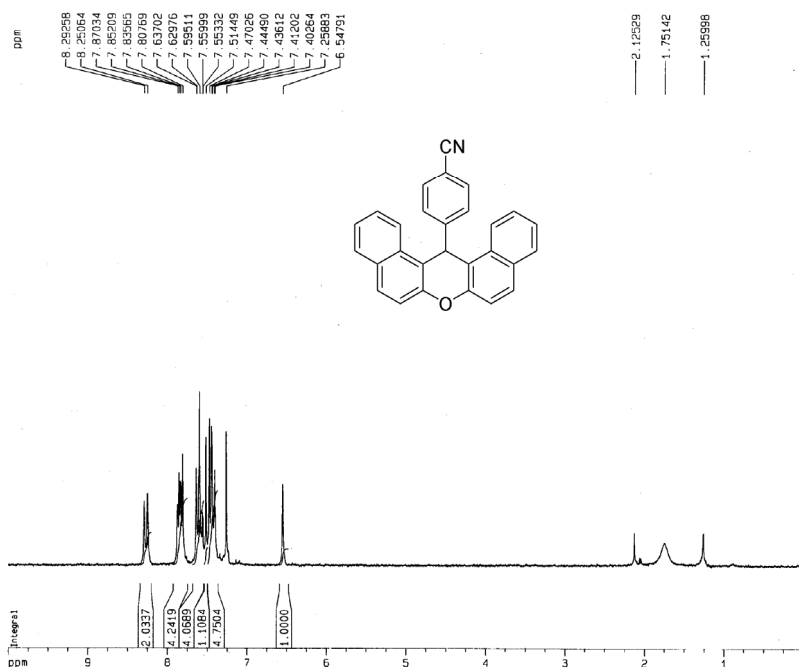
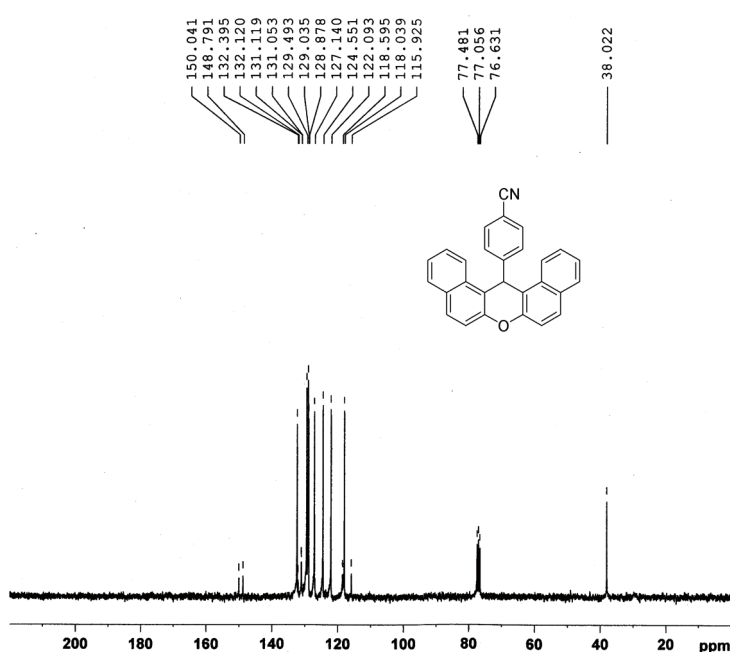
Fig. S-7. ^1H -NMR spectrum of **4c**.Fig. S-8. ^{13}C -NMR spectrum of **4c**.

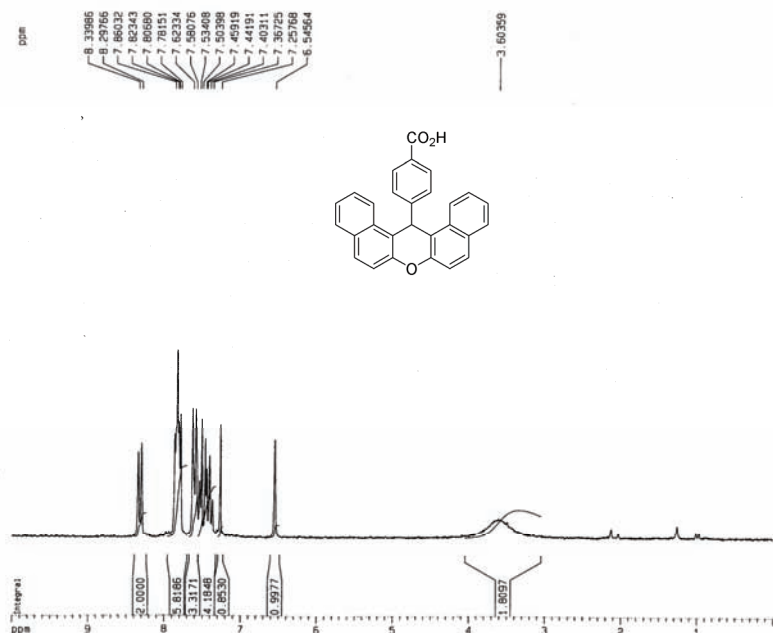
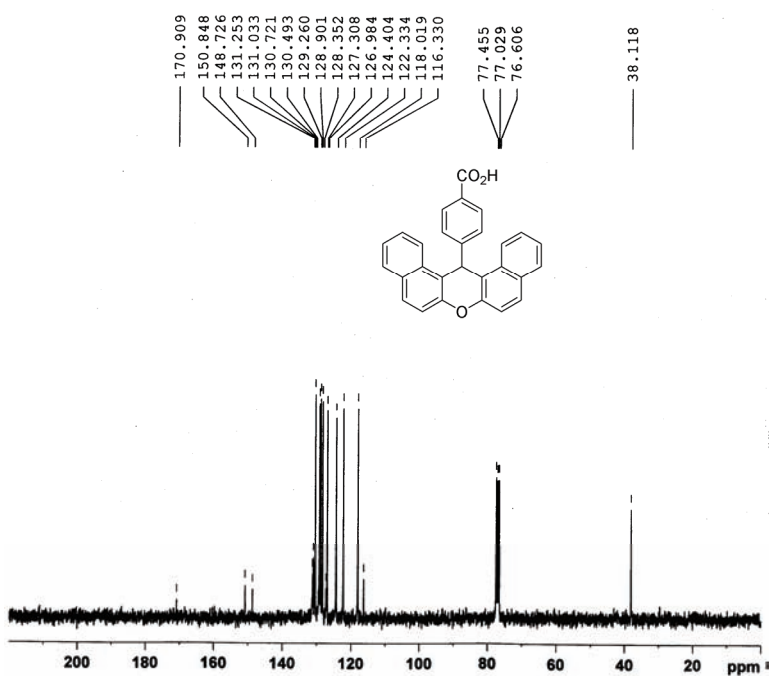
Fig. S-9. ¹H-NMR spectrum of 4d.Fig. S-10. ¹³C-NMR spectrum of 4d.

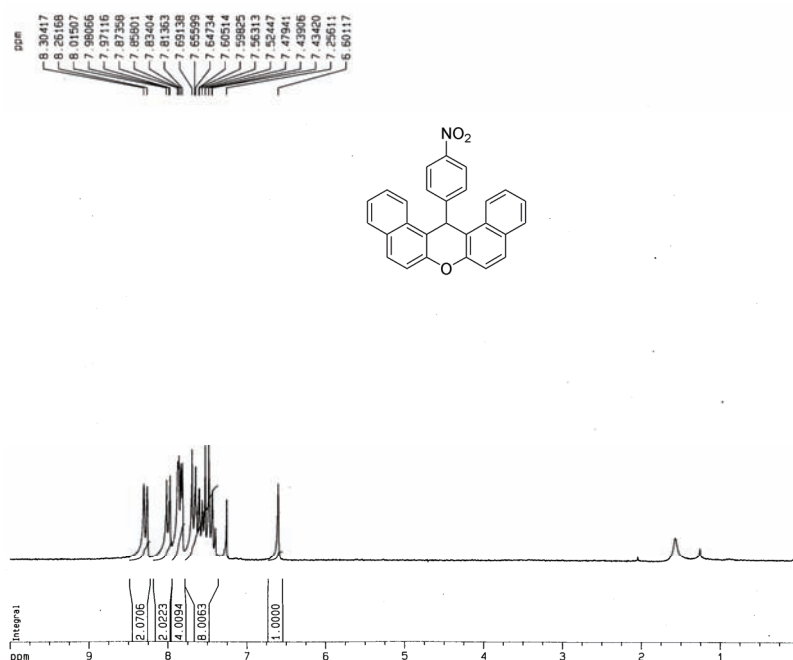
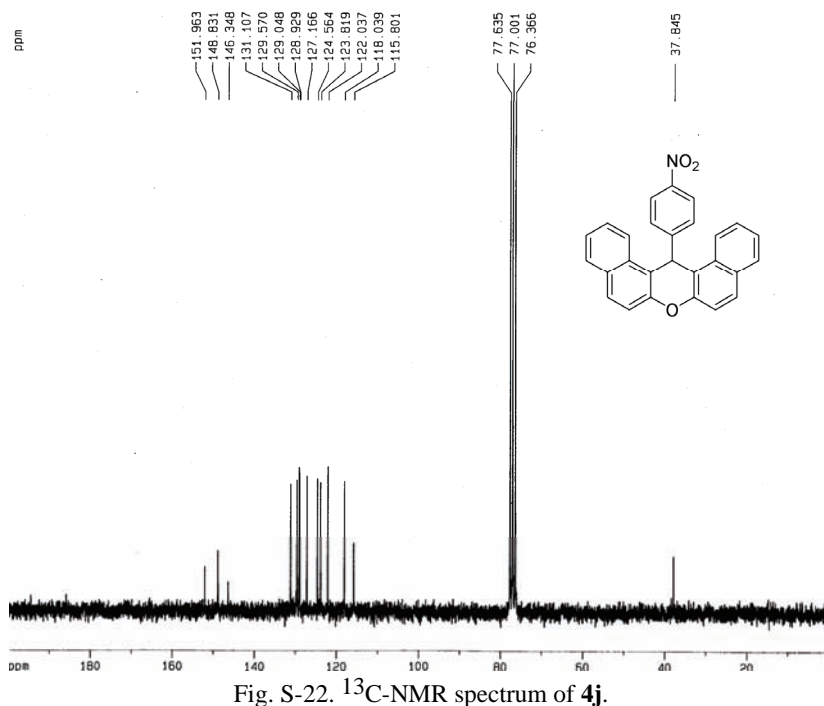
Fig. S-11. ¹H-NMR spectrum of 4e.Fig. S-12. ¹³C-NMR spectrum of 4e.

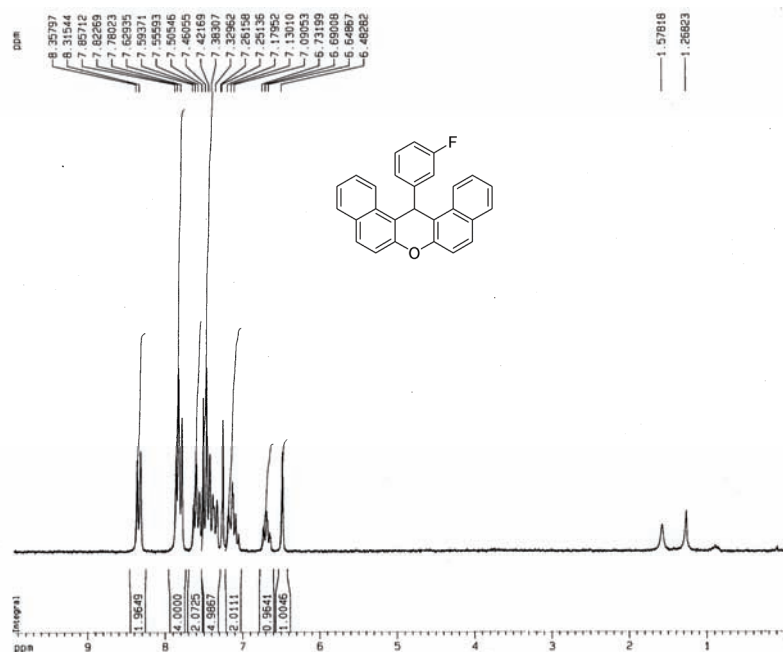
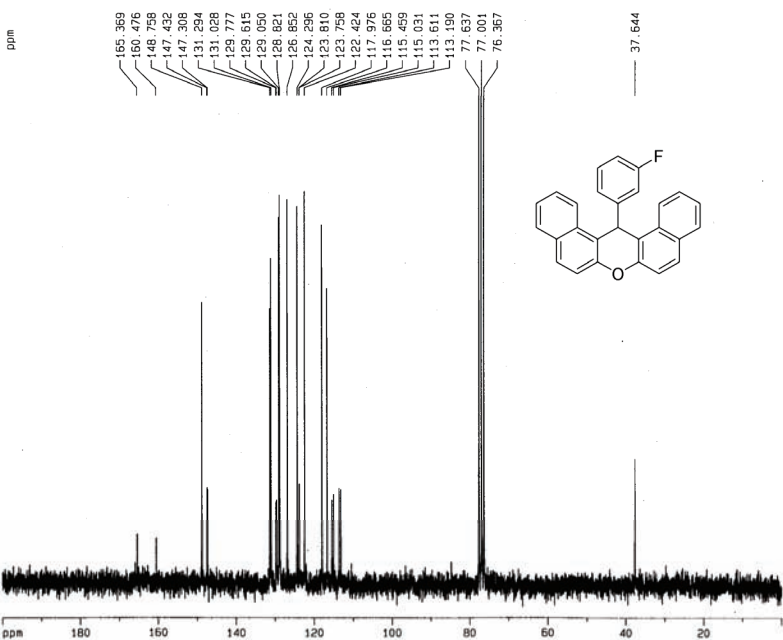
Fig. S-13. ¹H-NMR spectrum of 4f.Fig. S-14. ¹³C-NMR spectrum of 4f.

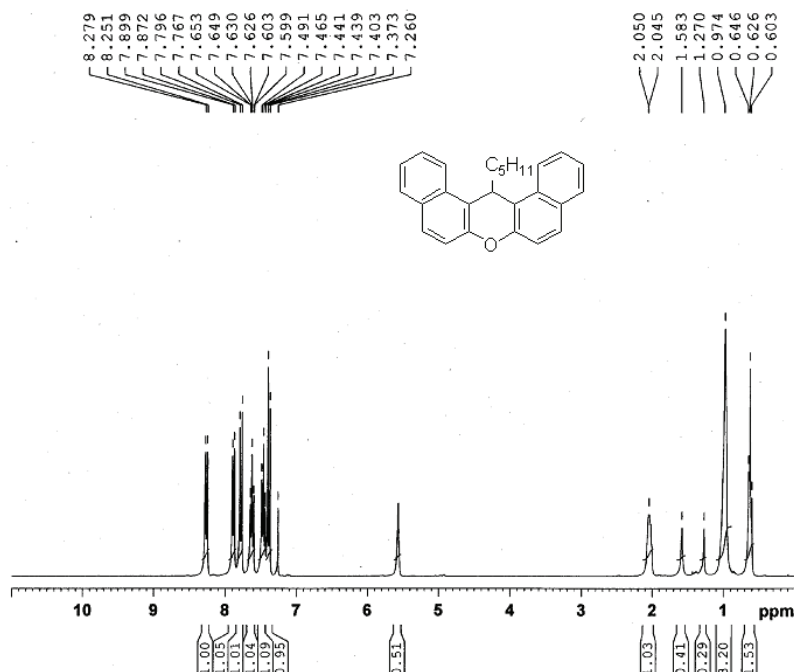
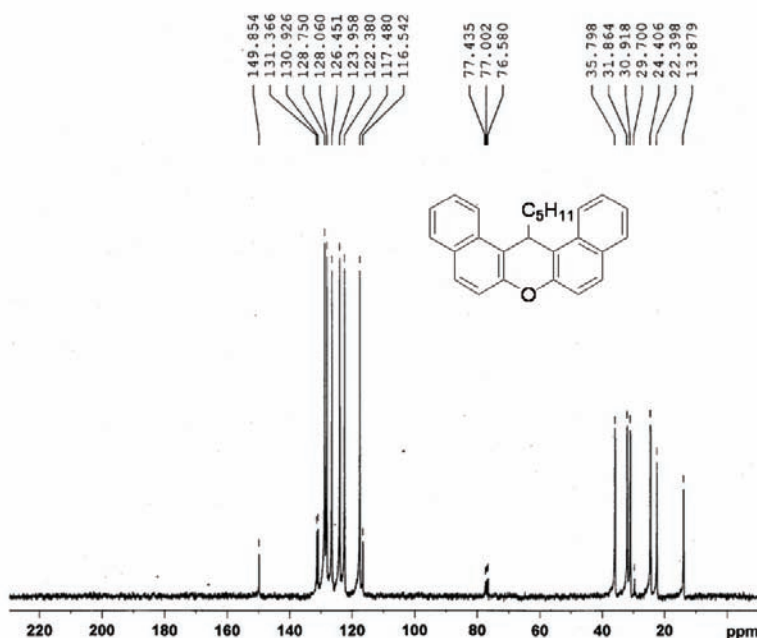
Fig. S-15. ¹H-NMR spectrum of 4g.Fig. S-16. ¹³C-NMR spectrum of 4g.

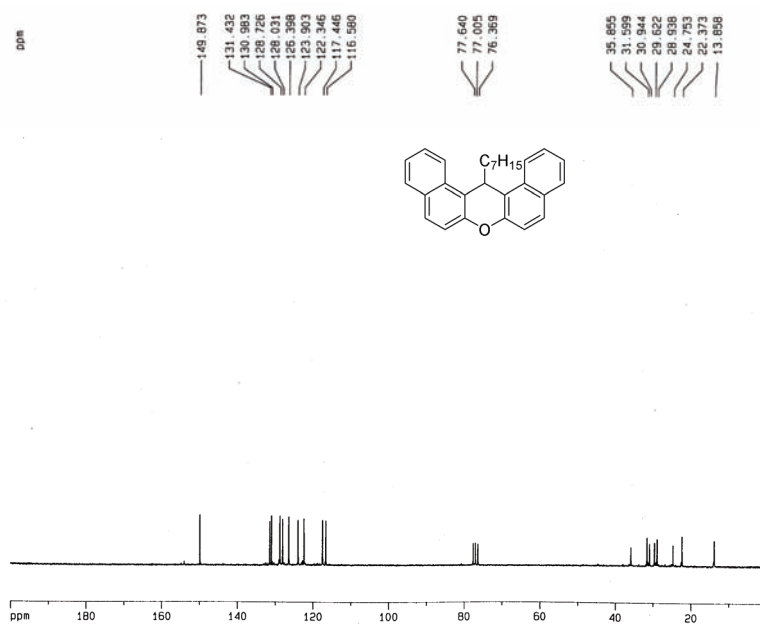
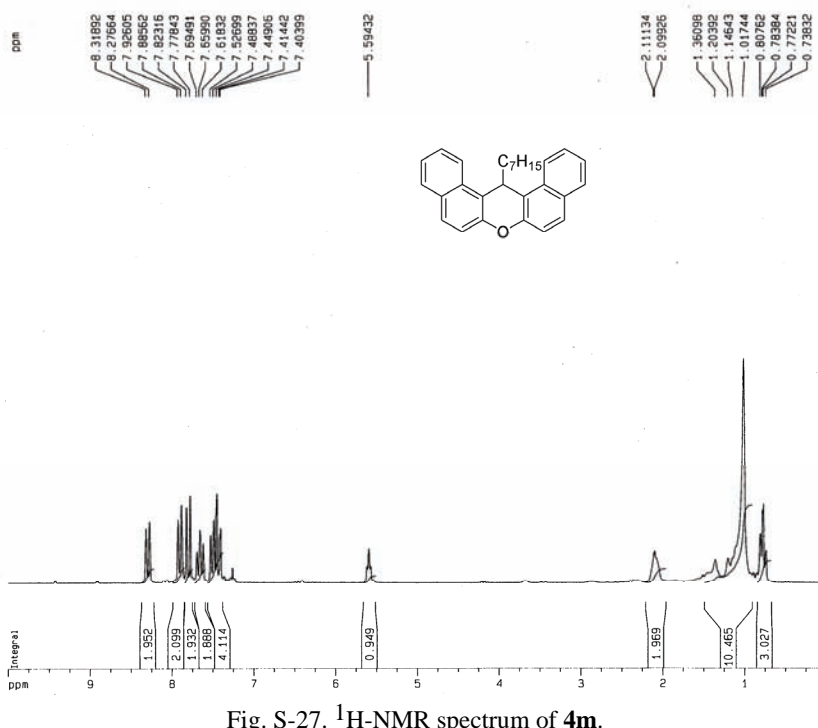
Fig. S-17. ¹H-NMR spectrum of 4h.Fig. S-18. ¹³C-NMR spectrum of 4h.

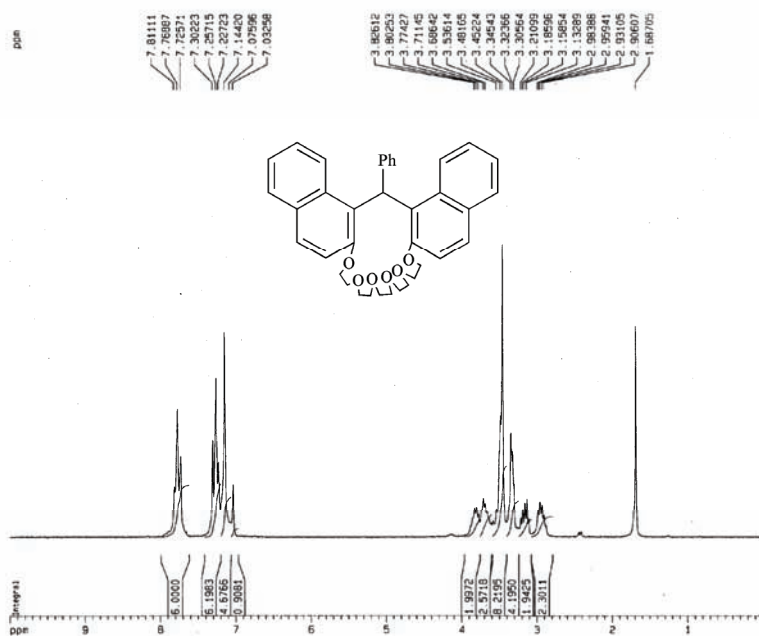
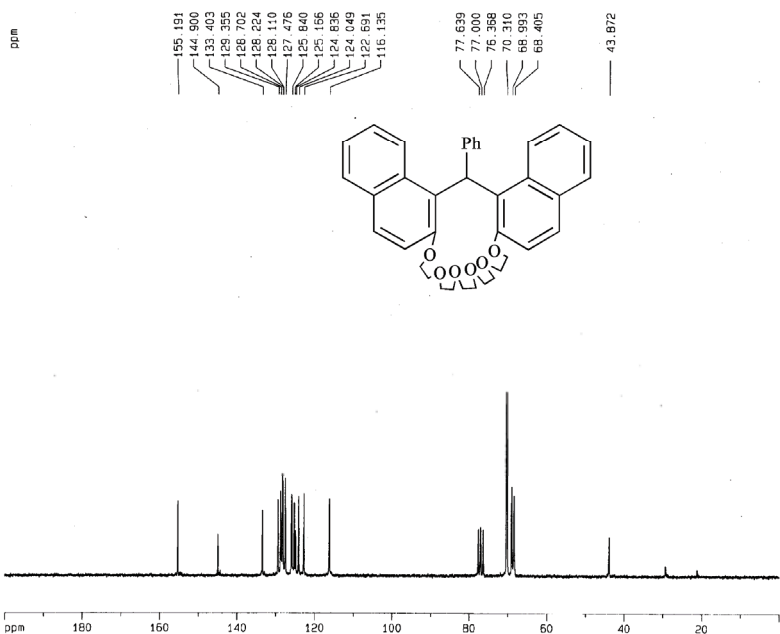
Fig. S-19. ¹H-NMR spectrum of 4i.Fig. S-20. ¹³C-NMR spectrum of 4i.

Fig. S-21. ¹H-NMR spectrum of 4j.Fig. S-22. ¹³C-NMR spectrum of 4j.

Fig. S-23. ^1H -NMR spectrum of **4k**.Fig. S-24. ^{13}C -NMR spectrum of **4k**.

Fig. S-25. ^1H -NMR spectrum of **4l**.Fig. S-26. ^{13}C -NMR spectrum of **4l**.



Fig. S-29. ^1H -NMR spectrum of **5**.Fig. S-30. ^{13}C -NMR spectrum of **5**.

REFERENCES

1. W. Su, D. Yang, C. Jin, B. Zhang, *Tetrahedron Lett.* **49** (2008) 3391
2. A. K. Bhattacharya, K. C. Rana, M. Mujahid, I. Sehar, A. K. Saxena, *Bioorg. Med. Chem.* **19** (2009) 5590
3. R. Kumar, G. C. Nandi, R. K. Verma, M. S. Singh, *Tetrahedron Lett.* **51** (2010) 442
4. M. Hong, C. Cai, *J. Fluorine Chem.* **130** (2009), 989
5. B. Rajitha, B. Sunil Kumar, Y. Thirupathi Reddy, P. Narsimha Reddy, N. Sreenivasulu, *Tetrahedron Lett.* **46** (2005) 8691.





Synthesis of various fused pyrimidine rings and their pharmacological and antimicrobial evaluation

MOUNIR A. SALEM*, MAGDA I. MARZOUK and NAGLAA F. MAHMOUD

Heterocyclic Synthetic Laboratory, Chemistry Department, Faculty of Science, Ain Shams University Cairo, Egypt

(Received 28 May 2013, revised 13 February, accepted 4 March 2014)

Abstract: Various fused pyrimidines, such as furo[2,3-*d*]pyrimidine, triazolo[1,5-*d*]pyrimidine and tetrazolo[1,5-*a*]pyrimidine, were synthesized in the reactions of thioxopyrimidine-6(1*H*)-ones with ethyl chloroacetate (under different reaction conditions), thiourea and sodium nitrite. Pyrimidine thiones reacted with $\text{POCl}_3/\text{PCl}_5$ to give the chloro derivatives which reacted with sodium azide and thiourea to give tetrazolo[1,5-*c*]pyrimidines, and pyrimido pyrimidines. Thioxopyrimidine-6(1*H*)-ones reacted with benzylamine to give pyrrolo[2,3-*d*]pyrimidinethiones. Theoretical calculation using MIDO/3, Fukui indices and the heat of formation of some compounds were carried out. The pharmacological and antimicrobial activities of some of the synthesized products were also evaluated.

Keywords: fused pyrimidine; thiazoles; pyrimidopyrimidines; antitumor; anti-oxidants; antimicrobial.

INTRODUCTION

Heterocyclic compounds are of great importance in the synthesis of pharmaceutically active compounds.^{1–4} Pyrimidine nuclei are the active core of various bioactive molecules and are best known as the heterocyclic core of nucleic acid bases.

In general, heterocyclics encompassing a pyrimidine moiety have found applications in a wide spectrum of biological^{5–7} and therapeutic areas.^{8–13} Such a ring system is often incorporated into drugs designed as anticancer,^{14,15} anti-viral,¹⁶ antihypertensive,¹⁷ analgesic,^{18,19} antipyretic,²⁰ anti-inflammatory,²¹ antifungal,²² antibacterial²² and anti-psoriasis agents.²³ Some derivatives are active on the blood circulatory system,²⁴ stimulate skin preparative regeneration and increase the efficacy of antibiotic therapy of *Staphylococcus* and *proteus*-infected wounds.²⁵ As part of ongoing interest in the synthesis of heterocyclic com-

*Corresponding author. E-mail: salemmai1947@yahoo.com
doi: 10.2298/JSC130528016M

pounds, convenient syntheses of 5-substituted 2-thioxo-4-aryl-1,2,3,6-tetrahydro-pyrimidin-6-ones and 4-aryl-2-(methylthio)-6-oxo-1,6-dihydropyrimidine-5-carbonitrile were reported.²⁶ The study presented herein dealt with the efficient synthesis of a variety of fused pyrimidine derivatives, and an investigation of their biological activities.

RESULTS AND DISCUSSION

Chemistry

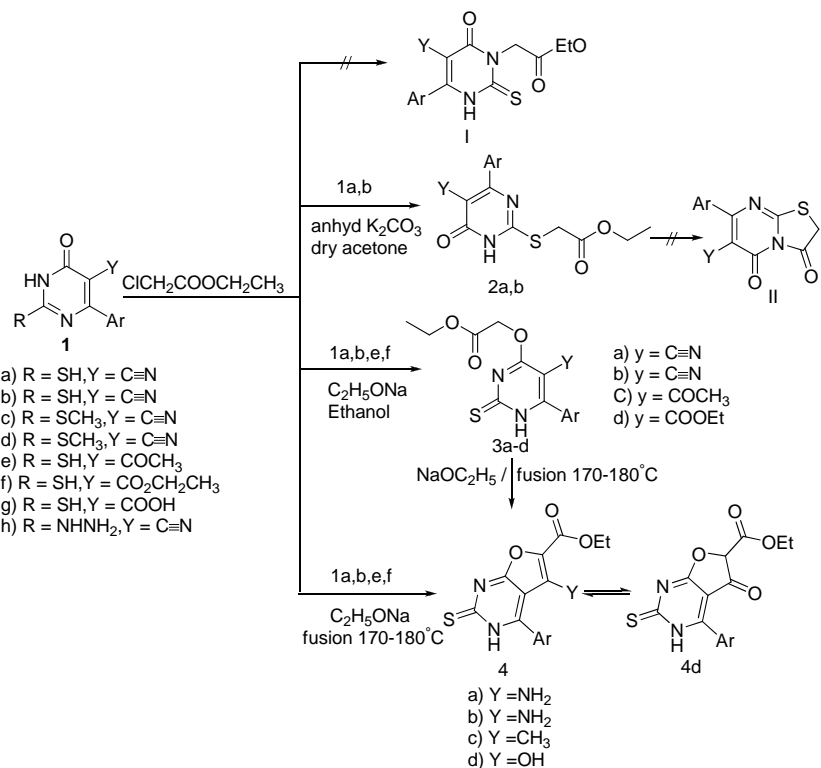
The hydrolysis of nitriles is generally considered one of the best methods for the preparation of carboxylic acids. The hydrolysis of nitriles proceeds in the distinct steps under acid or base treatment to achieve amides and carboxylic acids. The hydrolysis of the 5-cyano group in 2-thioxopyrimidine **1a** in basic medium was unsuccessful due to the low reactivity of the group. However, the hydrolysis was successfully achieved with 70 % sulfuric acid as the weakly nucleophilic nitrile was activated by protonation using H₂SO₄ to make it more electrophilic. This facilitates the reaction to give the corresponding 2-thioxopyrimidine-5-carboxylic acid (**1g**), Scheme 1. The structure of compound **1g** was confirmed by spectroscopic data, the IR spectrum revealed the presence of ν_{OH} at 3416 cm⁻¹, the ¹H-NMR spectrum showed a band at δ 11.0 ppm for the acidic OH and the ¹³C-NMR spectrum showed the presence of a carboxylic C=O at δ 165.2 ppm and the absence of C≡N.

Reaction of **1a** and **c** with hydrazine hydrate afforded the corresponding 2-hydrazino derivative **1h** by nucleophilic substitution of the SH or CH₃S group, respectively.

Masumoto *et al.* reported that treatment of 1-phenylpyrazolin-5-one with a base afforded a mixture of three adducts through carbon, nitrogen and oxygen anions.²⁷ On the other hand, some pyrimidinethiones in the presence of K₂CO₃/dry acetone yielded *S*-alkylated and/or *S*-and *N*-dialkylated products.^{28–30} Thienopyridin-2-one bearing a cyano group at the α-position to oxygen, reacted with ethyl chloroacetate in the presence of sodium ethoxide to give the oxygen alkylated derivative as the sole product, which cyclized to afford the corresponding furothiopyridine.^{31,32}

The reaction of **1a** and **b** with ethyl chloroacetate in the presence of a base depended on the reaction conditions. Furthermore, it was found that treatment of **1a** and **b** with ethyl chloroacetate in dry acetone, as a polar aprotic solvent, under reflux conditions in the presence of anhydrous K₂CO₃ afforded the *S*-alkylated products **2a** and **b** (Scheme 1). The *N*-alkylated product (**I**) and the corresponding cyclic product 7-aryl-2,3-dihydro-3,5-dioxo-5*H*-thiazolo[3,2-*a*]pyrimidine-6-carbonitrile (**II**) were not isolated.

To account for these results, theoretical calculations using MIDO/3 and Fukui indices were performed. As expected, the predicted electron density of the



Scheme 1. Synthesis of compounds **2a** and **b**; **4a** and **d**; Ar = C₆H₃-3,4-(O-CH₂-O) for **1a**, **c**, **g** and **h**, **2a**, **3a** and **4a**; Ar = C₆H₃-3,4-(OCH₃)₂ for **1b**, **d**, **e**, **f**, **2b**, **3b-d** and **4b-d**.

oxygen atom (-0.298 and -3.05 for **1a** and **b**, respectively) is larger than that of the sulfur atom (-0.172 and -0.188 for **1a** and **b**, respectively). However, since the size of the atom plays a significant role in the extent of its nucleophilicity, the S atom is more nucleophilic than the O atom. Consequently, the reaction proceeded *via* S-alkylation and afforded the thermodynamically more stable products **2a** ($\Delta H_f^\ominus = -82.03$ kcal* mol⁻¹, $\Delta E = E_{\text{LUMO}} - E_{\text{HOMO}} = 8.048$ eV) and **2b** ($(\Delta H_f^\ominus = -83.667$ kcal mol⁻¹, $\Delta E = E_{\text{LUMO}} - E_{\text{HOMO}} = 8.45$ eV). The structure of **2a** was also confirmed by ¹³C-NMR spectroscopy, which evidenced the presence of S-CH₂COOC₂H₅ by the appearance of a signal at δ 159.98 ppm, which is attributable to -C=S, and not at $\delta \approx 180$ ppm.

On the other hand, refluxing **1a** and **b** with ethyl chloroacetate in ethanol and sodium ethoxide gave the corresponding *O*-alkylated products **3a** and **b**, respectively, Scheme 1. It should be noted that, although **3a** and **b** were predicted to be thermodynamically less stable, where the (ΔH_f^\ominus of **3a** is -55.95 kcal mol⁻¹ and $\Delta E = E_{\text{LUMO}} - E_{\text{HOMO}} = 7.018$ eV, and that of **3b** is -56.595 kcal mol⁻¹ and $\Delta E =$

* 1 kcal = 4184 J

$= E_{\text{LUMO}} - E_{\text{HOMO}} = 7.44 \text{ eV}$, and in addition, the keto (lactam) form is more stable than the enol (lactim) form by *ca.* 13 kcal mol⁻¹, the formation of the *O*-alkylated products **3a** and **b** where the O atom with its higher electron density acted as the nucleophile were facilitated by the presence of the high boiling point, polar protic solvent and the strengthening of the employed base. In addition, analysis of the local reactivity of **1b** through an evaluation of the Fukui indices indicated that the Fukui indices for the S atom were $f_k^- = 0.643$, $f_k^+ = 0.133$ and $q_N = -0.589$, while for the O atom they were $f_k^- = 0.026$, $f_k^+ = 0.046$ and $q_N = 0.527$. The presence of electron withdrawing group (C≡N) in the α -position to the carbonyl of the amide also acts as an effective factor in the reaction pathway leading to the formation of **3a** and **b**. In order to confirm this assumption, **1e** and **f** were prepared and allowed to react under reflux with ethyl chloroacetate in ethanol and sodium ethoxide, whereby the *O*-alkylated products **3c** and **d** were isolated in a good yield as the sole products.

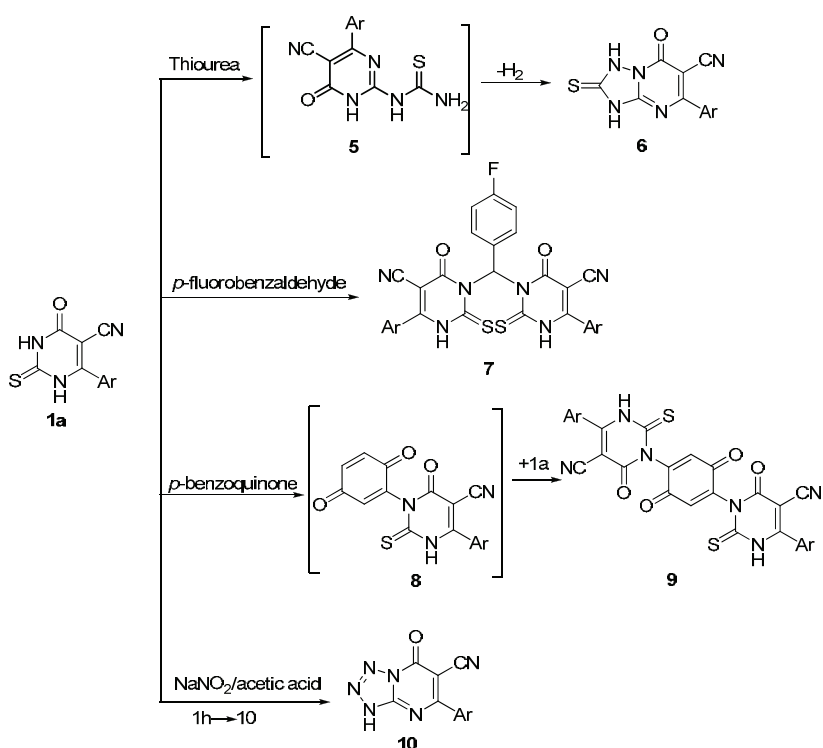
The ethyl 5-substituted-4-aryl-2-thioxo-1,2-dihydrofuro[2,3-*d*]pyrimidine-6-carboxylates **4a-d** were obtained *via* either fusion of **1a**, **b**, **e** and **f** with ethyl chloroacetate at 170–180 °C in the presence of sodium ethoxide or cyclization of the open chain products **3a-d** under similar reaction conditions (Scheme 1).

Treatment of **1a** with thiourea in *n*-butanol afforded the triazolo pyrimidine **6** without isolation of the intermediate **5** (Scheme 2). The ¹H-NMR spectrum of **6** showed the lack of an NH group adjacent to the C=O.

It was of interest to condense **1a** with 4-fluorobenzaldehyde³³ and also with *p*-benzoquinone,³⁴ to obtain the bis(pyrimidine-5-carbonitriles) **7** and **9** in 73 % and 68 % yield, respectively (Scheme 2).

It was found that the reaction of **1h** with aqueous sodium nitrite solution in the presence of acetic acid at 5 °C afforded the corresponding unisolated diazonium salt followed by cyclization to give the tetrazolo pyrimidine **10** in 52 % yield (Scheme 2). The IR spectra and the ¹H-NMR bands showed the absence of the NH₂ group and the appearance of a signal at δ 151.37 ppm in the ¹³C-NMR spectrum indicated the formation of the tetrazolo ring.

Treatment of 2-thioxopyrimidines **1a**, **b** and **d** with a mixture of phosphorus oxychloride and phosphorus pentachloride afforded the corresponding 4-chloro-2-thioxopyrimidines **11a-c** in 62–74 % yield (Scheme 3). The structures of compounds **11b** and **c** were confirmed by their ¹³C-NMR spectra, which showed signals for –C–Cl at δ 153.80 and 158.8 ppm, respectively, rather than at $\delta \approx 166$ ppm, which is attributable to –C=O. Such compounds were utilized for the synthesis of several new fused heterocyclic systems bearing 2-thioxo-pyrimidin-4(1*H*)-one moieties as an active core of bioactive molecules with expected antimicrobial and pharmacological activities.^{35–37}



Scheme 2. Synthesis of compounds **5–10**; Ar = C₆H₃-3,4-(O-CH₂-O) for **6**, **7**, **9** and **10**.

Treatment of **11a** with bi-functional nucleophilic substrates, *i.e.*, sodium azide and thiourea, afforded the tetrazolo pyrimidine **13**, and pyrimido pyrimidine **15**, respectively (Scheme 3).

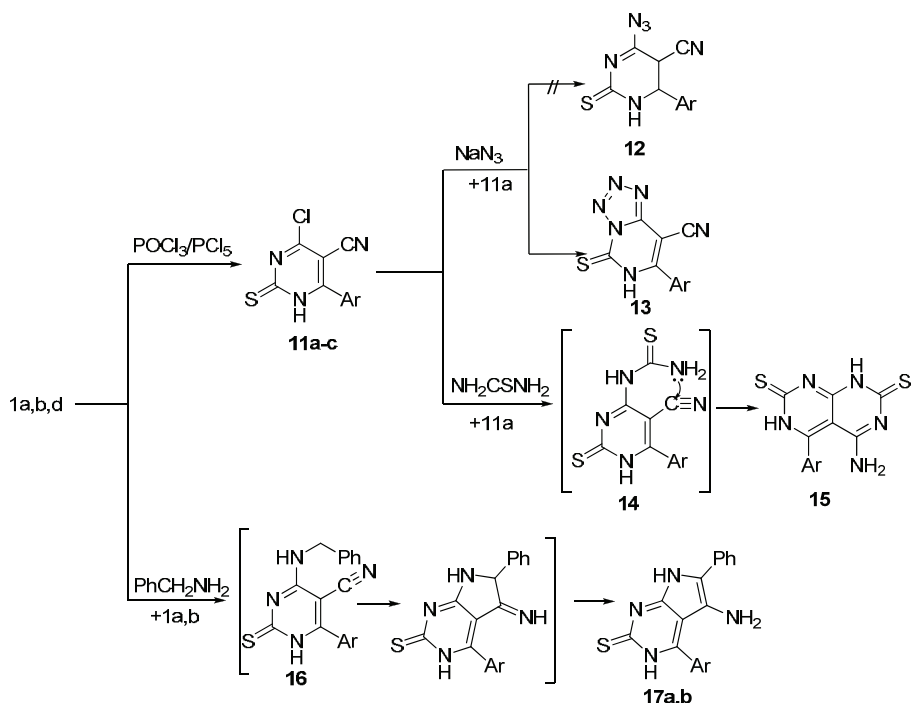
Reaction of 2-thioxopyrimidines **1a** and **b** with benzylamine in *n*-butanol afforded the pyrrolo pyrimidine-2-thiones **17a** and **b**, respectively, *via* the formation of the intermediate **16**.

Biological activities

Antimicrobial, anticancer and antioxidant activities of some compounds were investigated using standard methods and the results were compared with those of standard drugs.

Antimicrobial activity

It was observed that some of the thirteen tested compounds showed good activities against Gram-positive and Gram-negative bacteria, and the fungi *Candida albicans* and *Aspergillus niger*. Compounds **3b**, **3d**, **4a** and **11a** showed inhibition towards all the tested organisms (Table I).



Scheme 3. Synthesis of compounds **11a–c**, **13**, **15** and **17a** and **b**; Ar = $\text{C}_6\text{H}_3\text{-}3,4\text{-(O-CH}_2\text{-O)}$ for **11a** and **c**, **13**, **15** and **17a**; Ar = $\text{C}_6\text{H}_3\text{-}3,4\text{-(OCH}_3)_2$ for **11b** and **17b**.

The following points were noticed. On comparison between the compounds **1a**, **1c** and **1g**, it was noticed that compound **1a** did not inhibit any of the tested organisms, while conversion of the C=S group to CSCH₃ or CN group into COOH groups in compounds **1c** and **1g**, respectively, resulted in activity of **1c** against *Staphylococcus aureus*, *Escherichia coli* and *Pseudomonas aeruginosa* and of **1g** against *S. aureus*, *P. aeruginosa* and *C. albicans*.

Comparing the esters **2a** and **2b**, it was noticed that compound **2a** showed activity against *S. aureus*, *E. coli* and *P. aeruginosa* only, while compound **2b** exhibited activity against all the tested organisms, indicating that the presence of the 3,4-dimethoxy phenyl group in **2a** was more effective than the 1,3-benzodioxole group in **2b**.

The (aryloxy)acetate compounds **3b** and **3d** showed activity against all the tested organisms, while the (aryloxy)acetate **3a** showed activity against *S. aureus*, *E. coli* and *P. aeruginosa* only; this indicated that the presence of the 3,4-dimethoxyphenyl group in **3b** and **3d** is more effective than the 1,3-benzodioxole group in **3a**.

The furocarboxylate compound **4a** showed activity against all the tested organisms while **4c** showed activity against *S. aureus*, *E. coli*, *P. aeruginosa* and

C. albicans. **4d** exhibited activity against *Bacillus subtilis*, *S. aureus*, *C. albicans* and *A. niger*; this indicated that the NH₂ group in **4a** is more effective than the CH₃ and OH groups in **4c** and **4d**, respectively.

TABLE I. Antimicrobial activity for some of the products; the well diameter was 1 cm (100 µL of each one was tested); St = standard, that is chloramphenicol at 1 mg mL⁻¹ for Gram-positive bacteria, cefalexin for Gram-negative bacteria at 1 mg mL⁻¹, fluconazole for *A. niger* at 1 mg mL⁻¹ and flucoral for *C. albicans* at 1 mg mL⁻¹

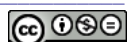
| Compound | Inhibition zone diameter, mm | | | | | |
|------------|------------------------------|------------------|----------------|----------------------|--------------------|-----------------|
| | <i>B. subtilis</i> | <i>S. aureus</i> | <i>E. coli</i> | <i>P. aeruginosa</i> | <i>C. albicans</i> | <i>A. niger</i> |
| 1a | — | — | — | — | — | — |
| 1c | — | 24 | 21 | 14 | — | — |
| 1g | — | 23 | — | 18 | 23 | — |
| 2a | — | 19 | 18 | 21 | — | — |
| 2b | 24 | 21 | 26 | 23 | — | — |
| 3a | — | 26 | 18 | 24 | — | — |
| 3b | 22 | 26 | 24 | 23 | 19 | 20 |
| 3d | 24 | 28 | 26 | 26 | 21 | 22 |
| 4a | 20 | 21 | 22 | 24 | 22 | 20 |
| 4c | — | 22 | 20 | 23 | 22 | — |
| 4d | 20 | 26 | — | — | 24 | 26 |
| 7 | — | — | — | 24 | — | 26 |
| 11a | 20 | 26 | 22 | 18 | 22 | 20 |
| St | 32.5 | 32.5 | 32.5 | 32.5 | 28 | 23 |

Compound **7** exhibited activity against *P. aeruginosa* and *A. niger*. Conversion of C=O group in **1a** to a chlorine atom in **11a** resulted in inhibition of all the tested organisms.

Pharmacological activity

Antitumor activity using the in vitro Ehrlich ascites assay. Cancer still continues to be a major health problem worldwide. The development of new anti-cancer therapeutic agents is one of the fundamental goals in medicinal chemistry. Compound **4d** proved to have the highest cytotoxic activity, 100 % mortality with 5-fluorouracil as a standard, followed by **4b**, **11b**, **1b** and **6**, having mortalities of 97.5, 93.5, 91 and 84.1 %, respectively, at 100 µg mL⁻¹. Compounds **1e**, **1a** and **11a** exhibited medium activity, while compounds **17a**, **1f**, **10** and **2b** showed low activity. The variations of inhibition of the Ehrlich antitumor activity with concentration of the test compounds are listed in Table II.

Antioxidant activity using 2,2'-azinobis(3-ethylbenzothiazoline-6-sulfonic acid) (ABTS) inhibition. Twelve compounds were tested for antioxidant activity as reflected in their ability to inhibit oxidation in rat brain and kidney homogenates, Table II. Compounds **4d**, **11b**, **6**, **4b** and **1b** showed a similar antioxidant



activity to ascorbic acid, used as standard. Compounds **1e**, **1a**, **10** and **11a** exhibited moderate antioxidant activity, while **1f**, **17a** and **2b** showed lower activity.

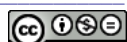
TABLE II. Antitumor (dead, %) and antioxidant activities (ABTS method) for some of the products

| Compound | Antitumor activity <i>c / μ mL⁻¹</i> | | | Antioxidant activity | | Bleomycin dependent-DNA damage |
|----------------------------|----------------------------------------------------|------|------|----------------------|---------------|--------------------------------|
| | 100 | 50 | 25 | Absorbance | Inhibition, % | |
| 1a | 68.9 | 37 | 20 | 0.213 | 59.4 | 0.118 |
| 1b | 91 | 43 | 18 | 0.038 | 89.1 | 0.079 |
| 1e | 79.8 | 38.6 | 21.1 | 0.201 | 61.7 | 0.124 |
| 1f | 45.7 | 28.6 | 14 | 0.447 | 14.8 | 0.140 |
| 2b | 33.1 | 28.6 | 14 | 0.485 | 7.6 | 0.173 |
| 4b | 97.5 | 63 | 36.7 | 0.056 | 89.3 | 0.090 |
| 4d | 100 | 100 | 98.2 | 0.033 | 93.7 | 0.086 |
| 6 | 84.1 | 11.4 | 25.6 | 0.049 | 91.4 | 0.089 |
| 10 | 36.8 | 19.1 | 11.6 | 0.22 | 56.4 | 0.129 |
| 11a | 56 | 30 | 17.2 | 0.300 | 42.8 | 0.138 |
| 11b | 93.5 | 48 | 21.4 | 0.045 | 92.8 | 0.084 |
| 17a | 48.2 | 27.3 | 13.8 | 0.453 | 13.7 | 0.159 |
| St ^a | 98 | 62.7 | 37 | — | — | — |
| ABTS | — | — | — | 0.525 | — | — |
| Ascorbic acid ^b | — | — | — | 0.029 | 94.5 | 0.093 |

^a5-Flourouracil was used as standard for the antitumor activity; ^bstandard for the antioxidant activity

Bleomycin-dependent DNA damage. The bleomycins are a family of glycopeptide antibiotics³⁸ that are routinely used as antitumor agents. The bleomycin assay has been adopted for assessing the pro-oxidant activity of food antioxidants. The antitumor antibiotic bleomycin binds iron ions and DNA. If the samples to be tested are able to reduce bleomycin-Fe³⁺ to bleomycin-Fe²⁺, DNA degradation in the system will be stimulated, resulting in a positive test for pro-oxidant activity. DNA degradation is accompanied by the formation of a product similar to malondialdehyde. L-ascorbic acid was used as the reducing agent to reduce Fe³⁺ to Fe²⁺. Twelve compounds were selected for bleomycin-dependent DNA-damage testing (Table II).

Results in Table II showed that compounds **1b**, **4d**, **4b**, **6** and **11b** have the ability to protect DNA from the damage induced by bleomycin. On the other hand, the rest of the compounds exhibited weak activities. By comparing the obtained results of the investigated compounds to their structures the following structure-activity relationships were postulated; *i*) compounds **1b**, **4b**, **4d**, **6** and **11b** were more potent than ascorbic acid, which may be attributed to the presence of the thioxopyrimidine moiety in **1b**, **4b**, **4d**, and **11b**, and the thioxo triazolo moiety in **6**; *ii*) compounds **4b** and **11b** were less potent than **1b**, which may be due to the replacement of the C=O and C≡N moieties into ethyl aminofuran-



carboxylate in compound **4b** and C=O into chlorine atom in compound **11b**; *iii)* compound **6** was more potent than compound **1a**, which may be attributable to the presence of the thioxotriazolo moiety.

EXPERIMENTAL

Chemistry

Chemicals were obtained from Alfa Aesar and used as provided. Melting points were measured on a Gallenkamp or a Griffin melting point apparatus. The infrared absorption spectra were measured on a Pye Unicam SP 2000 infrared spectrophotometer using the KBr wafer technique. The EI-MS spectra were determined using an AE1 MS 902 mass spectrometer. The ¹H-NMR and ¹³C-NMR spectra were recorded on a Bruker AC-300 instrument at 300 and 75 MHz, respectively, using DMSO-*d*₆ as the solvent. Chemical shifts are expressed as δ / ppm and TMS was used as an internal standard. All the spectral measurements were performed at the Micro analytical Center of Cairo University, Egypt, the Micro analytical Center of Ain Shams University or the Main Defense Chemical Laboratory. Elemental analysis were realized at the Faculty of Science, Ain Shams University, using a Perkin–Elmer 2400 C, H and N elemental analyzer and satisfactory analytical data (±0.3 %) were obtained for all compounds. The antimicrobial activities were determined at Al-Azhar University, Faculty of Science, Fermentation Biotechnology and Applied Microbiology (Ferm-BAM) Center, Egypt. The pharmacological activities were performed at the Pharmacology Department, Faculty of Pharmacy, Mansoura University, Egypt. The completion of chemical reactions was monitored by TLC. Compounds **1a–f** were prepared according to the literature.²⁶

The physical, analytic and spectral data for the prepared compounds are given in Supplementary Material to this paper.

*Synthesis of 6-(1,3-benzodioxol-5-yl)-4-oxo-2-thioxo-1,2,3,4-tetrahydropyrimidine-5-carboxylic acid (**1g**).* A mixture of **1a** (2.73 g, 10.0 mmol) and sulfuric acid (15 mL, 70 %) was heated under reflux for 3 h. The reaction mixture was left to cool and then poured onto cold water. The obtained solid was filtered off, dried and recrystallized from benzene. Pale brown crystals, Yield: 53 %

*Synthesis of 4-(1,3-benzodioxol-5-yl)-2-hydrazino-6-oxo-1,6-dihydropyrimidine-5-carbonitrile (**1h**).* To a solution of **1a** or **1c** (0.01 mol) in *n*-butanol (40 mL), hydrazine hydrate (0.75 mL, 0.015 mol, 98 %) was added and the reaction mixture was heated under reflux for 6 h. The solvent was evaporated and the obtained solid was collected by filtration, washed with water, dried and then recrystallized from methanol. Brown crystals, yield: 65 % from **1a** and 72 % from **1c**.

*General procedure for the synthesis of (dihydropyrimidin-2-ylthio)acetates **2a** and **b**.* A mixture of **1a** or **1b** (0.01 mol), ethyl chloroacetate (1.3 mL, 0.012 mol) and anhydrous K₂CO₃ (5.0 g, 40 mmol) in dry acetone (60 mL) was refluxed for 18 h and then filtered while hot, concentrated to half its volume and poured onto cold water. The obtained solid was filtered off, dried and recrystallized from a suitable solvent to afford **2a** and **2b**, respectively. **2a:** brown crystals (acetic acid), yield: 71 %, and **2b:** orange crystals (toluene/few drops of light petroleum 60–80 °C), yield: 72 %.

*General procedure for the synthesis of (dihydropyrimidin-4-yloxy)acetates **3a–d**.* A mixture of **1a**, **1b**, **1e** or **1f** (0.01 mol) and ethyl chloroacetate (1.3 mL, 0.012 mol) in sodium ethoxide solution (0.46 g of Na in 20 mL of absolute ethanol) was heated under reflux for 2 h.

Most of the solvent was evaporated and then the remaining acidified with cold diluted HCl (20 mL, 2 M). The oily residue obtained was extracted with ethyl acetate (3×50 mL) and dried over anhydrous MgSO₄. The solid obtained after evaporation of the solvent was filtered off, dried and recrystallized from a suitable solvent to give **3a–d**. **3a**: brown crystals (acetic acid), yield: 57 %; **3b**: orange crystals (toluene/light petroleum, 60–80 °C, 1:1 V/V), yield: 61 %; **3c**: yellow crystals (acetic acid), yield: 70 %; **3d**: pale brown crystals (acetic acid), yield: 64 %.

*General procedure for the synthesis of furo[2,3-d]pyrimidine-6-carboxylates **4a–d**.* A mixture of **1a**, **1b**, **1e** or **1f** (0.01 mol) and ethyl chloroacetate (1.30 mL, 0.012 mol, 99 %) in sodium ethoxide solution (0.92 g of Na in 40 mL of absolute ethanol) was fused at 170–180 °C for 3 h. The reaction mixture was left to cool, poured onto ice water and acidified with HCl (15 mL, 2 M). The product was extracted with ethyl acetate (3×40 mL), dried over anhydrous MgSO₄ and most of the solvent was evaporated. The obtained solid was filtered off, dried and recrystallized from an appropriate solvent to give **4a–d**. **4a**: brown crystals (methanol), yield: 63 %; **4b**: brown crystals (ethanol), yield 61 %; **4c**: brown crystals (ethanol), yield 66 %; **4d**: brown crystals (toluene), yield 55 %.

*Synthesis of authentic samples of **4a** and **c**.* A mixture of **3a** or **3c** (0.01 mol) and sodium ethoxide (0.46 g of Na metal in 20 mL of absolute ethanol) was heated at 170–180 °C for 1 h. The reaction mixture was left to cool, poured onto ice water and then acidified with HCl (15 mL, 2 M). The solid obtained was filtered off, dried and recrystallized from a proper solvent to yield **4a** or **4c**.

*Synthesis of 5-(1,3-benzodioxol-5-yl)-7-oxo-2-thioxo-1,2,3,7-tetrahydro[1,2,4]triazolo[1,5-a]pyrimidine-6-carbonitrile (**6**).* A mixture of **1a** (2.73 g, 10.0 mmol) and thiourea (0.94 g, 0.012 mol, 97 %) in *n*-butanol (40 mL) was heated under reflux for 4 h. Most of the solvent was evaporated and the obtained solid was filtered off, washed with water, dried and recrystallized from ethanol. Brown crystals, yield: 76 %.

*Synthesis of 3,3'-(4-fluorophenyl)methylenebis[6-(1,3-benzodioxol-5-yl)-4-oxo-2-thioxo-1,2,3,4-tetrahydropyrimidine-5-carbonitrile] (**7**).* A mixture of **1a** (5.46 g, 20.0 mmol) and 4-fluorobenzaldehyde (1.27 g, 10.0 mol) in acetic anhydride (15 mL) in the presence of a catalytic amount of anhydrous K₂CO₃ was heated at 70–80 °C for 3.5 h. The solid obtained after cooling was filtered off, dried and then recrystallized from ethanol. White crystals, yield: 73 %.

*Synthesis of 3,3'-(3,6-dioxocyclohexa-1,4-diene-1,4-diyl)bis[6-(1,3-benzodioxol-5-yl)-4-oxo-2-thioxo-1,2,3,4-tetrahydropyrimidine-5-carbonitrile] (**9**).* A mixture of **1a** (5.46 g, 0.02 mol) and *p*-benzoquinone (1.30 g, 0.012 mol) in aqueous acetone (80 mL, 50 %) was stirred for 6 h at room temperature. The reaction mixture was kept overnight and then poured onto ice/water. The obtained solid was filtered off, washed with hot water, dried and recrystallized from ethanol/toluene (2:1 by volume). Pale brown crystals, yield: 68 %.

*Synthesis of 5-(1,3-benzodioxol-5-yl)-7-oxo-1,7-dihydrotetrazolo[1,5-a]pyrimidine-6-carbonitrile (**10**).* An aqueous solution of sodium nitrite (1.07 g, 15.0 mol) in water (10 mL) was added to a stirred cold (0 °C) solution of **1h** (2.7 g, 10 mmol) in acetic acid (30 mL). The reaction mixture was stirred at 0 °C for 3 h, poured onto ice/saturated NaHCO₃ (40 mL) and the product was extracted with ethyl acetate (60 mL). The organic layer was dried over anhydrous MgSO₄ and half of the solvent was removed. The obtained solid was filtered off, and recrystallized from dioxane. Brown crystals, yield: 52 %.

*General procedure for the synthesis of dihydropyrimidine-5-carbonitriles **11a–c**.* A mixture of **1a**, **1b** or **1d** (0.01 mol), phosphorus oxychloride (20 mL) and phosphorus pentachloride (1.5 g, 7.0 mmol) was heated on a water bath for 4 h. The reaction mixture was



poured onto cold water. The obtained solid was filtered off, washed several times with light petroleum 60–80 °C, dried and recrystallized from a suitable solvent. **11a**: brown crystals (ethanol), yield: 74 %; **11b**: brown crystals (ethanol), yield: 62 %; **11c**: brown crystals (ethanol), Yield: 64 %.

Synthesis of 7-(1,3-benzodioxol-5-yl)-5-thioxo-5,6-dihydrotetrazolo[1,5-c]pyrimidine-8-carbonitrile (13). To a stirred solution of **11a** (2.9 g, 10 mmol) in DMF (30 mL), sodium azide (0.76 g, 12 mmol) was added in portions and the mixture was stirred at room temperature for 4 h. The mixture was poured onto ice water and the obtained solid was filtered off, dried and then recrystallized from methanol. Yellow crystals, yield: 54 %.

Synthesis of 4-amino-5-(1,3-benzodioxol-5-yl)pyrimido[4,5-d]pyrimidine-2,7(1H,3H)-dithione (15). A mixture of **11a** (2.8 g, 0.010 mol), thiourea (0.69 g, 0.012 mol) and few drops of piperidine in *n*-butanol (40 mL) was heated at 130–140 °C for 4 h. The mixture was left to cool to room temperature and poured onto cold HCl (40 mL, 2 M). The obtained solid was filtered off, washed with water (3×30 mL), dried and recrystallized from *n*-butanol. Yellow crystals, yield: 62 %.

Synthesis of 5-amino-4-aryl-6-phenyl-1,3-dihydro-2H-pyrrolo[2,3-d]pyrimidine-2-thiones 17a and b. A mixture of chloropyrimidine **1a** or **b** (0.01 mol) and benzylamine (1.35 mL, 12.0 mmol) in *n*-butanol (40 mL) was heated under reflux for 4 h. The reaction mixture was concentrated to half its volume and poured onto cold water. The obtained solid was filtered off, dried and recrystallized from the proper solvent. **17a**: brown crystals (DMF), yield: 72 %; **17b**: brown crystals (*n*-butanol), yield: 67 %.

Biological and pharmaceutical activities

Antimicrobial activity. Some of the products were screened for their antimicrobial activity including Gram-positive bacteria (*B. subtilis* and *S. aureus*), Gram-negative bacteria (*E. coli* and *P. aeruginosa*) and antifungal activity (*C. albicans* and *A. niger*).

Agar well diffusion method. The agar well diffusion method³⁹ was used for the determination of the inhibition zone. DMSO was used as the solvent and the blank with appropriate drugs as standards. The results are given in Table I. With a sterile loop, pure colonies of the bacterial cultures were picked up. The colonies were suspended in 5 mL of sterile physiological saline. Using sterile forceps, the wells containing the biomaterial were placed onto the agar surface and gently pressed down to ensure contact. The plates were per-incubated for 1 h in a refrigerator followed by incubation at 37 °C for 24 h.

Cell line and cell culture. Different concentrations of the tested compounds were prepared (ED_{100} , ED_{50} and ED_{25} as µg/ml DMSO). The amount of DMSO was adjusted to give a final concentration of 0.1%. Ascites fluid was obtained from the peritoneal cavity of the donor animal from (National cancer Institute, Cairo, Egypt) contain Ehrlich cell was as aseptically aspirated. The cells were grown partially floating and attach in a suspension culture (RPMI 1660 medium, Sigma Chemical Co. St. Louis, USA), supplemented with 10% fetal bovine serum 9GIBCO, UK). They were maintained at 37 °C in humidified atmosphere with 5% CO₂ for 2 h. The viability in control experiments (DMSO only without drug) exceeded 95% as determined by microscopical examination using a hemocytometer and trypan blue stain (stains only the dead cells).⁴⁰

MTT assay. Briefly, cells were seeded in a 96-well plate at a density of 1×10^4 cells well⁻¹ as previously described.⁴¹⁻⁴³ Drugs at different concentrations were added to each well and cultured for 48 h, followed by incubation with 5 mg L⁻¹ MTT (3-(4,5-dimethylthiazol-2-yl)-2,5-diphenyltetrazolium bromide) for 4 h, after which the supernatant was removed after centrifugation. Finally, 100 µL of DMSO was added and the absorbance, *A*, at a wavelength



of 490 nm was measured by using an Elisa Reader EXL 800. The relative cell proliferation inhibition rate (*IR*) is given by:

$$IR = \left(1 - \frac{A_{490,\text{exp}}}{A_{490,\text{control}}} \right) \times 100$$

where $A_{490,\text{exp}}$ and $A_{490,\text{control}}$ are the absorbances at 490 nm for the experimental and control, respectively.

Cytotoxic activity. Ehrlich cells^{44–46} (Ehrlich ascites carcinoma, EAC) were derived from the ascitic fluid from diseased mouse (purchased from the National Cancer institute, Cairo, Egypt). The cells were grown in suspension culture, partly floating and partly attached, in RPMI 1640 medium, supplemented with 10 % fetal bovine serum. They were maintained at 37 °C in a humidified atmosphere with 5 % CO₂. The viability of the cells used in the control experiments (DMSO only without drug) exceeded 95 %, as determined with trypan blue. The test compounds were prepared initially at a concentration of 1 mg mL⁻¹ DMSO.

Antioxidant activity screening assay (ABTS method). For each of the investigated compounds,^{47,48} 2 mL of ABTS (2,2'-azino-bis(3-ethylbenzothiazoline-6-sulfonic acid)) solution (60 µM) was added to 3 mL MnO₂ suspension (25 mg mL⁻¹), all prepared in 5 mL aqueous phosphate buffer solution (pH 7, 0.1 M). The mixture was shaken, centrifuged, filtered and the absorbance of the resulting green blue solution (ABTS radical solution) at 734 nm was adjusted to *ca.* 0.5. Then, 50 µl of a 2 mM solution of a test compound in spectroscopic grade MeOH/phosphate buffer (1:1) was added. The absorbance was measured and the reduction in the color intensity was expressed as inhibition percentage. L-Ascorbic acid was used as the standard antioxidant (positive control). A blank sample was run without ABTS and using MeOH/phosphate buffer (1:1) instead of a test compound. A negative control was run with ABTS and MeOH/phosphate buffer (1:1) only.

Bleomycin-dependent DNA damage assay. To the reaction mixtures in a final volume of 1.0 mL, the following reagents at the final concentrations were added: DNA (0.5 mg mL⁻¹), bleomycin sulfate (0.05 mg mL⁻¹), FeCl₃ (0.025 mM), magnesium chloride (5 mM), KH₂PO₄–KOH buffer pH 7.0 (30 mM), and ascorbic acid (0.24 mM) or a test fraction diluted with MeOH to give a concentration of 0.1 mg mL⁻¹. The reaction mixtures were incubated in a water bath at 37 °C for 1 h. At the end of the incubation period, 0.1 mL ethylenediaminetetraacetic acid (EDTA) (0.1 M) was added to stop the reaction (the iron–EDTA complex is unreactive in the bleomycin assay).⁴⁹ DNA damage was assessed by adding 1 mL 1 % (w/V) thiobarbituric acid (TBA) and 1 mL of 25 % (V/V) hydrochloric acid followed by heating in a water-bath maintained at 80 °C for 15 min. The chromogen formed was extracted into 1-butanol, and the absorbance was measured at 532 nm.

CONCLUSIONS

The type of the products from reactions of thioxopyrimidin-6(1*H*)-ones with ethyl chloroacetate were found in dependence on the reaction conditions to afford *S*-alkylated or *O*-alkylated or furo[2,3-*d*]pyrimidine products. Reactions of 2-thioxo-4-chloropyrimidine with bi-functional nucleophiles provided a convenient route for the synthesis of the corresponding tetrazolo[1,5-*c*]pyrimidine, pyrimido[4,5-*d*]pyrimidine and pyrrolo[2,3-*d*]pyrimidine. Some of the products exhibited promising antimicrobial, antitumor and antioxidant activities.

SUPPLEMENTARY MATERIAL

The physical, analytic and spectral data for the prepared compounds are available electronically from <http://www.shd.org.rs/JSCS/>, or from the corresponding author on request.

ИЗВОД

СИНТЕЗА РАЗЛИЧИТИХ КОНДЕНЗОВАНИХ ПИРИМИДИНА И ИСПИТИВАЊЕ
ФАРМАКОЛОШКЕ И АНТИМИКРОБНЕ АКТИВНОСТИ

MOUNIR A. SALEM, MAGDA I. MARZOUK и NAGLAA F. MAHMOUD

*Heterocyclic Synthetic Laboratory, Chemistry Department, Faculty of Science,
Ain Shams University Cairo, Egypt*

Синтетисана је група деривата пириимида који садрже кондензоване прстенове, као што су фуро[2,3-*d*]пириимидин, триазоло[1,5-*a*]пириимидин и тетразоло[1,5-*a*]пириимидин, реакцијом тиоксопириимидин-6(1*H*)-она са етил-хлорацетатом, под различитим реакционим условима. Пириимидин-тиони у реакцији са $\text{POCl}_3/\text{PCl}_5$ дају хлор-деривате који реакцијом са натријум-азидом и тиоуреом дају као производе тетразоло[1,5-*c*]пириимидин и пириимидо-пириимидине. Тиоксопириимидин-6(1*H*)-он реагује са бензил-амином и као производ даје пироло[2,3-*d*]пириимидинтионе. Извршена су израчунавања топлота стварања једињења применом Фукуи индекса. Испитана је фармаколошка и антимикробна активност неким од синтетисаних деривата.

(Примљено 28. маја 2013, ревидирано 13. фебруара, прихваћено 4. марта 2014)

REFERENCES

1. T. Eicher, S. Hauptmann, *The Chemistry of Heterocycles*, Wiley–VCH, Weinheim, 2003, p. 572
2. C. G. Hartung, A. C. Backes, B. Felber, A. Missio, A. Philipp, *Tetrahedron* **62** (2006) 10055
3. C. J. Shishoo, V. S. Shirasath, I. S. Rathod, V. D. Yande, *Eur. J. Med. Chem.* **35** (2000) 351
4. R. V. Chambhare, B. G. Khadse, A. S. Bobde, R. H. Bahekar, *Eur. J. Med. Chem.* **38** (2003) 89
5. S. F. Wnuk, E. Lewandowska, D. R. Companioni, P. I. Garcia Jr., J. A. Secrist, III, *Org. Biomol. Chem.* **2** (2004) 120
6. M. Cushman, T. Sambaiah, G. Jin, B. Illarionov, M. Fischer, A. Bacher, *J. Org. Chem.* **69** (2004) 601
7. S. M. Sondhi, M. Johar, S. Rajvamki, S. G. Dastidar, R. Shukla, R. Raghbir, J. W. Lown, *Aust. J. Chem.* **54** (2001) 69
8. J. L. Bernier, J. P. Henichart, V. Warin, F. Baert, *J. Pharm. Sci.* **69** (1980) 1343
9. K. Senga, T. Novinson, H. R. Wilson, R.K. Robins, *J. Med. Chem.* **24** (1981) 610
10. S. S. Pharmaceutical Co. Ltd. *Jpn. Kokai Tokkyo Koho* JP 5,962,595, 1984 [*Chem. Abstr.* **1984**, 101, 72754]
11. L. D. S. Yadav, D. R. Pal, *Indian J. Chem., B* **36** (1997) 1034
12. K. J. Pees, G. Albert, *US Patent* 5,593,996, 1997 [*Chem. Abstr.* **1984**, 101, 72754]
13. W. Pfrengle, A. Franz, *Jpn Kokai Tokyo Koho* JP 1999, 1,135,581 [*Chem. Abstr.* **1997**, 126, 171605]
14. M. S. A. El-Gaby, S. G. Abdel-Hamide, M. M. Ghorab, S. M. El-Sayed, *Acta Pharm.* **49** (1999) 149



15. E. G. E. De Vries, J. A. Gietema, P. Workman, J. E. Scott, A. Crawshaw, H. J. Dobbs, I. Dennis, N. H. Mulder, D. T. H. Sleijfer, P. H. Willense, *Br. J. Cancer* **68** (1993) 641
16. M. N. Nasr, M. M. Gineinah, *Arch. Pharm.* **335** (2002) 289
17. O. Alam, S. Khan, N. Siddiqui, W. Ahsan, S. Verma, S. Gilani *Eur. J. Med. Chem.* **45** (2010) 5113
18. J. Gupta, P. Shama, R. Dudhe, A. Chaudhary, A. Singh, P. Verma, S. Mondal, R. Yadav, S. Kashyap, *Med. Chem. Res.* **21** (2012) 1625
19. N. A. Hassan, *Molecules* **5** (2000) 826
20. P. A. S. Smith, R. O. Kan, *J. Org. Chem.* **29** (1964) 2261
21. S. Vega, J. Alonso, A. Diaz, F. Junquera, *J. Heterocycl. Chem.* **27** (1990) 269
22. A. N. Srivastava, N. P. Singh, C. K. Shriwastaw, *J. Serb. Chem. Soc.* **78** (2013) 1
23. L. F. Kuypers, D. P. Baccanari, M. L. Jones, R. N. Hunter, R. L. Tansik, S. S. Joyner, C. M. Boytos, S. K. Rudolph, V. Knick, R. H. Wilson, J. M. Caddell, H. S. Friedman, J. C. W. Comley, J. N. Stables, *J. Med. Chem.* **39** (1996) 892
24. A. Hunger, K. Hoffman, *Helv. Chem. Acta* **40** (1957) 1319
25. LuB. Belousov, V. P. Komarova, O. V. Efremenkova, *Antibiot. Khimioter.* **43** (1998) 19
26. M. A. I. Salem, H. M. F. Madkour, M. I. Marzouk, M. E. Azab, N. F. H. Mahmoud, *Phosphorus Sulfur Silicon Relat. Elem.* **183** (2008) 2596
27. E. Masumoto, H. Maruoka, F. Okabe, S. Nishida, Y. Yoshimura, T. Fujioka, K. Yamagata, *J. Heterocycl. Chem.* **48** (2011) 96
28. H. M. F. Madkour, M. A. I. Salem, M. I. Marzouk, M. E. Azab, N. F. H. Mahmoud, *Am.-Eurasian J. Sci. Res.* **2** (2007) 161
29. M. A. Hassan, M. M. Mohamed, S. A. Shiba, M. K. Abou El-Regal, A. Kahlil, *Phosphorus Sulfur Silicon Relat. Elem.* **178** (2003) 2497
30. M. S. Amine, S. A. Nassar, M. A. El-Hashash, S. E. Essawy, A. A. Hashish, *Indian J. Chem., B* **35** (1996) 388
31. E. Kh. Ahmed, M. A. Ameen, *Chin. Chem. Lett.* **21** (2010) 669
32. R. K. Bansal, in *Heterocyclic Chemistry*, 4th ed., New Age International Pub., New Delhi, 2008, p. 514
33. R. Gašparová, K. Kotlebová, M. Lácová, *Nova Biotechnologica* **9** (2009) 349
34. S. Zhang, Z. Huang, L. An, X. Bu, L. Ma, Y. Li, A. Chan, L. Gu, *Org. Lett.* **6** (2004) 4853
35. A. H. Naser, *Molecules* **5** (2000) 826
36. U. S. Pathak, N. V. Gandhi, S. Singh, R. P. Warde, K. S. Jain, *Indian J. Chem., B* **31** (1992) 223
37. V. J. Ram, D. A. Vanden, A. J. Vlietinck, *J. Heterocycl. Chem.* **21** (1984) 1307
38. J. Gutteridge, D. Rowley, B. Halliwell, *Biochem. J.* **199** (1981) 263
39. National Committee for Clinical Laboratory Standards, *Methods for dilution antimicrobial susceptibility tests for bacteria that grow aerobically*, Approved Standards M7-A4 and M2-A6, Clinical and Laboratory Standards Institute, Wayne, PA, 1997
40. Lonza Group, http://bio.lonza.com/uploads/tx_mwaxmarketingmaterial/Lonza_Bench-Guides_Protocol_for_Performing_a_Trypan_Blue_Viability_Test_Technical_Reference_Guide.pdf (accessed Sep, 2014)
41. H. J. Mauceri, N. N Hanna, M. A. Beckett, D. H. Gorski, M. J. Staba, K. A. Stellato, K. Bigelow, R. Heimann, S. Gately, M. Dhanabal, G. A. Soff, V. P. Sukhatme, D. W. Kufe, R. R. Weichselbaum, *Nature* **394** (1998) 287
42. T. Mosmann, *J. Immunol. Methods* **65** (1983) 55
43. F. Denizot, R. Lang, *J. Immunol. Methods* **22** (1986) 271



44. K. Karrer, J. R. Rubini, *Pharmacology* **13** (1965) 124
45. A. A. Fadda, F. A. Badria, K. M. El-Attar, *Med. Chem. Res.* **19** (2010) 413
46. A. El-Shafei, A. A. Fadda, A. M. Khalil, T. A. E. Ameen, F. A. Badria, *Bioorg. Med. Chem.* **17** (2009) 5096
47. E. A. Lissi, B. Modak, R. Torres, J. Escobar, A. Urzua, *Free Radical Res.* **30** (1999) 471
48. A. B. A. El-Gazar, A. M. S. Youssef, M. M. Youssef, A. A. Abu-Hashem, F. A. Badria, *Eur. J. Med. Chem.* **44** (2009) 609
49. R. Aeschbach, J. L. liger, B. C. Scott, A. Murcia, J. Butler, B. Halliwell, O. I. Aruoma, *Food Chem. Toxicol.* **32** (1994) 31.





SUPPLEMENTARY MATERIAL TO
Synthesis of various fused pyrimidine rings and their pharmacological and antimicrobial evaluation

MOUNIR A. SALEM*, MAGDA I. MARZOUK and NAGLAA F. MAHMOUD

Heterocyclic Synthetic Laboratory, Chemistry Department, Faculty of Science, Ain Shams University Cairo, Egypt

J. Serb. Chem. Soc. 79 (9) (2014) 1059–1073

SOME PHYSICAL, ANALYTIC AND SPECTRAL DATA FOR THE PREPARED COMPOUNDS

6-(1,3-Benzodioxol-5-yl)-4-oxo-2-thioxo-1,2,3,4-tetrahydropyrimidine-5-carboxylic acid (1g**)**. Yield: 53 %; Pale brown crystals; m.p.: 223 °C; Anal. Calcd. for C₁₂H₈N₂O₅S: C, 49.31; H, 2.76; N, 9.58; S, 10.97 %. Found: C, 49.15; H, 2.70, N, 9.72; S, 10.98 %; IR (KBr, cm⁻¹): 3416 (–OH), 3280/2978 (–NH), 1718 (–C=O acid), 1657 (–C=O amide), 1635 (–C=N), 1595 (C=C– aromatic ring), 1195/2587 (C=S/SH); ¹H-NMR (300 MHz, DMSO-d₆, δ / ppm): 6.09 (2H, s, OCH₂O), 6.94–7.34 (3H, m, aromatic), 11.2 (1H, s, OH, D₂O exchangeable), 12.2, 12.8 (2H, s, 2 NH, D₂O exchangeable); ¹³C-NMR (75 MHz, DMSO-d₆, δ / ppm): 171.3 (C₂), 162.8 (C₄), 98.5 (C₅), 168.9 (C₆), 165.2 (COOH), 101.4 (O–CH₂–O), 130.1 (Ar-C), 117.7 (Ar-C), 111.7 (Ar-C), 147.4 (Ar-C), 149.1 (Ar-C), 110.3 (Ar-C); MS (m/z, (relative abundance, %)): 292 (M⁺, 13), 248, 128, 122, 98, 84, 78, 72, 60 (BP, 100).

4-(1,3-Benzodioxol-5-yl)-2-hydrazino-6-oxo-1,6-dihydropyrimidine-5-carbonitrile (1h**)**. Yield: 65 % from **1a**, and 72 % from **1c**; Brown crystals; m.p.: 240 °C; Anal. Calcd. for C₁₂H₉N₅O₃: C, 53.14; H, 3.34; N, 25.82 %. Found: C, 53.45; H, 3.27; N, 25.76 %; IR (KBr, cm⁻¹): 3584, 3435, 3327 (–NH, –NH₂), 2213 (–C≡N), 1686 (–C=O), 1634 (–C=N), 1594 (C=C– aromatic ring); ¹H-NMR (300 MHz, DMSO-d₆, δ / ppm): 6.19 (2H, s, OCH₂O), 7.82–7.16 (3H, m, aromatic), 8.43 (2H, s, 2 NH, D₂O exchangeable), 13.18 (2H, s, NH₂, D₂O exchangeable); MS (m/z, (relative abundance, %)): 273 ([M + 2]⁺, 37), 271 (M⁺, 44), 257 (BP, 100), 256, 241, 215, 214, 186, 148, 121, 118, 93, 76, 64, 63.

Ethyl 2-{{[4-(1,3-benzodioxol-5-yl)-5-cyano-6-oxo-1,6-dihydropyrimidin-2-yl]thio}acetate (2a**)**. Yield: 71 %; Brown crystals; m.p.: 221 °C; Anal. Calcd. for C₁₆H₁₃N₃O₅S: C, 53.48; H, 3.65; N, 11.69; S, 8.92 %. Found: C, 53.65; H, 3.77;

*Corresponding author. E-mail: salemmai1947@yahoo.com

N, 11.84; S, 9.02 %. IR (KBr, cm^{-1}): 3453 ($-\text{NH}$), 2795 ($-\text{CH}_2\text{--S}$), 2215 ($-\text{C}\equiv\text{N}$), 1737 ($-\text{C}=\text{O}$ ester), 1658 ($-\text{C}=\text{O}$ amide), 1632 ($-\text{C}=\text{N}$), 1610 ($\text{C}=\text{C}$ -aromatic ring); $^1\text{H-NMR}$ (300 MHz, DMSO- d_6 , δ / ppm): 1.26 (3H, *t*, J = 7.0 Hz, CH_3), 4.10 (2H, *q*, J = 7.0 Hz, CH_2), 4.13 (2H, *s*, CH_2S), 6.17 (2H, *s*, OCH_2O), 7.81–7.12 (3H, *m*, aromatic), 10.92 (1H, *s*, NH, D_2O exchangeable); $^{13}\text{C-NMR}$ (75 MHz, DMSO- d_6 , δ / ppm): 159.98 (C_2), 170.19 (C_4), 101.19 (C_5), 166.42 (C_6), 112.81 (CN), 49.69 (SCH_2), 168.34 (OCO), 61.09 (OCH_2), 13.93 (CH_3), 102.12 (OCH_2O), 147.34 (2 Ar-C), 111.81 (2 Ar-C), 121.73 (Ar-C), 124.44 (Ar-C); MS (*m/z*, (relative abundance, %)): 359 (M^+ , 6.13), 273, 229, 178 (BP, 100), 122, 83.

Ethyl 2-{{[5-cyano-4-(3,4-dimethoxyphenyl)-6-oxo-1,6-dihdropyrimidin-2-yl]thio}acetate (2b)}. Yield: 72 %; m.p.: 178 °C; orange crystals; Anal. Calcd. for $\text{C}_{17}\text{H}_{17}\text{N}_3\text{O}_5\text{S}$: C, 54.39; H, 4.56; N, 11.19; S, 8.54 %. Found: C, 54.46; H, 4.49; N, 11.12; S, 8.62 %. IR (KBr, cm^{-1}): 3446 ($-\text{NH}$), 2835 ($-\text{CH}_2\text{--S}$), 2218 ($-\text{C}\equiv\text{N}$), 1746 ($-\text{C}=\text{O}$ ester), 1648 ($-\text{C}=\text{O}$ amide), 1630 ($-\text{C}=\text{N}$), 1610 ($\text{C}=\text{C}$ -aromatic ring); $^1\text{H-NMR}$ (300 MHz, DMSO- d_6 , δ / ppm): 1.32 (3H, *t*, J = 7.0 Hz, CH_3), 3.85, 3.88 (6H, 2 *s*, 2 OCH_3), 4.08 (2H, *s*, SCH_2), 4.46 (2H, *q*, J = 7.0 Hz, CH_2), 7.76–7.12 (3H, *m*, aromatic), 12.35 (1H, *s*, NH, D_2O exchangeable); MS (*m/z*, (relative abundance, %)): 375 (M^+ , 46.7), 330, 194 (BP, 100), 151 (60.0).

Ethyl 2-{{[6-(1,3-benzodioxol-5-yl)-5-cyano-2-thioxo-1,2-dihdropyrimidin-4-yl]oxy}acetate (3a)}. Yield: 57 %; m.p.: 220 °C, brown crystals; Anal. Calcd. for $\text{C}_{16}\text{H}_{13}\text{N}_3\text{O}_5\text{S}$: C, 53.48; H, 3.65; N, 11.69; S, 8.92 %. Found: C, 53.29; H, 3.48; N, 11.82; S, 9.05 %. IR (KBr, cm^{-1}): 3335/2985 ($-\text{NH}$), 2810 ($\text{O--CH}_2\text{C=O}$), 2216 ($-\text{C}\equiv\text{N}$), 1728 ($-\text{C}=\text{O}$ ester), 1635 ($-\text{C}=\text{N}$), 1608 ($\text{C}=\text{C}$ -aromatic ring), 1168/2592 ($-\text{C=S/SH}$); $^1\text{H-NMR}$ (300 MHz, DMSO- d_6 , δ / ppm): 1.25 (3H, *t*, J = 7.0 Hz, CH_3), 4.13 (2H, *s*, OCH_2CO), 4.00 (2H, *q*, J = 7.0 Hz, CH_2), 6.17 (2H, *s*, OCH_2O), 7.82–7.31 (3H, *m*, aromatic), 11.17 (1H, *s*, NH, D_2O exchangeable); MS (*m/z*, (relative abundance, %)): 359 (M^+ , 15), 334, 314, 287, 273, 115 (BP, 100), 109, 93, 77.

Ethyl 2-{{[5-cyano-6-(3,4-dimethoxyphenyl)-2-thioxo-1,2-dihdropyrimidin-4-yl]oxy}acetate (3b)}. Yield: 61 %; m.p.: 178 °C; orange crystals; Anal. Calcd. for $\text{C}_{17}\text{H}_{17}\text{N}_3\text{O}_5\text{S}$: C, 54.39; H, 4.56; N, 11.19; S, 8.63 %. Found: C 54.46, H 4.48, N 11.39, S 8.74 %. IR (KBr, cm^{-1}): 3345/2955 ($-\text{NH}$), 2208 ($-\text{C}\equiv\text{N}$), 1732 ($-\text{C}=\text{O}$ ester), 1628 ($-\text{C}=\text{N}$), 1598 ($\text{C}=\text{C}$ -aromatic ring), 1210/2594 ($-\text{C=S/-SH}$); $^1\text{H-NMR}$ (300 MHz, DMSO- d_6 , δ / ppm): 1.37 (3H, *t*, J = 7.0 Hz, CH_3), 3.87, 3.83 (6H, 2 *s*, 2 OCH_3), 4.08 (2H, *s*, OCH_2), 4.43 (2H, *q*, J = 7.0 Hz, CH_2), 7.76–7.15 (3H, *m*, aromatic), 11.36 (1H, *s*, NH, D_2O exchangeable); MS (*m/z*, (relative abundance, %)): 375 (M^+ , 47), 330, 323, 230, 195, 194 (BP, 100), 77, 76, 69, 64, 63, 62, 53, 50.

Ethyl 2-{{[5-acetyl-6-(3,4-dimethoxyphenyl)-2-thioxo-1,2-dihdropyrimidin-4-yl]oxy}acetate (3c)}. Yield: 70 %; m.p.: 280 °C dec.; yellow crystals; Anal.



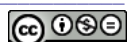
Calcd. for $C_{18}H_{20}N_2O_6S$: C, 55.09; H, 5.14; N, 7.14; S, 8.17 %. Found: C, 55.24; H 5.10; N, 7.20; S, 8.22 %; IR (KBr, cm^{-1}): 3115/3023/2934 ($-\text{NH}$), 2685 ($-\text{CH}_2\text{CO}$), 2218 ($-\text{C}\equiv\text{N}$), 1750 ($-\text{C}=\text{O}$ ester), 1678 ($-\text{C}=\text{O}$ acetyl), 1639 ($-\text{C}=\text{N}$), 1605 ($-\text{C}=\text{C}$ aromatic ring), 1280/2610 ($-\text{C}=\text{S}/\text{SH}$); $^1\text{H-NMR}$ (300 MHz, DMSO- d_6 , δ / ppm): 1.32 (3H, *t*, $J = 7.0$ Hz, CH_3), 2.06 (3H, *s*, COCH_3), 3.75, 3.82 (6H, 2 *s*, 2 OCH_3), 4.22 (2H, *q*, $J = 7.0$ Hz, CH_2), 5.02 (2H, *s*, OCH_2), 6.68–7.38 (3H, *m*, aromatic), 11.72 (1H, *s*, NH, D_2O exchangeable); MS (*m/z*, (relative abundance, %)): 392 (M^+ , 10), 360, 328, 209, 207 (BP, 100), 177, 97, 95, 90, 77, 63, 56, 55, 50.

Ethyl 6-(3,4-dimethoxyphenyl)-4-(2-ethoxy-2-oxoethoxy)-2-thioxo-1,2-dihydropyrimidine-5-carboxylate (3d). Yield: 64 %; m.p.: > 300 °C; pale brown crystals; Anal. Calcd. for $C_{19}H_{22}N_2O_7S$: C, 54.02; H, 5.25; N, 6.63; S, 7.59 %. Found: C, 53.94; H, 5.30; N, 6.56; S, 7.70 %; IR (KBr, cm^{-1}): 3119/3023 ($-\text{NH}$), 2682 ($-\text{CH}_2\text{CO}$), 2216 ($-\text{C}\equiv\text{N}$), 1732 ($-\text{C}=\text{O}$ ester), 1714 ($-\text{C}=\text{O}$ ester), 1640 ($-\text{C}=\text{N}$), 1597 ($\text{C}=\text{C}$ aromatic ring), 1265/2595 ($-\text{C}=\text{S}/\text{SH}$); $^1\text{H-NMR}$ (300 MHz, DMSO- d_6 , δ / ppm): 1.31 (6H, 2 *t*, $J = 7.0$ Hz, 2 CH_3), 3.85 (6H, *s*, 2 OCH_3), 4.28, 4.45 (4H, 2 *q*, $J = 7.0$ Hz, 2 CH_2), 5.12 (2H, *s*, OCH_2), 6.56–7.44 (3H, *m*, aromatic), 11.89 (1H, *s*, NH, D_2O exchangeable); MS (*m/z*, (relative abundance, %)): 422 (M^+ , 24), 377, 348, 142 (BP, 100), 141, 128, 126, 51.

Ethyl 5-amino-4-(1,3-benzodioxol-5-yl)-2-thioxo-1,2-dihydrofuro[2,3-d]pyrimidine-6-carboxylate (4a). Yield: 63 %; m.p.: 192 °C dec. brown crystals; Anal. Calcd. for $C_{16}H_{13}N_3O_5S$: C, 53.48; H, 3.65; N, 11.69; S, 8.92 %. Found: C, 54.16; H, 3.48; N, 11.74; S, 8.73 %; IR (KBr, cm^{-1}): 3382 /3194 /2910 ($-\text{NH}_2/-\text{NH}$), 1744 ($-\text{C}=\text{O}$ ester), 1635 ($-\text{C}=\text{N}$ stretching), 1612 ($\text{C}=\text{C}$ aromatic ring), 1208/2592 ($-\text{C}=\text{S}/\text{SH}$); $^1\text{H-NMR}$ (300 MHz, DMSO- d_6 , δ / ppm): 1.37 (3H, *t*, $J = 7.0$ Hz, CH_3), 4.54 (2H, *q*, $J = 7.0$ Hz, CH_2), 6.18 (2H, *s*, OCH_2O), 7.76–7.15 (3H, *m*, aromatic), 10.85 (1H, *s*, NH₂, D_2O exchangeable), 13.17 (2H, *s*, $\text{NHC}=\text{S}$, D_2O exchangeable); MS (*m/z*, (relative abundance, %)): 359 (M^+ , 44), 314, 313, 286, 285 (BP, 100), 271, 216, 148, 51.

Ethyl 5-amino-4-(3,4-dimethoxyphenyl)-2-thioxo-1,2-dihydrofuro[2,3-d]pyrimidine-6-carboxylate (4b). Yield: 61 %; mp > 300 °C; brown crystals; Anal. Calcd. for $C_{17}H_{17}N_3O_5S$: C, 54.39; H, 4.56; N, 11.19; S, 8.54 %. Found: C, 54.32; H, 3.68; N, 11.14; S, 8.65 %; IR (KBr, cm^{-1}): 3372/3185/2928 ($-\text{NH}_2/-\text{NH}$), 1738 ($-\text{C}=\text{O}$ ester), 1640 ($-\text{C}=\text{N}$), 1608 ($\text{C}=\text{C}$ aromatic ring), 1185/2584 ($-\text{C}=\text{S}/\text{SH}$); $^1\text{H-NMR}$ (300 MHz, DMSO- d_6 , δ / ppm): 1.35 (3H, *t*, $J = 7.0$ Hz, CH_3), 3.85 (6H, *s*, 2 OCH_3), 4.46 (2H, *q*, $J = 7.0$ Hz, CH_2), 7.16–7.45 (3H, *m*, aromatic), 10.48 (1H, *s*, NH₂, D_2O exchangeable), 13.37 (2H, *s*, $\text{NHC}=\text{S}$, D_2O exchangeable); MS (*m/z*, (relative abundance, %)): 376 ([$\text{M}-1$]⁺, 8.2), 274, 149 (BP, 100), 148, 104, 60.

Ethyl 4-(3,4-dimethoxyphenyl)-5-methyl-2-thioxo-1,2-dihydrofuro[2,3-d]pyrimidine-6-carboxylate (4c). Yield: 66 %; m.p.: 262 °C dec. brown crystals; Anal.



Calcd. for C₁₈H₁₈N₂O₅S: C, 57.74; H, 4.85; N, 7.48; S, 8.56 %. Found: C, 57.62; H, 3.68; N, 7.60; S, 8.65 %; IR (KBr, cm⁻¹): 3185/3094 (-NH), 1716 (-C=O ester), 1650 (-C=N), 1598 (C=C- aromatic ring), 1205/2678 (-C=S/SH); ¹H-NMR (300 MHz, DMSO-*d*₆, δ / ppm): 1.92 (3H, *t*, *J* = 7.0 Hz, CH₃), 2.58 (3H, *s*, CH₃), 3.38 (6H, *s*, 2 OCH₃), 4.39 (2H, *q*, *J* = 7.0 Hz, CH₂), 6.58–7.36 (3H, *m*, aromatic), 10.81 (1H, *s*, NH, D₂O exchangeable); MS (*m/z*, (relative abundance, %)): 374 (M⁺, 9), 342, 149 (BP, 100), 94, 68, 66, 65, 55, 51, 50.

Ethyl 4-(3,4-dimethoxyphenyl)-5-oxo-2-thioxo-1,2,5,6-tetrahydrofuro[2,3-d]pyrimidine-6-carboxylate (4d). Yield: 55 %; m.p.: 190 °C; brown crystals; Anal. Calcd. for C₁₇H₁₆N₂O₆S: C, 54.25; H, 4.29; N, 7.44; S, 8.52 %. Found: C, 54.58; H, 4.33; N, 7.62; S, 8.48 %; IR (KBr, cm⁻¹): 3235 (-NH), 1723 (-C=O ester), 1646 (-C=O), 1606 (C=C- aromatic ring), 1215/2595 (-C=S/SH); ¹H-NMR (300 MHz, DMSO-*d*₆, δ / ppm): 1.26 (3H, *t*, *J* = 7.0 Hz, CH₂CH₃), 3.65, 3.72 (6H, 2 *s*, 2 OCH₃), 4.30 (2H, *q*, *J* = 7.0 Hz, CH₂), 5.31 (1H, *s*, CHCO₂), 6.78–7.44 (3H, *m*, aromatic), 10.87 (1H, *s*, NH, D₂O exchangeable); MS (*m/z*, (relative abundance, %)): 376 (M⁺, 18), 323, 319, 190, 184, 178, 150, 149 (BP, 100), 122, 75, 65, 50.

5-(1,3-Benzodioxol-5-yl)-7-oxo-2-thioxo-1,2,3,7-tetrahydro[1,2,4]triazolo[1,5-a]pyrimidine-6-carbonitrile (6). Yield: 76 %; brown crystals, m.p.: 270 °C; Anal. Calcd. for C₁₃H₇N₅O₃S: C, 49.84; H, 2.25; N, 22.35; S, 10.23 %. Found: C, 50.11; H, 2.39; N, 22.18; S, 10.41 %; IR (KBr, cm⁻¹): 3383/3275 (-NH), 2230 (-C≡N), 1705 (-C=O), 1626 (-C=N), 1605/2565 (-C=S/SH); ¹H-NMR (300 MHz, DMSO-*d*₆, δ / ppm): 6.07 (2H, *s*, OCH₂O), 7.56–8.20 (3H, *m*, aromatic), 8.68 (1H, *s*, NHC≡N, D₂O exchangeable), 12.08 (1H, *s*, NNHC=S, D₂O exchangeable); MS (*m/z*, (relative abundance, %)): 313 (M⁺, 15), 273, 250, 214, 192, 148, 76, 56, 41 (BP 100).

3,3'-(4-Fluorophenyl)methylenebis[6-(1,3-benzodioxol-5-yl)-4-oxo-2-thioxo-1,2,3,4-tetrahydropyrimidine-5-carbonitrile] (7). Yield: 73 %; white crystals; m.p.: 128 °C; Anal. Calcd. for C₃₁H₁₇FN₆O₆S₂: C, 57.05; H, 2.63; N, 12.88; S, 9.83 %. Found: C, 56.87; H, 2.71; N, 12.48; S, 9.80 %; IR (KBr, cm⁻¹): 3380/3185 (-NH), 2225 (-C≡N), 1658 (-C=O stretching), 1628 (-C=N), 1605 (C=C- aromatic ring); ¹H-NMR (300 MHz, DMSO-*d*₆, δ / ppm): 5.7 (1H, *s*, CHAr), 6.08 (4H, *s*, 2 OCH₂O), 6.88–7.85 (10H, *m*, aromatic), 12.35 (2H, 2*s*, 2 NH, D₂O exchangeable); MS (*m/z*, (relative abundance, %)): 652 (M⁺, 65), 272, 245, 214, 186, 149, 124, 91 (BP, 100) 50.

3,3'-(3,6-Dioxocyclohexa-1,4-diene-1,4-diyl)bis(1,3-benzodioxol-5-yl)-4-oxo-2-thioxo-1,2,3,4-tetrahydropyrimidine-5-carbonitrile (9). Yield: 68 %; pale brown crystals; m.p.: 216 °C; Anal. Calcd. for C₃₀H₁₄N₆O₈S₂: C, 55.38; H, 2.17; N, 12.92; S, 9.86 %. Found: C, 55.53; H, 2.09; N, 13.04; S, 9.98 %; IR (KBr, cm⁻¹): 3235/3165 (-NH), 2216 (-C≡N), 1704 (-C=O quinonoid), 1648 (-C=O amide), 1622 (-C=N), 1595 (C=C- aromatic ring); ¹H-NMR (300 MHz, DMSO-



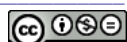
δ / ppm): 6.04 (4H, s, 2 OCH₂O), 6.18, 6.37 (2H, 2 s, 2 CHC=O) 6.82–7.68 (6H, m, aromatic), 12.43 (2H, 2 s, 2 NH, D₂O exchangeable); MS (*m/z*, (relative abundance, %)): 650 (M⁺, 44.12), 604, 217 (BP, 100), 78, 77.

5-(1,3-Benzodioxol-5-yl)-7-oxo-1,7-dihydrotetrazolo[1,5-a]pyrimidine-6-carbonitrile (10). Yield: 52 %; brown crystals; m.p.: 166 °C; Anal. Calcd. for C₁₂H₆N₆O₃: C, 51.07; H, 2.14; N, 29.78 %. Found: C, 50.96; H, 2.15; N, 29.89 %; IR (KBr, cm⁻¹): 3310 (–NH), 2231 (–C≡N), 1695 (–C=O), 1626 (–C=N), 1610 (C=C– aromatic ring), 1582 (–N=N); ¹H-NMR (300 MHz, DMSO-*d*₆, δ / ppm): 6.19 (2H, s, OCH₂O), 7.54–7.22 (3H, m, aromatic), 12.18 (1H, s, NH, D₂O exchangeable); ¹³C-NMR (75 MHz, DMSO-*d*₆, δ / ppm): 151.37 (C₂), 164.41 (C₄), 90.19 (C₅), 171.91 (C₆), 115.23 (CN), 101.59 (OCH₂O), 149.68 (Ar-C), 147.08 (Ar-C), 108.93 (Ar-C), 108.73 (Ar-C), 124.17 (Ar-C), 122.46 (Ar-C); MS (*m/z*, (relative abundance, %)): 161 (34.12), 136 (31.76), 77 (30.59), 69 (BP, 100).

6-(1,3-Benzodioxol-5-yl)-4-chloro-2-thioxo-1,2-dihdropyrimidine-5-carbonitrile (11a). Yield: 74 %; brown crystals; m.p.: 106 °C; Anal. Calcd. for C₁₂H₆ClN₃O₂S: C, 49.41; H, 2.07; Cl, 12.15; N, 14.40; S, 10.99 %. Found: C, 49.50; H, 1.99; Cl, 12.21; N, 14.35; S, 11.05 %; IR (KBr, cm⁻¹): 3144 (–NH), 2217 (–C≡N), 1681 (–C=N), 1185/2630 (–C=S/C–SH); ¹H-NMR (300 MHz, DMSO-*d*₆, δ / ppm): 6.10 (2H, s, OCH₂O), 6.74–7.33 (3H, m, aromatic), 12.4 (1H, s, NH, D₂O exchangeable); MS (*m/z*, (relative abundance, %)): 276, 275, 274, 257, 216 (BP, 100), 170, 121, 77.

4-Chloro-6-(3,4-dimethoxyphenyl)-2-thioxo-1,2-dihdropyrimidine-5-carbonitrile (11b). Yield: 62 %; m.p.: 183 °C; brown crystals; Anal. Calcd. for C₁₃H₁₀ClN₃O₂S: C, 50.73; H, 3.28; Cl, 11.52; N, 13.65; S, 10.42 %. Found: C, 50.49; H, 3.79; Cl, 11.21; N, 13.35; S, 11.05 %; IR (KBr, cm⁻¹): 3195 (–NH), 3089 (–CH aromatic), 2993 (–CH aliphatic), 2229 (–C≡N nitrile), 1619 (–C=N), 1539 (C=C– aromatic ring), 1168/2620 (–C=S/C–SH); ¹H-NMR (300 MHz, DMSO-*d*₆, δ / ppm): 3.81 (6H, s, 2 OCH₃), 6.82–7.24 (3 H, m, aromatic), 12.76 (1H, s, NH, D₂O exchangeable); ¹³C-NMR (75 MHz, DMSO-*d*₆, δ / ppm): 178.20 (C₂), 162.10 (C₄), 101.37 (C₅), 153.80 (C₆), 114.42 (CN), 147.88 (Ar-C), 128.97 (Ar-C), 121.94 (Ar-C), 109.03 (Ar-C), 108.53 (Ar-C), 55.81 (2 OCH₃); MS (*m/z*, (relative abundance, %)): 307 (M⁺, 75.34), 276, 246, 221, 188, 85 (BP, 100), 86.

4-(1,3-Benzodioxol-5-yl)-6-chloro-2-(methylthio)pyrimidine-5-carbonitrile (11c). Yield: 64 %; m.p.: 296 °C; brown crystals; Anal. Calcd. for C₁₃H₈ClN₃O₂S: C, 51.07; H, 2.64; Cl, 11.60; N, 13.74; S, 10.49 %. Found: C, 51.31; H, 2.68; Cl, 11.09; N, 13.99; S, 10.89 %; IR (KBr, cm⁻¹): 2216 (–C≡N), 1635 (–C=N), 1605 (C=C– aromatic ring); ¹³C-NMR (75 MHz, DMSO-*d*₆, δ / ppm): 172.1 (C₂), 160.0 (C₄), 108.6 (C₅), 158.8 (C₆), 114.8 (CN), 109.2 (CCN), 14.4 (SCH₃), 103.3 (OCH₂O), 162.5 (Ar-C), 126.3 (Ar-C), 120.8 (Ar-C), 110.2



(Ar-C), 145.8 (2 Ar-C); MS, (*m/z*, (relative abundance, %)): 288, 287 (BP, 100), 286, 241, 200, 148, 120, 100, 63, 62, 53, 50.

7-(1,3-Benzodioxol-5-yl)-5-thioxo-5,6-dihydrotetrazolo[1,5-c]pyrimidine-8-carbonitrile (13). Yield: 54 %; yellow crystals; m.p.: 202 °C; Anal. Calcd. for C₁₂H₆N₆O₂S: C, 48.32; H, 2.03; N, 28.17; S, 10.75 %. Found: C, 48.29; H, 2.11; N, 28.33; S, 10.73 %; IR (KBr, cm⁻¹): 3148 (–NH), 2213 (–C≡N nitrile), 1642 (–C=N), 1210/2585 (–C=S/SH); ¹H-NMR (300 MHz, DMSO-*d*₆, δ / ppm): 6.10 (2H, *s*, OCH₂O), 8.24–7.57 (3H, *m*, aromatic), 8.77 (1H, *s*, NH, D₂O exchangeable); ¹³C-NMR (75 MHz, DMSO, δ / ppm): 158.4 (C₅), 154.1 (C₇), 134.9 (C₉), 106 (C₈), 138.1 (Ar-C), 137.9 (Ar-C), 131.90 (Ar-C), 131.97 (C≡N), 116.9 (Ar-C), 117.1 (Ar-C), 113 (O–CH₂–O); 70.5 (Ar-C); MS (*m/z*, (relative abundance, %)): 300 ([M + 2]⁺, 23), 299 ([M + 1]⁺, 30), 298 (M⁺, 72), 272, 244 (BP, 100), 238, 234, 211, 184, 152, 121, 109, 64, 54.

4-Amino-5-(1,3-benzodioxol-5-yl)pyrimido[4,5-d]pyrimidine-2,7(1H,3H)-dithione (15). Yield: 62 %; yellow crystals; m.p.: 244 °C; Anal. Calcd. for C₁₃H₉N₅O₂S₂: C, 47.12; H, 2.74; N, 21.13; S, 19.35 %. Found: C, 47.20; H, 2.65; N, 21.18; S, 19.23 %; IR (KBr, cm⁻¹): 3422, 3342 (–NH₂/NH), 1654 (–C=N), 1605 (C=C– aromatic ring), 1595/2615 (–C=S/SH); ¹H-NMR (300 MHz, DMSO-*d*₆, δ / ppm): 3.40 (2H, *s*, NH₂, D₂O exchangeable), 6.15 (2H, *s*, OCH₂O), 7.33–7.78 (3H, *m*, Ar-H); 12.3 (s, 2H, 2NH, D₂O exchangeable) MS (*m/z*, (relative abundance, %)): 331 (M⁺, 96.27), 301, 280, 252, 134 (BP, 100), 78.

5-Amino-4-(1,3-benzodioxol-5-yl)-6-phenyl-1,3-dihydro-2H-pyrrolo[2,3-d]-pyrimidine-2-thione (17a). Yield: 72 %; brown crystals; m.p.: 208 °C; Anal. Calcd. for C₁₉H₁₄N₄O₂S: C, 62.97; H, 3.89; N, 15.46; S, 8.85 %. Found: C, 63.12; H, 3.95; N, 15.43; S, 8.76 %; IR (KBr, cm⁻¹): 3448 (–NH, NH₂), 2895 (–CH aliphatic), 1616 (–C=N); ¹H-NMR (300 MHz, DMSO-*d*₆, δ / ppm): 1.94 (1H, *s*, NH, D₂O exchangeable), 4.14 (2H, *s*, NH₂, D₂O exchangeable), 6.2 (2H, *s*, OCH₂O), 7.28–7.85 (8H, *m*, aromatic), 8.12 (1H, *s*, NHC=S, D₂O exchangeable); MS (*m/z*, (relative abundance, %)): 362 (M⁺, 59.78), 318, 241, 112 (BP, 100), 122, 78.

5-Amino-4-(3,4-dimethoxyphenyl)-6-phenyl-1,3-dihydro-2H-pyrrolo[2,3-d]-pyrimidine-2-thione (17b). Yield: 67 %; brown crystals; m.p.: 190 °C; Anal. Calcd. for C₂₀H₁₈N₄O₂S: C, 63.47; H, 4.79; N, 14.80; S 8.47 %. Found: C, 63.52; H, 4.89; N, 14.95; S, 8.62 %; IR (KBr, cm⁻¹): 3466 (–NH,NH₂), 3090 (–CH aromatic), 1632 (–C=N); ¹H-NMR (300 MHz, DMSO-*d*₆, δ / ppm): 2.1 (1H, *s*, NH, D₂O exchangeable), 3.58 (6H, *s*, 2 OCH₃), 4.78 (2H, *s*, NH₂, D₂O exchangeable), 6.78–7.55 (8H, *m*, aromatic), 8.28 (1H, *s*, NHC=S, D₂O exchangeable), ¹³C-NMR (75 MHz, DMSO-*d*₆, δ / ppm): 174.4 (C₂), 159.8 (C₄), 109.3 (C₅), 161.6 (C₆), 118.7 (C=CNH₂), 121.7 (CNH₂), 51.1 (2 OCH₃), 147.7(Ar-C), 147.1 (Ar-C), 135.9 (Ar-C), 126.5 (Ar-C), 126.1 (Ar-C), 125.8 (Ar-C), 124.4



(Ar-C), 123.8 (Ar-C), 119.6 (Ar-C), 119.0 (Ar-C), 115.8 (Ar-C), 111.9 (Ar-C); MS, (*m/z*, (relative abundance, %)): 378 (M⁺, 42.31), 301, 287, 109, 55 (BP, 100).





The effect of chlorsulfuron and MCPB-Na on the enzymatic activity of microorganisms

MARIOARA NICOLETA FILIMON^{1,2}, SORIN OCTAVIAN VOIA^{3*},
ROXANA POPESCU⁴, DESPINA-MARIA BORDEAN⁵, DIANA LARISA
VLADOIU^{1,2}, MIHAI MITULETU^{1,2} and VASILE OSTAFE^{1,2}

¹West University of Timișoara, Faculty of Chemistry-Biology-Geography, Department of Biology-Chemistry, Pestalozzi, 16, Timisoara, 300115, Romania, ²West University of Timisoara, Laboratory of Advanced Research in Environmental Protection, Oituz 4, Timisoara 300086, Romania, ³Banat University of Agricultural Sciences and Veterinary Medicine, Faculty of Animal Science and Biotechnology, Calea Aradului, 119, Timisoara, 300645, Romania, ⁴University of Medicine and Pharmacy "Victor Babes", Department of Cellular and Molecular Biology, E. Murgu, 2, Timisoara, 300041, Romania and ⁵Banat University of Agricultural Sciences and Veterinary Medicine from Timisoara, Faculty of Food Processing and Technology, Calea Aradului, 119, Timisoara, 300645, Romania

(Received 15 January, revised 25 March, accepted 27 March 2014)

Abstract: Sulphonylureic herbicides have a broad spectrum effect on weeds in relatively low doses and with a much reduced toxicity to livestock. In this study, two herbicides: dacsulfuron with the active substance chlorsulfuron (0.005–0.035 µg g⁻¹ soil) and butoxone with the active substance MCPB-Na (0.005–0.035 mg L⁻¹ g⁻¹ soil) were investigated. The samples were collected from a depth of 0–20 cm from chernozem soil. The effects of the herbicides were estimated by measuring the activities of catalase, actual and potential dehydrogenase, urease and cellulase. All samples were incubated for 10 days at 27 °C using Stapp medium for the isolation and study of cellulosolytic bacteria. The inhibitory effect of the tested herbicides was the most intense on the enzymatic activities of urease and dehydrogenase. The most resistant cellulosolytic bacteria to the effects of dacsulfuron were *Cellfalcicula fusca*, *C. viridis*, *Cellvibrio fulvus* and *Cellfalcicula* sp., and for butoxone *C. mucosa*, *C. viridis* and *C. fulvus*.

Keywords: herbicides; soil; cellulosolytic bacteria.

INTRODUCTION

Soil microorganisms play an important role on soil processes, influencing soil structure, plant cultivation, medium resources and soil quality.¹ Soil structure and stability are strictly related to the presence and activity of microorganisms.

*Corresponding author. E-mail: voia@animalsci-tm.ro
doi: 10.2298/JSC140115031F

Microbial activity in soil, being susceptible to xenobiotics, can be a useful tool to assess soil quality.² Xenobiotics can have both direct and indirect effects upon the enzymatic activities in soil. Enzymes such as hydrolases (invertase, protease, phosphatase and urease) and oxidases (dehydrogenase, catalase and peroxidase) can be used as sensitive bioindicators of soil pollution.^{3,4} Enzymatic activities of soil microorganisms are of major interest in assessing the effects of herbicides on the quality of soil. Studies have shown that dehydrogenase activity may represent an important indicator of the secondary effects associated with the administration of sulphonylureic herbicides.^{5–7} Depending on the employed type of herbicide, other enzymatic activities present in soils undergo quantitative and qualitative variations. Thus, urease, amylase and protease activities are inhibited by some sulphonylureic herbicides. Herbicides from the glyphosate group inhibit enzymatic activities in soil with increasing herbicide dose.^{8,9}

Herbicide degradation in soil is due to intra- and extracellular enzymes produced by soil microorganisms, especially bacteria, but also fungi. Most studies on herbicide degradation were conducted on bacteria.^{10,11} However, the role of fungi in herbicide degradation must also be considered.^{12–14}

Herbicide impact on microorganism communities in soil, especially their metabolic activity, depends on various factors, such as: soil structure and texture,^{15,16} physical and chemical factors (pH, temperature, humidity and organic matter content), intensity and activity spectrum of the herbicide and herbicide persistence in the soil.^{16–18}

Chlorophenoxy derivatives, most commonly γ -phenoxybutyric acids, are selective herbicides used against broadleaf weeds. The application of herbicides to destroy weeds in crops has advantageous effects on agricultural production but negatively influences soil microorganism growth,^{19,20} population dynamics^{19–21} and metabolic activity.^{15,17,20}

The detection of bacterial ecophysiological groups is useful for identifying structural changes that occur in soil due to xenobiotic substances. Cellulosolytic bacteria are a group with a very important role due to the fact that cellulose is present in soil in large amounts, being the main component of plant organic matter. The isolation and identification of cellulosolytic bacteria and the effect of different xenobiotics on these bacterial species led to different studies.^{6,22}

Sulphonylureic herbicides are a group of herbicides frequently used to destroy weeds in crops; their large scale administration is due to the need for relatively low doses, high efficiency and low toxicity for small mammals.²³

The present study aimed at establishing the effects of the two herbicides on soil quality, based on the fact that soil enzymes could be considered as early indicators in soil quality change in the context of land management. The present study brings an important contribution in establishing the effects of anthropo-



genic influences (the use of herbicides) on soil quality, and their relation to enzymatic activity and their potentials.

EXPERIMENTAL

Materials

Chlorsulfuron (CAS 79793-81-0-64902-72-3) also known as 1-(2-chlorophenylsulphonyl)-3-(4-methoxy-6-methyl-1,3,5-triazin-2-yl)urea, may also be found in commercial herbicides under the trade name Dacsulfuron 750SP (Strand Group Holdings Ltd.). MCPB-Na also known as sodium 4-(4-chloro-2-methylphenoxy)butanoate (CAS 6062-26-6), may also be found in commercial herbicides under the trade name Butoxone M40 (Nufarm Ltd., UK). Microorganisms were isolated from chernozem soil samples collected from a depth of 0-20 cm, in the spring, before sowing and fertilization. The collected soil samples were treated with chlorsulfuron and MCPB-Na and analyzed in the Laboratory of Advanced Research in Environmental Protection.

Soil treatment with herbicides

The soil was sieved through a 2 mm sieve and placed in polyethylene bags in order to ensure soil moisture. The conversion rate: pesticides g⁻¹ of soil applied in the field was calculated according to a uniform distribution of herbicides in the soil.²⁴

An untreated sample was preserved as a control sample, while the experimental samples were treated with increasing doses of herbicide. The following experimental variants were obtained after applying the herbicides: normal doses (ND, 0.2 µg chlorsulfuron, 0.2 mg MCPB-Na), 2 times the normal doses (2×ND, 0.4 µg chlorsulfuron, 0.4 mg MCPB-Na), 5 times the normal doses (5×ND, 1 µg chlorsulfuron, 1.0 mg MCPB-Na) and 7 times the normal doses (7×ND, 1.4 µg chlorsulfuron, 1.4 mg MCPB-Na). The samples were incubated for 7 days at 24 °C.

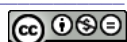
The enzymatic activity

The experimental variants were considered for comparative studies of the activities of enzymes. The following enzymatic activities were chosen for assay: dehydrogenase (DA, EC 1.1.1.1), urease (EC 3.5.1.5), catalase (CA, EC 1.11.1.6) and cellulase (Cel A, EC 3.2.1.91). The enzymatic activity was determined using a T90 UV–Vis spectrophotometer (PG Instruments, UK).

The actual dehydrogenase activity (ADA) was measured using 2,3,5-triphenyltetrazolumchloride (TTC), incubating soil samples (5 g) mixed with distilled water Tris-buffer (2 mL, 1 M, pH 7.6) at 37 °C for 48 h. To determine the potential dehydrogenase activity (PDA), glucose was added to the reaction mix. The formed triphenyl formazan was extracted with acetone and the absorbance of the supernatants measured at 485 nm. The activity of dehydrogenase was expressed as mg triphenyl formazan g⁻¹ soil.²⁵

The urease activity was determined in accordance with the method described by Alef and Nannpieri.²⁶ Reaction mixtures consisting of 3 g soil, 2 mL toluene, 5 mL phosphate buffer (0.6 M, pH 6.8) and 5 mL of a 3 % urea solution were incubated at 37 °C for 24 h. The absorbance was measured at 445 nm. The activity was expressed as mg NH₄ g⁻¹ soil.

The catalase activity was determined using the permanganometric method described by Dragan-Bularda.²⁷ The reaction mixtures consisted of 3 g soil, 2 mL H₂O₂, 10 ml of a 3 %, phosphate buffer solution (0.4 M, pH 6.7). After 1 h incubation at 37 °C, the catalase activity was recorded as mg H₂O₂ decomposed by 1 g of soil in 1 h.



The cellulase activity (Cel A, EC 3.2.1.91) was determined by assessing the amount of cellulose consumed through decomposition.²⁸ On the basis of the difference between the initial and the final quantity of decomposed cellulose, specifically related to the amount of analyzed soil sample. All the assays of the enzymes activities were performed in triplicate, in a controlled laboratory environment, by the same researcher during the same day.

Isolation and identification of cellulolytic microorganisms was made from 10⁻³ dilution soil experimental variants inoculated on a solid growth medium (Stapp medium). The inoculated Petri dishes were incubated for 10 days at 27 °C. After the incubation, the main cellulolytic bacterial species were identified based on the specificity of the substrate degradation and the morphologic aspects of the colonies.

Statistical data interpretation

The data were analyzed using analysis of variance (ANOVA) of simple correlations as 2nd degree polynomial regression equations. The software MINITAB 14 was employed.²⁹ All data are presented as mean values with standard deviation ($X \pm SD$). Significant differences in variables were tested using the *F*-test at the 0.05 level of probability. Cluster analysis was performed using the Past Statistical Program, version 2.12, employing the Algorithm Single Linkage and Bray-Curtis Indices³⁰ were used as a similarity measure.

Cluster analysis divides the data into groups (clusters) that have an important similar effect. The clusters confine the meaningful groups and present the natural structure of the data as well as data summarization. “The greater the similarity within a group and the greater the difference between groups, the better or more distinct is the clustering”.³¹ The use of cluster analysis in microbiology and molecular microbial ecology was mentioned by de Bruijn in 2011³² as a possible method to analyze microbiological data.

The distance between two clusters using the algorithm single linkage clustering, is defined as the distance between the closest members of the two groups.³³ Bray-Curtis is a popular similarity index for abundance data:

$$y_{jk} = 1 - \frac{\sum_i |x_{ji} - x_{ki}|}{\sum_i (x_{ji} + x_{ki})}$$

Similarly, y_{ik} is the count for the i^{th} species in the k^{th} sample, representing the entry in the i^{th} row and j^{th} column of the data matrix, *i.e.*, the abundance for the i^{th} species in the j^{th} sample ($i = 1, 2, \dots, p; j = 1, 2, \dots, n$).³⁴

RESULTS AND DISCUSSION

The statistical analyses of the values of the enzymatic activities from the soil samples treated with herbicides are presented in Table I.

The values of the catalase activity measured in the soil samples decreased with increasing herbicide dosage: 3.13 % decrease when dacsulfuron was applied and 9.24 % on application of butoxone. From a statistical point of view, the observed decrease in the experimental variants was significant, the *p* value being < 0.05. Thus, the catalase activity was more negatively influenced by butoxone than by dacsulfuron, probably due to the effect of other non-enzymatic catalysts on the catalase activity in soil.



The dehydrogenase activity reflects the respiratory processes in the soil, which are directly proportional to the number of microorganisms in the soil; the greater the number of microorganisms in the soil, the higher is the intensity of the dehydrogenase activity. Thus, analysing the effect of dacsulfuron in the experimental samples, a decrease of 39.82 % for the actual dehydrogenase activity and a 41.12 % decrease in the potential dehydrogenase activity were observed. The treatment with the herbicide butoxone induced a 51.37 % decrease in the actual dehydrogenase activity and a 25.44 % decrease in the potential dehydrogenase activity. Therefore, butoxone shown a stronger effect based on the fact that the potential dehydrogenase activity was significantly lower compared to the dehydrogenase activities of corresponding untreated (batch) and dacsulfuron-treated samples. Similar results, with decreased dehydrogenase activity of up to 25 or 50 % in soils treated with herbicides (metsulfuron-methyl and 2,4-D, glyphosate) were obtained in previous studies, such as those of Araújo *et al.* and Zabaloy *et al.*^{5,7}

TABLE I. Enzymatic activity values in the analyzed soil samples; statistic analysis: $X \pm SD$; D – dacsulfuron; B – butoxone; ND – normal dose; $2 \times ND$ – 2 times normal dose; $5 \times ND$ – 5 times normal dose; $7 \times ND$ – 7 times normal dose; X – mean value; SD – standard deviation; SEM – standard error of mean; * – the mean difference is significant at the 0.05 level between the batch and the experimental variants

| Exp. variants | CA ^a | ADA ^b | PDA ^c | UA ^d | Cel A ^e |
|-----------------|-------------------|-------------------|-------------------|-------------------|--------------------|
| Batch | 3.485 \pm 0.085 | 1.421 \pm 0.019 | 0.800 \pm 0.013 | 2.660 \pm 0.010 | 0.091 \pm 0.001 |
| D ND | 3.126 \pm 0.143 | 1.371 \pm 0.019 | 0.696 \pm 0.019 | 1.132 \pm 0.011 | 0.071 \pm 0.001 |
| D 2 \times ND | 3.094 \pm 0.093 | 1.238 \pm 0.013 | 0.625 \pm 0.013 | 0.945 \pm 0.012 | 0.062 \pm 0.003 |
| D 5 \times ND | 3.082 \pm 0.128 | 1.054 \pm 0.059 | 0.563 \pm 0.013 | 0.720 \pm 0.011 | 0.004 \pm 0.001 |
| D 7 \times ND | 3.028 \pm 0.128 | 0.825 \pm 0.012 | 0.375 \pm 0.013 | 0.218 \pm 0.007 | 0.001 \pm 0.000 |
| SEM | 0.0508 | 0.0588 | 0.0381 | 0.2196 | 0.0062 |
| B ND | 3.094 \pm 0.131 | 0.763 \pm 0.013 | 0.621 \pm 0.019 | 1.143 \pm 0.004 | 0.005 \pm 0.000 |
| B 2 \times ND | 3.060 \pm 0.085 | 0.643 \pm 0.006 | 0.587 \pm 0.013 | 0.987 \pm 0.002 | 0.003 \pm 0.000 |
| B 5 \times ND | 3.021 \pm 0.045 | 0.446 \pm 0.019 | 0.500 \pm 0.025 | 0.966 \pm 0.003 | 0.002 \pm 0.000 |
| B 7 \times ND | 2.808 \pm 0.085 | 0.371 \pm 0.019 | 0.463 \pm 0.013 | 0.760 \pm 0.003 | 0.000 \pm 0.000 |
| SEM | 0.0619 | 0.0890 | 0.0295 | 0.1842 | 0.0021 |

^aCatalase activity (mg H₂O₂ not decomposed per g soil); ^bactual dehydrogenase activity (mg triphenyl formazan g⁻¹ soil); ^cpotential dehydrogenase activity (mg triphenyl formazan g⁻¹ soil); ^durease activity (mg NH₄ g⁻¹ soil); ^ecellulase activity

Dehydrogenase activity was proved to be an important indicator of the secondary effects following the administration of the two herbicides. Similar studies on the influence of herbicides on dehydrogenase activity of soil microorganisms also revealed that herbicides cause a decrease in the activity of this enzyme.⁵⁻⁷

The urease activity registered significantly lower values after application of the herbicides compared to the untreated sample, showing that this enzymatic activity seems to be the most sensitive to the herbicides. Experimental values,



showed a 80.74 % decrease in the urease activity in soil samples treated with 7×normal dose (7×ND, 1.4 µg chlorsulfuron) of dacsulfuron, compared to the soil sample treated with the normal dose (ND, 0.2 µg chlorsulfuron) of dacsulfuron. The experimental variants treated with butoxone presented a of 33.50 % decrease in the urease activity compared to the control sample.

For both herbicides, a decrease in urease activity with increasing herbicide dose was observed, the effect of dacsulfuron being stronger than that of butoxone. Similar studies on the influence of herbicides on the enzymatic activities of soil microorganisms confirmed the effect of herbicides (glyphosate, gluphosinate and sulphonylureic) on urease activity.^{8,9,35}

The cellulase activity decreased in the experimental samples with the increased dose of the applied herbicides. In the case of butoxone, for the (7×ND, 1.4 mg MCPB-Na) experimental sample, the cellulase activity could not be measured on the experimental level. Significantly reduced cellulase activities were also identified in other studies which analyzed the effects of herbicides on microorganism communities in soil.^{6,22,36}

The sensitivity of different enzymatic activities to dacsulfuron and butoxone decreased in the following order: urease activity > potential dehydrogenase activity > actual dehydrogenase activity > catalase activity > cellulase activity.

The correlations between the cellulase activity and the number of cellulosolytic bacterial colony forming units showed a positive correlation ($r = +0.809$) for the herbicide dacsulfuron and a negative correlation ($r = -0.838$) for the herbicide butoxone. Therefore, it could be argued that the number of cellulosolytic bacteria is less important than the bacterial species present and their enzymatic capacity.

In the control samples, the following species of cellulolytic bacteria were identified: *Cellfalcicula fusca*, *C. mucosa*, *C. viridis*, *Cellvibrio fulvus*, *Cellvibrio ochreus*, *Cytophaga aurantica* and *Sporocytophaga congregata*. In the soil experimental variants qualitative and quantitative variations of cellulolytic bacteria species were recorded. *Cellfalcicula fusca* was well represented in soils treated with dacsulfuron compared to those treated with butoxone, while *C. mucosa* showed the opposite distribution. *C. viridis* was found in soils treated with dacsulfuron and absent in those treated with butoxone. *Cellvibrio fulvus* showed large quantitative variations in the experimental variants compared to the control sample, which demonstrated its increased sensitivity to the action of herbicides. Toxicity of dacsulfuron was manifested on *Cytophaga* sp., as shown by its absence in the experimental variants treated with dacsulfuron (Fig. 1).

Cluster analysis showed, in the soil samples treated with increasing doses of chlorsulfuron, the species *Cellvibrio flavescent*, *Cellfalcicula fusca*, *C. mucosa*, *Cellulomonas pusilla*, *Cellfalcicula viridis* and *Cellvibrio fulvus* had a similar behaviour on exposure to dacsulfuron (0.329, Fig. 2). For the soil samples treated

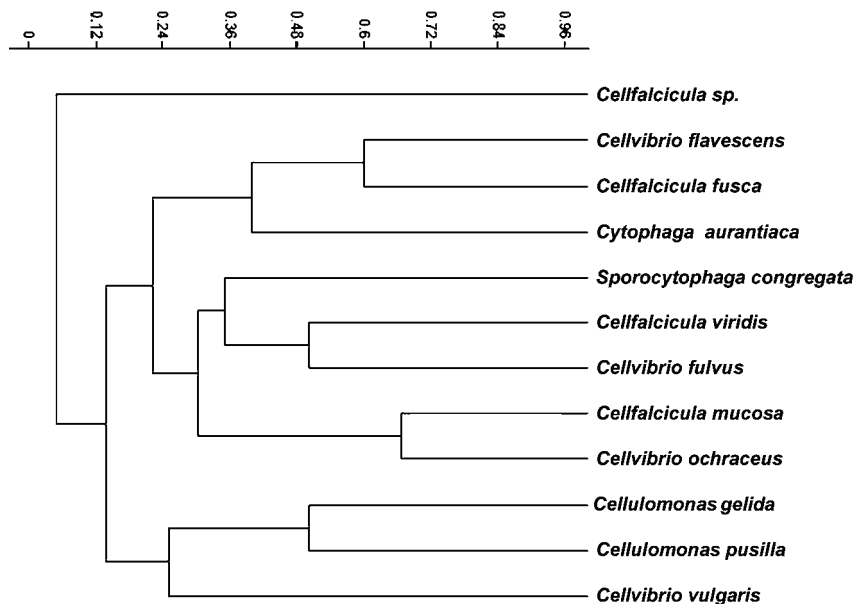


Fig. 1. Cluster analysis of cellulosolytic bacteria from soil samples treated with chlorsulfuron.

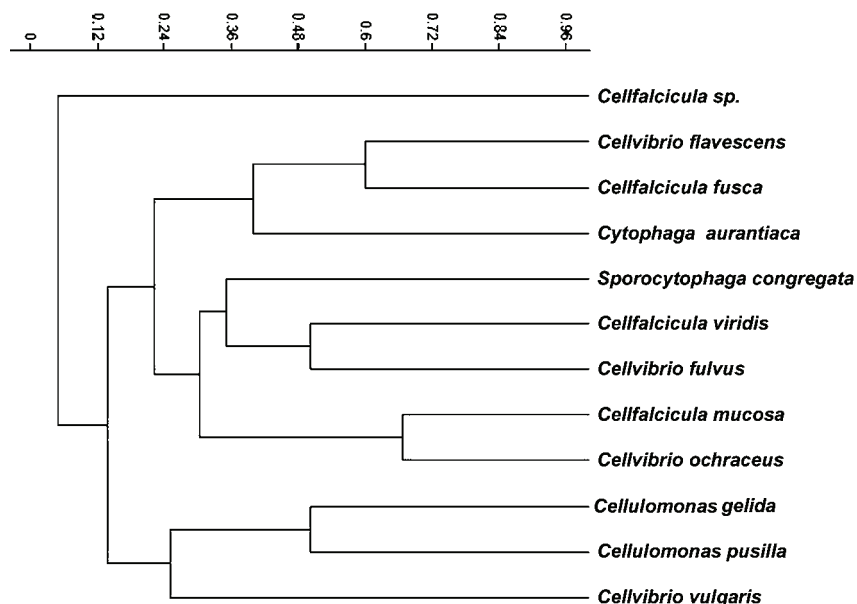


Fig. 2. Cluster analysis of cellulosolytic bacteria from soil samples treated with MCPB-Na.

with MCPB-Na, cluster analysis showed that the species *C. fulvus*, *Cytophaga aurantiaca*, *C. fusca* (0.365), *C. mucosa* and *Cellvibrio ochraceus* (0.259), as

well as *Cellfalcicula viridis* and *S. congregata* (0.517), also exhibited similar behaviour when exposed to the herbicide butoxone.

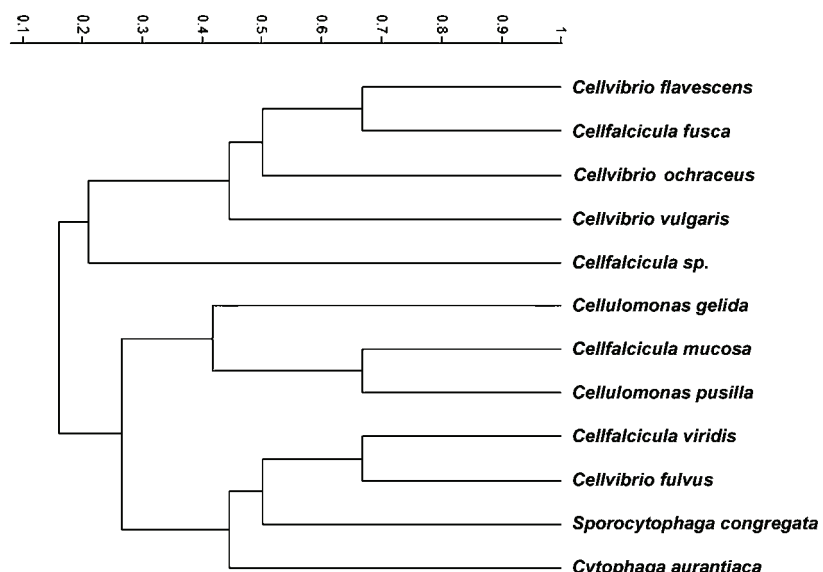


Fig. 3. Cluster analysis of cellulolytic bacteria from soil samples treated with herbicides.

Based on cluster analysis, it was established that *C. flavesiensis*, *Cellfalcicula fusca* (0.400), *C. mucosa* and *Cellvibrio ochraceus* (0.345), *Cellfalcicula viridis* and *Cellvibrio fulvus* (0.513), *Cellulomonas pussilla* and *Cellvibrio vulgaris* (0.533) presented a similar behaviour on exposure to dacsulfuron and butoxone (Fig. 3).

CONCLUSIONS

In conclusion, the use of microorganisms in monitoring programs is necessary because the changes in the structure of the microorganism communities may indicate changes in environment quality. In order to accurately identify the possible changes caused by the use of xenobiotics, many impact indicators must be considered – key microorganisms, quantitative and qualitative variations in microorganism groups and metabolic activities (enzymatic).

The urease and dehydrogenase enzymatic activities were the most sensitive to the action of chlorsulfuron and MCPB-Na. The inhibition of dehydrogenase activity indicates to the toxic effect of chlorsulfuron and MCPB-Na on the microorganism communities in soil.

The most resistant species to the effect of dacsulfuron were *Cellfalcicula fusca*, *C. viridis*, *Cellvibrio fulvus*, *Cellfalcicula* sp., *Cellfalcicula mucosa*, *C. viridis* and *Cellvibrio fulvus* to the action of butoxone.

ИЗВОД

ЕФЕКТИ ХЛОРСУЛФУРОНА И MCPB-Na НА ЕНЗИМСКУ АКТИВНОСТ
МИКРООРГАНИЗАМА

MARIOARA NICOLETA FILIMON^{1,2}, SORIN OCTAVIAN VOIA³, ROXANA POPESCU⁴, DESPINA-MARIA
BORDEAN⁵, DIANA LARISA VLADOIU^{1,2}, MIHAI MITULETU^{1,2} и VASILE OSTAFE^{1,2}

¹West University of Timișoara, Faculty of Chemistry-Biology-Geography, Department of Biology-Chemistry,
Pestalozzi, 16, Timisoara, 300115, Romania, ²West University of Timisoara, Laboratory of Advanced
Research in Environmental Protection, Oituz 4, Timisoara 300086, Romania, ³Banat University of
Agricultural Sciences and Veterinary Medicine, Faculty of Animal Science and Biotechnology, Calea Aradului,
119, Timisoara, 300645, Romania, ⁴University of Medicine and Pharmacy "Victor Babes", Departament of
Cellular and Molecular Biology, E. Murgu, 2, Timisoara, 300041, Romania и ⁵Banat University of
Agricultural Sciences and Veterinary Medicine from Timisoara, Faculty of Food Processing & Technology
Calea Aradului, 119, Timisoara, 300645, Romania

Хербициди имају широк спектар дејства у сузбијању корова у релативно ниским дозама, и показују смањену токсичност код животиња. У истраживању су примењени хербициди даксулфурон, са активном супстанцом хлорсулфурон (0,005–0,035 µg g⁻¹ земљишта) и бутоксон, са активном супстанцом MCPB-Na (0,005–0,035 mg L⁻¹ g⁻¹ земљишта). Земљиште типа чернозем је узорковано до дубине од 20 см. Ефекат хербицида је био оцењен преко анализе ензимске активности: каталитичке, тренутне и потенцијалне дехидрогеназне, уреазне и целулолитичне активности. За изоловање и развој бактерија целулолитика коришћена је подлога Stapp. Инкубација је трајала 10 дана на 27 °C. Инхибициони ефекат тестиралих хербицида био је најинтензивнији у случају дехидрогеназне и уреазне ензимске активности. Најотпорније бактерије целулолитици на дејство даксулфурона биле су *Cellfalcicula fusca*, *C. viridis*, *Cellvibrio fulvus* и *Cellfalcicula* sp., а на деловање бутоксона *Cellfalcicula mucosa*, *C. viridis* и *Cellvibrio fulvus*.

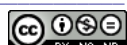
(Примљено 15. јануара, ревидирано 25. марта, прихваћено 27. марта 2014)

REFERENCES

1. J. E. Stach, R. G. Burns, *Environ. Microbiol.* **4** (2002) 169
2. L. Gianfreda, M. A. Rao, *Enzyme Microb. Technol.* **35** (2004) 339
3. J. P. Taylor, B. Wilson, M. S. Mills, R. G. Burns, *Soil Biol. Biochem.* **34** (2002) 387
4. E. Benitez, R. Melgar, R. Nogales, *Soil Biol. Biochem.* **36** (2004) 1615
5. A. S. F. Araújo, R. T. R. Monteiro, R. B. Abarkeli, *Chemosphere* **52** (2003) 799
6. M. E. Pampulha, A. Oliveira, *Curr. Microbiol.* **53** (2006) 238
7. M. C. Zabaloy, M. A. Gómez, *Commun. Soil Sci. Plant Anal.* **39** (2008) 370
8. C. Accinelli, C. Scarpanti, G. Dinelli, A. Vicari, *Int. J. Environ. Anal. Chem.* **82** (2002) 519
9. N. Z. Lupwayi, K. G. Hanson, K. N. Harker, R. E. Blackshawab, G. W. C. O'Donovan, J. T. Johnson, E. N. Gan, Y. Irvine, M. A. Monreal, *Soil Biol. Biochem.* **39** (2007) 1418
10. E. El-Bestawy, H.-J. Albrechtsen, *Int. Biodeter. Biodegr.* **59** (2007) 193
11. S. R. Sørensen, C. N. Albers, J. Aamand, *Appl. Environ. Microbiol.* **74** (2008) 2332
12. C. Tixier, M. Sancelme, S. Ait-Aissa, P. Widéhem, F. Bonnemoy, A. Cuer, N. Truffaut, H. Veschambre, *Chemosphere* **46** (2002) 519
13. N. Badawi, S. Ronhede, S. Olsson, B. B. Kraglund, A. H. Johnsen, O. S. Jacobsen, J. Aamand, *Environ. Pollut.* **157** (2009) 2806
14. H. Harms, D. Schlosser, L. Y. Wick, *Nat. Rev. Microbiol.* **9** (2011) 177
15. A. Monkiedje, M. O. Ilori, M. Spitteler, *Soil Biol. Biochem.* **34** (2002) 1939



16. S. Beulke, C. D. Brown, C. J. Fryer, W. van Beinum, *Chemosphere* **57** (2004) 481
17. F. Sannino, L. Gianfreda, *Chemosphere* **45** (2001) 417
18. J. Singh, D. K. Singh, *J. Environ. Sci. Heal. B* **40** (2005) 785
19. S. Thiele-Bruhn, I. C. Beck, *Chemosphere* **59** (2005) 457
20. C. B. Zhang, J. Wang, W. L. Liu, S. X. Zhu, H. L. Ge, S. X. Chang, J. Chang, Y. Ge, *Ecol. Eng.* **36** (2010) 62
21. W. Liu, N. Pan, W. Chen, W. Jiao, M. Wang, *Plant Soil Environ.* **58** (2012) 295
22. S. A. Omar, M. A. Abdel-Sater, *Water Air Soil Pollut.* **127** (2001) 49
23. A. K. Sarmah, J. Sabadie, *J. Agric. Food Chem.* **50** (2002) 6253
24. R. M. Atlas, D. Parmer, R. Partha, *Soil Biol. Biochem.* **10** (1978) 231
25. F. Schinner, R. Öhlinger, E. Kandeler, R. Margesin, *Methods in Soil Biology*, Springer Verlag, Berlin Heidelberg, 1996, p. 241
26. K. Alef, P. Nannipieri, *Methods in Applied Soil Microbiology and Biochemistry*, Academic Press Ltd., London, 1995, p. 316
27. M. Dragan-Bularda, *Microbiologie generală-Lucrări practice*, Editura Universitatii Babes-Bolyai, Cluj-Napoca, 2000, p. 175 (in Romanian)
28. Gh. Stefanic, *Metode de analiză pedobiologică și chimică*, ICCPT, Fundulea, 2000, p. 21 (in Romanian)
29. Softonic, <http://en.softonic.com/s/minitab-14-free-download-full-version>
30. Ø. Hammer, D. A. T. Harper, P. D. Ryan, *Palaeontol Electronica*, 2001, http://palaeo-electronica.org/2001_1/past/issue1_01.htm (accessed in Sep, 2014)
31. P. N. Tan, M. Steinbach, V. Kumar, *Cluster Analysis: Basic Concepts and Algorithms*, 2006, <http://www-users.cs.umn.edu/~kumar/dmbook/ch8.pdf> (accessed in Sep, 2014)
32. F. J. de Bruijn, *Handbook of Molecular Microbial Ecology I*, Wiley, Hoboken, NJ, 2011, p. 514, books.google.ro/books?isbn=1118010442 (accessed in Sep, 2014)
33. Ø. Hammer, D. A. T. Harper, *Paleontological Data Analysis*, Wiley–Blackwell, Hoboken, NJ, 2005, p. 68
34. Ø. Hammer, *PAleontological STatistics – Version 2.17*, http://www.nhm2.uio.no/norlex/past/past_part1.pdf (accessed in Sep, 2014)
35. D. C. Vlad, M. N. Filimon, R. Popescu, C. Gurban, V. Dumitrascu, *Ann. West Univer. Timisoara, Series Chem.* **20** (2012) 87
36. A. Ulrich, G. Klimke, S. Wirth, *Microb. Ecol.* **55** (2008) 512.





Effects of high dose olive leaf extract on the hemodynamic and oxidative stress parameters in normotensive and spontaneously hypertensive rats

DRAGANA DEKANSKI^{1*}, NEVENA MIHAJOVIĆ-STANOJEVIĆ², JELICA GRUJIĆ², MILANOVIC², ĐURĐICA JOVOVIĆ² and ZORAN MILORADOVIĆ²

¹Biomedical Research, R & D Institute, Galenika a.d., Pasterova 2, Belgrade, Serbia and

²Department of Cardiovascular Physiology, Institute for Medical Research, University of Belgrade, Dr Subotića 4, P. O. Box 102, Belgrade, Serbia

(Received 18 February, revised 26 March, accepted 27 March 2014)

Abstract: The antihypertensive activity of olive leaf extract (OLE), a natural antioxidant is recognized, but its influence on the cardiovascular system when administered in a high dose has not yet been investigated. The aim of the present study was to determine the acute effects of excessive intake of standardized OLE on blood pressure, heart rate and oxidative status in both spontaneously hypertensive rats and normotensive Wistar rats. The systolic arterial pressure and heart rate were measured using a tail-cuff and pneumatic pulse detector before and 60 and 120 min after intragastric OLE administration. The activities of catalase, glutathione peroxidase, superoxide dismutase (SOD) and glutathione reductase in erythrocytes, as well as lipid peroxidation in plasma (pTBARS) were measured spectrophotometrically at the same time points. A high-dose of OLE did not influence blood pressure, heart rate or pTBARS in normotensive rats, while the SOD, catalase and glutathione reductase activities were significantly increased. The same dose significantly decreased blood pressure in hypertensive rats, but increased the pTBARS and SOD activity. Excessive oral intake of OLE induced moderate hypotensive effects only in spontaneously hypertensive rats, suggesting the absence of harmful hemodynamic effects after an oral overdose in both rat strains. However, its pro-oxidative role when given in a high dose in hypertensive organisms should not be neglected.

Keywords: *Olea europaea* L.; hypertension; acute oral toxicity; spontaneously hypertensive rat; oxidative stress.

INTRODUCTION

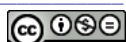
Hypertension is the most important cardiovascular risk factor worldwide, contributing nearly 50 % to prevalent coronary heart disease and approximately

*Corresponding author. E-mail: ddekan@sezampro.rs
doi: 10.2298/JSC140218030D

70 % of prevalent cerebrovascular disease burdens.¹ It is widely known that dietary changes play an important role in managing blood pressure. A number of studies showed that the Mediterranean food pattern plays a significant role in the prevention of cardiovascular disease.² It was reported that olive oil represents a key healthy component of Mediterranean diet and that dietary intake of virgin olive oil, thanks to its minor constituents, exhibits cardio-protective effects.³ Moreover, there is evidence that daily doses of blood pressure medication could be reduced during olive oil diet. This finding could be partly attributed to the polyphenols, which enhance nitric oxide (NO) concentrations and may help vaso-dilatation, which reduces blood pressure.⁴

The results of recent investigations suggested beneficial effects of phenolic-rich olive leaf extracts (OLE) as dietary supplements in modifying cardiovascular risk biomarkers, such as blood pressure, hyperglycemia, oxidative stress and inflammation, as well as in improving vascular function and lipid profiles.⁵ Several preclinical studies confirmed the antihypertensive activity of OLE or its active constituents on different experimental models,^{6,7} and the mechanisms of this action are continuously being studied. Moreover, the dual effect of OLE in both reducing blood pressure and improving lipid profile was presented as the result of clinical trials.^{8,9} OLE contains large amounts of potentially useful phytochemicals, many of the same phenolics as in olive oil, but in much higher concentrations.¹⁰ Its chemical content makes olive leaf one of the most potent natural antioxidants. The main constituent is oleuropein, an iridoide monoterpenone. This compound, obtained by decoction of olive leaves, has been recognized as one of the constituents responsible for vasodilating activity on isolated rat aorta.¹¹ Moreover, as a constituent of aqueous OLE, it showed high angiotensin-converting-enzyme (ACE) inhibitor activity.¹² Furthermore, olive leaf contains triterpenes (oleanolic, ursolic and maslinic acid) with confirmed antihypertensive, anti-atherosclerotic and antioxidant activity on a Dahl salt-sensitive, insulin-resistant genetic model of hypertension.¹³ Flavonoids, including luteolin, apigenin and quercetin, are also important antihypertensive components of OLE.^{14,15} The beneficial properties of olive leaf are further enhanced by the good absorption of its phenolic constituents and their bioavailability, which is a necessary pre-condition for its bioactivity.¹⁶

Herbal medicines are classified as dietary supplements or foods rather than drugs and do not require approval by regulatory drug agencies to be marketed. Hence, their efficacy and potential toxicity is not evaluated thoroughly. Due to traditional use, there is general opinion that these products are safe and harmless. However, many of them previously used in other forms, a diluted tea for example, may now be available as concentrated and potent extract formulations and thus potentially harmful.¹⁷ Based on the available safety/toxicity studies of total olive leaf extract and its constituents, and the history of the use of the components of



the extract through table olives, olive products and olive oil, the consumption of OLE could be considered as safe.¹⁸ A recent investigation showed that no report has indicated the negative effects of recommended, moderate doses of OLE over longer periods. However, there is an issue with many different commercial extracts of olive leaf since the composition of OLE in these products varies. There is data available that concerns the correct dosage and the side effects from long-term intake of mega doses of OLE. Recently, findings regarding the effects of different concentrations of OLE on the function of mice liver over the course of 14 weeks revealed that alanine aminotransferase and alkaline phosphatase serum enzyme activities increased significantly, and hepatic fibrosis was observed in the groups in which higher (0.5 and 0.75 %) OLE concentrations were used. All the groups exposed to OLE exhibited hyperplasia of the bile ducts, cholestasis, and hepatocyte necrosis.¹⁹ It was also shown that feeding doses of 0.2–0.9 % of OLE to Wistar rats for a period of 6 weeks may induce hematological, biochemical as well as hepatocellular and renal abnormalities of experimental animals.²⁰ Hitherto, the effects of acute excessive intake of concentrated, oleuropein-rich OLE have not been seriously investigated, in particular effects on the cardiovascular system. Hence, the safety of high-dose intake of this “cardiovascular friendly” natural product has been quite neglected.

The aim of the present study was to investigate the acute *in vivo* blood pressure effects of high doses of this natural antihypertensive agent administered to spontaneously hypertensive and to normotensive rats. In addition, the effects of high-dose of this natural antioxidant on the plasma lipid peroxidation and antioxidant defense system in erythrocytes of the both strains of experimental rats were investigated.

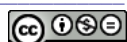
EXPERIMENTAL

Chemicals

Olive leaf extract EFLA® 943, standardized to 18–26 % of oleuropein, was purchased from Frutarom Switzerland Ltd. (Wadenswil, Switzerland). The extract was manufactured from the dried leaves of *Olea europaea* L., applying an ethanol (80 vol. %) extraction procedure. After a patented filtration process (EFLA® Hyperpure), the crude extract was dried. The stability and microbiological purity of the extract were confirmed by the manufacturer. A comprehensive phytochemical analysis was performed previously.²¹ In this study, the same batch of EFLA® 943 was used. It was kept in sealed microtubes, stored at room temperature and protected from light until use. All other chemicals used for biochemical analyses were obtained from Sigma (St Louis, MO, USA).

Animals

Male, adult, age matched spontaneously hypertensive rats (SHR) and Wistar (normotensive) rats, weighing about 280–330 g, were bred in the Institute for Medical Research, University of Belgrade. The rats were housed 4 in a cage under constant environmental conditions (20–24 °C; 12h light-dark cycle), and fed *ad libitum* with a standard chow for laboratory rats (Veterinary Institute, Subotica, Serbia).



The experimental protocol was approved by the Ethical Committee of the Institute for Medical Research, University of Belgrade, Serbia (No. 0316-1/11) according to the National Law on Animal Welfare ("Official Gazette of RS" No. 6/10, in Serbian) that is consistent with guidelines for animal research and principles of the European Convention for the Protection of Vertebrate Animals Used for Experimental and Other Purposes (Official Daily N. L 358/1-358/6, 18, December 1986) and EU Directive on the protection of animals used for scientific purposes (Directive 2010/63).

Acute oral toxicity study

Acute oral toxicity test was run strictly in accordance with OECD Guidelines for the Testing of Chemicals, Section 4: Health Effects: Test No. 423: Acute Oral toxicity – Acute Toxic Class Method, which was described in details in a recent publication.²² Briefly, three male and three female young adult Wistar rats (ten weeks old, weight 190 to 230 g) were fasted 16 h before the experiment. A single dose of 2000 mg kg⁻¹ b.w. of OLE was administered intragastrically (*i.g.*) through a metal gavage tube. Three hours after treatment, diet was available *ad libitum*. The rats were observed for abnormal behavioral signs, somnolence, dizziness, restlessness, neurological signs, respiratory distress or mortality, and weighed daily after administration of OLE. At the end of the test (day 14), the rats were sacrificed by cervical dislocation, and gross pathological changes in the main organs (brain, liver, kidney, spleen, gastric and intestinal mucosa) were evaluated.

Blood pressure and heart rate measurements

The systolic blood pressure and heart rate were indirectly measured using a tail-cuff, pneumatic pulse detector and a direct recorder (Physiograph Four, Narco Bio-System, Houston, TX, USA). Before the experiment, two separate baseline determinations of body weight and systolic blood pressure were made for all experimental animals over a span of 4 days and the rats were divided into six groups, three groups for each rat species (8 rats per group).

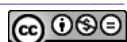
The cardiovascular effect of a high dose (2000 mg kg⁻¹, dissolved in 0.5 mL of tap water) of *i.g.*-administered OLE was investigated. The study was performed on six experimental groups according to strains and treatment they received as follows: W Control – Wistar rats received tap water (0.5 mL *i.g.*); WOLE60' and WOLE120' – Wistar rats in which the measurements of blood pressure, heart rate and oxidative stress parameters were performed 60 or 120 min after OLE administration, respectively; SH Control – spontaneously hypertensive rats (SHR) received tap water (0.5 mL *i.g.*); SHOLE60' and SHOLE120' – SHR received OLE and the measurement of hemodynamic and oxidative stress parameters were performed in 60 or 120 min after OLE administration, respectively. After cardiovascular measurement, animals were anaesthetized (35 mg kg⁻¹ sodium pentobarbital; *i.p.*) and blood samples were collected immediately. At the end of the experiment, the animals were sacrificed by a pentobarbital overdose injection.

Biochemical measurements

Blood samples were centrifuged at 4 °C at 3000 rpm for 15 minutes and erythrocytes were separated. Hemoglobin (Hb) content was estimated by the method of Drabkin and Austin.²³

All spectrophotometric analyses of the activities of the antioxidant enzymes in the plasma or erythrocytes were performed using an Ultrospec 3300 pro UV/Vis spectrophotometer (Amersham Biosciences Corp., USA).

The plasma thiobarbituric acid reactive substances (pTBARS), as a marker of plasma lipid peroxidation, were measured using 2-thiobarbituric acid (2,6-dihydrooxypyrimidine-2-



-thiol; TBA). An extinction coefficient of $156,000 \text{ M}^{-1} \text{ cm}^{-1}$ was used for the calculation²⁴ and level of pTBARS is expressed as nmol mL⁻¹ plasma.

The endogenous antioxidant status of the red blood cell was investigated in all experimental groups. The activity of catalase (CAT) was determined according to the procedure of Beutler by following the absorbance of hydrogen peroxide at 230 nm.²⁵ The activity of catalase is expressed as U g⁻¹ of hemoglobin where one unit of CAT activity is defined as mmol H₂O₂ min⁻¹.

Glutathione reductase (GR) activity was estimated according to the method of Glatzle.²⁶ The GR activity is expressed as U g⁻¹ hemoglobin, where one unit of GR activity is defined as (mmol oxidized NADPH) min⁻¹ g⁻¹ hemoglobin.

Glutathione peroxidase (GSH-Px) activity was determined according to the previously described method suggested by Paglia and Valentine.²⁷ One unit of GSH-Px activity is defined as (μmol oxidized NADPH) min⁻¹.

Activity of superoxide dismutase (SOD) was measured spectrophotometrically using a previously described method of epinephrine auto-oxidation²⁸ and is expressed as U g⁻¹ Hb.

Statistical analysis

The data are given as mean \pm SEM. One-way analysis of variance (ANOVA) was used for comparison between the experimental groups of the same rat strain, while the Fisher LSD test was performed for *post hoc* multiple comparisons. Comparison between normotensive Wistar control rats and control SHRs was made using Student's *t*-tests. *P* values less than 0.05 were considered as significant (Statistica 8.0 for Windows).

RESULTS

Acute oral toxicity

For the evaluation of acute oral toxicity of the OLE, a single dose (2000 mg kg⁻¹) was orally administered to Wistar rats. During the study period of two weeks, no death occurred in the treated animals. The body weight did not vary after drug administration, and the autopic analysis failed to show appreciable macroscopic alterations of the internal organs. The absence of adverse effects at concentrations as high as 2000 mg kg⁻¹ b.w. did not allow the calculation of the median lethal dose (*LD*₅₀) value. In principle, the method used is not intended to allow the calculation of a precise *LD*₅₀ value. Exceptionally, and only when justified by specific regulatory needs, may the use of an additional upper dose level of 5000 mg kg⁻¹ b.w. be considered. In accordance with OECD Guidelines and for concern of animal welfare, the testing of animals in GHS Category 5 ranges (2000–5000 mg kg⁻¹) is discouraged. Thus, the standardized OLE EFLA® 943 used in this study belongs to the so-called Category 5 or unclassified.

Hemodynamic and oxidative stress parameters after excessive oral intake of OLE

As expected, a significant difference (*P* < 0.001) was recorded in the systolic blood pressure and heart rate values between W Control and SHR Control (Fig. 1). Orally ingested OLE, even in high doses, did not influence the blood pressure of normotensive experimental animals. The same dose had reduced the blood pressure in SHR 60 and 120 min after the treatment by 20 and 13 %, respectively

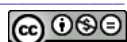


(Fig. 1A). The heart rate remained unaffected in the Wistar strain of rats. In the hypertensive rats, the heart rate was significantly higher in the SHOLE120' than in the SHOLE60' group, but there was no significant difference in comparison to the SH control group (Fig. 1B).

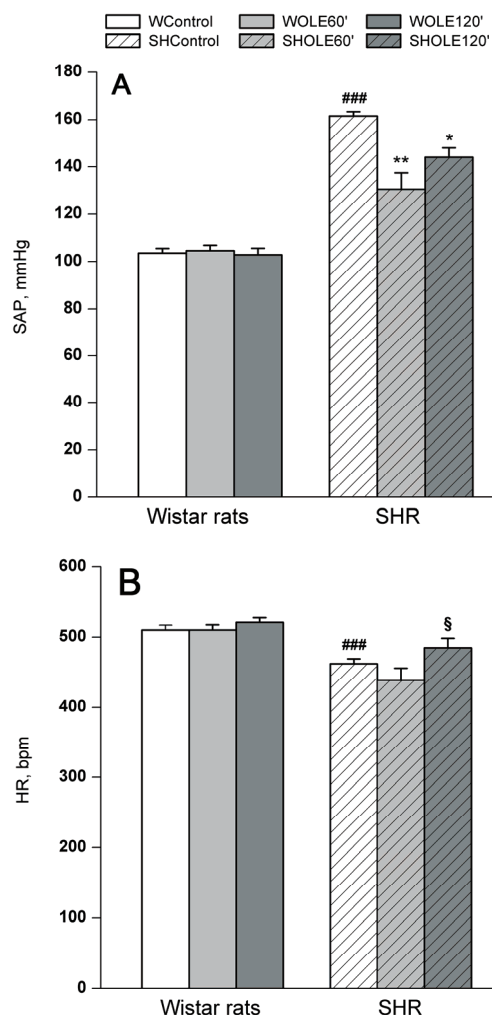


Fig. 1. Effect of *Olea europaea* L. leaf extract (OLE, 2000 mg kg⁻¹; i.g.) on: A) systolic arterial pressure (SAP, 1 mm Hg = = 133.3 Pa) and B) heart rate (HR) of normotensive Wistar (W) rats and spontaneously hypertensive rats (SHR). WControl – W rats treated with water; WOLE60' – W rats, 60 min after OLE treatment; WOLE120' – W rats, 120 min after OLE treatment; SHControl – SHR treated with water; SHOLE60' – SHR, 60 min. after OLE treatment; SHOLE120' – SHR, 120 min. after OLE treatment; *P < 0.05 and **P < 0.01, indicates statistical significance difference compared to the respective control; ###P < 0.001, the difference between SHControl and WControl groups; § indicates the difference (P < 0.05) between SHOLE120' and SHOLE60'.

In normotensive rats, pTBARS levels were unchanged in both the OLE treated groups compared to the control. However, the level of lipid peroxidation in the plasma of hypertensive animals increased significantly ($P < 0.05$) after excessive oral intake of OLE at both the examined time points (Fig. 2).

The results of the determination of the activity of four anti-oxidative enzymes at three time points, before, 60 and 120 min after OLE administration, are pre-

sented in Fig. 3. It is evident that activities of CAT and GR were significantly higher in the SH Control in comparison to the W Control group. After OLE administration to normotensive Wistar rats, the activities of CAT, SOD and GR (Fig. 3A, C and D) were significantly higher in comparison to the W Control group, while the activity of GSH-Px (Fig. 3B) was significantly lower. Administration of OLE did not influence the activities of CAT, GSH-Px and GR (Fig. 3A, B and D) in SHR, but the SOD activity was markedly increased 120 min after OLE treatment (Fig. 3C).

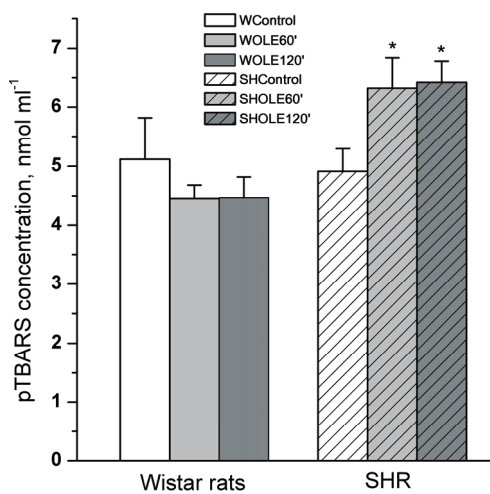


Fig. 2. Effects of *Olea europaea* L. leaf extract (OLE, 2000 mg kg⁻¹; i.g.) on the plasma concentration of thiobarbituric acid reactive substances (pTBARS) of normotensive Wistar (W) rats and spontaneously hypertensive rats (SHR). WControl – W rats treated with water; WOLE60' – W rats, 60 min after OLE treatment; WOLE120' – W rats 120 min after OLE treatment; SHControl – SHR treated with water; SHOLE60' – SHR, 60 min after OLE treatment; SHOLE120' – SHR, 120 min after OLE treatment; * indicates statistical significance ($P < 0.05$) of the difference compared to the respective control.

DISCUSSION

The purpose of this study was to evaluate the effects of excessive intake of standardized, oleuropein-rich olive leaf extract on blood pressure, heart rate and oxidative stress parameters in an established experimental model of genetically induced hypertension and in normotensive animals. To the best of our knowledge, this is the first *in vivo* study on the effects of a single high-dose OLE intake on lipid peroxidation and the activities of anti-oxidative enzymes in experimental hypertension. Thus, the results of this study represent a contribution to the overall safety assessment of *Olea europaea*-derived constituents as dietary supplements.

As a basic step in this study, OLE was assessed for acute toxicity using the OECD Test Guideline 423 (Acute Oral Toxicity – Acute Toxic Class Method). The limit test was applied since data from the literature indicated that OLE is likely to be non-toxic. There are only few preclinical safety data for various olive leaf extracts and some incomplete toxicological data concerning the toxicity of oleuropein. The LD_{50} of an extract of olive leaf was not precise when it was given intraperitoneally (*i.p.*) as a single dose of 1300 mg kg⁻¹ or as dose of 3000 mg kg⁻¹

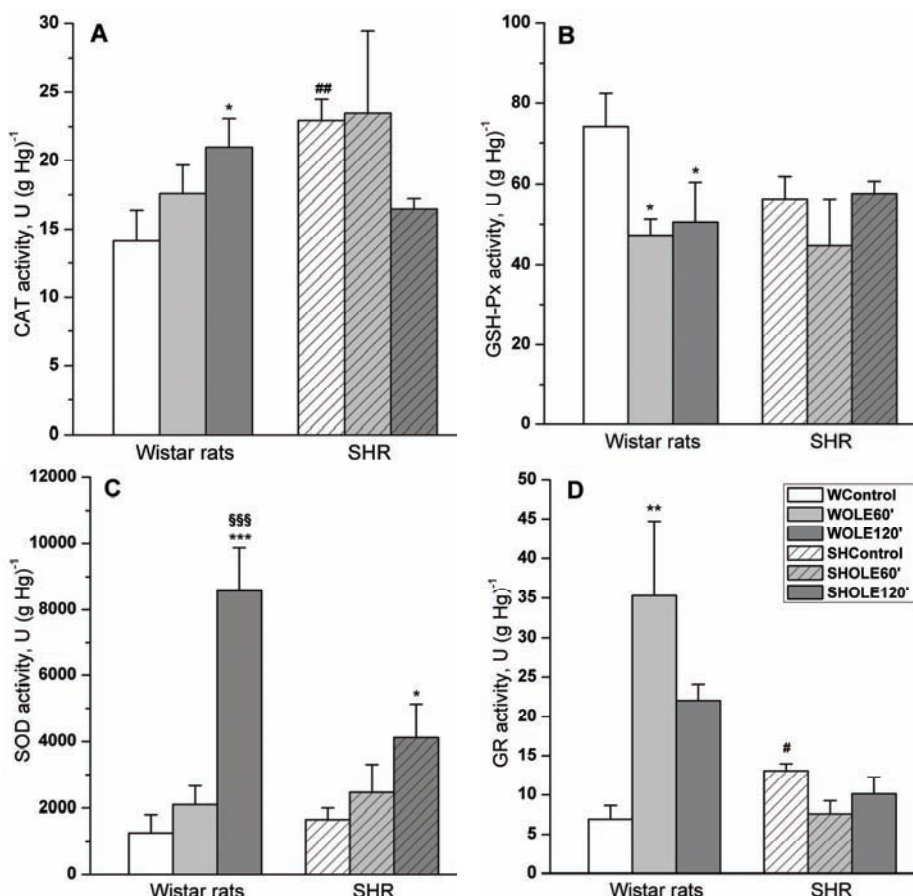


Fig. 3. Effect of *Olea europaea* L. leaf extract (OLE, 2000 mg kg⁻¹; *i.g.*) on: A) catalase (CAT), B) glutathione peroxidase (GSH-Px), C) superoxide dismutase (SOD) and D) glutathione reductase (GR) activity of normotensive Wistar (W) rats and spontaneously hypertensive rats (SHR). WControl – W rats treated with water; WOLE60' – W rats, 60 min after OLE treatment; WOLE120' – W rats, 120 min after OLE treatment; SHControl – SHR treated with water; SHOLE60' – SHR, 60 min after OLE treatment; SHOLE120' – SHR, 120 min after OLE treatment; *P < 0.05, **P < 0.01 and ***P < 0.001 indicates statistical significance difference in the enzyme activity compared to the respective control. #P < 0.05 and ##P < 0.01 represent the difference between SHControl and WControl groups; §§§ indicates the difference (P < 0.001) between WOLE120' and WOLE60'.

orally in mouse.²⁹ The LD₅₀ of a standardized aqueous olive pulp extract with hydroxytyrosol as the major constituent of biological significance was also reported to be greater than 2000 mg kg⁻¹. Moreover, in a subchronic study, the no-observed-adverse-effect-level (NOAEL) of the same extract in rats was found to be 2000 mg kg⁻¹ day⁻¹. In developmental and reproductive toxicity studies, the studied extract did not cause toxicity at levels up to 2000 mg kg⁻¹ daily.¹⁸

The results of the present acute oral toxicity study are consistent with previous findings, and confirmed that OLE EFLA® 943 is a safe material when administered *via* oral gavage to rats in a single dose of 2000 mg kg⁻¹. Clinical signs and gross findings of treatment-related adverse effects were not observed in the experimental rats.

Different experimental models were used with the intention of investigating the hypotensive effect of total olive leaf extract. In a study by Khayyal *et al.*, oral administration of OLE EFLA® 943 showed a dose dependent prophylactic effect against the rise in blood pressure induced by L-NAME.⁶ Commercial *Olea europaea* L. leaf extract caused a concentration-dependent decrease in systolic left ventricular pressure and heart rate on isolated rabbit hearts.⁷ Nevertheless, no information is available regarding its high dose activity in normotensive conditions and on an experimental model of genetically induced hypertension, such as SHR. Hence, the cardiovascular effect of excessive oral intake of OLE under hypertensive and normotensive conditions was the next step in the present study. It is known that oleuropein, the main component of OLE, is rapidly absorbed after oral administration, with maximum plasma concentration occurring after two hours.³⁰ According to this data, the tested time intervals 60 and 120 min after OLE oral administration were chosen to obtain more detailed information on the dynamic changes in the cardiovascular parameters and the oxidative stress rate in blood. The results obtained revealed that orally ingested OLE, even at the high dose of 2000 mg kg⁻¹, did not influence blood pressure and heart rate in normotensive experimental animals. The same dose reduced blood pressure by approximately 20 and 13 %, 60 and 120 min after the treatment, respectively. These findings could be explained by the dissimilar oxidative status in the normotensive and hypertensive strains of the studied rats. Namely, while multiple diverse factors likely contribute to the development of hypertension, the pathogenesis of this disease appears related, at least in part, to the development of a state of excessive oxidative stress. Local excessive superoxide production in the kidney, CNS, and vasculature, along with inflammatory activation, are central findings in hypertension models, including spontaneous hypertension in rats.^{31,32} It was previously reported that either excess production of oxidants or a deficiency of antioxidant systems may contribute to high blood pressure and the endothelium-dependent impairment of vascular relaxation in SHR.³³ The results of the same study suggested that different antioxidants (ascorbic acid, aminotriazole and glutathione), administered *in vivo* as a single dose, significantly decreased blood pressure in SHR, but not in Wistar Kyoto rats. In a previous study, the high anti-oxidative potential of OLE EFLA® 943 was confirmed *in vitro* using 2,2-diphenyl-1-picrylhydrazyl radical (DPPH[•]).³⁴ Additional findings suggested its strong anti-oxidative potential *in vivo*, in global cerebral ischemia and the reperfusion experimental model and in cold restraint stress-induced oxidative

changes in rat liver.^{34,35} According to these results and to the results from the present study, antihypertensive activity of OLE, at least partly, could be attributed to its anti-oxidative potential.

It was recently reported that extracts of *Olea europaea* L. leaves induced an increase in protein oxidation products in a concentration dependent manner.³⁶ The pro-oxidant activity of these plant extracts could be attributed to the unstable state of their phenoxy radicals. Therefore, it was reasonable to expect pro-oxidative effects of the high-dose OLE intake in the present study. It is obvious from the obtained results that OLE did not cause changes in plasma lipid peroxidation of normotensive animals. This could be explained by effective anti-oxidative protection in normotensive rats. Namely, increased CAT activity in response to enhanced H₂O₂ production (due to intensive SOD activity) probably could be responsible for the unchanged pTBARS. The antioxidant status in the SH Control group was compromised in the present study, as in the study by Yuan *et al.*³⁷ The activities of catalase, which converts hydrogen peroxide into water and molecular oxygen, and glutathione reductase, which reduces the antioxidant glutathione from its oxidized to its reduced form, were significantly higher in SHR in comparison to the activities of these enzymes in normotensive Wistar rats before OLE administration. It is important to note that anti-oxidative enzymes have a bimodal behavior. In the short term, as was the case in some other experimental models,^{34,35} their activity decreases after acute oxidative damage, while in the long term, as in the case of genetically induced hypertension,¹³ it increases; in both cases, this may be an indicator of increased oxidative damage. Good oral bioavailability, good safety profile with limited side effects, efficacy in hypertension originating from disparate etiologies, as well as limited potential for their pro-oxidative role are the recognized conditions for an optimal profile of natural antioxidant agent for anti-hypertensive therapy.³⁸ Excessive oral intake of OLE reduced high blood pressure, but induced the lipid peroxidation process in the plasma of SHR, one and two hours after administration. In parallel, the activities of anti-oxidative enzymes, except SOD, remained unaffected in SHR.

According to the results obtained in this study, it could be stated that OLE, like other dietary phenols, may be beneficial in the correct dosage. It could be considered for antihypertensive therapy in appropriate doses only, and its pro-oxidative role when given in high dose (which could not be effectively buffered by increased SOD activity) in hypertensive organism should not be neglected.

Acknowledgements. This study was supported by the Ministry of Education, Science and Technological Development of the Republic of Serbia (Grant No. 175096).

ИЗВОД

ЕФЕКТИ ВИСОКЕ ДОЗЕ ЕКСТРАКТА ЛИСТА МАСЛИНЕ НА ХЕМОДИНАМСКЕ И ПАРАМЕТРЕ ОКСИДАТИВНОГ СТРЕСА КОД НОРМОТЕНЗИВНИХ И СПОНТАНО ХИПЕРТЕНЗИВНИХ ПАЦОВА

ДРАГАНА ДЕКАНСКИ¹, НЕВЕНА МИХАИЛОВИЋ-СТАНОЈЕВИЋ², ЈЕЛИЦА ГРУЛИЋ МИЛАНОВИЋ², ЂУРЂИЦА ЈОВОВИЋ² и ЗОРАН МИЛОРАДОВИЋ²

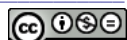
¹Биомедицинска истраживања, Институут за истраживање и развој, Галеника а.г., Пасјерова 2, 11000 Београд и ²Група за кардиоваскуларну физиологију, Институут за медицинска истраживања, Универзитет у Београду, Др Суботића 4, Београд

Антихипертензивно дејство природног антиоксиданса, екстракта листа маслине (OLE) је познато, али до сада није испитиван његов утицај на кардиоваскуларни систем када се примењује у високој дози. Наш циљ је био да одредимо акутне ефекте прекомерног уноса стандардизованог екстракта на крвни притисак, срчану фреквенцију и оксидативни статус како код пацова са урођеном хипертензијом, тако и код Вистар пацова са нормалним артеријским притиском. Систолни притисак и фреквенција рада срца мерењи су помоћу уређаја за индиректно регистровање крвног притиска у репној артерији, пре интрагастричног апликовања OLE, 60 и 120 min након давања. У истим временским тачкама, спектрофотометријски су мерење активности каталазе, глутатион-пероксидазе, супероксид дисмутазе (SOD) и глутатион редуктазе у еритроцитима, као и липидна пероксидација у плазми (rTBARS). OLE у дози од 2000 mg kg⁻¹ није утицао на крвни притисак, срчану фреквенцију и rTBARS код нормотензивних пацова, док су се активности SOD, каталазе и глутатион-редуктазе значајно повећале. Иста доза довела је до значајног смањења крвног притиска код хипертензивних животиња, али је повећала вредности rTBARS и активност SOD. Унос OLE у дози од 2000 mg kg⁻¹ изазвао је умерен хипотензивни ефекат само код пацова са спонтаном хипертензијом, указујући на одсуство штетних хемодинамских дејстава након предозирања код оба соја пацова, али не би требало занемарити прооксидативно дејство његових високих доза у хипертензивном организму.

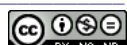
(Примљено 18. фебруара, ревидирано 26. марта, прихваћено 27. марта 2014)

REFERENCES

1. G. Mancia, R. Fagard, K. Narkiewicz, J. Redón, A. Zanchetti, M. Böhm, T. Christiaens, R. Cifkova, G. De Backer, A. Dominiczak, M. Galderisi, D. E. Grobbee, T. Jaarsma, P. Kirchhof, S. E. Kjeldsen, S. Laurent, A. J. Manolis, P. M. Nilsson, L. M. Ruilope, R. E. Schmieder, P. A. Sirnes, P. Sleight, M. Viigimaa, B. Waeber, F. Zannad, *J. Hypertens.* **31** (2013) 1281
2. R. Estruch, M. A. Martínez-González, D. Corella, J. Salas-Salvadó, V. Ruiz-Gutiérrez, M. I. Covas, M. Fiol, E. Gómez-Gracia, M. C. López-Sabater, E. Vinyoles, F. Arós, M. Conde, C. Lahoz, J. Lapetra, G. Sáez, E. Ros, *Ann. Intern. Med.* **145** (2006) 1
3. M. I. Covas, K. Nyysönen, H. E. Poulsen, J. Kaikkonen, H. J. Zunft, H. Kiesewetter, A. Gaddi, R. de la Torre, J. Mursu, H. Bäumler, S. Nascenti, J. T. Salonen, M. Fitó, J. Virtanen, J. Marrugat, *Ann. Intern. Med.* **145** (2006) 333
4. L. A. Ferrara, A. S. Raimondi, L. d' Episcopo, L. Guida, A. Dello Russo, T. Marotta, *Arch. Intern. Med.* **160** (2000) 837
5. S. Lockyer, P. Yaqoob, J. P. E. Spencer, I. Rowland, *Nutr. Aging* **1** (2012) 125
6. M. T. Khayyal, M. A. El-Ghazaly, D. M. Abdallah, N. N. Nassar, S. N. Okpanyi, M. H. Kreuter, *Arzneim.-Forsch.* **52** (2002) 797



7. A. Scheffler, H. W. Rauwald, B. Kampa, U. Mann, F. W. Mohr, S. Dhein, *J. Ethnopharmacol.* **120** (2008) 233
8. T. Perrinjaquet-Moccetti, A. Busjahn, C. Schmidlin, A. Schmidt, B. Bradl, C. Aydogan, *Phytother. Res.* **22** (2008) 1239
9. E. Susalit, N. Agus, I. Effendi, R. R. Tjandrawinata, D. Nofiarny, T. Perrinjaquet-Moccetti, M. Verbruggen, *Phytomedicine* **18** (2011) 251
10. S. Silva, L. Gomes, F. Leitão, A. V. Coelho, L. V. Boas, *Food Sci. Technol. Int.* **12** (2006) 385
11. A. Zarzuelo, J. Duarte, J. Jiménez, M. González, M. P. Utrilla, *Planta Med.* **57** (1991) 417
12. K. Hansen, A. Adsersen, S. Brøgger Christensen, S. Rosendal Jensen, U. Nyman, U. Wagner Smitt, *Phytomedicine* **2** (1996) 319
13. L. I. Somova, F. O. Shode, P. Ramnanan, A. Nadar, *J. Ethnopharmacol.* **84** (2003) 299
14. M. Sánchez, M. Galisteo, R. Vera, I. C. Villar, A. Zarzuelo, J. Tamargo, F. Perez-Vizcaino, J. Duarte, *J. Hypertens.* **24** (2006) 75
15. S. K. Shukla, S. Gupta, S. K. Ojha, S. B Sharma, *Nat. Prod. Res.* **24** (2010) 873
16. M. Kendall, M. Batterham, D. L. Callahan, D. Jardine, P. D. Prenzler, K. Robards, D. Ryan, *Food Chem.* **130** (2012) 651
17. C. B. Rasmussen, J. K. Glisson, D. S. Minor, *J. Clin. Hypertens. (Greenwich)* **14** (2012) 467
18. M. G. Soni, G. A. Burdock, M. S. Christian, C. M. Bitler, R. Crea, *Food Chem. Toxicol.* **44** (2006) 903
19. R. Arantes-Rodrigues, A. Henriques, M. J. Pires, B. Colaço, A. M. Calado, P. Rema, A. Colaço, T. Fernandes, P. L. De la Cruz, C. Lopes, L. Fidalgo-Gonçalves, S. Vilela, T. Pedrosa, F. Peixoto, P. A. Oliveira, *Food Chem. Toxicol.* **49** (2011) 1989
20. S. A. Omer, M. A. Elobeid, M. H. Elamin, Z. K. Hassan, P. Virk, M. H. Daghestani, E. M. Al-Olayan, N. A. Al-Eisa, Z. M. Almarhoon, *Asian J. Anim. Vet. Adv.* **7** (2012) 1175
21. D. Dekanski, S. Janićijevic-Hudomal, V. Tadić, G. Marković, I. Arsić, D. M. Mitrović, *J. Serb. Chem. Soc.* **74** (2009) 367
22. D. Dekanski, T. Todorović, D. Mitić, N. Filipović, N. Polović, K. Andelković, *J. Serb. Chem. Soc.* **78** (2013) 1503
23. D. L. Drabkin, J. H. Austin, *J. Biol. Chem.* **112** (1935) 51
24. H. Ohkawa, N. Ohishi, K. Yagi, *Anal. Biochem.* **95** (1979) 351
25. E. Beutler, *Red Cell Metabolism, a Manual of Biochemical Methods*, Grune and Stratton, New York, 1982, p. 105
26. D. Glatzle, J. P. Vuilleumier, F. Weber, K. Decker, *Experientia* **30** (1974) 665
27. D. E. Paglia, W. N. Valentine, *J. Lab. Clin. Med.* **70** (1967) 158
28. H. P. Misra, I. Fridovich, *J. Biol. Chem.* **247** (1972) 3170
29. J. A. Duke, *Handbook of Medicinal Herbs*, CRC Press, Boca Raton, FL, 2002, p. 535
30. P. Del Boccio, A. Di Deo, A. De Curtis, N. Celli, L. Iacoviello, D. Rotilio, *J. Chromatogr., B* **785** (2003) 47
31. J. Friedman, E. Peleg, T. Kagan, S. Shnizer, T. Rosenthal, *Am. J. Hypertens.* **16** (2003) 1049
32. D. G. Harrison, M. C. Gongora, *Med. Clin. North Am.* **93** (2009) 621
33. M. J. Akpaffiong, A. A. Taylor, *Am. J. Hypertens.* **11** (1998) 1450
34. D. Dekanski, V. Selaković, V. Piperski, Ž. Radulović, A. Korenić, L. Radenović, *Phytomedicine* **18** (2011) 1137



35. D. Dekanski, S. Ristić, N. V. Radonjić, N. D. Petronijević, A. Dekanski, D. M. Mitrović., *J. Serb. Chem. Soc.* **76** (2011) 1207
36. O. Y. El-Khawaga, M. A. Abou-Seif, *Eur. Rev. Med. Pharmacol.* **14** (2010) 731
37. Y. V. Yuan, D. D. Kitts, D. V. Godin, *Can. J. Physiol. Pharmacol.* **74** (1996) 290
38. T. J. Kizhakekutty, M. E. Widlansky, *Cardiovasc. Ther.* **28** (2010) e20.





Anatase titania–vanadium polyphosphomolybdate as an efficient and reusable nano catalyst for the desulphurization of gas oil

MOHAMMAD ALI REZVANI^{1*}, ABDOLLAH FALLAH SHOJAEI²
and FAROKHZAD MOHAMADI ZONOZ³

¹Department of Chemistry, Faculty of Science, University of Zanjan, 45371-38791 Zanjan,

Iran, ²Department of Chemistry, Faculty of Science, University of Guilan, 419961-3769

Rasht, Iran and ³Department of Chemistry, Hakim Sabzevari University, Sabzevar, 397, Iran

(Received 25 October 2013, revised 20 February, accepted 24 February 2014)

Abstract: $(Bu_4N)_4H[PMo_{10}V_2O_{40}]$ –TiO₂ nanocomposite has been synthesized by a reaction of $(Bu_4N)_4H[PMo_{10}V_2O_{40}]$ with titanium tetraisopropoxide at 100 °C via the sol–gel method. The crushed nano layer of the anatase phase was 20 nm in nature and the fixing of $(Bu_4N)_4H[PMo_{10}V_2O_{40}]$ decreased its size. This nano polyphosphomolybdate was shown to be able to oxidatively desulphurize simulated gas oil with a high S conversion (more than 98 %). In the present work, the efficient oxidative desulphurization of gas oil and simulated gas oil using the formic acid/hydrogen peroxide system is reported. This system provides an efficient, convenient and practical method for scavenging sulfur compound.

Keywords: polyoxometal; desulfurization; anatase; gas oil; nanocomposite.

INTRODUCTION

The catalytic function of heteropolyacids (HPAs) has attracted much attention because of their uncommon ability to accept an electron without deformation of their structure or reversible reduction.^{1–4} Keggin type polyoxoanions have been widely studied as homogeneous and heterogeneous catalyst for the oxidation of organic compounds, whereas the application of Wells–Dawson type polyoxoanions is mostly limited to homogeneous or gas phase applications and only a few of them have demonstrated catalytic activity in the heterogeneous form.^{5–7} Generally, Keggin structures show more acidity and catalytic activity among the heteropolyacids.⁸ These solid acids are usually insoluble in non-polar solvents but highly soluble in polar ones. They can be used in bulk or supported forms in both homogeneous and heterogeneous systems.⁹ Further catalytically important subclasses of the Keggin compounds are the mixed-addenda vanadium

*Corresponding author. E-mail: marezvani2010@gmail.com
doi: 10.2298/JSC131026015A

(V) substituted HPAs with the general formula $H_{3+n}PM_{12-n}V_nO_{40}$ ($M = Mo$ and W ; $n = 1$ to 6). The best known of these HPAs is the 10-molybdo-2-vanado-phosphoric acid $H_5PV_2Mo_{10}O_{40}$). This compound contains a central PO_4 tetrahedron, surrounded by 12 MO_6 ($10MoO_6 + 2VO_6$) octahedra arranged in four M_3O_{13} group-edge-sharing octahedra. The edge-sharing M_3O_{13} groups are linked to each other and to the central tetrahedron by shared corners. $H_5PV_2Mo_{10}O_{40}$ has been extensively used as an effective redox catalyst in homogeneous oxidation processes.¹⁰ There are fewer reports regarding the application of $H_5PV_2Mo_{10}O_{40}$ as an acid catalyst for organic transformations for the simple reason that V^{5+} is the most strongly oxidizing element and can be readily reduced to V^{4+} with concomitant oxidation of an organic substrate. In fact, the introduction of V^{5+} into the Keggin framework shifts its catalytic activity from acid-dominated to redox-dominated. Deep desulphurization of transportation fuels has become an important research subject due to the increasingly stringent regulations and fuel specifications in many countries for the purpose of environmental protection.^{11–13} In the conventional hydrodesulphurization (HDS) process, it is difficult to remove alkyl-substituted dibenzothiophenes, such as 4,6-dimethylbenzothiophene, which are refractive to HDS due to steric hindrance. In order to produce ultralow sulfur diesel fuel using the HDS process, higher temperature, higher pressure, larger reactor volume and catalysts that are more active are required. Therefore, alternative desulphurization techniques have been widely investigated, among which oxidative desulphurization (ODS) is considered to be one of the promising new methods for super deep desulphurization of fuel oil.^{12–14} Various oxidants have been used in ODS, such as NO_2 , O_3 , H_2O_2 and solid oxidizing agents.^{11–16} Among these oxidants, H_2O_2 is mostly chosen as an oxidant, as only water is produced as a byproduct. Peracids produced *in situ* from organic acids catalysts and H_2O_2 are reported to be very effective for rapid oxidation of sulfur compounds in fuel oils under mild conditions. Homogeneous catalysts cannot be separated from the reaction media and, consequently, cannot be reused. Fixation of homogeneous catalysts onto a solid support may be a strategy to overcome this problem. Recently, supported heteropolyacids have been synthesized and applied as effective catalyst in organic reactions.^{17–19} Supporting the heteropolyacids on solids with high surface areas improve their catalytic performance in various liquid–solid and solid surface heterogeneous reactions. Titanium dioxide is a wide-band-gap semiconductor material that has received intense scrutiny for a broad range of applications, thanks to its intriguing physicochemical properties, as well as being cheap, abundant, and reasonably nontoxic. TiO_2 , also a widely used catalyst and catalyst support is known to enhance the catalytic activity in many cases because of the strong interaction between the active phase and the support.¹⁷

In continuation of ongoing research into the synthesis and application of polyoxometalates (POM) and anatase,^{18–26} anatase TiO₂ crushed nano leaf coupled by a sandwich type polyoxometalate was fabricated at 100 °C via the sol-gel method under oil bath conditions. The chemical characterization of this fabrication was accomplished by means of elemental analysis, IR, ³¹P- and ¹¹³Cd-NMR spectroscopy, and XRD and TEM analyses. The catalytic performance of these homogenous and heterogeneous catalysts were tested on the oxidative desulphurization of model sulfur compounds, *i.e.*, benzothiophene (BT), dibenzothiophene (DBT), 4-methyldibenzothiophene (4-MDBT), and 4,6-dimethyldibenzothiophene (4,6-DMDBT) and gas oil, using formic acid/hydrogen peroxide as the oxidizing reagent. The POM-TiO₂ nanocomposite presented much higher catalytic activity than those of unsupported polyoxometalates. The catalyst could be easily separated and reused at the end of the reaction without significant loss of its catalytic activity, which suggests that the catalyst is stable under different conditions.

EXPERIMENTAL

All employed reagents and solvents were commercially available and used as received, unless otherwise indicated. The model compounds and chemicals, including BT, DBT, 4-MDBT and 4,6-DMDBT, solvent (*n*-heptane) for the experiments and analyses and hydrogen peroxide (30 vol. %) were obtained from Aldrich Chemical Company. Preparation of the H₅PV₂Mo₁₀O₄₀ catalyst and other mixed heteropolyacids and salts were based on a literature procedure with modifications.^{20,21} Titanium (IV) tetra-isopropoxide and glacial acetic acid were obtained from Merck Chemical Company. Gas oil (density 0.8361 g mL⁻¹ at 15 °C, total sulfur content 0.98 wt. %) was supplied from the terminal of the North Iranian Oil Company (Table I).

TABLE I. Properties of the actual gas oil; abbreviations: API GR.: API gravity (API – American Petroleum Institute); API = 141.5/Specific gravity–131.5; Viscosity KIN: Kinematic viscosity

| Entry | Properties of gas oil | Method | Results |
|-------|--------------------------------------|------------|---------|
| 1 | Specific gravity at 60/60, °F | ASTM D1298 | 0.8365 |
| 2 | Density at 15 °C, g cm ⁻³ | ASTM D1298 | 0.8361 |
| 3 | API GR. 60/60, °F | Calculated | 37.66 |
| 4 | Flash point, °C | ASTM D93 | 142 |
| 5 | Water content, vol. % | ASTM D4006 | 0.025 |
| 6 | Total sulfur content, wt. % | ASTM D4294 | 0.98 |
| 7 | Cloud point, °C | ASTM D2500 | –4 |
| 8 | Color test | ASTM D156 | 1.5 |
| 9 | Viscosity KIN at 50 °C, CST | ASTM D445 | 2.8 |
| 10 | Pour point, °C | ASTM D97 | –9 |
| 11 | Mercaptans, ppm | ASTM D3227 | 286 |
| 13 | Initial boiling point (IBP), °C | ASTM D86 | 157.8 |
| 14 | 10 % Distillation, °C | ASTM D86 | 194.6 |



TABLE I. Continued

| Entry | Properties of gas oil | Method | Results |
|-------|-------------------------------|----------|---------|
| 15 | 20 % Distillation, °C | ASTM D86 | 213.4 |
| 16 | 50 % Distillation, °C | ASTM D86 | 268.6 |
| 17 | 90 % Distillation, °C | ASTM D86 | 353.9 |
| 18 | Final boiling point (FBP), °C | ASTM D86 | 384.9 |
| 19 | Distillation residue, vol. % | ASTM D86 | 1.5 |
| 20 | Distillation loss, vol. % | ASTM D86 | 1 |
| 21 | Distillation recovery, vol. % | ASTM D86 | 97.5 |

Preparation of the catalyst

$(\text{Bu}_4\text{N})_4\text{H}[\text{PMo}_{10}\text{V}_2\text{O}_{40}]$ was prepared as follows: Sodium metavanadate (12.2 g, 100 mmol) was dissolved by boiling in 50 mL of water and then mixed with 3.55 g (25.0 mmol) of Na_2HPO_4 in 50 mL of water. After the solution had cooled, concentrated sulfuric acid (5 mL, 17 M, 85 mmol) was added, whereby the solution developed a red color. Then, $\text{Na}_2\text{MoO}_4 \cdot 2\text{H}_2\text{O}$ (60.5 g, 250 mmol) dissolved in 100 mL of water was added to the red solution under vigorous stirring, followed by the slow addition of a solution of 1.0 g (3.7 mmol) of tetrabutylammonium bromide in 5.0 mL of H_2O . The mixture was stirred at 60 °C for 3 h. The formed white precipitate was filtered off, recrystallized from acetonitrile and diethyl ether, and air dried.²¹

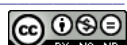
Preparation of the nanocatalyst

The $(\text{Bu}_4\text{N})_4\text{H}[\text{PMo}_{10}\text{V}_2\text{O}_{40}]$ – TiO_2 nanoparticle was prepared as follows: titanium tetraisopropoxide was added into glacial acetic acid with stirring. Next, a solution of $(\text{Bu}_4\text{N})_4\text{H}[\text{PMo}_{10}\text{V}_2\text{O}_{40}]$ in water was added drop-wise. The mixture was stirred to dissolve any solid. Then, the sol was heated to 100 °C under oil bath conditions until a homogenous $(\text{Bu}_4\text{N})_4\text{H}[\text{PMo}_{10}\text{V}_2\text{O}_{40}]$ – TiO_2 hydrogel was formed. Finally, the gel was filtered, washed with deionized water–acetone and dried in oven at 50 °C overnight.¹⁷

Oxidative desulphurization (ODS) of simulated gas oil using the formic acid/ H_2O_2 system

Some typical benzothiophenes and dibenzothiophenes, which represent easy, hard and very hard to remove sulfur species in gas oil, were selected to evaluate the catalysts and the reactivity of the benzothiophenes and dibenzothiophenes in the oxidation reaction. The water bath was first heated up and stabilized to the desired reaction temperature (25–80 °C). A model sulfur compound (BT, DBT, 4-MDBT or 4,6-DMDBT) was dissolved in *n*-heptane to make a stock solution with a sulfur content of 500 ppm. Then, 5 mL of the model sulfur compound, mixed with 2 mL formic acid/ H_2O_2 (performic acid, formic acid/hydrogen peroxide mole ratio of 1) was added into the flask. The flask was immersed in a heating bath and stirred at 500 rpm for 2 h. The biphasic mixture was separated by decantation. It reached the reaction temperature in about 15 min. After withdrawing the first sample, 0.1 g of the nanocomposite $(\text{Bu}_4\text{N})_4\text{H}[\text{PMo}_{10}\text{V}_2\text{O}_{40}]$ – TiO_2) catalyst was added to the flask to initiate the reaction. The sulfur concentration of the sample was determined using a Tanaka Scientific RX-360 SH X-ray fluorescence spectrometer (ASTM D-4294 method and D-3227).

ASTM D-4294. This test method covers the measurement of sulfur in hydrocarbons, such as diesel, naphtha, kerosene, residuals, lubricating base oils, hydraulic oils, jet fuels, crude oils, gasoline (all unleaded) and other distillates. Compared to the other test methods for sulfur determination, the test method D-4294 has a high throughput, minimal sample preparation, good precision, and is capable of determining sulfur over a wide range of concentrations. The



equipment specified is in most cases less costly than that required for alternative methods. In the case of petroleum materials that contain suspended water, it is recommended that the water be removed before testing or that the sample be thoroughly homogenized and immediately tested. The interference is greatest if the water creates a layer over the transparent film, as this would attenuate the X-ray intensity for sulfur. One such method to accomplish the removal of water is to centrifuge the sample first under ambient sealed conditions, taking care that the sample integrity is not compromised. The results are given in Table II.

TABLE II. Oxidative desulphurization of gas oil by $(Bu_4N)_4H[PMo_{10}V_2O_{40}]$ – TiO_2

| Entry | Properties of gas oil | Before ODS | After ODS ^a | After ODS ^b |
|-------|--------------------------------------|------------|------------------------|------------------------|
| 1 | Total sulfur content, wt. % | 0.98 | 0.068 | 0.072 |
| 2 | Density at 15 °C, g cm ⁻³ | 0.8361 | 0.8358 | 0.8364 |
| 3 | Mercaptans, ppm | 286 | 8 | 11 |
| 4 | Flash point, °C | 142 | 142 | 142 |
| 5 | Water content, vol. % | 0.025 | 0.025 | 0.025 |
| 6 | Cloud point, °C | –4 | –4 | –4 |
| 7 | Color test | 1.5 | 1.5 | 1.5 |
| 8 | Viscosity KIN at 50 °C, CST | 2.8 | 2.7 | 2.5 |
| 9 | Pour point, °C | –9 | –9 | –9 |
| 10 | Distillation IBP, °C | 157.8 | 156.9 | 157.5 |
| 11 | Distillation FBP, °C | 384.9 | 382.6 | 384.0 |

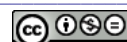
^aConditions for the desulphurization: 5 mL of gas oil (9800 ppm S), 0.1 g nano-catalyst, 2 mL oxidant, 5 mL extraction solvent, time = 2 h, temperature = 80 °C; ^breuse of the catalyst in the desulphurization of gas oil

Oxidative desulphurization (ODS) of gas oil using the formic acid/ H_2O_2 system

In the same manner as the oxidation of the model sulfur compounds but using actual gas oil (sulfur 2300 ppm, 10 mL) with 0.1 g nanocatalyst ($(Bu_4N)_4H[PMo_{10}V_2O_{40}]$ – TiO_2), 2 mL formic acid/ H_2O_2 (formic acid/hydrogen peroxide mole ratio of 1) and temperature 80 °C. After completion of the oxidation, the oxidized sulfur in the gas oil was extracted with acetonitrile at room temperature. The acetonitrile/oil ratio used was 1/2 by volume. The biphasic mixture was separated by decantation. The oil phase was separated and weighed to calculate % recovery of gas oil (for three times reaction: 98, 96 and 95 %). The sulfur content in the oil before and after reaction was determined using X-ray fluorescence spectrometer (ASTM D-4294 method). According to data in Table II, after the oxidation process, the total sulfur content (Entry 1) and content of mercaptans (Entry 2) were much lower, while numerous other properties of gas oil showed in Table II remained unaffected. From the results obtained in this work, it was demonstrated that the nanocomposite ($(Bu_4N)_4H[PMo_{10}V_2O_{40}]$ – TiO_2) could catalyze the oxidative desulphurization reaction in 2 h and could reduce the total sulfur content in the gas oil from 0.98 to 0.068 wt. % and reduce content of mercaptans from 286 to 8 ppm. The addition of formic acid enhanced the conversion.

Recycling of the catalyst

At the end of the oxidative desulphurization of the model sulfur compounds and gas oil, the catalyst was filtered and washed with dichloromethane. In order to determine whether the catalyst would succumb to poisoning and lose its catalytic activity during the reaction, the reusability of the catalyst was investigated. For this purpose, we carried out the desulphurization reaction of gas oil and model compounds in the presence of fresh and recovered catalyst (Table II). Even after three runs for the reaction, the catalytic activity of



$(Bu_4N)_4H[PMo_{10}V_2O_{40}]$ – TiO_2) was almost the same as that of freshly used catalyst. The results are summarized in Table II.

RESULT AND DISCUSSION

Characterization of synthesized catalysts

The XRD pattern corresponding to pure TiO_2 was found to match with that of fully anatase phase. No peaks from any impurities or the rutile phase were observed, which indicates the high purity of the obtained powders. The sharp diffraction peaks confirmed that the obtained TiO_2 was of high crystallinity. When $(Bu_4N)_4H[PMo_{10}V_2O_{40}]$ was bound to the TiO_2 surface, $(Bu_4N)_4H[PMo_{10}V_2O_{40}]$ had disappeared and the final pattern matched that of fully anatase phase of TiO_2 (JCPDS No. 21-1272), which was most likely because $(Bu_4N)_4H[PMo_{10}V_2O_{40}]$ formed only a thin coating on the TiO_2 surface and thus the majority of the observed signals were due to the crystal phases of anatase TiO_2 . A TEM image of the obtained fully anatase phase of TiO_2 as a crushed nano leaf indicate an average size of about 25 nm. After modification of anatase with $(Bu_4N)_4H[PMo_{10}V_2O_{40}]$, a significant change in the morphology and size occurred. In the TEM image, most of the obtained powders consisted of nano particles with an average size of about 10 nm but there were some nano rods. In ultraviolet light regions, which are shorter than 332 nm, pure nano- TiO_2 , the band gap energy of which corresponds to around 320 nm (3.60 eV), shows the highest absorbance because of charge-transfer from the valence band (mainly formed of the 2p orbitals of the oxide anions) to the conduction band (mainly formed by 3d t_{2g} orbitals of Ti^{4+}).¹⁷ In addition, $(Bu_4N)_4H[PMo_{10}V_2O_{40}]$ showed an absorbance maximum at 230 nm attributed to charge transfer (CT) from O 2p to W 5d of the Keggin units at the W–O and W–O–W bonds. The $(Bu_4N)_4H[PMo_{10}V_2O_{40}]$ – TiO_2 nanocomposite showed strong and broad optical absorption in the range from 220 to 330 nm, and a red shift is observed compared with the parent $(Bu_4N)_4H[PMo_{10}V_2O_{40}]$, and a blue shift compared with anatase. The above UV–Vis results indicate that the introduction of $(Bu_4N)_4H[PMo_{10}V_2O_{40}]$ into TiO_2 framework has an influence on the coordination environment of crystalline TiO_2 .^{17,20}

Catalytic results

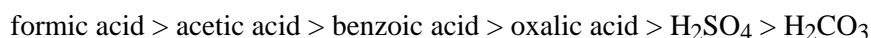
Effect of the oxidation system on the oxidative desulphurization of gas oil or simulated gas oil. In this study, many types of oxidative systems, such as H_2O_2 /organic acids, H_2O_2 /POMs, H_2O_2 /POMs– TiO_2 , were investigated. Formic acid, benzoic acid, oxalic acid, acetic acid, H_2SO_4 and H_2CO_3 were selected to acidify the system, and were added into the gas oil or simulated gas oil solutions in a mole ratio of 1:1 with 30 % H_2O_2 . The reactions were performed at 80 °C for 2 h. The results given in Table III show that the oxidation reactivities of the inorganic acids, H_2SO_4 and H_2CO_3 , were lower than those of the organic acids

because the inorganic acids are insoluble in the gas oil and simulated gas oil solutions.

TABLE III. Effect of different acids in the presence of hydrogen peroxide and $(Bu_4N)_4H[PMo_{10}V_2O_{40}]$ -TiO₂ in the oxidative desulfurization of different sulfur compounds; conditions for the desulfurization: 2 mL acid/H₂O₂ as oxidant, 0.1 mmol nanocatalyst ($(Bu_4N)_4H[PMo_{10}V_2O_{40}]$ -TiO₂), 5 mL DMF as extraction solvent, time 2 h, temperature 80 °C

| Entry | Acid used | Conversion, % | | | |
|-------|--------------------------------|---------------|--------|-----------|----|
| | | DBT | 4-MDBT | 4,6-DMDBT | BT |
| 1 | Formic acid | 98 | 96 | 97 | 94 |
| 2 | Benzoic acid | 94 | 90 | 94 | 90 |
| 3 | Oxalic acid | 92 | 86 | 92 | 92 |
| 4 | Acetic acid | 97 | 96 | 97 | 93 |
| 5 | H ₂ SO ₄ | 79 | 75 | 78 | 72 |
| 6 | H ₂ CO ₃ | 77 | 73 | 77 | 71 |

The order of the oxidative reactivity of the different acids in the presence of hydrogen peroxide and $(Bu_4N)_4H[PMo_{10}V_2O_{40}]$ -TiO₂ was:



Effect of types of the sulfur compound on the desulphurization of simulated gas oil. The reactivities of different sulfur-containing compounds, including benzothiophene (BT), 4-methyldibenzothiophene (4-MDBT), dibenzothiophene (DBT) and 4,6-dimethyldibenzothiophene (4,6-DMDBT), were investigated for oxidative desulphurization using hydrogen peroxide and formic acid. The electron densities of the thiophene derivatives varied between 5.696 (thiophene) and 5.760.¹⁶ Thiophene is usually oxidized with difficulty because of its low electron density. BT (electron density 5.739) and the other model compounds with higher electron densities were oxidized to form their corresponding sulfones. The apparent rate constants (*k*) for these oxidations decreased as follows: 4,6-DMDBT > 4-MDBT > DBT > BT.¹⁶ This result indicates that the rate constant increased with increasing electron density. The oxidation reactivities decreased according to DBT > 4-MDBT > 4,6-DMDBT, and the same reactivity trend was found for ODS. The apparent activation energies of DBT, 4-MDBT, and 4,6-DMDBT oxidation were 53.8, 56.0, and 58.7 kJ mol⁻¹, respectively. These results indicate that DBT oxidation was achieved under mild reaction conditions and it was easy to increase the reaction temperature or reaction time to achieve high conversions, even for the least reactive 4,6-DMDBT that showed a lower reactivity compared with DBT, as methyl substituents were present at the 4 and 6 positions on the DBT rings. In addition, the formic acid/H₂O₂ and polyoxometalates/H₂O₂ biphasic catalytic systems have completely different reactivity orders for the oxidation of DBTs because of the important role of the molecular size of the catalyst.¹⁸ For the formic acid catalyzed reaction, the formic acid can interact with sulfur with-



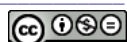
out any steric hindrance from alkyl groups. Therefore, the reactivity trend obtained in the formic acid catalyzed reactions reflected the intrinsic oxidative reactivity of the DBTs. Phosphotungstic compounds convert to polyoxoperoxo complexes in the presence of hydrogen peroxide.^{18,19} The tungsten atom in this polyoxoperoxo species is in a highly crowded rigid structure. The effects of different catalysts in the oxidative desulphurization of different sulfur-containing compounds are listed in Table IV. The alkyl groups of dialkyl DBT likely sterically hinder the polyoxoperoxo species from interacting with DBT *via* the sulfur atom to form a transition state. Therefore, the oxidation reactivity trend in polyoxometalates/H₂O₂ in a biphasic catalytic system imply the presence of steric hindrance because of the alkyl groups. These results suggest that there is little steric hindrance in the amphiphilic compounds. The oxidation reactivity decreased in the order of DBT > 4,6-DMDBT > 4-MDBT > BT. BT exhibited the lowest reactivity, and this was related to the different electron density on the sulfur atom. Difference in electron density on the sulfur atom is for DBT and 4,6-DMDBT very small. The oxidation reactivity was governed by the strict hindrance of the methyl groups, which become an obstacle for the approach of the sulfur atom to the catalytically active spaces. The electron density for 4,6-DMDBT is the highest, but its oxidation reactivity is lower than DBT, this is due to the steric effect from the alkyl groups at the 4 and 6 position.

TABLE IV. Effect of different catalysts on the oxidative desulphurization of different sulfur compounds; conditions for the desulphurization: 2 mL H₂O₂/formic acid as oxidant, 0.1 mmol catalyst, 5 mL DMF as extraction solvent, time 2 h, temperature 80 °C

| Entry | Catalyst | Conversion, % | | | |
|-------|--------------------------------------------------------------------------------------------------------|---------------|--------|-----------|----|
| | | DBT | 4-MDBT | 4,6-DMDBT | BT |
| 1 | (Bu ₄ N) ₄ H[PMo ₁₀ V ₂ O ₄₀]–TiO ₂ | 98 | 96 | 97 | 94 |
| 2 | (Bu ₄ N) ₄ H[PMo ₁₀ V ₂ O ₄₀] | 93 | 92 | 93 | 90 |
| 3 | H ₅ PMo ₁₀ V ₂ O ₄₀ | 92 | 91 | 92 | 89 |
| 4 | H ₄ PMo ₁₁ VO ₄₀ | 91 | 90 | 91 | 88 |
| 5 | H ₆ PMo ₉ V ₃ O ₄₀ | 91 | 88 | 90 | 87 |
| 6 | H ₃ PMo ₁₂ O ₄₀ | 90 | 88 | 90 | 86 |
| 7 | H ₃ PW ₁₂ O ₄₀ | 90 | 87 | 90 | 85 |
| 8 | H ₄ SiW ₁₂ O ₄₀ | 86 | 84 | 86 | 82 |
| 9 | H ₁₄ [NaP ₅ W ₃₀ O ₁₁₀] | 81 | 77 | 80 | 74 |
| 10 | Na ₃ PMo ₁₂ O ₄₀ | 80 | 75 | 80 | 72 |
| 11 | Na ₃ PW ₁₂ O ₄₀ | 78 | 74 | 77 | 70 |
| 12 | (NH ₄) ₃ H[PMo ₁₁ VO ₄₀] | 78 | 72 | 78 | 68 |
| 13 | H ₆ P ₂ Mo ₁₈ O ₆₂ | 74 | 71 | 73 | 70 |
| 14 | H ₆ P ₂ W ₁₈ O ₆₂ | 70 | 67 | 70 | 65 |

Effect of the catalyst structure

The effects of the catalyst structure on the oxidation of the simulated gas oil by formic acid/H₂O₂ are presented in Table IV. BT, DBT, 4-MDBT and 4,6-



DMDBT were taken as model compounds. The amount of each catalyst used was the same. POM-TiO₂ nanocomposite presented a much higher catalytic activity than that of the unsupported polyoxometalates. The (Bu₄N)₄H[PMo₁₀V₂O₄₀]-TiO₂ nanoparticle was a very active catalyst system for the oxidation of the model compound, while other polyoxometalate systems were much less active. In the series of Keggin-type polyoxometalates, H₅[PMo₁₀V₂O₄₀] showed the highest catalytic activity. In general, heteropoly salt-type catalysts were less efficient than the heteropolyacids. The Keggin-type polyoxometalates lead to more effective reactions in comparison with the Wells-Dawson-type polyoxometalates. Moreover, H₆[P₂Mo₁₈O₆₂] was more effective than H₆[P₂W₁₈O₆₂], which may be due to the difference in the reduction potentials of tungsten and molybdenum. However, the results indicate that the highest yield of oxidation was obtained when the oxidation of the substrates was realized with the (Bu₄N)₄H[PMo₁₀V₂O₄₀]-TiO₂ as catalyst.

Effect of the amount formic acid

Effect of the amount of formic acid on the oxidative desulphurization of different sulfur compounds was studied and the results are given in Table V. In the formic acid catalyzed reaction, the formic acid can interact with sulfur without any steric hindrance from alkyl groups. Therefore, the reactivity trend obtained in the formic acid catalyzed reactions reflects the intrinsic oxidation reactivity of the DBTs. The % sulfur removal of the simulated gas oil increased with increasing formic acid. It could be seen that a formic acid/H₂O₂ mole ratio of 1.0 (98 % conversion of DBT) was better than the other mole ratio. Therefore, in all the subsequent experiments, this formic acid/DBT mole ratio was used. The fuel mixed with H₂O₂/formic acid (performic acid) and the oxidative reaction occurred below 100 °C under atmospheric pressure. This was followed by liquid/liquid extraction to obtain a fuel with a low sulfur and an extract with a high sulfur content. Finally, the low sulfur fuel may require additional treatment. The extraction solvent was then removed from the extract for reuse and the concen-

TABLE V. Effect of formic acid amount on the oxidative desulphurization of different sulfur compounds using (Bu₄N)₄H[PMo₁₀V₂O₄₀]-TiO₂ as catalyst; conditions for the desulphurization: 2 mL H₂O₂/formic acid as oxidant, 0.1 mmol nanocatalyst, 5 mL DMF as extraction solvent, time 2 h, temperature 80 °C

| Entry | Formic acid/sulfur compound mole ratio | Conversion, % | | | |
|-------|-------------------------------------------|---------------|--------|-----------|----|
| | | DBT | 4-MDBT | 4,6-DMDBT | BT |
| 1 | 0.25 | 48 | 45 | 48 | 39 |
| 2 | 0.5 | 68 | 62 | 67 | 59 |
| 3 | 0.75 | 84 | 82 | 84 | 78 |
| 4 | 1 | 98 | 96 | 97 | 94 |
| 5 | 1.25 | 96 | 94 | 96 | 87 |
| 6 | 1.5 | 91 | 85 | 89 | 82 |



trated extract was made available for further processing to remove sulfur and to produce hydrocarbons.

Effect of temperature on the oxidative desulphurization of gas oil or simulated gas oil

The reaction was carried out at different temperatures under the same conditions using $(Bu_4N)_4H[PMo_{10}V_2O_{40}]$ – TiO_2 as the nanocatalyst and the formic acid/ H_2O_2 system. The results are given in Table VI, from which it can be seen that the yields of the products were a function of temperature. Conversion of the sulfur compounds was increased at higher reaction temperatures and longer reaction times. The conversion of sulfur in the simulated gas oil was the highest at 80 °C, at which temperature, a conversion of sulfur of 98% was obtained. The catalytic activities of the $(Bu_4N)_4H[PMo_{10}V_2O_{40}]$ – TiO_2 in the oxidation of DBT at different temperatures, 30–80 °C, were compared. At 80 °C, percent conversion was higher than that at 30 and 40 °C. In 120 min, up to 98 % removal of sulfur was obtained at 80 °C for the $(Bu_4N)_4H[PMo_{10}V_2O_{40}]$ – TiO_2 catalyst, which was superior to the $(Bu_4N)_4H[PMo_{10}V_2O_{40}]$ catalyst, with which 94 % conversion was achieved.

TABLE VI. Effect of temperature on the oxidative desulfurization of different sulfur compounds (conversion, %) using $(Bu_4N)_4H[PMo_{10}V_2O_{40}]$ – TiO_2 as catalyst; conditions for the desulphurization: 2 mL H_2O_2 /formic acid as an oxidant, 0.1 mmol nanocatalyst, 5 mL DMF as an extraction solvent, time = 2 h

| Entry | Temperature, °C | Compound | | | |
|-------|-----------------|----------|--------|-----------|----|
| | | DBT | 4-MDBT | 4,6-DMDBT | BT |
| 1 | 30 | 55 | 47 | 49 | 42 |
| 2 | 40 | 67 | 59 | 62 | 55 |
| 3 | 50 | 74 | 65 | 76 | 65 |
| 4 | 60 | 88 | 82 | 84 | 79 |
| 5 | 70 | 96 | 94 | 95 | 91 |
| 6 | 80 | 98 | 96 | 97 | 94 |

CONCLUSIONS

A $(Bu_4N)_4H[PMo_{10}V_2O_{40}]$ – TiO_2 nanocomposite was synthesized at a low temperature *via* the sol–gel method under oil bath conditions. Fixing of $(Bu_4N)_4H[PMo_{10}V_2O_{40}]$ into TiO_2 decreases the particle size of the crushed nano leaf of the anatase phase. The $(Bu_4N)_4H[PMo_{10}V_2O_{40}]$ – TiO_2 nanocomposite was a very active catalyst system for the model compound oxidation, while unmodified $(Bu_4N)_4H[PMo_{10}V_2O_{40}]$ was much less active. The oxidation reaction was selective as only sulfone was detected. For this polyoxometalates/ H_2O_2 /formic acid system, the oxidation reactivity decreased in the following order: DBT > 4,6-DMDBT > BT. The percent conversion increased when the



amounts of oxidant and catalyst were increased. The addition of formic acid enhanced the conversion.

Acknowledgment. The authors are grateful to the Research Council of the University of Zanjan, Guilan and the terminal of North Iranian Oil Company for their partial support of this study.

ИЗВОД

АНАТАЗНИ ОКСИД ТИТАНА-ВАНАДИЈУМ-ПОЛИФОСФОМОЛИБДАТ КАО ЕФИКАСАН И ПРАКТИЧАН НАНОКАТАЛИЗАТОР ЗА ДЕСУЛФУРИЗАЦИЈУ ГАСНОГ УЉА

MOHAMMAD ALI REZVANI¹, ABDOLLAH FALLAH SHOJAEI² и FAROKHZAD MOHAMADI ZONOZ³

¹Department of Chemistry, Faculty of Science, University of Zanjan, 45371-38791 Zanjan, Iran,

²Department of Chemistry, Faculty of Science, University of Guilan, 419961-3769 Rasht, Iran и

³Department of Chemistry, Hakim Sabzevari University, Sabzevar, 397, Iran

Нанокомпозит $(Bu_4N)_4H[PMo_{10}V_2O_{40}]$ - TiO_2 је синтетисан у реакцији $(Bu_4N)_4H[PMo_{10}V_2O_{40}]$ и титан-тетраизопропоксида на 100 °C применом сол-гел методе. Дебљина слоја анатазне фазе, која износи 20 nm, се смањује додатком $(Bu_4N)_4H[PMo_{10}V_2O_{40}]$. За овај полифосфомолибдат је нађено да оксидује гасно уље са високим процентом конверзије (више од 98 %). У овом раду је приказана ефикасна оксидативна десулфуризација гасног уља помоћу система мравља киселина/водоник-пероксид. Овај систем омогућава ефикасан, погодан и практичан метод за везивање сумпорних једињења.

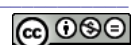
(Примљено 25. октобра 2013, 20. фебруара, прихваћено 24. фебруара 2013)

REFERENCES

1. C. A. S. Regino, D. E. Richardson: *Inorg. Chim. Acta* **360** (2007) 3971
2. M. M. Heravi, Kh. Bakhtiari, F. F. Bamoharram, *Catal. Commun.* **7** (2006) 373
3. M. T. Pope, in *Comprehensive Coordination Chemistry*, Vol. 3, G. Wilkinson, D. Gillard, J. A. McCleverty, Eds., Pergamon Press, New York, 1987, p. 1023
4. F. F. Bamoharram, M. M. Heravi, M. Roshani, M. Jahangir, A. Gharib, *J. Appl. Catal., A* **302** (2006) 42
5. M. M. Heravi, F. K. Behbahani, F. F. Bamoharram, *J. Mol. Catal., A* **253** (2006) 16
6. V. Kesavan, D. Bonnet-Delpon, J. P. Begue, *Synthesis* (2000) 223
7. Y. Izumi, K. Urabe, M. Onaka, *Zeolites Clay and Heteropolyacid in Organic Reactions*, Vol. 99, Kodansha, Tokyo, 1992
8. I. V. Kozhevnikov, *Chem. Rev.* **98** (1998) 171
9. I. V. Kozhevnikov, *Catalysis for Fine Chemical Synthesis*, Vol. 2, *Catalysis by Polyoxometalates*, Wiley, New York, 2002
10. X. López, *PhD Thesis*, Universitat Rovira i Virgili, Tarragona, 2003
11. P. S. Tam, J. R. Kittrrell, J. W. Eldridge, *Ind. Eng. Chem. Res.* **29** (1990) 321
12. S. Otsuki, T. Nonaka, W. Qian, A. Ishihara, T. Kabe, *Bull. Chem. Soc. Jpn.* **31** (1998) 1939
13. D. Wang, E. W. Qian, H. Amano, K. Okata, A. Ishihara, T. Kabe, *Appl. Catal., A* **253** (2003) 91
14. T. V. Rao, B. Sain, S. Kafola, Y. K. Sharma, S. M. Nanoti, M. O. Garg, *Energy Fuels* **21** (2007) 3420.
15. S. Z. Liu, B. H. Wang, B. C. Cui, L. L. Sun, *Fuel* **87** (2008) 422



16. Z. Jiang, H. Lü, Y. Zhang, C. Li, *Chin. J. Catal.* **32** (2011) 707
17. S. Tangestaninejad, V. Mirkhani, M. Moghadam, I. Mohammadpoor, E. Shams, H. Salavati, *Ultrason. Sonochem.* **15** (2008) 438
18. A. Fallah Shojaie, M. A. Rezvani, M. H. Loghmani, *Fuel Process. Technol.* **118** (2014) 1
19. M. A. Rezvani, A. Fallah Shojaie, M. H. Loghmani, *Catal. Commun.* **25** (2012) 36
20. A. Fallah Shojaie, M. A. Rezvani, F. M. Zonozi, *J. Serb. Chem. Soc.* **78** (2013) 129
21. A. Fallah Shojaei, M. H. Loghmani, *Chem. Eng. J.* **157** (2010) 263
22. A. Fallah Shojaei, M. A. Rezvani, M. Heravi, *J. Serb. Chem. Soc.* **76** (2011) 955
23. A. Fallah Shojaei, M. A. Rezvani, M. Heravi, *J. Serb. Chem. Soc.* **76** (2011) 1513
24. R. Harutyunyan, M. A. Rezvani, M. M. Heravi, *Synth. React. Inorg., Met.-Org. Nano-Met. Chem.* **41** (2011) 94
25. M. A. Rezvani, R. Harutyunyan, Majid M. Heravi, *Synth. React. Inorg., Met.-Org. Nano-Met. Chem.* **42** (2012) 1232
26. M. Sharifzadeh Baei, M. A. Rezvani, *Asian J. Chem.* **12** (2011) 5381.





QSAR studies for assessing the acute toxicity of nitrobenzenes to *Tetrahymena pyriformis*

DAN-DAN WANG¹, LIN-LIN FENG¹, GUANG-YU HE² and HAI-QUN CHEN^{1*}

¹School of Environmental and Safety Engineering, Changzhou University, Jiangsu Province, Changzhou, 213164, China and ²Key Laboratory of Advanced Catalytic Materials and Technology, Changzhou University, Jiangsu Province, Changzhou, 213164, China

(Received 10 September, 2013, revised 11 November, accepted 6 December 2013)

Abstract: Quantitative structure–activity relationship (QSAR) models play a key role in finding the relationship between molecular structures and the toxicity of nitrobenzenes to *Tetrahymena pyriformis*. In this work, a genetic algorithm along with partial least square (GA–PLS) was employed to select the optimal subset of descriptors that significantly contribute to the toxicity of nitrobenzenes to *T. pyriformis*. A set of five descriptors, namely G2, HOMT, G(Cl···Cl), Mor03v and MAXDP, was employed for the prediction of the toxicity of 45 nitrobenzene derivatives and then they were used to build the model by the multiple linear regression (MLR) method. It transpired that the built model, the stability of which was confirmed using the leave-one-out validation and external validation test, showed high statistical significance ($R^2 = 0.963$, $Q_{LOO}^2 = 0.944$). Moreover, the y-scrambling test indicated there were no chance correlations in the model.

Keywords: quantitative structure–activity relationship; multiple linear regressions.

INTRODUCTION

Nitrobenzenes are important fine organic intermediates that are widely used in many fields, such as the synthesis of pharmaceuticals, dyestuffs and explosives.^{1,2} Since most of nitrobenzenes and their derivatives are hazardous and have high potential to pollute the environment, it is of great significance to study their acute toxicity. With the rapid development of industry and agriculture, a growing number of nitrobenzenes leak into the environment, especially in aquatic ecosystems.³ There is little possibility of testing the acute toxicity of each compound, since it would be time-consuming and expensive. Hence, great attention is being paid to finding tools capable of assessing the acute toxicity of nitroben-

*Corresponding author. E-mail: hqchenyf@hotmail.com
doi: 10.2298/JSC130910025W

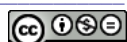
zenes, among which the quantitative structure–activity relationship (QSAR) method is the most powerful one.

The quantitative structure–activity relationship (QSAR) method focuses on the motto that the properties of chemical compounds are determined by their molecular structures.⁴ Thus, based on accurate experimental data of only some of the chemicals in one group, the activities of chemicals in the whole group can be predicted using suitable models, including compounds that have not yet been experimentally synthesized.^{5–9}

For many years, QSARs have been efficiently used in the study of toxicity mechanisms of various reactive chemicals. Dearden *et al.* reviewed the attempts to model the acute toxicity of nitrobenzenes.¹⁰ Due to the reactive electrophilic nature of nitrobenzenes, the global electrophilicity and local maximum philic power ($\omega_{C_{max}}^+ / \omega_{C_{max}}^-$), along with the total Hartree–Fock energy (E_{HF}), were used as independent variables, while the toxicity of 174 selected aromatic compounds to *T. pyriformis* were considered as the dependent variable.¹¹ Roy and Ghosh introduced extended topochemical atom (ETA) indices to model the toxicity of nitrobenzene derivatives to *T. pyriformis*.¹² Furthermore, quantum chemical methods were used to calculate molecular descriptors by Gu *et al.*, making it easier to understand the built models.^{13,14} Estrada and Uriarte obtained a good quantitative structure–toxicity model of 42 nitrobenzenes by their original topological sub-structural molecular design (TOPS–MODE) approach.¹⁵ Artemenko *et al.* studied the toxicity of 95 diverse nitroaromatics to *T. pyriformis* and discussed possible modes of action by hierarchical technology for quantitative structure–activity relationships (HiT QSAR).¹⁶ In some of the above-mentioned models, external validation and proof of passing the γ -scrambling test were absent, causing serious doubts about the reliability of the interpretation and making it hard to assess their predictive power, which is a very important part of QSAR studies.

The selection of the molecular descriptors most relevant to acute toxicity is the key problem involved in the QSAR method, as well as the application of appropriate techniques for constructing the models. At present, the genetic algorithm (GA) is well known as an interesting and more widely used variable selection method.^{17–19} GA is a stochastic method to solve the optimization problems defined by fitness criteria, applying the evolution hypothesis of Darwin and different genetic functions, *i.e.*, crossover and mutation.²⁰ Nowadays, many different techniques, such as multiple linear regression (MLR), partial least squares (PLS) and different types of artificial neural networks (ANN), have been widely used in building QSAR models.^{21,22}

The aim of this study was to develop a reliable and predictive QSAR model using the MLR method for identifying the factors governing the acute toxicity of nitrobenzenes to *T. pyriformis* and to predict their acute toxicity from their mole-



cular structures. For this purpose, a group of 45 nitrobenzene compounds having the structure of a single nitrobenzene ring with different substituent groups, such as nitro-, halogens (fluorine, chlorine, bromine), was chosen as the sample set. The leave-one-out cross-validation, a γ -scrambling test and outer samples prediction were performed to validate the developed model.

MATERIAL AND METHODS

Dataset

The QSAR modeling was applied on a set of nitrobenzenes (their molecular structures are given in Fig. S-1 of the Supplementary Material to this paper). The dataset used in this study was extracted from a single literature source.²³ It consists of 45 nitrobenzene compounds based on a nitrobenzene ring structure with different halogen substituents. Herein, $-\log IGC_{50}$ means the inverse logarithm of the concentration causing 50 % growth inhibition of *T. pyriformis*, which was used as a measure of the toxicity of the compounds. The experimental acute toxicity values of the nitrobenzenes to *T. pyriformis* are listed in Table I, as well as the corresponding names, molecular formulas and CAS numbers. The bigger the value of $-\log IGC_{50}$, the higher is the acute toxicity of the compound.

TABLE I. List of the 45 compounds considered in the study, including corresponding names, molecular formulas, CAS numbers and $-\log IGC_{50}$ values

| No. | Compound | Formula | CAS | $-\log (IGC_{50} / \text{mmol mL}^{-1})$ |
|-----|------------------------------------|-----------------------------------------------------------------------------|------------|------------------------------------------|
| 1 | 1,3-Dinitrobenzene | C ₆ H ₄ N ₂ O ₄ | 99-65-0 | 0.89 |
| 2 | 1-Bromo-4-nitrobenzene | C ₆ H ₄ BrNO ₂ | 586-78-7 | 0.38 |
| 3 | 1,3,5-Trimethyl-2-nitrobenzene | C ₉ H ₁₁ NO ₂ | 603-71-4 | 0.86 |
| 4 | 1-Methyl-2,4-dinitrobenzene | C ₇ H ₅ N ₂ O ₄ | 121-14-2 | 0.87 |
| 5 | 1,2-Dichloro-3-nitrobenzene | C ₆ H ₃ Cl ₂ NO ₂ | 3209-22-1 | 1.07 |
| 6 | 1,2-Dinitrobenzene | C ₆ H ₄ N ₂ O ₄ | 528-29-0 | 1.25 |
| 7 | 1,4-Dinitrobenzene | C ₆ H ₄ N ₂ O ₄ | 100-25-4 | 1.30 |
| 8 | 1,3-Dimethyl-2-nitrobenzene | C ₈ H ₉ NO ₂ | 81-20-9 | 0.30 |
| 9 | 1,2-Dimethyl-3-nitrobenzene | C ₈ H ₉ NO ₂ | 83-41-0 | 0.56 |
| 10 | 1,3,5-Trichloro-2-nitrobenzene | C ₆ H ₂ Cl ₃ NO ₂ | 18708-70-8 | 1.43 |
| 11 | 1,2,3-Trichloro-4-nitrobenzene | C ₆ H ₂ Cl ₃ NO ₂ | 17700-09-3 | 1.51 |
| 12 | 4-Chloro-1-methyl-2-nitrobenzene | C ₇ H ₆ ClNO ₂ | 89-59-8 | 0.82 |
| 13 | 1,4-Dichloro-2-nitrobenzene | C ₆ H ₃ Cl ₂ NO ₂ | 89-61-2 | 1.13 |
| 14 | 1-Chloro-2,4-dinitrobenzene | C ₆ H ₃ ClN ₂ O ₄ | 97-00-7 | 1.98 |
| 15 | 1,2,3,4-Tetrachloro-5-nitrobenzene | C ₆ HCl ₄ NO ₂ | 879-39-0 | 1.78 |
| 16 | 1-Methyl-4-nitrobenzene | C ₇ H ₇ NO ₂ | 99-99-0 | 0.17 |
| 17 | 1,3,5-Trichloro-2,4-dinitrobenzene | C ₆ HCl ₃ N ₂ O ₄ | 6284-83-9 | 2.19 |
| 18 | 1-Bromo-2,4-dinitrobenzene | C ₆ H ₃ BrN ₂ O ₄ | 584-48-5 | 2.31 |
| 19 | 1,5-Dichloro-2,3-dinitrobenzene | C ₆ H ₂ Cl ₂ N ₂ O ₄ | 28689-08-9 | 2.42 |
| 20 | 1,3-Dichloro-5-nitrobenzene | C ₆ H ₃ Cl ₂ NO ₂ | 618-62-2 | 1.13 |
| 21 | 1-Fluoro-3-nitrobenzene | C ₆ H ₄ FNO ₂ | 402-67-5 | 0.20 |
| 22 | 1-Fluoro-2-nitrobenzene | C ₆ H ₄ FNO ₂ | 1493-27-2 | 0.23 |
| 23 | 1-Ethyl-4-nitrobenzene | C ₈ H ₉ NO ₂ | 100-12-9 | 0.43 |
| 24 | 1,2-Dimethyl-4-nitrobenzene | C ₈ H ₉ NO ₂ | 99-51-4 | 0.59 |
| 25 | 1-Chloro-2-nitrobenzene | C ₆ H ₄ ClNO ₂ | 88-73-3 | 0.68 |
| 26 | 1-Chloro-2-fluoro-3-nitrobenzene | C ₆ H ₃ ClFNO ₂ | 21397-07-9 | 0.80 |



TABLE I. Continued

| No. | Compound | Formula | CAS | $-\log (IGC_{50} / \text{mmol mL}^{-1})$ |
|-----------------|----------------------------------------|--------------------------|------------|------------------------------------------|
| 27 | 1-Chloro-3-nitrobenzene | <chem>C6H4ClNO2</chem> | 121-73-3 | 0.84 |
| 28 | 1-Bromo-3-nitrobenzene | <chem>C6H4BrNO2</chem> | 585-79-5 | 1.22 |
| 29 | 1,2,4,5-Tetrachloro-3-nitrobenzene | <chem>C6HCl4NO2</chem> | 117-18-0 | 1.47 |
| 30 | 1-Fluoro-2,4-dinitrobenzene | <chem>C6H3FN2O4</chem> | 70-34-8 | 1.71 |
| 31 | 1,2,3,5-Tetrafluoro-4-nitrobenzene | <chem>C6HF4NO2</chem> | 314-41-0 | 1.87 |
| 32 | 1,5-Difluoro-2,4-dinitrobenzene | <chem>C6H2F2N2O4</chem> | 327-92-4 | 2.03 |
| 33 | 1,2,3,4,5-Pentafluoro-6-nitrobenzene | <chem>C6F5NO2</chem> | 880-78-4 | 2.43 |
| 34 ^a | Nitrobenzene | <chem>C6H5NO2</chem> | 98-95-3 | 0.14 |
| 35 ^a | 1-Chloro-4-nitrobenzene | <chem>C6H4ClNO2</chem> | 100-00-5 | 0.43 |
| 36 ^a | 2,4-Dichloro-1-nitrobenzene | <chem>C6H3Cl2NO2</chem> | 611-06-3 | 0.99 |
| 37 ^a | 1,2-Dichloro-4-nitrobenzene | <chem>C6H3Cl2NO2</chem> | 99-54-7 | 1.16 |
| 38 ^a | 1,4-Dibromo-2-nitrobenzene | <chem>C6H3Br2NO2</chem> | 3460-18-2 | 1.37 |
| 39 ^a | 1-Chloro-2-methyl-3-nitrobenzene | <chem>C7H6ClNO2</chem> | 83-42-1 | 0.68 |
| 40 ^a | 1,2,4-Trichloro-5-nitrobenzene | <chem>C6H2Cl3NO2</chem> | 89-69-0 | 1.53 |
| 41 ^a | 1,2-Dichloro-4,5-dinitrobenzene | <chem>C6H2Cl2N2O4</chem> | 6306-39-4 | 2.21 |
| 42 ^a | 1,2,4,5-Tetrachloro-3,6-dinitrobenzene | <chem>C6Cl4N2O4</chem> | 20098-38-8 | 2.74 |
| 43 ^a | 1-Fluoro-4-nitrobenzene | <chem>C6H4FNO2</chem> | 350-46-9 | 0.25 |
| 44 ^a | 1-Bromo-2-nitrobenzene | <chem>C6H4BrNO2</chem> | 577-19-5 | 0.86 |
| 45 ^a | 1,2,3-Trifluoro-4-nitrobenzene | <chem>C6H2F3NO2</chem> | 771-69-7 | 1.89 |

^aTest set

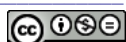
The compounds in Table I were sorted from low value to high value of their acute toxicity. Then, the first, the fifth, the ninth sample, *etc.* were chosen to create a test set, and the remaining 33 samples were regarded as the training set. The 33 training samples were utilized to construct the model. The other 12 samples were utilized to evaluate the predictive ability of the obtained model.

Molecular descriptor calculation and selection

Constructing numerical descriptors of a set of molecules is necessary for QSAR models. Descriptor reflects some of molecular properties, which can then be related with biological activity. For the compounds studied in this article, up to 1644 molecular descriptors were calculated using DRAGON software, which is a sophisticated program for the calculation of molecular descriptors.^{24,25} To date, a wide variety of descriptors have been reported for QSAR analysis, such as topological descriptors, constitutional descriptors, geometric descriptors and charge related descriptors.^{26,27} The geometries of all molecules were optimized by MM+ force field and then by the AM1 semi-empirical method with an SCF convergence of 10^{-5} and a RMS gradient of 10^{-2} kcal* Å⁻¹·mol⁻¹.²⁸ The DRAGON software users' guide can be referred to for a detailed description on the types of the molecular descriptors that DRAGON can calculate as well as the calculation procedures.²⁹

The molecular descriptors that remained constant or near constant for all molecules were removed from the descriptor pool, since such descriptors could not encode the structural differences between the compounds, which account for the differences between their acute

* 1 kcal = 4184 J



toxicity. Further reduction of the descriptor pool was attained by examining pair-wise correlations between descriptors so that only one descriptor was retained from a pair contributing similar information (correlation coefficient > 0.95 in this study). Finally, a total set of 521 remaining descriptors was achieved and used to select the optimal subset of descriptors that significantly contribute to the acute toxicity.

The selection of molecular descriptors plays a significant role in QSAR analysis. With hundreds of descriptors remaining, a more powerful optimization method was required to find the optimum quantitative relationships between the molecular descriptors and the acute toxicity. The genetic algorithm (GA), which was developed to simulate processes observed in natural evolution, is a popular solution to solve this problem.³⁰ In this study, the GA, a powerful optimization method, along with the partial least square method (PLS), which is a robust statistical method for variable selection, was used to find the molecular descriptors closely related to acute toxicity. The GA–PLS programs were implemented using the software package PLS–Algorithm Toolbox written by Leardi and Lupiáñez.³¹ A detailed description of how to use GA–PLS and the parameters required can be found in the literature.³¹ In this work, all calculation programs implementing GA–PLS were written in M-file using the MATLAB package.³²

MLR method

MLR is a widely-used statistical analysis method to model the relationship between a scalar dependent variable Y and several explanatory variables denoted X , which can build a simple and interpretable model.³³ In multiple linear regression, n compounds with a known dependent variable (acute toxicity) and independent variables (molecular structure descriptors) are used for building the model. It is assumed that the acute toxicity of each compound can be represented as:

$$y_i = b + b_1x_{i,1} + b_2x_{i,2} + \dots + b_mx_{i,m} + \varepsilon_i \quad (1)$$

where y_i is the i^{th} acute toxicity ($i = 1, 2, \dots, n$), $x_{i,k}$ is the value of k^{th} descriptor for compound i ($k = 1, 2, \dots, m$) and ε_i is the i^{th} residual and with b as the vector of the regression coefficients. In matrix notation:

$$\mathbf{y} = \mathbf{X}\mathbf{b} + \boldsymbol{\varepsilon} \quad (2)$$

where \mathbf{y} is the vector of the toxicity values for different compounds, \mathbf{X} is the matrix of descriptors for different compounds and $\boldsymbol{\varepsilon}$ is the vector of the residuals.

When the matrix $\mathbf{X}^T\mathbf{X}$ is non-singular, the least square estimate of b is therefore obtained as:

$$\mathbf{b} = (\mathbf{X}^T\mathbf{X})^{-1}\mathbf{X}^T\mathbf{y} \quad (3)$$

The estimated acute toxicity value can be calculated as:

$$\hat{y} = \mathbf{X}\hat{\mathbf{b}} \quad (4)$$

In this work, the multiple linear regressions were performed using the statistics software SPSS.³⁴ The linear relationship between the acute toxicity data of the compounds and their structure parameters was fitted by the multiple stepwise regression method in 95 % confidence intervals. The qualities of the statistics of the MLR equation were judged by parameters such as the R^2 value (coefficient of determination), the F value (Fischer statistics) and the S value (standard deviation).



Model validation

In order to check the reliability and the stability of QSPR model elaborated by MLR method, both the internal and external validations were conducted. The goodness of the fitting was firstly characterized by the coefficient of determination (R^2) and the root mean squared error ($RMSE$) between calculated and experimental values for the molecules of the training set. The two formulas are given by Eqs. (5) and (6), respectively:

$$R^2 = 1 - \frac{\sum_{i=1}^n (y_i - y'_i)^2}{\sum_{i=1}^n (y_i - \bar{y})^2} \quad (5)$$

and:

$$RMSE = \sqrt{\frac{\sum_{i=1}^n (y'_i - y_i)^2}{N}} \quad (6)$$

where y_i , y'_i and \bar{y} are the observed property, calculated property and mean value of the property, respectively, and N is the number of observations.

Cross-validation is one of the most popular methods of estimating the robustness of a model. In this work, the internal predictive capability of the model was evaluated by the leave-one-out cross-validation (Q_{LOO}^2), following the mathematic form:

$$Q_{LOO}^2 = 1 - \frac{\sum_{i=1}^{\text{training set}} (y_i - y'_i)^2}{\sum_{i=1}^{\text{training set}} (y_i - \bar{y})^2}. \quad (7)$$

A good Q_{LOO}^2 often indicates a good robustness and high internal predictive power of a QSPR model. The cross-validation coefficient between predicted and observed values of the test set Q_{ext}^2 was used to verify the external predictive ability of the MLR model, which can be calculated at the model development step by properly employing a prediction set for validation as follows:

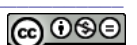
$$Q_{ext}^2 = 1 - \frac{\sum_{i=1}^{\text{test set}} (x_i - x'_i)^2}{\sum_{i=1}^{\text{test set}} (x_i - \bar{y}_{tr})^2} \quad (8)$$

where x_i , x'_i , and \bar{y}_{tr} are the observed property, the calculated property in the test set and the mean value of the property in the training set, respectively.

In addition, the mean absolute error (AAE) was also used to assess the obtained model, which was calculated according to the following equation:

$$AAE = \frac{\sum_{i=1}^n |y'_i - y_i|}{N} \quad (9)$$

where y_i , and y'_i are the observed property and calculated property, respectively.



A y -scrambling test reveals the robustness of a QSAR model, being a measure of the model overfit. This test is realized by deliberately destroying the connection between the target variable y and the independent variables x (in QSAR: molecular descriptors). Thus, the y -data was randomly permuted, while all x data were left untouched. This y -scrambling was repeated 100 times. After this procedure, the obtained MLR model must have the minimal R^2 value.

RESULTS AND DISCUSSION

Results of descriptors selection

The GA-PLS procedure was performed to select the optimal set of descriptors. A set of five descriptors were finally selected and used to build the following model of MLR. The correlation matrix for these descriptors used in the present study is shown in Table II, from which it can be seen that no high correlations existed between these descriptors.

TABLE II. Correlation matrix between the selected descriptors

| | <i>Mor03v</i> | <i>G2</i> | <i>HOMT</i> | <i>G(Cl···Cl)</i> | <i>MAXDP</i> |
|-------------------|---------------|-----------|-------------|-------------------|--------------|
| <i>Mor03v</i> | 1 | -0.094 | 0.074 | -0.209 | -0.124 |
| <i>G2</i> | | 1 | 0.195 | 0.354 | -0.019 |
| <i>HOMT</i> | | | 1 | 0.006 | 0.291 |
| <i>G(Cl···Cl)</i> | | | | 1 | -0.176 |
| <i>MAXDP</i> | | | | | 1 |

The physical meanings of these descriptors are interpreted as follows.²⁷ *Mor03v* (3D-MoRSE – signal 03/weighted by atomic van der Waals volumes) is a 3D-MoRSE descriptor based on the idea of obtaining information from the 3D atomic coordinates by the transform used in electron diffraction studies for preparing theoretical scattering curves. A generalized scattering function, called the molecular transform, can be used as a functional basis for deriving the specific analytic relationship of X-ray and electron diffraction from a known molecular structure.

G(Cl···Cl) is a 3D atom pair descriptor and one of the primary dimensional features of chemicals. It is mainly related to the sum of the geometrical distances between Cl···Cl. For a compound without a Cl atom, this value will be zero.

G2 is a gravitational index (bond restricted), defined as:

$$G2 = \sum_{b=1}^B \left(\frac{m_i m_j}{r_{ij}^2} \right)$$

where m_i and m_j are the atomic masses of the considered atoms, r_{ij} is the corresponding interatomic distance and B is the number of bonds in the molecule. The *G2* index is restricted to pairs of bonded atoms and is related to the bulk cohesiveness of the molecules, accounting for both atomic masses and their dis-



tribution within the molecule space and can be extended to any atomic property other than the atomic mass, such as atomic polarizability, atomic van der Waals volume, *etc.* The *G*2 descriptor can be related to the size of the molecule – *G*2 is larger for large molecules.

Harmonic oscillator model of aromaticity index total (*HOMT*) is also a geometrical descriptor. It is based on the degree of alternation of single/double bonds and is used to measure the bond length deviation from the optimal length attributed to the typical aromatic state. In this work, it depended on the variation of the number, position, and nature of the substituents. To illustrate the effects of the substituents on *HOMT*, the title compounds were divided into 17 groups according to the type of ring. Table III presents the values of the *HOMT* indices for the 17 groups of differently substituted benzene rings, labeled in column 3.

TABLE III. *HOMT* values of the compounds with different types of ring substitution

| Number of substituents | Type of ring | Class | Compound number | <i>HOMT</i> |
|------------------------|--------------------------------|-------|----------------------------------------------------------------------------------------|----------------------------------------------------------|
| 1 | Unsubstituted nitrobenzene | 1 | 34 | 5.844 |
| 2 | 2-Substituted nitrobenzene | 2 | 6 22 25 44 | 5.944 5.959 5.955 5.955 |
| | 3-Substituted nitrobenzene | 3 | 1 21 27 28 | 5.944 5.959 5.955 5.955 |
| | 4-Substituted nitrobenzene | 4 | 2 7 16 23 35 43 | 5.95 5.944 5.944 5.944 5.955 5.961 |
| 3 | 2,4-Disubstituted nitrobenzene | 5 | 36 | 5.96 |
| | 2,5-Disubstituted nitrobenzene | 6 | 4 12 13 14 18 30 38 | 5.95 5.955 5.96 5.955 5.953 5.959 5.96 |
| | 3,4-Disubstituted nitrobenzene | 7 | 24 37 | 5.953 5.963 |
| | 3,5-Disubstituted nitrobenzene | 8 | 20 | 5.96 |
| | 2,3-Disubstituted nitrobenzene | 9 | 26 39 | 5.962 5.955 |
| | 2,6-Disubstituted nitrobenzene | 10 | 8 | 5.953 |

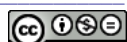


TABLE III. Continued

| Number of substituents | Type of ring | Class | Compound number | <i>HOMT</i> |
|------------------------|-----------------------------------------|-------|-----------------|-------------|
| 4 | 2,3,4-Trisubstituted nitrobenzene | 11 | 11 | 5.964 |
| | | | 45 | 5.973 |
| | | | 3 | 5.944 |
| | 2,4,6-Trisubstituted nitrobenzene | 12 | 10 | 5.961 |
| | | | 19 | 5.96 |
| | | | 32 | 5.969 |
| | 2,4,5-Trisubstituted nitrobenzene | 13 | 40 | 5.963 |
| | | | 41 | 5.958 |
| | | | 15 | 5.97 |
| 5 | 2,3,4,5-Tetrasubstituted nitrobenzene | 14 | 29 | 5.97 |
| | | | 31 | 5.983 |
| | 2,3,5,6-Tetrasubstituted nitrobenzene | 15 | 17 | 5.961 |
| 6 | 2,3,4,5,6-Pentasubstituted nitrobenzene | 16 | 33 | 5.988 |
| | | 17 | 42 | 5.97 |

Analyzing the data in Table III, several interesting results could be found. 1) Among the compounds with the same nitrobenzene ring, the halogen-substituted nitrobenzene compounds had higher *HOMT* indices than nitrobenzene compounds with alkyl groups; 2) when the H atoms were substituted by F atoms, the *HOMT* index was higher than for compounds with Cl and Br atoms; 3) for the isomers, the variance in the *HOMT* values was subtle.

The relation between the median *HOMT* value of each group and the number of substituents is illustrated in Fig. 1, from which it could be seen that the *HOMT* index, in general, incrementally increases with the number of substituents attached to the ring. As is well known, halogen and nitro groups are electron-withdrawing groups that are responsible for a decrease in the electronic density of a benzene ring to which they are attached.

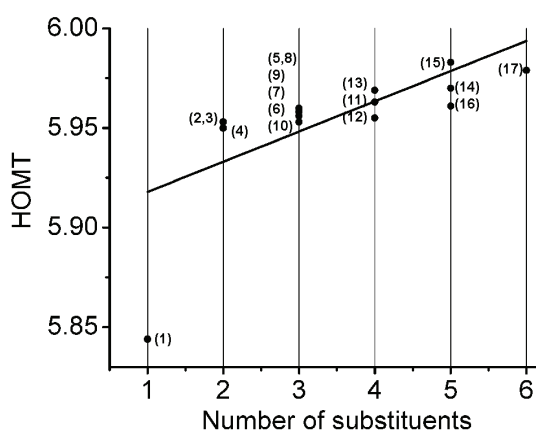


Fig. 1. Plot of the median values of *HOMT* against the number of substituents.

MAXDP is a topological descriptor defined as the maximal electrotopological positive variation, which can be related to the electrophilicity of a molecule.³⁵ The nitrobenzenes are representatives of electrophilic toxicants in that, depending on the substitution pattern, they may undergo a number of different electrophilic reactions.³⁶ Due to the reactive electrophilic nature of the nitrobenzenes, it is not surprising that previous modeling efforts focused on the use of electronic molecular descriptors.^{37–40} The mechanisms of toxic action have been simplistic in that toxicity was modeled as a function of the ability of the toxicant to reach the active site and its ability to react covalently with some biological macromolecule.⁴¹ Previous studies proposed a number of mechanisms of toxic action.^{10,42–44} Despite the lack of knowledge regarding specific mechanisms of toxic action for some compounds, it was recognized that, while it is not easy to qualify, electrophilicity is an important property governing the toxicity of these compounds.

In general, the descriptors that appear in the QSAR model can encode different electronic, steric and electrophilic aspects of the molecules, which affect the acute toxicity of the compound.

Multiple linear regressions were found in SPSS in Analyze/Regression/Linear. The method for the multiple linear regression analysis in this study was “Stepwise”, which is an automated procedure used to select the most statistically significant variables from several explanatory variables. In this study, the experimental acute toxicity values of the 33 compounds in the training set as dependent variables and the *G*2, *HOMT*, *G(Cl··Cl)*, *Mor03v* and *MAXDP* as independent variables had to be entered into the multiple linear regression model. The types and definitions of these descriptors are listed in Table IV.

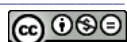
TABLE IV. Molecular descriptors selected by GA–PLS

| Descriptor | Independent variable | Type |
|------------------|----------------------|-------------------------|
| <i>Mor03v</i> | x_1 | 3D-MoRSE descriptors |
| <i>G(Cl··Cl)</i> | x_2 | 3D Atom pairs |
| <i>G</i> 2 | x_3 | Geometrical descriptors |
| <i>HOMT</i> | x_4 | Geometrical descriptors |
| <i>MAXDP</i> | x_5 | Topological descriptors |

The MLR model built by stepwise regression⁴⁵ on the training set is given as Eq. (10):

$$\begin{aligned} -\log IGC_{50} = & -120.042 - 0.538x_1 - 0.026x_2 + \\ & + 19.745x_3 + 0.462x_4 - 0.216x_5 \\ N = 33, R^2 = 0.963, F = 140.273, S = 0.142 \end{aligned} \quad (10)$$

The model was assessed with the *R*² value (coefficient of determination), the *F* value (Fischer statistics), and the *S* value (standard deviation). The number of



observations N was also noted. Generally, the higher the correlation coefficient and the lower the standard error, the more reliable is the model. High values of F indicate the significance of Eq. (10), which reflects the ratio of variance explained by the model and the variance due to the error in the model.

Based on Eq. (10), the independent variables x_3 and x_4 were positively correlated with the dependent variable acute toxicity, while the independent variable x_1 , x_2 and x_5 were in negative correlations with acute toxicity. As discussed in the section above, this also indicates positive contributions of molecular bulk (size), halogen and additional nitro substitutions in the nitrobenzene ring and negative contributions of $-Cl$ group and molecular electrophilicity to the toxicity.

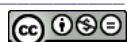
The relative influence of the various parameters on the targeted value were determined by their standardized regression coefficients in the equation, which were 0.210, -0.282, 0.842, 0.304 and -0.168, respectively. According to these values, the importance of the descriptors involved in the model decreased in the following order: $G2 > HOMT > G(Cl\cdots Cl) > Mor03v > MAXDP$. The most significant descriptor is the mass distribution $G2$. The second significant descriptor is $HOMT$.

Model validation

In order to check the reliability and the stability of the QSAR model elaborated by the MLR method, both internal and external validations were conducted. The leave-one out cross-validation correlation coefficient (Q_{LOO}^2) was 0.944, showing the good robustness of the model. Moreover, predictions realized on the test set were in good agreement with the experimental values ($R_{ext}^2 = 0.927$, $Q_{ext}^2 = 0.918$, $RMSE_{ext} = 0.220$). The value of the cross-validation correlation coefficient (Q_{LOO}^2) was similar to R^2 ($R^2 - Q_{LOO}^2 = 0.019$), which disclosed that the linear modeling method had a good generalization performance.

The dependences between the predicted acute toxicity values *vs.* the observed values for both the training and test sets are shown in Fig. 2, which shows good correlations between the parameters. In addition, the residuals of the predicted values of the acute toxicity against the observed values for the model are shown in Fig. 3. As most of the calculated residuals were distributed on both sides of the zero line, the conclusion could be drawn that there was no systematic error in the development of the developed model.

Moreover, the obtained model was tested for chance correlations by the y -scrambling experiment. In this work, the y -scrambling was conducted using the "MLR Y-Randomization Test 1.0" java program.⁴⁶ This y -scrambling was repeated 100 times. Every run yielded estimates of R^2 and Q^2 , which are presented in Table S-I of the Supplementary Material to this paper. The obtained mean value of R^2 and Q^2 after a 100-time scrambling of the data set and modeling were



0.1625 ($R^2 < 0.3$) and -0.2871 ($Q^2 < 0.0$), respectively. It could thus be concluded that chance correlation had little or no effect in the presented model.

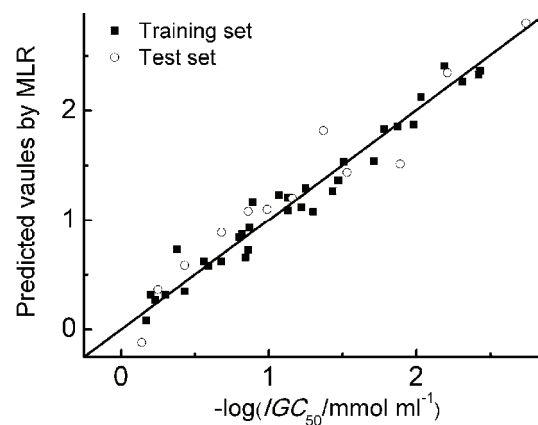


Fig. 2. Comparison between the predicted and the experimental $-\log IGC_{50}$ values.

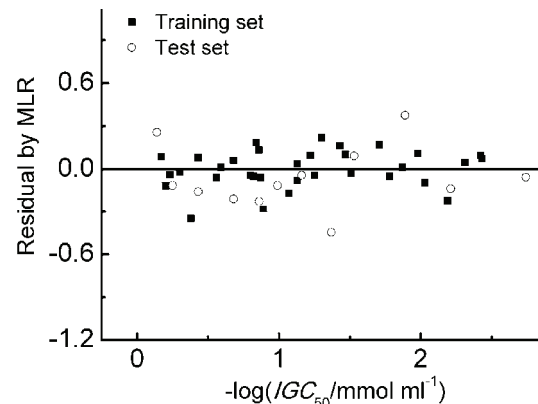


Fig. 3. Plots of the residuals *vs.* the experiment $-\log IGC_{50}$ values for the MLR model.

All the results discussed above showed that the presented MLR model could be effectively used to predict the acute toxicity of nitrobenzenes to *T. pyriformis*.

Model comparison

In order to estimate acute toxicity of nitrobenzenes to the *T. pyriformis*, several important relationships were previously proposed, which are reported in Table V.

As seen from Table V, these models were mainly based on three different typologies of descriptors: experimental parameters, quantum-chemical descriptors and molecular structure descriptors. Unfortunately, it is not possible to verify whether one model is better than another is; at most, it is possible to discuss the quality and the drawbacks of each model, because the size and composition of the training sets were usually different. Furthermore, the literature often reports

only the fitting power of a model expressed by R^2 , while the predictive power is unknown. A γ -scrambling test was not always performed. However, the MLR model presented in this paper is derived only from knowledge of molecular structure and it shows good predictive ability and strong robustness.

TABLE V. Comparison of some models for the prediction of nitrobenzenes' acute toxicity to *T. pyriformis*

| Literature | <i>N</i> | Model descriptors | Q^2 a | R^2 a |
|------------|----------|-------------------------------------------------------------------------------------------------------------|---------|---------|
| 12 | 42 | $[\eta'_F]_{\text{Cl}}, [\eta'_F]_{\text{Br/I}}, [\eta'_F]_{\text{NO}_2}, [\eta'_F]_{\text{CH}_2\text{OH}}$ | 0.88 | 0.920 |
| 15 | 42 | $\mu_0, \mu_1, \mu_2, \mu_0$ | 0.901 | 0.910 |
| 9 | 42 | $\log K_{\text{OW}}, \log K_{\text{OW}}, E_{\text{LUMO}}$ | 0.866 | 0.881 |
| 13 | 36 | $E_{\text{HOMO}}, E_{\text{LUMO}}, \Delta E, P, \mu, V, Q_{\text{-NO}_2}$ | 0.874 | 0.896 |
| 14 | 20 | E_{LUMO} | – | 0.889 |
| 47 | 97 | $E_{\text{en}}^{\min}(\text{C}-\text{C}), {}^2\chi, E^{\text{SOMO}}, \bar{V}_0, FNSA_{\text{PNSA}}^{(2)}$ | – | 0.815 |
| 10 | 47 | $\log D, E_{\text{LUMO}}, dC_{\text{ox}} $ | 0.826 | 0.858 |
| 36 | 50 | $\omega, \log E_{\text{LUMO}}, \log P$ | – | 0.870 |

aThe model with best predictive ability in the literature

CONCLUSIONS

In this study, GA-PLS was used to search for molecular descriptors closely related to the acute toxicity of nitrobenzenes for *T. pyriformis*. A set of five descriptors were finally selected and used to build a model by MLR. The most significant descriptor was the *G2* molecular descriptor. This descriptor is a geometrical descriptor related to the size of the molecule. Moreover, the number of substituents on the aromatic ring of the nitrobenzenes, connected with the geometrical descriptor *HOMT*, also played a key role in the acute toxicity. Furthermore, internal and external validations were conducted to check the reliability and the stability of the QSAR model elaborated by the MLR method. The results showed the established model had a good predictive ability and strong robustness, with $R^2 = 0.963$, $Q^2_{\text{LOO}} = 0.944$ and $Q^2_{\text{ext}} = 0.918$. Thus, the presented model could be efficiently employed for estimating the toxicity of nitrobenzene derivatives for which experimental data are unavailable.

SUPPLEMENTARY MATERIAL

The molecular structures of the 45 titled compounds (Fig. S-1) and the results of the γ -randomization validation (Table S-I) are available electronically from <http://www.shd.org.rs/JSCS/>, or from the corresponding author on request.

Acknowledgements. Financial support from the National Natural Science Foundation of China (Nos. 51202020 and 51472035), the International S & T Cooperation Program of Changzhou City (CZ20110022), the Science and Technology Department of Jiangsu Province (BY2013024-04, BE2014089) and the Qing Lan Project of Jiangsu Province are gratefully acknowledged.



И З В О Д

QSAR СТУДИЈЕ АКУТНЕ ТОКСИЧНОСТИ НИТРОБЕНЗЕНА ЗА ПРАЖИВОТИЊУ
Tetrahymena pyriformis

DAN-DAN WANG¹, LIN-LIN FENG¹, GUANG-YU HE² и HAI-QUN CHEN¹

¹School of Environmental and Safety Engineering, Changzhou University, Jiangsu Province, Changzhou, 213164, China и ²Key Laboratory of Advanced Catalytic Materials and Technology, Changzhou University, Jiangsu Province, Changzhou, 213164, China

Квантитативни модели за релације између структуре и активности (QSAR) имају важну улогу у проучавању структурне зависности токсичности нитробензена за праживотињу *Tetrahymena pyriformis*. У овом раду је применењен генетички алгоритам, заједно са методом парцијалних најмањих квадрата. Токсичност 45 деривата нитробензена описан је помоћу пет дескриптора, наиме *G2*, *HOMT*, *G(Cl··Cl)*, *Mor03v* и *MAXDP*. Показало се да је добијени модел статистички значајан ($R^2 = 0,963$, $Q_{LOO}^2 = 0,944$). Осим тога, одговарајућим статистичком провером (*y-scrambling test*) показали смо да у моделу нема случајне корелације.

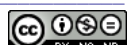
(Примљено 10. септембра, ревидирано 11. новембра, прихваћено 6. децембра 2013)

REFERENCES

1. S. Ikeno, C. Ogino, T. Ito, N. Shimizu, *Biochem. Eng. J.* **15** (2003) 193
2. H. Feuer, A. T. Nielsen, *Nitro Compounds: Recent Advances in Synthesis and Chemistry*, VCH Publishing, New York, 1990, p. 35
3. Y. H. Zhao, X. Yuan, G. D. Ji, L. X. Sheng, L. S. Wang, *Chemosphere* **34** (1997) 1837
4. D. J. W. Blum, R. E. Speece, *Ecotoxicol. Environ. Safety* **22** (1991) 198
5. F. R. Burden, D. A. Winkler, *Chem. Res. Toxicol.* **13** (2000) 436
6. E. Estrada, *SAR QSAR Environ. Res.* **11** (2000) 55
7. D. Ivan, L. Crisan, S. Funar-Timofei, M. Mracec, *J. Serb. Chem. Soc.* **78** (2013) 495
8. M. H. Fatemi, H. Malekzadeh, *Bull. Chem. Soc. Jpn.* **83** (2010) 233
9. M. T. D. Cronin, B. W. Gregory, T. W. Schultz, *Chem. Res. Toxicol.* **11** (1998) 902
10. J. C. Dearden, M. T. D. Cronin, T. W. Schultz, D. T. Lin, *Quant. Struct.-Act. Relat.* **14** (1995) 427
11. D. R. Roy, R. Parthasarathi, V. Subramanian, P. K. Chattaraj, *QSAR Comb. Sci.* **25** (2006) 114
12. K. Roy, G. Ghosh, *QSAR Comb. Sci.* **23** (2004) 99
13. Y. L. Gu, J. Q. Tao, Z. H. Fei, G. C. Zhang, *Chin. J. Struct. Chem.* **29** (2010) 86
14. X. F. Yan, H. M. Xiao, *Chin. J. Struct. Chem.* **26** (2007) 7
15. E. Estrada, E. Uriarte, *SAR QSAR Environ. Res.* **12** (2001) 309
16. A. G. Artemenko, E. N. Muratov, V. E. Kuz'min, N. N. Muratov, E. V. Varlamova, A. V. Kuz'mina, L. G. Gorb, A. Golius, F. C. Hill, J. Leszczynski, A. Tropsha, *SAR QSAR Environ. Res.* **22** (2011) 575
17. U. Depczynski, V. J. Frost, K. Molt, *Anal. Chim. Acta* **420** (2000) 217
18. B. K. Alberg, N. M. Geneste, R. D. King, *Chemom. Intell. Lab. Syst.* **54** (2000) 75
19. D. Jouanrimbaud, D. L. Massart, R. Leardi, O. E. de Noord, *Anal. Chem.* **67** (1995) 4295
20. G. V. Dijck, M. M. V. Hulle, *Chemom. Intell. Lab. Syst.* **107** (2011) 318
21. M. Goodarzi, M. P. Freitas, R. Jensen, *Chemom. Intell. Lab. Syst.* **98** (2009) 123
22. Q. Shen, J. H. Jiang, C. X. Jiao, G. L. Shen, R. Q. Yu, *Eur. J. Pharm. Sci.* **22** (2004) 145
23. M. P. Gonzalez, H. G. Diaz, M. A. Cabrera, R. M. Ruiz, *Bioorg. Med. Chem.* **12** (2004) 735



24. V. Consonni, R. Todeschini, A. Mauri, M. Pavan, *Dragon software: Calculation of molecular descriptors*, Department of Environmental Sciences, University of Milano-Bicocca and Talete, srl, Milan, Italy, 2003, <http://www.vcclab.org/lab/edragon/> (accessed in Sep. 2014)
25. I. V. Tetko, J. Gasteiger, R. Todeschini, A. Mauri, D. Livingstone, P. Ertl, V. A. Palyulin, E. V. Radchenko, N. S. Zefirov, A. S. Makarenko, V. Y. Tanchuk, V. V. Prokopenko. *J. Comput.-Aided Mol. Des.* **19** (2005) 453
26. M. Karelson, V. S. Lobanov, A. R. Katritzky, *Chem. Rev.* **96** (1996) 1027
27. V. Consonni, R. Todeschini, *Methods and Principles in Medicinal Chemistry*, in *Handbook of Molecular Descriptors*. Vol. 11, R. Mannhold, H. Kubinyi, H. Timmerman, Eds., Wiley-VCH, Weinheim, 2000
28. Hypercube HyperChem, Inc., <http://www.hyper.com> (accessed in Sep, 2014)
29. V. Consonni, R. Todeschini, M. Pavan, *DRAGON. Software for the calculation of and web version 2.1 molecular descriptors*, 2002, <http://michem.disat.unimib.it/chm/> (accessed in Sep, 2014)
30. J. H. Holland, *Adaptation in Natural and Artificial Systems*, University of Michigan Press, Ann Arbor, MI, 1975
31. R. Leardi, A. Lupiáñez, *Chemom. Intell. Lab. Syst.* **41** (1998) 195
32. MATLAB 7.4. <http://www.mathworks.com/products/matlab/> (accessed in Sep, 2014)
33. M. Mahani, H. S. Ghomi, *Anal. Methods* **4** (2012) 3381
34. SPSS for Windows, Rel. 10.0.0, SPSS Inc., Chicago, IL, 1999
35. P. Gramatica, M. Corradi, V. Consonni, *Chemosphere* **41** (2000) 763
36. K. Bellifa, S. M. Mekelleche, *Arab. J. Chem.* <http://dx.doi.org/10.1016/j.arabjc.2012.04.031>
37. J. W. Deneer, T. L. Sinnige, W. Seinen, J. L. M. Hermens, *Aquat. Toxicol.* **10** (1987) 115
38. G. D. Veith, O. G. Mekenyan, *Quant. Struct.-Act. Relat.* **12** (1993) 349
39. X. Yuan, G. Lu, P. Lang, *Bull. Environ. Contam. Toxicol.* **58** (1997) 123
40. P. Z. Lang, X. F. Ma, G. H. Lu, Y. Wang, Y. Bian, *Chemosphere* **32** (1996) 1547
41. O. G. Mekenyan, G. D. Veith, *SAR QSAR Environ. Res.* **2** (1994) 129
42. T. W. Schultz, M. T. D. Cronin, *Environ. Toxicol. Chem.* **16** (1997) 357
43. D. W. Roberts, *Chem. Res. Toxicol.* **8** (1995) 545
44. G. Dupuis, C. Benezra, *Allergic Contact Dermatitis to Simple Chemicals*, Marcel Dekker, New York, 1982
45. D. L. Massart, B. G. M. Vandeginste, L. M. G. Buydens, S. Dejong, P. J. Lewi, J. Smeyers-Verbeke, *Handbook of Chemometrics and Qualimetrics: Part A*, Elsevier, Amsterdam, 1977
46. MLR Y-Randomization Test 1.0 java program, <http://dtclab.webs.com/> software-tools (accessed in Sep, 2014)
47. A. R. Katritzky, P. Oliferenko, A. Oliferenko, A. Lomaka, M. Karelson, *J. Phys. Org. Chem.* **16** (2003) 811.





SUPPLEMENTARY MATERIAL TO
**QSAR studies for assessing the acute toxicity of nitrobenzenes to
*Tetrahymena pyriformis***

DAN-DAN WANG¹, LIN-LIN FENG¹, GUANG-YU HE² and HAI-QUN CHEN^{1*}

¹School of Environmental and Safety Engineering, Changzhou University, Jiangsu Province, Changzhou, 213164, China and ²Key Laboratory of Advanced Catalytic Materials and Technology, Changzhou University, Jiangsu Province, Changzhou, 213164, China

J. Serb. Chem. Soc. 79 (0) (2014) 000–000

TABLE S-I. Results of the y -randomization validation

| Model | R^2 | Q^2 | Model | R^2 | Q^2 |
|-----------|--------|---------|-----------|--------|---------|
| Random 1 | 0.1358 | -0.2708 | Random 51 | 0.1478 | -0.2123 |
| Random 2 | 0.4068 | -0.0344 | Random 52 | 0.238 | -0.2097 |
| Random 3 | 0.1997 | -0.245 | Random 53 | 0.2662 | -0.0487 |
| Random 4 | 0.027 | -0.4036 | Random 54 | 0.1726 | -0.2493 |
| Random 5 | 0.1244 | -0.2722 | Random 55 | 0.113 | -0.5259 |
| Random 6 | 0.0657 | -0.4161 | Random 56 | 0.0907 | -0.3946 |
| Random 7 | 0.1167 | -0.4297 | Random 57 | 0.1956 | -0.2543 |
| Random 8 | 0.169 | -0.206 | Random 58 | 0.1963 | -0.3116 |
| Random 9 | 0.2548 | -0.1416 | Random 59 | 0.0217 | -0.4579 |
| Random 10 | 0.0493 | -0.5385 | Random 60 | 0.1344 | -0.4856 |
| Random 11 | 0.0859 | -0.5537 | Random 61 | 0.1518 | -0.2407 |
| Random 12 | 0.0817 | -0.5627 | Random 62 | 0.2178 | -0.1744 |
| Random 13 | 0.1884 | -0.3312 | Random 63 | 0.2399 | -0.1354 |
| Random 14 | 0.0783 | -0.3652 | Random 64 | 0.0806 | -0.4553 |
| Random 15 | 0.0815 | -0.3685 | Random 65 | 0.0867 | -0.4405 |
| Random 16 | 0.1508 | -0.1935 | Random 66 | 0.1739 | -0.3648 |
| Random 17 | 0.2424 | -0.0816 | Random 67 | 0.1055 | -0.4815 |
| Random 18 | 0.1629 | -0.4217 | Random 68 | 0.1838 | -0.4349 |
| Random 19 | 0.0274 | -0.4958 | Random 69 | 0.0963 | -0.3776 |
| Random 20 | 0.0737 | -0.2858 | Random 70 | 0.2123 | -0.1789 |
| Random 21 | 0.1724 | -0.2384 | Random 71 | 0.2245 | -0.1861 |
| Random 22 | 0.1011 | -0.4897 | Random 72 | 0.1035 | -0.456 |
| Random 23 | 0.3505 | 0.0922 | Random 73 | 0.4003 | 0.1303 |
| Random 24 | 0.3104 | -0.0892 | Random 74 | 0.1107 | -0.2842 |
| Random 25 | 0.1264 | -0.3953 | Random 75 | 0.0527 | -0.5697 |
| Random 26 | 0.2193 | -0.195 | Random 76 | 0.1486 | -0.2057 |

*Corresponding author. E-mail: hqchenyf@hotmail.com

TABLE S-I. Continued

| Model | R^2 | Q^2 | Model | R^2 | Q^2 |
|----------------------|--------|---------|------------|--------|---------|
| Random 27 | 0.0714 | -0.4154 | Random 77 | 0.1269 | -0.3869 |
| Random 28 | 0.1653 | -0.3346 | Random 78 | 0.2844 | -0.1379 |
| Random 29 | 0.1001 | -0.2356 | Random 79 | 0.3716 | 0.0884 |
| Random 30 | 0.0579 | -0.448 | Random 80 | 0.1852 | -0.2434 |
| Random 31 | 0.1234 | -0.3085 | Random 81 | 0.0795 | -0.4541 |
| Random 32 | 0.1502 | -0.1818 | Random 82 | 0.2168 | -0.1933 |
| Random 33 | 0.0663 | -0.4397 | Random 83 | 0.0269 | -0.5164 |
| Random 34 | 0.219 | -0.298 | Random 84 | 0.0636 | -0.4222 |
| Random 35 | 0.2231 | -0.3232 | Random 85 | 0.2222 | -0.1293 |
| Random 36 | 0.285 | -0.0902 | Random 86 | 0.2445 | -0.1094 |
| Random 37 | 0.2525 | -0.0109 | Random 87 | 0.0223 | -0.433 |
| Random 38 | 0.1614 | -0.2618 | Random 88 | 0.1899 | -0.4443 |
| Random 39 | 0.1511 | -0.3019 | Random 89 | 0.048 | -0.6216 |
| Random 40 | 0.1492 | -0.2454 | Random 90 | 0.0823 | -0.4262 |
| Random 41 | 0.1898 | -0.1992 | Random 91 | 0.0766 | -0.3398 |
| Random 42 | 0.1685 | -0.3456 | Random 92 | 0.3163 | 0.0506 |
| Random 43 | 0.1489 | -0.2463 | Random 93 | 0.1601 | -0.1501 |
| Random 44 | 0.1061 | -0.3298 | Random 94 | 0.2543 | 0.0004 |
| Random 45 | 0.1179 | -0.5352 | Random 95 | 0.0845 | -0.4744 |
| Random 46 | 0.1962 | -0.1834 | Random 96 | 0.3105 | -0.2083 |
| Random 47 | 0.3078 | 0.0595 | Random 97 | 0.1234 | -0.2445 |
| Random 48 | 0.2635 | -0.0631 | Random 98 | 0.1498 | -0.2165 |
| Random 49 | 0.3353 | -0.0816 | Random 99 | 0.1379 | -0.2898 |
| Random 50 | 0.1327 | -0.4471 | Random 100 | 0.168 | -0.2025 |
| Average value | 0.1625 | -0.2871 | | | |



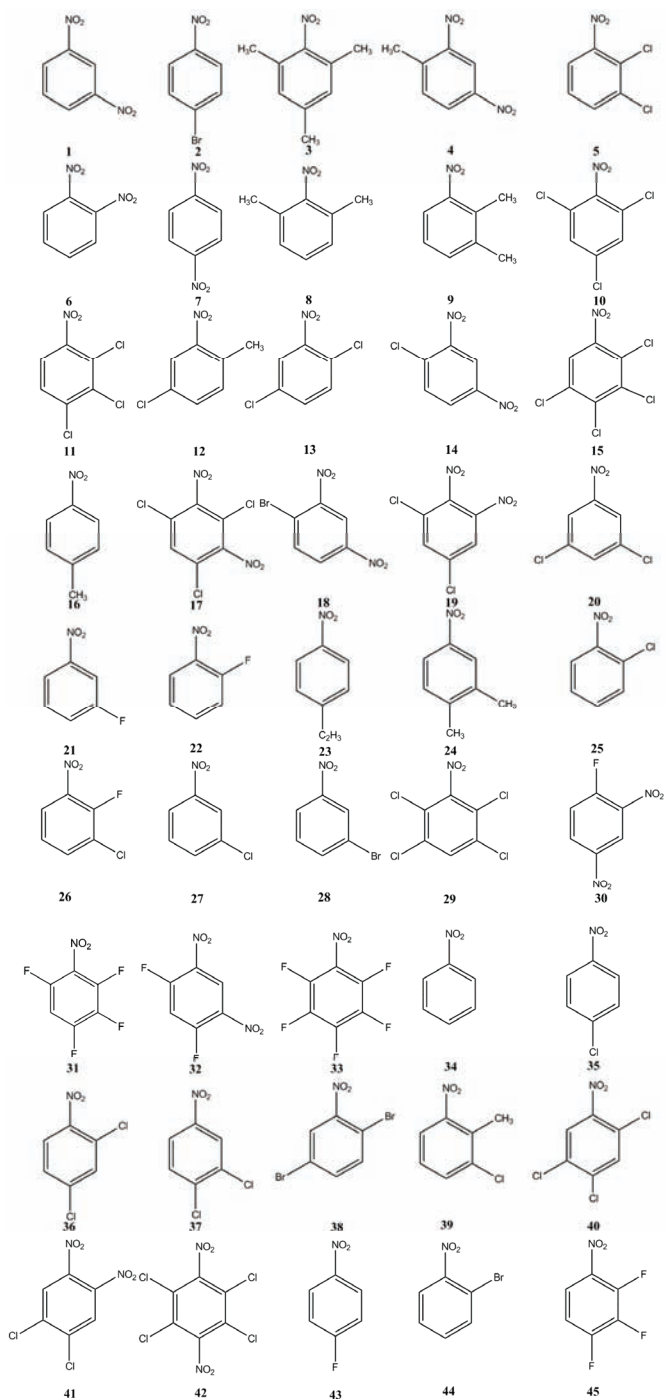


Fig. S-1. Molecular structures of the 45 titled compounds.



Photocatalytic efficiency of titania photocatalysts in saline waters

ASMA JUMA ALBRBAR¹, ANDJELIKA BJELAJAC^{2#}, VELJKO DJOKIĆ^{1#},
JELENA MILADINOVIC¹, DJORDJE JANAČKOVIC^{1#} and RADA PETROVIĆ^{1**#}

¹Faculty of Technology and Metallurgy, University of Belgrade, Karnegijeva 4, 11000 Belgrade, Serbia and ²Innovation Center of the Faculty of Technology and Metallurgy, Karnegijeva 4, University of Belgrade, 11000 Belgrade, Serbia

(Received 11 November 2013, revised 20 February, accepted 11 March 2014)

Abstract: The photocatalytic efficiency of a recently synthesized TiO₂ powder, denoted P160, for the degradation of the Dye C.I. Reactive Orange 16 in natural and artificial seawater was investigated in comparison to its efficiency in deionized water and the efficiency of a standard TiO₂ powder, Degusa P25. It was shown that the photocatalytic efficiency of P160 was slightly higher than that of P25, probably due to slightly higher specific surface area, higher pore volume and larger pores of the powder P160. The efficiency of both photocatalysts in natural and artificial seawater was significantly lower than in deionized water. The overall rate of dye degradation for both types of photocatalysts was slightly higher in artificial seawater than in natural seawater, which shows the influence of organic compounds naturally present in seawater on the photocatalysts activity. A saturation Langmuir-type relationship between the initial degradation rate and the initial dye concentration indicated that adsorption plays a role in the photocatalytic reaction. The photodegradation rate constant, *k*, which represents the maximum reaction rate, had similar values for P25 and P160 in all types of water due to the similar properties of the photocatalysts.

Keywords: photocatalysis; titanium dioxide; dye degradation; seawater; Langmuir–Hinshelwood model.

INTRODUCTION

The removal of organic pollutants from water is an important challenge for water treatment worldwide. In the last few years, seawater has become an important source for drinking water preparation mainly by reverse osmosis membrane filtration. However, the organic matter in seawater, which may deposit on the

* Corresponding author. E-mail: radaab@tmf.bg.ac.rs

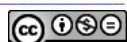
Serbian Chemical Society member.

doi: 10.2298/JSC131114020A

membrane surface and thus stimulate biofouling, should be removed in advance. The conventional treatment methods are unable to remove trace organic contaminants and large amounts of secondary pollutants are released into the environment. To overcome this, the semiconductor photocatalytic process has provided a satisfactory and economically viable solution by enabling complete mineralization of many organic pollutants into CO₂ and H₂O.^{1,2}

The semiconductor TiO₂ has been widely used as a photocatalyst for inducing a series of reductive and oxidative reactions on its surface. The photo-induced reactions are basically initiated by band gap excitation to generate valence band holes (h⁺) and conduction band electrons (e⁻). In TiO₂-assisted oxidation processes of organic compounds, there are two important processes: the direct oxidation on the TiO₂ surface by h⁺ and the indirect oxidation by reactive oxygen species, such as superoxide (O₂^{•-}), singlet oxygen (¹O₂), the hydroxyl radical (•OH), the hydroperoxyl radical (HO₂[•]), and hydrogen peroxide (H₂O₂), which are formed *via* the reduction of O₂ by e⁻ and by the reaction of h⁺ with hydroxyls or water at the TiO₂ surface.³⁻⁵ The efficiency of heterogeneous photocatalysis depends primarily on the properties of the photocatalyst, such as: the band gap energy, specific surface area, pore size distribution, crystal structure, crystal size, *etc*. However, the efficiency of a photocatalyst could greatly depend on environmental factors, in other words some components found in water that processed may affect the efficiency.⁶⁻¹⁰ Previous investigations of the photocatalytic efficiency of some photocatalysts in saline waters showed that salinity generally decreases the efficiency.^{7,8,10-13}

The aim of this work was to compare the photocatalytic efficiency of a recently synthesized¹⁴ TiO₂ powder P160 and a standard TiO₂ powder Degusa P25 on the degradation of dissolved organic substances in saline waters, using artificial (ASW) and natural (SW) seawaters. Previous investigations^{14,15} showed the very good photocatalytic efficiency of P160 on the degradation of dyes CI Reactive Orange 16 and CI Basic Yellow 28 in deionized water. In this paper, the efficiency of P160 and of P25 in saline waters were compared to the efficiency in deionized water (DIW) according to the degree of decomposition of the dye C.I Reactive Orange 16, as a model for dissolved organic substances, under UV irradiation at room temperature. Due to the natural decomposition of plants, fish and microorganisms, SW usually contains a complex mixture of organic constituents that could also react during photocatalytic experiments. ASW was used to assess the influence of the major seawater ions on the efficiency of the photocatalysts and to establish the relevance of ASW as a model for the study. The effect of the initial dye concentration on the initial reaction rate of photodecolorization by both photocatalysts in DIW, SW and ASW was also studied.



EXPERIMENTAL

Materials

Recently synthesized powder P160¹⁴ was used in the experiments, together with a commercially available photocatalyst powder Degussa P25, since it has become the standard for photoreactivity in environmental applications.¹⁶⁻¹⁹ The specific surface area of P25 powder was 45.7 m²·g⁻¹, the pore volume was 0.177 cm³·g⁻¹, the average pore size was 7.57 nm, the crystalline size was 29.5 nm and it consisted of 72.7 % anatase and 27.3 % rutile,¹⁹ while the point of zero charge, pH_{PZC}, of P25 was 6.4.²⁰ P160 was synthesized by a non-hydrolytic sol-gel process combined with a solvothermal treatment.¹⁴ Titanium isopropoxide, Ti(O'Pr)₄, titanium tetrachloride, TiCl₄, and carbon tetrachloride, CCl₄, were mixed in the mole ratio 1:1:1 under a nitrogen atmosphere in a glove box. The obtained mixture was subjected to gelation in an autoclave at 160 °C for 3 h. The gel was dried at 100 °C under a nitrogen flow and calcined at 500 °C for 3 h. The thus obtained powder P160 consisted of pure anatase and its specific surface area was 52.8 m²·g⁻¹, the average pore size was 11.1 nm, the pore volume was 0.209 cm³·g⁻¹ and the crystalline size was 26.4 nm.¹⁴ The point of zero charge of P160, determined by a batch equilibration technique,²¹ was 6.5. Scanning electron micrographs (SEM) of the titania powders, obtained using a Tescan Mira3 XMU microscope operated at 20 kV, are presented in Fig. 1.

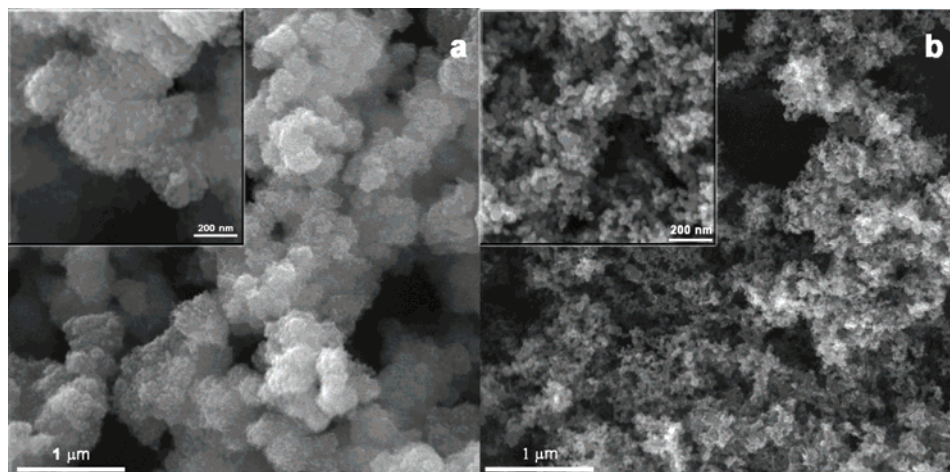


Fig. 1. Scanning electron micrographs (SEM) of a) P160 and b) P25.

The anionic dye C.I Reactive Orange 16 (RO16) was obtained from Bezema (commercial name Bezaktiv Orange V-3R) and used without further purification. Its molecular formula is C₂₀H₁₉N₃O₁₁S₃.

The three types of water were used: deionized water (DIW) from a Millipore Waters Milli Q purification unit; natural seawater (SW), obtained off the coast of Greece and passed through 2 μm filter and artificial seawater (ASW).

Analysis of natural seawater and preparation of artificial seawater

The concentrations of major cations and anions in the natural seawater were determined on a Metrohm ion chromatography instrument, 861 Advanced Compact IC MSM II, and the results are presented in Table I. The instrument specifications were: conductivity detector with

chemical suppression; controlled flow ranging from 0.2 to 2.5 mL min⁻¹ and maximum pressure of 35 MPa. The columns specifications were: Metrosep A Supp 5–150 (for anion analysis), anion eluent – 3.2 mmol Na₂CO₃/1.0 mmol NaHCO₃; Metrosep C2–150 (for cation analysis), cation eluent – 4 mmol tartaric acid/0.75 mmol dipicolinic acid; suppressor solution – 50 mmol H₂SO₄. Prior to the analysis, all samples were filtered through 0.45 µm filters and degassed in an S100 Elmasonic ultrasonic bath. The standard solutions were prepared with demineralized water and standard ion solutions.

TABLE I. Ionic composition of SW

| Ion | Concentration, mmol L ⁻¹ |
|-------------------------------|-------------------------------------|
| Cl ⁻ | 564.1 |
| Na ⁺ | 488.9 |
| K ⁺ | 8.74 |
| Mg ²⁺ | 45.22 |
| Ca ²⁺ | 8.56 |
| SO ₄ ²⁻ | 27.91 |

The quantities of salts for the ASW preparation were calculated according to the composition of SW given in Table I. The prepared ASW had the following composition: 488.9 mmol L⁻¹ NaCl, 8.74 mmol L⁻¹ KCl, 25.91 mmol L⁻¹ MgCl₂·6H₂O, 19.36 mmol L⁻¹ MgSO₄·7H₂O and 8.56 mmol L⁻¹ CaSO₄.

Photocatalytic degradation experiments

A batch-type quartz reactor (cylindrical shape, inner diameter 4 cm, volume 50 mL) was used for the catalytic runs and the set up was in a closed housing to prevent the effect of external light. The reactor had water-cooling jacket, and the illumination was provided for by a Philips HPR 125 W lamp, having the strongest emission wavelength of 364 nm. The lamp was placed 100 mm from the surface of the reaction mixture. The catalyst was maintained in suspended form by using a magnetic stirrer (500 rpm).

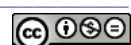
The photocatalytic efficiencies of P25 and P160 were investigated in DIW, SW and ASW under the following experimental conditions: dye concentration in the range of 20–80 mg L⁻¹, TiO₂ powders concentration of 1 g L⁻¹ and UV irradiation at room temperature.

In all the experiments, a suspension of 25 mg of TiO₂ powder and 25 mL of solution was mixed ultrasonically for 10 min, followed by magnetically stirring for 30 min in the dark, to attain adsorption/desorption equilibrium. The pH values of the suspensions were between 6.5 and 6.8 in DIW and ASW and about 7.7 in SW, for both photocatalysts. Then, the UV light was switched on to perform the photocatalytic reaction. The concentrations of dye in the starting solutions and of dye remaining in the solutions after stirring in the dark and after 5, 10, 15 and 30 min of irradiation were determined by UV–Vis spectroscopy (Shimadzu UV-160A 145 instrument). The solutions for analysis by UV–Vis spectroscopy were prepared by passing through a syringe filter (pore size of 0.22 µm) in order to remove the particles of the photocatalyst.

RESULTS AND DISCUSSION

Comparison of the photocatalysts efficiency in different types of water

The results of photodegradation of dye RO16 in DIW, SW and ASW by photocatalysts P25 and P160 are presented in the form of the dependence of the



normalized concentration, c/c_0 , vs. time t , where c_0 is the concentration of RO16 after adsorption in the dark and c is the concentration of RO16 after illumination time t (Figs. 2 and 3). The degradation efficiency of the photocatalysts can be assessed by using the expression: $1 - c/c_0$.

The Langmuir–Hinshelwood (L–H) model was used to describe the kinetics of photodegradation of dye.^{22–25} This model basically relates the degradation rate r and reactant concentration c in water after an illumination time t . The simple rate expression for the L–H model is given by Eq. (1):

$$r = -\frac{dc}{dt} = \frac{kKc}{1 + Kc} \quad (1)$$

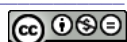
where k is the rate constant, which is dependent on the diffusion of the reactant into the pores and the reaction at the interface,¹⁶ and K is the Langmuir adsorption to desorption equilibrium constant. According to the L–H model, a limiting reaction rate ($r = k$) is observed at high reactant concentrations ($Kc \gg 1$). When the adsorption is relatively weak and/or the reactant concentration is low ($Kc \ll 1$) and Eq. (1) can be simplified to pseudo-first order kinetics with an apparent first-order rate constant k_{app} :^{26–28}

$$-\ln\left(\frac{c}{c_0}\right) = kKt = k_{app}t \quad (2)$$

The dependences of $-\ln(c/c_0)$ vs. illumination time t for the data in Figs. 2 and 3 are linear (insets of Figs. 2 and 3), as confirmed by the correlation coefficient R^2 values of ≈ 1 (Tables II–IV). The derived k_{app} values corresponding to their respective initial dye concentration, c_0 , are also presented in Tables II–IV.

From the results presented in Figs. 2 and 3, it could be seen that the efficiency of photocatalytic degradation of RO16 by P25 and P160 in DIW, SW and ASW decreased as the initial concentration increased, which is in good agreement with decreasing trend of k_{app} values, shown in Tables II–IV. This could be explained in terms of saturation of the limited number of accessible active sites on the photocatalytic surface. When the dye concentration increased, the amount of dye adsorbed on the catalyst surface also increased (data not shown), resulting in a reduction in the light intensity reaching the photocatalyst,¹¹ since the absorption of RO16²⁹ well matches the absorption of titania¹⁹ in the UV part of the spectrum. It is well known that the absorption edge of titania powders is about 400 nm,¹⁹ while RO16 had three absorption bands in the UV region, centered at 388, 302 and 254 nm.²⁹

Both photocatalysts showed their highest photocatalytic activity in DIW, where the dye concentration decreased more rapidly with time than in SW and ASW, as seen in Figs. 2 and 3. Consequently, the k_{app} values were much higher



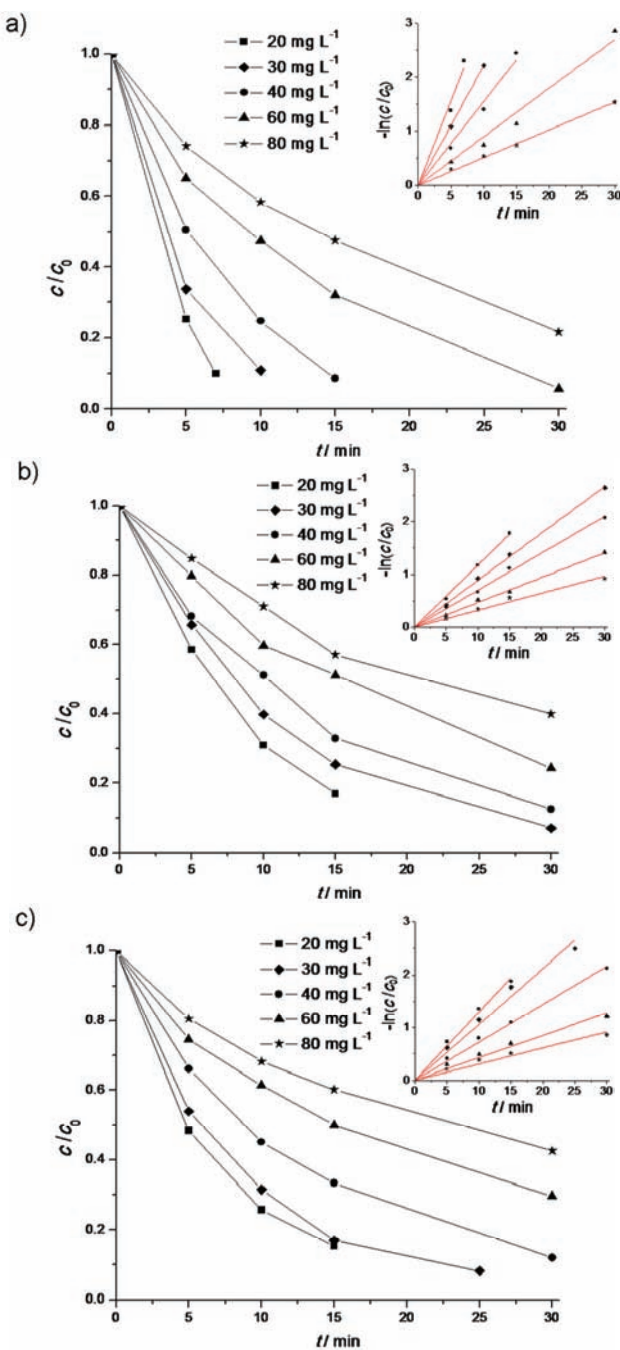


Fig. 2. Photocatalytic degradation of the dye RO16 by P25 powder in a) DIW, b) SW and c) ASW (UV irradiation at room temperature; the P25 concentration was 1 g L^{-1}). The corresponding linear plots of the photocatalytic decolorization kinetics are given in the insets.

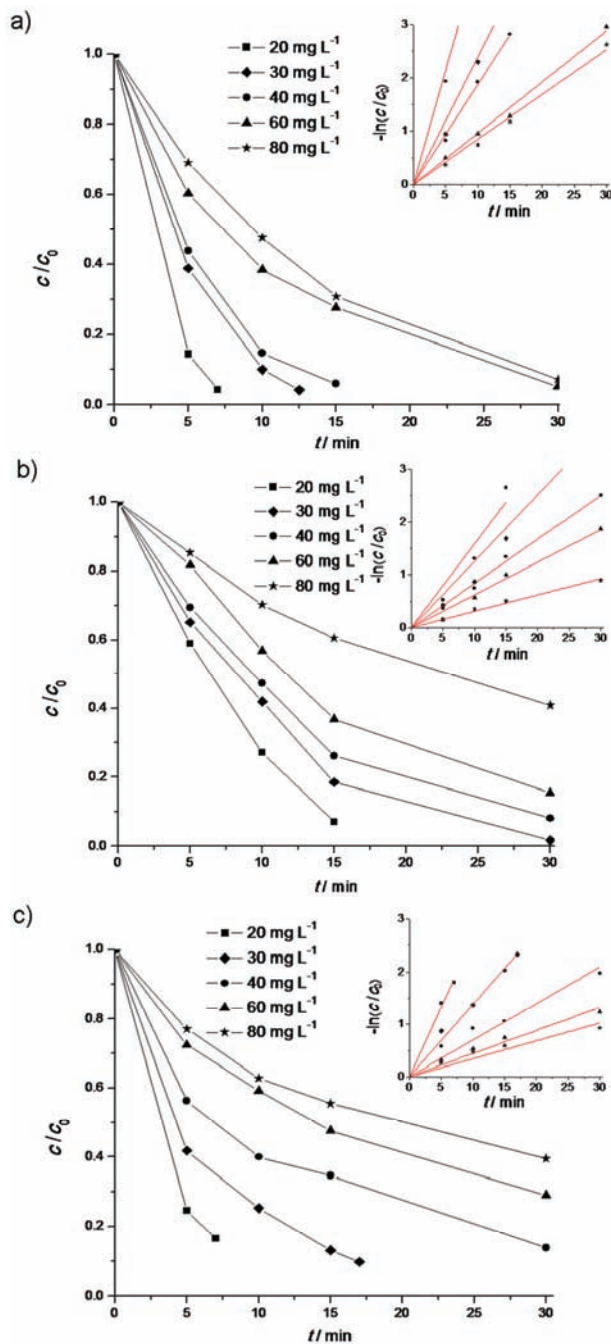


Fig. 3. Photocatalytic degradation of the dye RO16 by P160 powder in a) DIW, b) SW and c) ASW (UV irradiation at room temperature; the P160 concentration was 1 g L^{-1}). The corresponding linear plots of the photocatalytic decolorization kinetics are given in the insets.

TABLE II. The k_{app} values for the photodegradation of RO16 by P25 and P160 in DIW in dependence on the initial dye concentration (UV irradiation at room temperature; TiO_2 concentration was 1 g L^{-1})

| $c_0 / \text{mg L}^{-1}$ | Type of titania | | | |
|--------------------------|-----------------------------|--------|-----------------------------|--------|
| | P25 | | P160 | |
| | $k_{app} / \text{min}^{-1}$ | R^2 | $k_{app} / \text{min}^{-1}$ | R^2 |
| 20 | 0.3109 | 0.9902 | 0.4267 | 0.9934 |
| 30 | 0.2207 | 0.9999 | 0.2389 | 0.9917 |
| 40 | 0.1545 | 0.9936 | 0.1874 | 0.9983 |
| 60 | 0.0898 | 0.9887 | 0.0962 | 0.9966 |
| 80 | 0.0512 | 0.9988 | 0.0846 | 0.9959 |

Table III. The k_{app} values of photodegradation of RO16 by P25 and P160 in SW in dependence on the initial dye concentration (UV irradiation at room temperature; TiO_2 concentration was 1 g L^{-1})

| $c_0 / \text{mg L}^{-1}$ | Type of titania | | | |
|--------------------------|-----------------------------|--------|-----------------------------|--------|
| | P25 | | P160 | |
| | $k_{app} / \text{min}^{-1}$ | R^2 | $k_{app} / \text{min}^{-1}$ | R^2 |
| 20 | 0.1173 | 0.9902 | 0.1590 | 0.9671 |
| 30 | 0.0890 | 0.9995 | 0.1260 | 0.9810 |
| 40 | 0.0700 | 0.9926 | 0.0827 | 0.9974 |
| 60 | 0.0470 | 0.9887 | 0.0620 | 0.9915 |
| 80 | 0.0322 | 0.9988 | 0.0310 | 0.9955 |

Table IV. The k_{app} values of photodegradation of RO16 by P25 and P160 in ASW in dependence on the initial dye concentration (UV irradiation at room temperature; TiO_2 concentration was 1 g L^{-1})

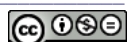
| $c_0 / \text{mg L}^{-1}$ | Type of titania | | | |
|--------------------------|-----------------------------|--------|-----------------------------|--------|
| | P25 | | P160 | |
| | $k_{app} / \text{min}^{-1}$ | R^2 | $k_{app} / \text{min}^{-1}$ | R^2 |
| 20 | 0.1299 | 0.9969 | 0.2651 | 0.9973 |
| 30 | 0.1062 | 0.9917 | 0.1380 | 0.9964 |
| 40 | 0.0723 | 0.9980 | 0.0699 | 0.9774 |
| 60 | 0.0426 | 0.9908 | 0.0441 | 0.9841 |
| 80 | 0.0306 | 0.9831 | 0.0341 | 0.9683 |

for the photodegradation of the dye in DIW than those in SW and ASW. The observed decrease of dye photodegradation efficiency in salt waters was explained by the fouling effects of the inorganic ions on the photoactivity of titania. Several mechanisms for the fouling effects of inorganic ions on the photoactivity of titania were proposed.⁸ These include UV screening, competitive adsorption to surface active sites, competition for photons, surface deposition of precipitates and elemental metals, radical and hole scavenging and direct reaction with the photocatalyst.



Furthermore, according to the k_{app} values for the photodegradation of the dye in saline waters, it could be seen that the photocatalytic efficiency was higher in ASW at lower concentrations (20 and 30 mg L⁻¹), while at higher concentrations, the efficiency was slightly higher in SW for both photocatalysts. It could be assumed that the better efficiency in ASW than in SW was because SW contains some other ions (carbonate and bicarbonate) and organic substances besides the major cations and anions (Table I). It was reported that carbonate and bicarbonate both act as electron scavengers and thus they are expected to be responsible for the observed lowering of the degradation rate.¹² However, when the photocatalysis occurs in an air atmosphere, oxygen is a more powerful scavenger of electrons formed in TiO₂ after illumination than carbonate and bicarbonate ions. In addition, the reaction rate constants of hydroxyl radicals with carbonate and bicarbonate ions are much smaller than the values given for the other ions.³⁰ Therefore, it is likely that the organic substances present in SW influenced the activity of the titania powders by adsorption onto their surface and the resulting blocking of the active sites. The differences in the photocatalytic activities in ASW and SW may also be the result of the different pH values of the suspensions during the reaction. The pH values of the suspensions in SW were higher than pH_{PZC} of the titania, while in the case of suspension in ASW, the pH values were approximately equal to the pH_{PZC}. Accordingly, the adsorption of the dye anions should be less favorable at the negatively charged titania surface in SW than in ASW. However, the adsorption in SW was comparable (for P160) and even higher (for P25) than in ASW, which suggests that the organic substances present in SW strongly influenced dye adsorption onto the titania powders. These results show that, besides the major ions, organic compounds naturally present in seawater had a large influence on the photocatalytic activity of the titania powders. Consequently, the artificial seawater that contained only the major seawater ions cannot be used as a model for the prediction of the activity of the photocatalysts in natural seawaters.

By comparing the photocatalysts P25 and P160, it could be observed that P160 had a slightly better photocatalytic efficiency than P25 in all three types of water. The values of k_{app} in all three types of water for P160 were higher than those for P25 (with experimental uncertainty for the higher concentration of the dye). It is well known that the efficiency of semiconductors is influenced by many factors, such as crystalline structure, particle size, specific surface area, adsorption capacity, and prevention of electron–hole pair recombination reactions. In comparison with P25, the P160 powder had a slightly higher specific surface area, higher pore volume and larger pores, which contributed to its better photocatalytic efficiency with respect to P25. On the other hand, the P25 crystallites were slightly larger than those of P160 were and P25 contained 72.7 % anatase and 27.3 % of rutile, while P160 contained pure anatase. These features

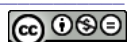


should contribute to a better photoactivity of P25. It was shown³¹ that, in comparison to pure anatase, mixed-phase titania catalysts show greater photoeffectiveness in the UV region due to stabilization of the charge separation by electron transfer from rutile to anatase, which slows recombination. Despite the fact that P160 contained pure anatase, its photocatalytic efficiency was slightly higher compared to that of P25, probably due to its higher specific surface area and larger pores. For the same quantity of adsorbed dye, the surface coverage would be higher in the case of the TiO₂ with a lower specific surface area, which causes a greater reduction of the light intensity reaching the photocatalyst and, consequently, lower photocatalytic activity. In addition, different types of aggregation of the primary particles of P160 and P25 (Fig. 1) caused the powders to have different pore volumes and pore sizes. The pore size is a very important parameter for photocatalysis, because large dye molecules cannot enter small pores and, in that way, the surface of such pores is inaccessible for reaction.

The influence of initial dye concentration on the initial photodegradation rate

The effects of the initial dye concentration c_0 (after 30 min in the dark) on its initial photodegradation rate r_0 with P25 and P160 in DIW, SW and ASW are demonstrated in Fig. 4. Values of r_0 (in mg L⁻¹ min⁻¹) were obtained according to the results presented in Figs. 2 and 3, as the dye concentration decay at 5 min of photoreaction. It could be observed from Fig. 4 that the initial degradation rate increased with increasing initial dye concentration and then remained almost constant. According to the L–H model^{32,33} (Eq. (1), $r = r_0$ and $c = c_0$), such a dependence of r_0 on c_0 indicates that the oxidation rate is first-order at lower concentrations and becomes zero-order at higher concentrations, when the reaction rate becomes independent of the dye concentration (meaning a saturation-type Langmuir kinetics). Such a Langmuir-type relationship between the initial degradation rate and concentration indicates that adsorption played a role in the photocatalytic reaction.

It is well known that photocatalytic reactions can occur independently of the degree of adsorption of organic compounds on TiO₂ both in the dark or during the photocatalytic process. The radical species produced during irradiation can react with dye on the surface of the TiO₂ but also in the bulk of the solution. It was suggested³⁴ that in the case of radical formation on a UV-illuminated TiO₂ surface, adsorption of the organic compound would increase the reaction rates, but it is not a prerequisite for the reaction to occur since the reactive OH· radicals and other oxidizing species can diffuse into the solution bulk where they react with the organic pollutant. In the present case, the adsorption was included in photocatalytic process: for both photocatalysts and for all types of water, the reaction rate increased as the adsorption increased, but in the case of a particular photocatalyst for different types of water, the highest adsorption did not mean the



highest reaction rate. For example, in the case of P25, the adsorption for all initial concentrations was higher in SW than in ASW, but reaction rates were lower. Thus, the adsorption plays a role in the photocatalytic reaction, but it is not the main factor that influences the reaction rate and the efficiency of the photocatalyst.

From Fig. 4 it is obvious that the highest values of initial reaction rate for both photocatalysts were observed for in DIW, than in ASW, and the lowest in SW, as was found for the efficiency of the photocatalysts according to the overall reaction rate for the different dye concentrations.

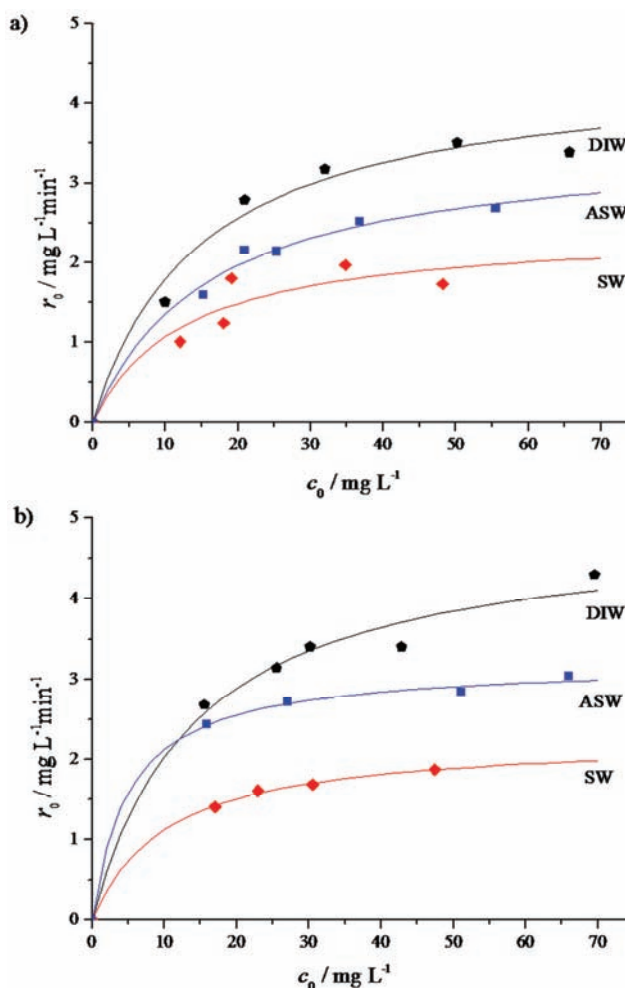


Fig. 4. Effect of the initial RO16 dye concentration on its initial photodegradation rate by a) P25 and b) P160 in DIW, SW and ASW (UV irradiation at room temperature; the RO16 concentration was in the range of 20–80 mg L⁻¹; the TiO₂ concentration was 1 g L⁻¹).

The experimental data presented in Fig. 4 were fitted to a hyperbolic function, expressed by Eq. (3):³⁵

$$Y = \frac{abx}{1+bx} \quad (3)$$

in which $Y = r_0$, $x = c_0$, $b = K$ and $a = k$.

The parameters K and k were estimated by an optimization procedure using MATLAB and are presented in Table V.

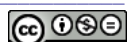
TABLE V. The parameters k and K obtained by fitting the experimental data of the photocatalytic degradation of the dye by P25 and P160 in DIW, SW and ASW (UV irradiation at room temperature; RO16 concentration was in the range of 20–80 mg L⁻¹; TiO₂ concentration was 1 g L⁻¹); MSE – mean standard error

| Type of water | Type of titania | | | | | |
|---------------|--------------------------------------------|--------------------------|--------|--------------------------------------------|--------------------------|--------|
| | P25 | | | P160 | | |
| | k / mg L ⁻¹ min ⁻¹ | K / L mg ⁻¹ | MSE | k / mg L ⁻¹ min ⁻¹ | K / L mg ⁻¹ | MSE |
| DIW | 4.4364 | 0.0669 | 0.0487 | 4.9546 | 0.0695 | 0.0362 |
| ASW | 3.5383 | 0.0622 | 0.0119 | 3.1995 | 0.1964 | 0.0035 |
| SW | 2.4275 | 0.0786 | 0.0631 | 2.2746 | 0.0975 | 0.0005 |

The results given in Table V show that the values of the photodegradation rate constant k for both types of photocatalysts were higher in DW than in saline waters, which indicates that inorganic ions have inhibiting effect on the photoactivity of both titania samples. In addition, the values of photodegradation rate constant for both photocatalysts were lower in natural seawater than in artificial seawater. The value of k of the photocatalytic decolorization of the dye in DIW with P160 was slightly higher than with P25, probably because of the higher surface area and larger pores. However, the values of k for P160 in ASW and SW were lower than those for P25 in these waters, which indicates that influence of inorganic ions in ASW and SW was more pronounced for P160 than for P25.

CONCLUSIONS

The efficiency of recently synthesized TiO₂ powder P160 in the degradation of the dye C.I. Reactive Orange 16 in deionized and saline waters under UV irradiation is comparable and even slightly better than the efficiency of a standard TiO₂ powder Degusa P25. The higher specific surface area, higher pore volume and larger pores of P160 with respect to P25 contributed to its better photocatalytic efficiency. Water salinity decreased the efficiency of P160 to approximately the same extent as the efficiency of P25 was decreased. Some organic compounds naturally present in seawater have a large influence on the efficiency of both photocatalysts; hence, artificial seawater that contains only the major ions of seawater cannot be used as a model for the prediction of photocatalyst activity in natural seawaters. The dependence of the initial degradation rate on the initial



dye concentration followed the Langmuir–Hinshelwood (L–H) model. The photodegradation rate constant k , which represents the maximum reaction rate, has similar values for P25 and P160 in all types of water due to similar properties of the photocatalysts.

Acknowledgements. The authors would like to acknowledge the financial support of the Ministry of Education, Science and Technological Development of the Republic of Serbia, Project No. III 45019.

ИЗВОД

ЕФИКАСНОСТ ФОТОКАТАЛИЗАТОРА НА БАЗИ TiO₂ У СЛАНИМ ВОДАМА

ASMA JUMA ALBRBAR¹, АНЂЕЛИКА БЈЕЛАЈАЦ², ВЕЉКО ЂОКИЋ¹, ЈЕЛЕНА МИЛАДИНОВИЋ¹, ЂОРЂЕ ЈАНАЌКОВИЋ¹ и РАДА ПЕТРОВИЋ¹

¹Технолошко–мешавински факултет, Универзитет у Београду, Карнеијева 4, 11000 Београд и

²Иновациони центар Технолошко–мешавинској факултета, Универзитет у Београду,
Карнеијева 4, 11000 Београд

Фотокаталитичка ефикасност TiO₂ праха P160, синтетизованог нехидролитичким сол–гел поступком, испитивана је у процесу разградње боје C.I. Reactive Orange 16 у природној и лабораторијски припремљеној морској води у поређењу са ефикасношћу у дејонизованој води, као и у поређењу са ефикасношћу комерцијалног фотокатализатора Degussa P25. Показано је да је ефикасност P160 мало већа од ефикасности P-25 због веће специфичне површине, већих пора и веће запремине пора. Ефикасност оба катализатора у природној и лабораторијски припремљеној морској води значајно је мања него у дејонизованој води. Просечна брзина разградње боје за оба фотокатализатора је у малој мери већа у лабораторијски припремљеној него у природној морској води, што показује утицај органских компоненти присутних у природној морској води на фотокаталитичку ефикасност. Зависност почетне брзине разградње од почетне концентрације боје се покорава Ленгмیر–Хиншелвудовом моделу, што указује на то да адсорпција има улогу у фотокаталитичкој реакцији разградње боје. Слична својства фотокатализатора су узроковала блиске вредности константе брзине фотокаталитичке разградње, k , која представља максималну брзину реакције, за P25 и P160 у свим испитиваним врстама воде.

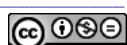
(Примљено 11. новембра 2013, ревидирано 20. фебруара, прихваћено 11. марта 2014)

REFERENCES

1. N. Daneshvar, D. Salari, A. R. Khataee, *J. Photochem. Photobiol., A* **162** (2004) 317
2. M. Karkmaz, E. Puzenat, C. Guillarad, J. M. Herrmann, *Appl. Catal., B* **51** (2004) 183
3. M. A. Fox, M. T. Dulay, *Chem. Rev.* **93** (1993) 341
4. S. S. Shinde, C. H. Bhosale, K. Y. Rajpure, *J. Photochem. Photobiol., B* **103** (2011) 111
5. T. Tachikawa, T. Majima, *Langmuir* **25** (2009) 7791
6. D. Friedmann, C. Mendive, D. Bahnemann, *Appl. Catal., B* **99** (2010) 398
7. M. J. Kim, K. H. Choo, H. S. Park, *J. Photochem. Photobiol., A* **216** (2010) 215
8. M. N. Chong, B. Jin, C. W. K. Chow, C. Saint, *Water Res.* **44** (2010) 2997
9. S. Parra, *PhD Thesis*, EPFL, Lausanne, 2001, p. 48
10. M. Makita, A. Harata, *Chem. Eng. Process.* **47** (2008) 859
11. R. Al-Rasheed, D. J. Cardin, *Chemosphere* **51** (2003) 925
12. R. Al-Rasheed, D. J. Cardin, *Appl. Catal., A* **246** (2003) 39



13. S. W. Bennett, A. A. Keller, *Appl. Catal., B* **102** (2011) 600
14. R. Petrović, N. Tanasković, V. Đokić, Ž. Radovanović, I. J. Častvan, I. Stamenković I, Dj. Janačković, *Powder Technol.* **219** (2012) 239
15. V. Djokić, J. Vujović, A. Marinković, R. Petrović, Dj. Janačković, A. Onjia, D. Mijin, *J. Serb. Chem. Soc.* **77** (2012) 1747
16. M. R. Hoffmann, S. T. Martin, W. Choi, D. W. Bahnemann, *Chem. Rev.* **95** (1995) 69
17. A. Mills, S. L. Hunte, *J. Photochem. Photobiol., A* **108** (1997) 1
18. M. I. Litter, *Appl. Catal., B* **23** (1999) 89
19. G. Wang, L. Xu, J. Zhang, T. Yin, H. Deyan, *Int. J. Photoenergy* **2012** (2012) 265760
20. M. Kosmulski, *Adv. Colloid Interface Sci.* **152** (2009) 14
21. S. Milonjić, A. Ruvarac, M. Šušić, *Thermochim. Acta* **11** (1975) 161
22. I. K. Konstantinou, T. A. Albanis, *Appl. Catal., B* **49** (2004) 1
23. V. Belessi, D. Lambropoulou , I. Konstantinou, A. Katsoulidis, P. Pomonis, D. Petridis, T. Albanis, *Appl. Catal., B* **73** (2007) 292
24. A. H. Gordillo, A. G. Romero, F. Tzompanzi, R. Gomez, *J. Photochem. Photobiol., A* **257** (2013) 44
25. A. H. Gordillo, A. G. Romero, F. Tzompanzi, R. Gomez, *Appl. Catal., B* **144** (2014) 507
26. M. Movahedi, A. R. Mahjoub, S. J. Darzi, *J. Iran. Chem. Soc.* **6** (2009) 570
27. O. Moradi, K. Zare, *Fuller. Nanotub. Car. N.* **19** (2011) 628
28. J. H. Suna, K. E. Wang, R. X. Sun, S. Y. Dong, *Mater. Chem. Phys.* **115** (2009) 303
29. D. Mijin, M. Radulović, D. Zlatić, P. Jovančić, *Chem. Ind. Chem. Eng. Q.* **13** (2007) 179
30. C. Guillard, E. Puzenat, H. Lachheb, A. Houas, J.-M. Herrmann, *Int. J. Photoenergy* **7** (2005) 1
31. D. C. Hurum, A. G. Agrios, K. A. Gray, T. Rajh, M. C. Thurnauer, *J. Phys. Chem., B* **107** (2003) 4545
32. X. Wang, Y. Liu, Z. Hu, Y. Chen, W. Liu, G. Zhao, *J. Hazard. Mater.* **169** (2009) 1061
33. Z. Sun, L. Zheng, S. Zheng, R. L. Frost, *J. Colloid Interf. Sci.* **404** (2013) 102
34. C. S. Turchi, D. F. Ollis, *J. Catal.* **122** (1990) 178
35. A. V. Emeline, V. K. Ryabchuk, N. Serpone, *J. Phys. Chem., B* **109** (2005) 18515.





The changes of $\text{Ba}_{0.5}\text{Sr}_{0.5}\text{Co}_{0.8}\text{Fe}_{0.2}\text{O}_{3-\delta}$ perovskite oxide on heating in oxygen and carbon dioxide atmospheres

SAŠA ZELJKOVIĆ^{1*}, TONI IVAS², SEBASTIEN VAUCHER³, DIJANA JELIĆ⁴
and LUDWIG J. GAUCKLER²

¹University of Banja Luka, Faculty of Natural Sciences and Mathematics, Mladena Stojanovića 2, 78 000 Banja Luka, Bosnia and Herzegovina, ²ETH Zürich, Department of Materials, Wolfgang-Pauli-Str. 10, CH-8093 Zürich, Switzerland, ³Swiss Federal Institute for Materials Research and Testing, EMPA, Feuerwerkerstraße 39, CH-3602 Thun, Switzerland and ⁴University of Banja Luka, Faculty of Medicine, Save Mrkalja 14, 78000 Banja Luka, Bosnia and Herzegovina

(Received 24 October 2013, revised 5 March, accepted 7 March 2014)

Abstract: In the first part of this study, the oxygen deficiency, δ , in $\text{Ba}_{0.5}\text{Sr}_{0.5}\text{Co}_{0.8}\text{Fe}_{0.2}\text{O}_{3-\delta}$ (BSCF) was measured by means of thermogravimetry as a function of the oxygen partial pressure, $p(\text{O}_2)$, in the range of 1.1×10^{-6} –41.67 % at elevated temperatures in the range 873–1073 K. It was shown that δ becomes more pronounced with increasing T and with decreasing $p(\text{O}_2)$. The isotherms δ vs. $p(\text{O}_2)$ were determined. The second part of this study relates to the reaction of CO_2 with $\text{Ba}_{0.5}\text{Sr}_{0.5}\text{Co}_{0.8}\text{Fe}_{0.2}\text{O}_{3-\delta}$ perovskite oxide in the absence and presence of O_2 at temperatures ranging from 673 to 973 K, also by thermogravimetry. The reactivity of CO_2 with BSCF increased with increasing temperature and increasing exposure to CO_2 . The reaction of CO_2 with BSCF was described by equilibrium reaction isotherms. The results of X-ray diffractometry evidenced that exposure to CO_2 leads to the formation of carbonates.

Keywords: BSCF; perovskite; oxygen; carbon dioxide.

INTRODUCTION

Among mixed conducting perovskite-type oxides, $\text{Ba}_{0.5}\text{Sr}_{0.5}\text{Co}_{0.8}\text{Fe}_{0.2}\text{O}_{3-\delta}$ (BSCF) has recently received much attention.^{1–4} BSCF has been proposed as the cathode material for a new SOFC (solid oxide fuel cell)^{5,6} and as an oxygen permeable membrane material.⁷ After a first report by Shao *et al.*,⁸ the preparation, phase structure, thermal expansion coefficient and performance of BSCF materials were investigated.^{9–16}

*Corresponding author. E-mail: zeljkovics@yahoo.com
doi: 10.2298/JSC131024018Z

McIntosh *et al.*¹⁷ investigated oxygen non-stoichiometry of BSCF up to 1273 K in the $p(\text{O}_2)$ range 1.01325×10^5 to $1.01325 \cdot 10^2 \times \text{Pa}$ using a neutron diffraction technique. It was found that BSCF maintained cubic symmetry at all temperatures and oxygen partial pressures covered by the performed experiments. Zeng *et al.*¹⁸ measured the non-stoichiometry of BSCF at room temperature using iodometry and found a high oxygen non-stoichiometry of $\delta = 0.318$ (2.682) for an air-calcined sample. They also measured the oxygen partial pressure and temperature dependence of the oxygen non-stoichiometry by the thermogravimetric analysis (TGA) method up to 1273 K under an air and nitrogen atmosphere. Bucher *et al.*¹⁹ also investigated the oxygen non-stoichiometry of BSCF by thermogravimetry at temperatures ranging from 873 to 1173 K and $p(\text{O}_2)$ pressures from 10 to 4×10^4 Pa. In addition, oxygen exchange kinetics was measured by electrical conductivity relaxation and the chemical diffusion coefficients and surface exchange coefficient were calculated from the relaxation experiments.²⁰ Vente *et al.*²¹ measured the oxygen transport, oxygen non-stoichiometry of BSCF and $\text{SrCo}_{0.8}\text{Fe}_{0.2}\text{O}_{3-\delta}$ for oxygen transport membranes. Combined TGA, temperature programmed desorption (TPD) and neutron diffraction measurements were performed. The oxygen non-stoichiometry measurements were realized in oxygen partial pressures from 100 to 1×10^5 Pa in the temperature range 873 to 1073 K. Using TGA, Wang *et al.*²² determined the oxygen content of the starting material to be $3 - \delta = 2.79$ at room temperature. They determined the oxygen ion–electron hole diffusion coefficient, the oxygen content and the diffusion coefficient of the oxygen vacancy. Perovskite oxides of type $\text{A}_{1-a}\text{A}'_a\text{B}_{1-b}\text{B}'_b\text{O}_{3-\delta}$ (with A A' = La, Ba, Sr and B B' = Mn, Fe, Co) were investigated by Giradauskaite *et al.*²³ The non-stoichiometry of oxygen was measured using a micro-thermo balance with partial oxygen pressures from 10^{-3} to 10^5 Pa.

The use of BSCF in practical applications, such as fuel cell cathodes, demands a certain degree of chemical stability. It is well known^{24–28} that some perovskites containing alkaline elements react with CO_2 . As CO_2 is one of the components of air, which is often used as an oxidizer for the fuel cell, there may be a chemical interaction between a BSCF and CO_2 , leading to degradation of the cathode.

Yan *et al.*²⁹ investigated the interaction between CO_2 and BSCF using TPD in the presence and absence of O_2 and H_2O . They found that CO_2 could be adsorbed and reacted with BSCF in the temperature range from 673 to 973 K, thereby forming $\text{Sr}_{0.6}\text{Ba}_{0.4}\text{CO}_3$. In the case of adsorption of CO_2 without O_2 , the reactivity of CO_2 on the surface of BSCF increased with increasing temperature. CO_2 and O_2 were competitively adsorbed on the BSCF. At 973 K, the oxygen adsorption was the dominant reaction on the surface of BSCF. The presence of water accelerated the “toxicity” of CO_2 , which probably resulted in the formation



of bicarbonate. Moreover, Yan *et al.* calculated important kinetic parameters, such as activation energy, to see how strongly the adsorbent was bound to the surface of the adsorbate.

Nomura *et al.*³⁰ emphasized that oxygen vacancy in perovskite structures could contribute to the formation of carbonates. They suggested that the perovskite oxides with oxygen vacancy in the crystal lattice, which are formed at elevated temperatures, could easily adsorb CO₂. The higher the temperature at which the pretreatment was performed, the more oxygen vacancies were present, which, as explained by the author, may be the reason for the reaction of BSCF with CO₂ being facilitated at high temperatures.

Arnold *et al.*³¹ reported the competitive adsorption of CO₂ and O₂. They noticed strong acceleration in the degradation of a BSCF membrane with increasing CO₂ content in the supply air.

Yan *et al.*³² found that CO₂ desorption starts at 713 K and reaches its peak at 980 K. Small particles of SrCO₃, BaCO₃ and Sr_xBa_{1-x}CO₃ may decompose from 873 to 1023 K. They concluded that complete decomposition of carbonate requires temperatures above 973 K. Finally, they indicated that extremely clean air should be used as an oxidizer when a BSCF cathode is operated at low temperatures. In another study, Yan *et al.*³³ examined the effects of CO₂ concentration and temperature on the performance of BSCF cathodes in SOFC at temperatures from 673 to 1023 K and CO₂ concentrations from 0.28 to 3.07 %. They concluded that BSCF cathode is not suitable for single chamber fuel cells that use hydrocarbons as fuel, especially at lower temperatures.

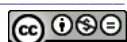
Yang *et al.*³⁴ reported on the catalytic activity of Ba_{0.2}Sr_{0.8}Co_{0.8}Fe_{0.2}O_{3-δ}, which was degraded in a carbon dioxide atmosphere from 773 to 1073 K due to the formation of carbonate on the surface.

In this paper, we present the results of an investigation of the reactivity of BSCF with oxygen and carbon dioxide, in various gas mixtures and under various temperatures. Six different gas mixtures were used. Results were fitted to reaction isotherms based on the well-known mathematical models 1 (Freundlich)³⁵ and 2 (Langmuir).³⁶ The performed calculations based on the reaction isotherms provided valuable insight into the *in situ* behavior of BSCF.

EXPERIMENTAL

Phase pure BSCF powder (Praxair) was annealed in air at 1273 K for 6 h. XRD analysis (Siemens D5000 diffractometer using a Cu-K_α X-ray tube ($\lambda = 154$ nm)) was performed on the resulting material, confirming the presence of single phase BSCF. The employed BSCF had a specific surface area close to 2 m² g⁻¹ as determined by the Brunauer–Emmett–Teller (BET) method.

Non-stoichiometric ratios of oxygen and CO₂ adsorption were measured by a set of TGA measurement (Netzsch STA 449 C with rhodium–platinum furnace) as a function of oxygen partial pressure and temperature. The gas flows were controlled using flow meters (Bronkhorst, GmbH, Germany) with magnetic valves. The platinum crucible and slip-on plate were

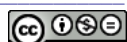


conditioned for the measurement by heating to 1073 K. The non-stoichiometric ratio of oxygen was measured under isobaric conditions under an atmosphere of Ar or Ar and O₂. Six different gas mixtures were used (60 cm³ min⁻¹ Ar, 55 cm³ min⁻¹ Ar + 5 cm³ min⁻¹ O₂, 50 cm³ min⁻¹ Ar + 10 cm³ min⁻¹ O₂, 45 cm³ min⁻¹ Ar + 15 cm³ min⁻¹ O₂, 40 cm³ min⁻¹ Ar + 20 cm³ min⁻¹ O₂ and 35 cm³ min⁻¹ Ar + 25 cm³ min⁻¹ O₂). Temperature program included heating to 1073 K at a heating rate of 10 K min⁻¹ with a 30-min-long isothermal dwell time. Isothermal dwell times were chosen in order to keep the system in a state of dynamic equilibrium. Subsequently, the sample was cooled to 973 K and then to 873 K at a cooling rate of 0.5 K min⁻¹ with 30-min-long isothermal dwells. In all experiments, the samples were considered in a thermodynamic equilibrium when the sample mass attained a constant value. The equilibration time was chosen according to this condition. After cooling to 873 K, samples were again heated to 1073 K with an isothermal dwell at 973 K. All measurements were corrected by the results of a correction measurement, which was performed under the same conditions as a sample run. For each measurement, the sample mass was 700 mg.

The absolute oxygen non-stoichiometry was determined by complete reduction of a BSCF sample in a 5 vol. % mixture of Ar and H₂ under isothermal conditions at 1073 K for about 24 h. The oxygen partial pressure of the reducing atmosphere was measured by a Rapidox 2100 oxygen sensor (Cambridge Sensotec Ltd., UK). After the reduction experiment, the X-ray diffraction pattern of the sample confirmed the complete decomposition of the perovskite phase into the constituent oxides. Experiments measuring carbon adsorption were performed using different CO₂/O₂ gas mixtures with a constant gas flow (10 cm³ min⁻¹). Ba_{0.5}Sr_{0.5}Co_{0.8}Fe_{0.2}O_{3-δ} was subjected to the initial treatment in air at 773 K for 60 min in order to remove traces of moisture. The sample weight in all experiments was 200 mg. All measurements were performed in a Pt crucible. The TG analysis of CO₂ adsorption onto BSCF was performed at 673, 773, 873 and 973 K. Each isothermal step lasted 480 min with the intention of system mass equilibration. Gas mixtures of 1, 10 and 100 % CO₂ were used for the adsorption, as presented in Table I. The rate of heating/cooling was 10 K min⁻¹ in all experiments. The corrective measurement was performed with the same temperature and atmospheric parameters as used for the measurement in 100 % CO₂.

TABLE I. Gas mixtures used for measurements of CO₂ adsorption by Ba_{0.5}Sr_{0.5}Co_{0.8}Fe_{0.2}O_{3-δ}

| Gas mixture | Purity | Other characteristics | Producer |
|--------------------------------------------|--------------------------------------------------------------------------------------------------------------------------------------------------------------------------------------------|----------------------------------------------------------------------------------|-----------------------|
| 100 % CO ₂ gas | CO ₂ > 99.998 %, O ₂ < 2 ppm, H ₂ O < 3 ppm, N ₂ < 8 ppm, H ₂ < 0.5 ppm, CO < 1 ppm, C _n H _m < 5 ppm | 40 dm ³ Quality 48 | Carbagas, Switzerland |
| 10 % CO ₂ gas in O ₂ | CO ₂ by analysis 10 % (± 2 % rel.) | 40 dm ³ , CO ₂ quality 40, O ₂ quality 48 | Carbagas, Switzerland |
| 1 % CO ₂ gas in O ₂ | CO ₂ by analysis 0.997 % (± 2 % rel.) | 40 dm ³ CO ₂ quality 40, O ₂ quality 48 | Carbagas, Switzerland |



RESULTS AND DISCUSSION

Non-stoichiometric ratio of oxygen in oxidizing atmosphere ($p(O_2) > 21000$ Pa) was largely influenced by the temperature, as shown in Fig. 1. Change of the oxygen non-stoichiometric ratio by the oxygen partial pressure showed that, regardless of the temperature, a plateau of the partial pressure of oxygen occurred, near to the one that exists in the Earth's atmosphere, indicating temporary stabilization of the oxygen level in the material. Of course, such stabilization could be interpreted as a relative change in the diffusion energy of the oxygen ions in the BSCF material.

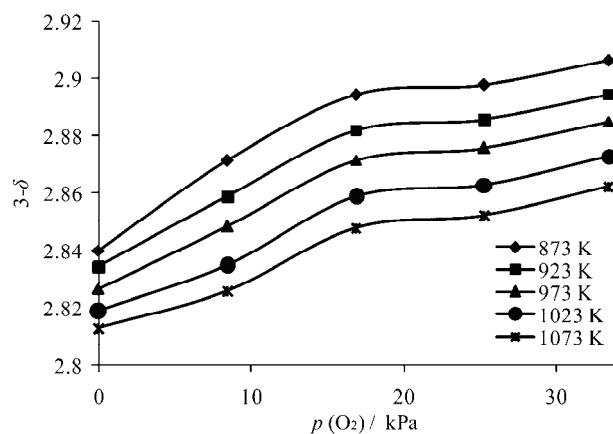


Fig. 1. Oxygen stoichiometry ($3 - \delta$) of BSCF as a function of oxygen partial pressure at different temperatures.

Although the process of change in the oxygen non-stoichiometric ratio in BSCF cannot be understood as an adsorption process, it is possible to determine the relation between the partial pressure of oxygen and the change in the mass of the sample. Reaction isotherms based on mathematical model 1, as shown in Fig. 2, followed a linear dependence that opened the possibility of determining the oxygen non-stoichiometric ratio in relation to oxygen partial pressure. The linear correlation coefficients had high values (>0.99) with a tendency to increase with temperature.

The sample mass changes obtained upon cooling were in strong agreement with those obtained upon heating. Between 973 and 873 K, the non-reversibility in mass change between the cooling and the heating process at a rate of 0.5 K min^{-1} was around 0.06 %. (Fig. 3) As shown in Fig. 4, the sample morphology, followed by scanning electron microscopy (SEM), remained the same before and after the experiment, implying that the non-reversibility was not a consequence of grain growth. Oxygen sorption and desorption are chemical processes responsible for the stoichiometric change of BSCF material. Thus, it could be concluded

that the adsorption hysteresis is due to the different chemical processes during heating and cooling.

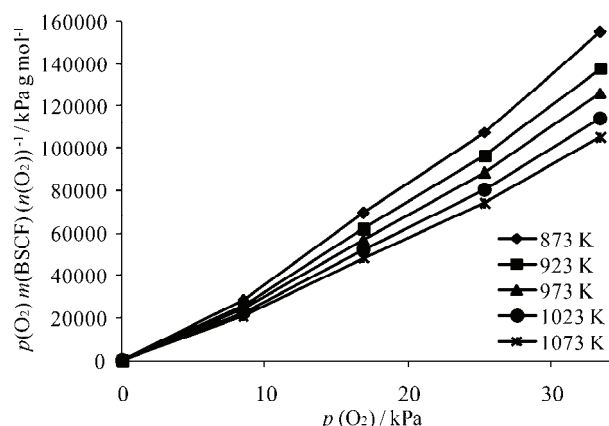


Fig. 2. Reaction isotherms based on mathematical model 1 for the system BSCF–O₂ with the corresponding equations and linear correlation coefficients ($y(873 \text{ K}) = 4636.9x - 5982$, $R^2 = 0.9924$; $y(923 \text{ K}) = 4123.1x - 4974$, $R^2 = 0.9934$; $y(973 \text{ K}) = 3779.3x - 4430$, $R^2 = 0.9937$; $y(1023 \text{ K}) = 3412.2x - 3818$, $R^2 = 0.9942$; $y(1073 \text{ K}) = 3144.5x - 3229$, $R^2 = 0.995$).

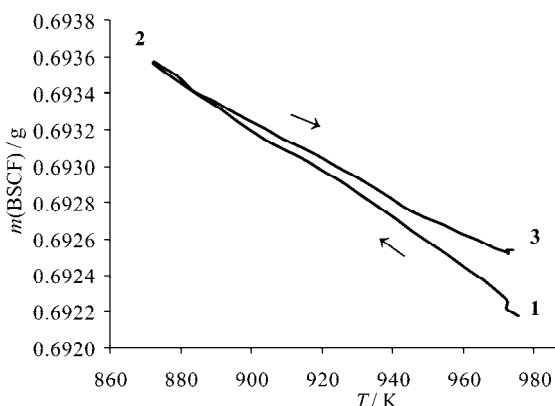


Fig. 3. The mass change of the BSCF sample at 0.5 K min^{-1} cooling (1→2) and heating (2→3) between 973 and 873 K under $10 \text{ cm}^3 \text{ min}^{-1}$ O₂ + $50 \text{ cm}^3 \text{ min}^{-1}$ Ar gas mixture.

The value of the initial oxygen stoichiometry obtained by the complete reduction of BSCF was $3-\delta \approx 2.6$. Initial oxygen stoichiometry, as found by various authors, is presented in Table II. Its value is determined by many factors, including the method of synthesis, and the values can vary from 2.48 to 2.79.

Concerning BSCF, it was assumed that the non-stoichiometry is governed by the reduction of iron from Fe³⁺ to Fe²⁺, and cobalt from Co³⁺ to Co²⁺. It is well known that Sr and Ba always keep their valence states and, therefore, do not influence oxygen non-stoichiometry.³⁷

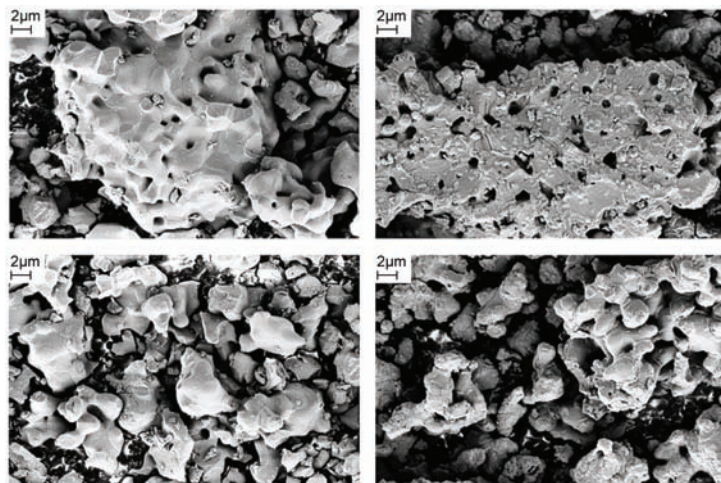


Fig. 4. Morphology of the BSCF samples before (left) and after (right) oxygen non-stoichiometry TG measurement.

TABLE II. Summary of the experimental results for $\text{Ba}_{0.5}\text{Sr}_{0.5}\text{Co}_{0.8}\text{Fe}_{0.2}\text{O}_{3-\delta}$ initial oxygen stoichiometry found by various authors

| Authors | Initial oxygen stoichiometry |
|------------------------------------------|------------------------------|
| McIntosh <i>et al.</i> ¹⁷ | 2.48 |
| Zeng <i>et al.</i> ¹⁸ | 2.68 |
| This study | 2.60 |
| Girdauskaite <i>et al.</i> ²³ | 2.75 |
| Wang <i>et al.</i> ²² | 2.79 |

Taking into consideration that Co^{3+} is reduced at a lower temperature³⁸ than Fe^{3+} , and that in BSCF, the molar fraction of Co is greater than the mole fraction of Fe; it could be presumed that oxygen non-stoichiometry is guided mainly by Co^{3+} reduction.

The BSCF sample mass as a function of temperature and CO_2 concentration was followed during reaction with CO_2 by thermogravimetry (Fig. 5). It should be noted that the equilibrium mass ratio established at a given temperature caused by the reaction with CO_2 was not corrected for changes in mass resulting from the temperature-dependent oxygen content in the material. There was no significant reaction with CO_2 at 673 K regardless of the relative CO_2/O_2 ratio in the atmosphere. Considerable variation in the reactivity of the BSCF– CO_2 system was observed at 773, 873 and 973 K. Increasing temperature and partial pressure of CO_2 resulted in an increased reaction rate and the creation of carbonate at the surface of BSCF. The reaction rate in 1 % CO_2 was relatively small and therefore, no weight stabilization could be observed during 480 min isothermal heating. Reaction rates in 10 % and especially in 100 % CO_2 were higher than in the

previous case, leading to equilibration of the BSCF sample mass. In the case of two-component gas mixtures (10 and 1 % CO₂ in oxygen), there was a possibility of competitive adsorption and reaction of both molecules. Oxygen is absorbed and desorbed from the perovskite structure depending on the oxygen partial pressure in the surrounding atmosphere and temperature. The concentration of surface oxygen vacancies depends on the stoichiometric ratio of oxygen in the BSCF structure. These surface vacancies represent possible active sites for further reaction of oxygen and other small molecules, in the present case, CO₂. Oxygen vacancies could play the role of active adsorption centers, enabling a chemical molecular mechanism. In the case of reaction with CO₂ and related reactions on the surface, various chemical forms may occur, bonded linearly or through a chemical bridge. Based on the experimental results related to the non-stoichiometric ratio of oxygen, it is clear that the change in the oxygen content in the material (due to changes in temperature and the oxygen partial pressure) occurs rapidly and that the system is continuously in a state of dynamic equilibrium. In this regard, after equilibration of the system (after a short time) at a constant temperature and partial pressure of oxygen in the atmosphere, the competitive adsorption and reaction of oxygen and CO₂ should not be considerable.

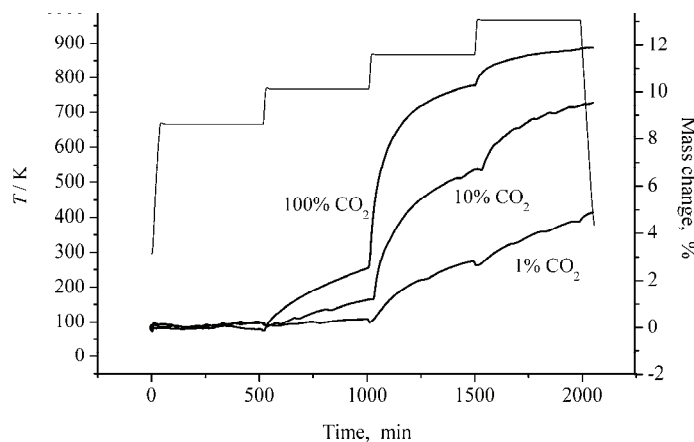


Fig. 5. Mass change of BSCF samples during isothermal steps (673, 773, 873 and 973 K) due to adsorption from 1, 10 and 100 % CO₂ mixtures.

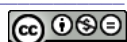
After adsorption, a molecule of CO₂ reacts with BSCF material to form carbonates.³⁴ It could be assumed that penetration and reaction of oxygen is provided through the entire structure of BSCF, while the penetration of CO₂, followed by the creation of carbonate is limited to the surface only.³⁴ It is clear from the experimental results that with increasing temperature, such a monolayer does not prevent further reaction with CO₂. Simultaneously with the temperature change, there is also a change in number and availability of oxygen vacancies

and a change in the reactivity of CO₂. The increase in the reaction rate with temperature and partial pressure of CO₂ could be explained by the above-mentioned effects. At 673 K in an atmosphere of CO₂, no reaction was recorded. The explanation for this may be the low reactivity of CO₂ with BSCF at this temperature and a slightly lower concentration of defects associated with the non-stoichiometric ratio of oxygen. As the experiments were realized in a dynamic (permanent fluctuating) atmosphere and that elemental carbon (C) is practically absent from the whole system, it could be assumed that the 100 % CO₂ system behaves in Boudouard balance³⁹ ($2\text{CO} \rightleftharpoons \text{CO}_2 + \text{C}$) and only negligible amounts of CO were formed. In the two-component systems, *i.e.*, with 10 and 1 % CO₂ in the O₂ mixture, the possibility of CO formation is even smaller.

Already at this stage and based on the very slow mass equilibration of the system, it could be concluded that studied interaction of CO₂ with BSCF may be described as chemical adsorption and reaction. At lower concentrations of carbon oxides (1 %), the adsorption process did not proceed to completion, which means that the weight at the end of the process is not the maximal and that the decrease in concentration increased the time required for equilibration, and the uncertainty in the formulation of the maximum adsorbed mass.

Adsorption is a very complex phenomenon.⁴⁰ For this main reason, there is no single model of adsorption that would give a universal mathematical description of adsorption isotherms that could be used at the borders of all phases and when any physical or chemical adsorption is present. In this study, the reaction of CO₂ on the surface of BSCF perovskite was described by reaction isotherms based on two mathematical models. As the content of oxygen in BSCF varies and the mass is dependent on temperature and partial pressure of oxygen in the surrounding atmosphere, it was difficult to obtain correct molar mass and amount of BSCF in a continually varying atmosphere. Therefore, in this study, the reaction isotherm based on mathematical model 1 was used in such a way that the amount of reacted substance was included as the mass (Fig. 6). An additional benefit of this approach is that the precise chemical form of the carbon oxides deposited on BSCF does not modify the used relation. The parameters k and $1/n$ of the corresponding line equation (Table III) were determined from the linear form of reaction isotherms based on mathematical model 1 (Fig. 7).

The reaction isotherm based on mathematical model 2 was modified in the same way as for the reaction isotherm based on the mathematical model 1 and it was applied to describe the reaction of CO₂ with BSCF (Fig. 8). The reaction isotherms based on mathematical model 2 are expressed by the equation given in Table IV, where k_1 and k_2 are constants. Experimental data are well described by this reaction isotherm, especially at 873 and 973 K, at which temperatures completion of the reaction was observed and it could be concluded that the system was in thermodynamic equilibrium. The coefficients of determination R^2 increase



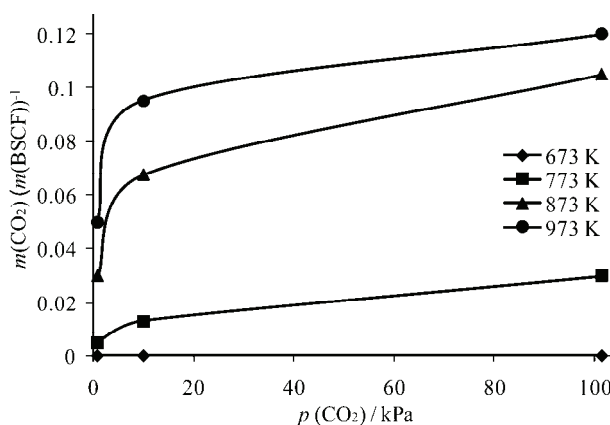


Fig. 6. Reaction isotherm based on mathematical model 1 for the system BSCF–CO₂.

TABLE III. Linear form of the reaction isotherm based on mathematical model 1. Values of the constants k and $1/n$

| Parameter | T / K | | |
|-------------------------|--------|--------|--------|
| | 773 | 873 | 973 |
| $k / \text{kPa}^{-1/n}$ | 7.9712 | 5.3278 | 4.2434 |
| $1/n$ | 0.3891 | 0.272 | 0.1901 |

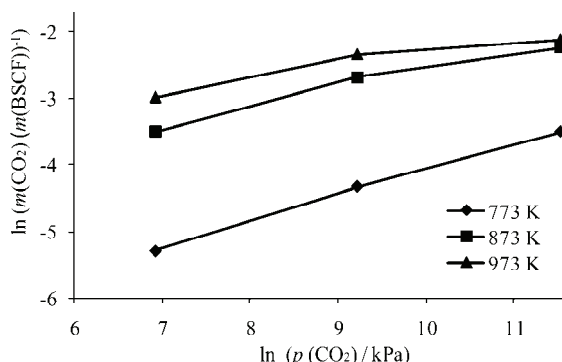


Fig. 7. Linear form of the reaction isotherm based on mathematical model 1 for the system BSCF–CO₂ with the corresponding equations and linear correlation coefficients ($y(973\text{ K}) = 0.190x - 4.243$, $R^2 = 0.932$; $y(873\text{ K}) = 0.272x - 5.327$, $R^2 = 0.971$; $y(773\text{ K}) = 0.389x - 7.971$, $R^2 = 0.998$).

with temperature for both linear isotherms, while their absolute values are in favor of the reaction isotherm based on mathematical model 2. Thus, it could be concluded that the reaction isotherm based on mathematical model 2 better described the reaction of CO₂ at the surface of the BSCF system.

The comparison of the XRD results of the different samples after completion of the experiments presented in Fig. 9 indicates that a chemical reaction of carbon oxides occurred during which the Sr_{0.6}Ba_{0.4}CO₃ phase forms. The intensity of the peaks attributed to the perovskite phase decreased with increasing concentration of carbon oxides in the atmosphere.

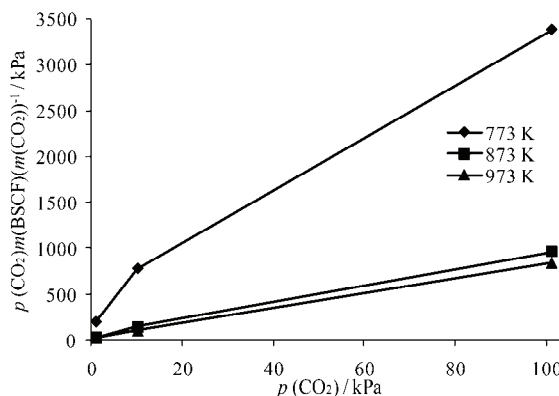


Fig. 8. Linear form of the reaction isotherm based on mathematical model 2 for the system BSCF–CO₂ with the corresponding equations and linear correlation coefficients ($y(773\text{ K}) = 30.36x + 314.6, R^2 = 0.992$; $y(873\text{ K}) = 9.142x + 40.20, R^2 = 0.998$; $y(973\text{ K}) = 8.164x + 17.67, R^2 = 0.999$).

TABLE IV. Linear form of the reaction isotherm based on mathematical model 2. Values of the constants k_1 and k_2

| Parameter | T / K | | |
|------------------------|----------------|-------|-------|
| | 773 | 873 | 973 |
| k_1 / Pa^{-1} | 0.0965 | 0.227 | 0.462 |
| k_2 | 0.0329 | 0.109 | 0.122 |

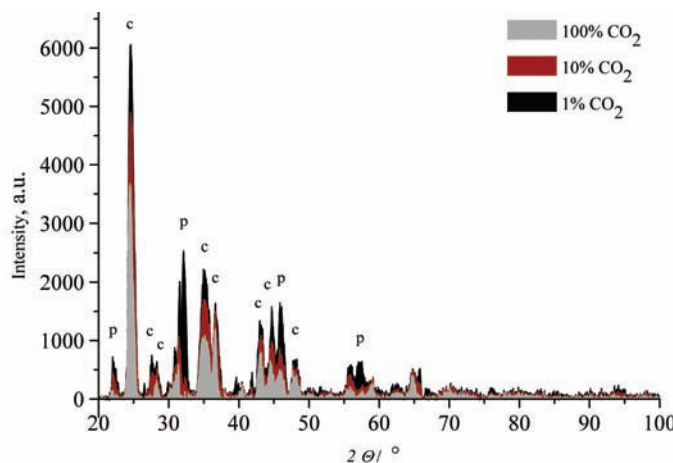


Fig. 9. Comparison of the XRD patterns of the BSCF samples after adsorption from 100, 10 and 1 % CO₂. p: perovskite, c: Sr_{0.6}Ba_{0.4}CO₃.

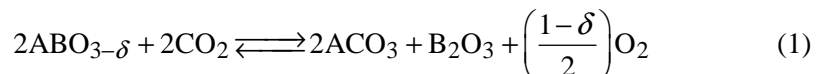
CONCLUSIONS

Oxygen non-stoichiometric property of BSCF has been presented and discussed in conjunction with the findings of other authors. Oxygen non-stoichio-

metry was investigated by thermogravimetry as a function of oxygen partial pressure in the temperature range 873–1073 K. The absolute oxygen non-stoichiometry was determined by the complete reduction of BSCF. Non-stoichiometry in an oxidizing atmosphere ($p(O_2) > 21000$ Pa) was found to be largely influenced by the temperature. Due to the higher molar fraction of Co vs. Fe and the greater affinity for Co^{2+} reduction, it could be argued that the oxygen non-stoichiometry is guided mainly by Co reduction. The defined reaction isotherms for the BSCF– O_2 system follow a linear dependence, opening the possibility for controlling the oxygen non-stoichiometry ratio by changing the partial pressure of oxygen.

The reaction of carbon oxides with BSCF perovskite was observed at 773, 873 and 973 K. The reaction rate increased with increasing temperature and with increasing concentration of CO_2 in the atmosphere. A reaction of CO_2 with BSCF perovskite was not observed at 673 K. The increase of reaction rate with the increasing temperature for the same mixture of gases (in terms of the initial concentrations) could be attributed to the increased concentrations of oxygen vacancies and/or increased reactivity of the CO_2 –BSCF system. Since there is no reaction present at 673 K, despite the presence of oxygen vacancies, it can be assumed that CO_2 does not react with BSCF at or below this temperature.

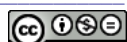
The XRD measurements clearly showed the presence of $Sr_{0.6}Ba_{0.4}CO_3$ phase indicating that chemical reaction occurred in the system. Such an interaction of adsorbate and adsorbent implies the presence of Lewis active sites on the surface of the perovskite, very likely oxygen vacancies sites. This chemical reaction of BSCF perovskite and CO_2 can be completely described by:



where ABO_3 is the general chemical formula for perovskite compound with A and B standing for cations of very different sizes. The formation of carbonate ions was realized by interactions with the negatively charged atomic oxygen ions $O^{\delta-}$ (Lewis bases) of the complex metal oxides and the positively charged carbon atoms $C^{\delta+}$ (Lewis acid).⁴¹

The maximum measured weight gain (at 973 K and in 100 % CO_2) was 12 %. During 480-min-long reaction with CO_2 from 1 and 10 % mixtures, no mass equilibration was attained, which suggests that the reaction of CO_2 with BSCF from these gas mixtures was not completed. Due to the very rapid changes in the material regarding the oxygen content related to the temperature and partial pressure of O_2 , it does not seem likely that competitive adsorption and reaction of O_2 and CO_2 is present during the period of 480 min.

It is recommended that extremely pure air be used as an oxidant when BSCF is operated as a cathode material at low temperatures. Furthermore, a BSCF cath-



ode is not suitable for single-chamber fuel cells that use hydrocarbons as a fuel, especially at lower temperatures.

By careful observation of the isotherm, it could be noticed that the reaction at 973 K went to completion and that a plateau formed. At 873 and especially at 773 K the plateaus were poorly defined. Both types of reaction isotherms, (linear forms) sufficiently describe the BSCF–CO₂ system. However, based on the results of the linear correlation coefficient, the linear form of reaction isotherm based on mathematical model 2 was more successful in describing the system, especially at higher temperatures. The reaction isotherms registered only one “plateau”.

И З В О Д

ПРОМЕНЕ ПЕРОВСКИНОГ ОКСИДА Ba_{0,5}Sr_{0,5}Co_{0,8}Fe_{0,2}O_{3-δ} ПРИ ГРЕЈАЊУ У АТМОСФЕРИ КИСЕОНИКА И УГЉЕН-ДИОКСИДА

SAŠA ZELJKOVIĆ¹, TONI IVAS², SEBASTIEN VAUCHER³, DIJANA JELIĆ⁴ и LUDWIG J. GAUCKLER²

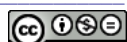
¹University of Banja Luka, Faculty of Natural Sciences and Mathematics, Mladena Stojanovica 2, 78000 Banja Luka, Bosnia and Herzegovina, ²ETH Zürich, Department of Materials, Wolfgang-Pauli-Str. 10, CH-8093 Zürich, Switzerland, ³Swiss Federal Institute for Materials Research and Testing, EMPA, Feuerwerkerstrasse 39, CH-3602 Thun, Switzerland and ⁴University of Banja Luka, Faculty of Medicine, Save Mrkalja 14, 78000 Banja Luka, Bosnia and Herzegovina

Мањак кисеоника, δ, у формули перовскита Ba_{0,5}Sr_{0,5}Co_{0,8}Fe_{0,2}O_{3-δ} (BSCF) мерен је термогравиметријски у функцији парцијалног притиска кисеоника, $p(O_2)$, у опсегу $1,1 \times 10^{-6}$ –41,67 % на повишеном температуром (873–1073 K). Мањак кисеоника постаје већи са повећањем T и са смањењем $p(O_2)$. Одређене су изотерме δ – $p(O_2)$ за различите температуре. Испитивана је реакција CO₂ са BSCF у одсуству и присуству O₂ на температуром од 673 до 973 K такође методом термогравиметрије. Реактивност CO₂ са BSCF се повећавала са повећањем температуре и изложености CO₂ гасу. За ову реакцију одређене су равнотежне реакционе изотерме. Резултати XRD указују да се реакцијом са CO₂ формирају карбонати.

(Примљено 24. октобра 2013, ревидирано 5. марта, прихваћено 7. марта 2014)

REFERENCES

1. Z. P. Shao, W. S. Yang, Y. Cong, H. Dong, J. H. Tong, G. X. Xiong, *J. Membr. Sci.* **172** (2000) 177
2. Z. P. Shao, G. X. Xiong, J. H. Tong, H. Dong, W. S. Yang, *Sep. Purif. Technol.* **25** (2001) 419
3. Z. P. Shao, G. X. Xiong, H. Dong, W. S. Yang, L. W. Lin, *Sep. Purif. Technol.* **25** (2001) 97
4. P. Y. Zeng, Z. H. Chen, W. Zhou, H. X. Gu, Z. P. Shao, S. M. Liu, *J. Membr. Sci.* **291** (2007) 148
5. C. K. Dyer, *J. Power Sources* **106** (2002) 31
6. F. Schulze-Küppers, S. Baumann, W. A. Meulenberg, D. Stöver, H. P. Buchkremer, *J. Membr. Sci.* **433** (2013) 121
7. H. Wang, C. Tablet, A. Feldhoff, J. Caro, *J. Memb. Sci.* **262** (2005) 20
8. Z. P. Shao, S. M. Haile, *Nature* **431** (2004) 170
9. J. Martynczuk, M. Arnold, H. Wang, J. Caro, A. Feldhoff, *Adv. Mater.* **19** (2007) 2134



10. L. Tan, X. H. Gu, L. Yang, W. Q. Jin, L. X. Zhang, N. P. Xu, *J. Membr. Sci.* **212** (2003) 157
11. C. Niedrig, S. Taufall, M. Burriel, W. Meneskou, S. F. Wagner, S. Baumann, E. Ivers-Tiffée, *Solid State Ionics* **197** (2011) 25
12. Z. P. Shao, H. Dong, G. X. Xiong, Y. Cong, W. S. Yang, *J. Membr. Sci.* **183** (2001) 181
13. S. K. Singh, J. Kumar, *J. Mater. Sci.* **42** (2007) 2105
14. A. Mosadeghkhah, M. A. Alaee, T. Mohammadi, *Mater. Des.* **28** (2007) 1699
15. H. H. Wang, Y. Cong, W. S. Yang, *Catal. Today* **82** (2003) 157
16. M. Arnold, H. H. Wang, A. Feldhoff, *J. Membr. Sci.* **293** (2007) 44
17. S. McIntosh, J. F. Vente, W. G. Haije, D. H. A. Blank, H. J. M. Bouwmeester, *Solid State Ionics* **177** (2006) 1737
18. P. Zeng, Z. Chen, W. Zhou, H. Gu, Z. Shao, S. Liu, *J. Membr. Sci.* **291** (2007) 148
19. E. Bucher, A. Egger, P. Ried, W. Sitte, P. Holtappels, *Solid State Ionics* **179** (2008) 1032
20. E. Girdauskaite, H. Ullmann, V. V. Vashook, U. Guth, G. B. Caraman, E. Bucher, W. Sitte, *Solid State Ionics* **179** (2008) 385
21. J. F. Vente, S. McIntosh, W. G. Haije, H. J. M. Bouwmeester, *J. Solid State Electrochem.* **10** (2006) 581
22. H. Wang, Y. Cong, W. Yang, *J. Membr. Sci.* **210** (2002) 259
23. E. Girdauskaite, H. Ullmann, M. Al Daroukh, V. Vashook, M. Bülow, U. Guth, *J. Solid State Electrochem.* **11** (2007) 469
24. C. Tofan, D. Klvana, J. Kirchnerova, *Appl. Catal., B* **36** (2002) 311
25. I. V. Khromushin, T. I. Aksanova, Z. R. Zhotabaev, *Solid State Ionics* **162–163** (2003) 37
26. V. V. Kharton, A. A. Yaremchenko, A. V. Kovalevsky, A. P. Viskup, E. N. Naumovich, P. F. Kerko, *J. Membr. Sci.* **163** (1999) 307
27. T. Hibino, K. Ushiki, Y. Kuwahara, *Solid State Ionics* **91** (1996) 69
28. Z. Zhao, L. Liu, X. Zhang, B. Tu, D. Ou, M. Cheng, *Int. J. Hydrogen Energ.* **37** (2012) 19036
29. A. Yan, B. Liu, Y. Dong, Z. Tian, D. Wang, M. Cheng, *Appl. Catal., B* **80** (2008) 24
30. K. Nomura, Y. Ujihira, T. Hayakawa, K. Takehira, *Appl. Catal., A* **137** (1996) 25
31. M. Arnold, H. Wang, A. Feldhoff, *J. Membr. Sci.* **293** (2007) 44
32. A. Yan, V. Maragou, A. Arico, M. Cheng, P. Tsakaratas, *Appl. Catal., B* **76** (2007) 320
33. A. Yan, M. Cheng, Y. Dong, W. Yang, V. Maragou, S. Song, P. Tsakaratas, *Appl. Catal., B* **66** (2006) 64
34. Z. Yang, A. S. Harvey, L. J. Gauckler, *Scripta Mater.* **61** (2009) 1083
35. H. Freundlich, *Kapillarchemie*, Akademische Verlagsgesellschaft, Leipzig, 1909
36. I. Langmuir, *J. Am. Chem. Soc.* **40** (1918) 1361
37. A. S. Harvey, F. Jochen-Litterst, Z. Yang, J. L. M. Rupp, A. Infortuna, L. J. Gauckler, *Phys. Chem. Chem. Phys.* **11** (2009) 3090
38. B. Tomic-Tucaković, D. Majstorović, D. Jelić, S. Mentus, *Thermochim. Acta* **541** (2012) 15
39. A. Jess, U. Kragl, P. Wasserscheid, *Chemical Technology: An Integral Textbook*, Wiley-VCH, Weinheim, 2013, p. 197
40. G. A. Somorjai, Y. Li, *Introduction to Surface Chemistry and Catalysis*, Wiley, Hoboken, NJ, 2010, p. 27
41. H. J. Freund, M. W. Roberts, *Surf. Sci. Rep.* **25** (1996) 225.





Ex situ integration of iron oxide nanoparticles onto exfoliated expanded graphite flakes in aqueous suspension

NATAŠA JOVIĆ^{1*}, MARIA P. CALATAYUD², BEATRIZ SANZ², AMELIA MONTONE³
and GERARDO F. GOYA²

¹Vinča Institute of Nuclear Sciences (020), University of Belgrade, P. O. Box 522, 11000

Belgrade, Serbia, ²Aragón Institute of Nanoscience and Department of the Physics of Condensed Matter, University of Zaragoza, Zaragoza, Spain and ³ENEA, Technical Unit Materials Technology, Research Centre of Casaccia, Via Anguillarese 301, 00123 Rome, Italy

(Received 21 November 2013, revised 3 March, accepted 10 March 2014)

Abstract: Hybrid structures composed of exfoliated expanded graphite (EG) and iron oxide nanocrystals were produced by an *ex situ* process. The iron oxide nanoparticles coated with *meso*-2,3-dimercaptosuccinic acid (DMSA), or poly(acrylic acid) (PAA) were integrated onto the exfoliated EG flakes by mixing their aqueous suspensions at room temperature under the support of 1-ethyl-3-(3-dimethylaminopropyl)carbodiimide (EDC) and *N*-hydroxysuccinimide (NHS). EG flakes both naked and functionalized with branched polyethylenimine (PEI) were employed. Complete integration of the two constituents was achieved and stability was maintained for more than 12 months. No preferential spatial distribution of anchoring sites for attachment of iron oxide nanoparticles was observed, regardless of whether the EG flakes were used naked or functionalized with PEI molecules. The structural and physicochemical characteristics of the exfoliated expanded graphite and its hybrid nanostructures were investigated by SEM, TEM, FTIR and Raman techniques.

Keywords: expanded graphite; iron oxide nanoparticles; nanocomposites; TEM; Raman spectroscopy.

INTRODUCTION

Due to its outstanding properties, graphene has been widely investigated. Recently, decoration of graphene platelets with different nanoparticles (quantum dots,¹ and magnetic² or noble metal nanoparticles^{3–5}) has attracted great attention. Such graphene-based hybrid structures combine the properties of both constituents. Depending on a kind of employed nanoparticles, multifunctional hybrids can express magnetic, optically active, conducting, catalytic and electrochemically active properties, thereby simultaneously keeping the good characteris-

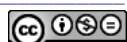
*Corresponding author. E-mail: natasaj@vinca.rs
doi: 10.2298/JSC131121019J

tics of graphene sheets, such as their stiffness, electrical conductivity and optical transparency. For example, graphene platelets decorated with transition metal or metal oxide nanoparticles were shown to be good candidates for the anode material in lithium-ion batteries,^{2,6} or as effective adsorbents for the removal of organic molecules and heavy metal ions from waste water.^{7–9} The properties of such hybrid structures are additionally dependent on the thickness of graphene platelets¹⁰ (mono- or few-layer graphene), the structural defects inside the basal graphene plane, and/or the number of oxygen-containing functional groups on the surface.^{11,12} Another important factor in defining the performances of hybrids could be related to the interfacial adhesion between the anchoring entities and the graphene support.⁶

The production of graphene platelets as substrates for hybrid structures is usually based on two different methods. The most common method to produce graphene platelets is the reduction of graphite oxide (GO) prepared from graphite according to the Hummers method.¹³ However, this process involves the use of strong and harmful reducing reactants, such as hydrazine. Simultaneously, the restacking of graphene sheets usually results in: *i*) a corrugated-sheet structure with damages in the basal plane and *ii*) a surface enriched with oxygen residues. Another method to produce graphene platelets is based on the exfoliation of graphite by means of ultrasonic treatment.^{14–16}

A hybrid structure with a graphene-based material as support matrix can be produced by different synthesis procedures, such as thermal decomposition of metal salts in the presence of graphene or graphene oxide sheets,^{17–19} hydrothermal/solvothermal methods^{20,21} or the simple mixing of solutions.²² Methods based on the *in situ* approach (the synthesis of nanoparticles occurs in the presence of graphene or graphene oxide sheets) are commonly in use. Only a few studies followed an *ex situ* approach in which previously synthesized and functionalized nanoparticles were used to anchor the graphene sheets.^{8,22} An overview of the literature data is presented in Table I, with emphases on the synthesis method, type of carbon-based matrix as support for the nanoparticles, type of bonding between constituents and possible application of graphene-based hybrid structures. Graphene-based hybrids can further be used as a filler in various polymer matrices,^{23,24} for the production of thin films¹ or as colloids.²⁵

In the present work, an *ex situ* process was used to decorate exfoliated expanded graphite (EG) sheets with *meso*-2,3-dimercaptosuccinic acid (DMSA)- or poly(acrylic acid) (PAA)-coated iron oxide nanoparticles (IONs). The aqueous suspensions of the two constituents were mixed at room temperature. This is one of the rare attempts where exfoliated expanded graphite,²⁷ obtained by reduction of graphene oxide, was used as the support instead of graphene sheets. The starting material was commercially available expanded graphite that was subjected to sonication in ethanol. The graphite flakes obtained in such a way were used



naked or grafted with PEI molecules and then were decorated with DMSA- or PAA-coated IONs in the presence of 1-ethyl-3-(3-dimethylaminopropyl)carbodiimide (EDC) and *N*-hydroxysuccinimide (NHS). The morphology and structural properties of the exfoliated expanded graphite sheets and its hybrid structures with IONs were studied by SEM, TEM, FTIR and Raman techniques.

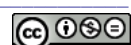
TABLE I. Iron oxide/carbon-based hybrid structures: methods of synthesis, types of support matrix/iron oxide nanoparticles, types of bonding, and potential applications of the hybrids; rGO – reduced graphene oxide

| Method of synthesis | Graphene-based support/IONs | Type of bonding | Potential application |
|--------------------------------------------------------------------------|------------------------------------------------------|--------------------------------------------|-------------------------------------------------------------------------|
| <i>In situ</i> | | | |
| Co-precipitation of iron salts in water | rGO ^a /Fe ₃ O ₄ | – | Electrochemical detection of chromium ¹⁷ |
| Thermal decomposition of iron precursor in organic solvents | Graphene or rGO/Fe ₃ O ₄ | – | Wave filters; superconductors ^{10,18} |
| Hydrothermal method | Graphene/Fe ₃ O ₄ | Direct bonding (without molecular linkers) | In polymer matrix for optical devices; bioimaging ²⁰ |
| Solvothermal reaction | Graphene/Fe ₃ O ₄ microspheres | – | Loading of doxorubicin hydrochloride ²¹ |
| Direct pyrolysis of Fe(NO ₃) ₃ ·9H ₂ O | Graphene/Fe ₃ O ₄ | Via Fe–O–C bond | In Li-ion batteries ⁶ |
| <i>Ex situ</i> | | | |
| Ultrasonication | GO/Fe ₃ O ₄ | Covalent bonding/ assisted by EDC/NHS | For removing cationic dyes (Methylene Blue; Neutral Red) ⁸ |
| Mixing of aqueous solutions | PEI-grafted rGO/Fe ₃ O ₄ | Covalent bonding/ assisted by EDC/NHS | For removal of antibiotics or aromatic anticancer drugs ²² |
| Mixing of aqueous solutions | Graphene/Fe ₃ O ₄ | Covalent bonding assisted by EDC | For drug delivery (loading and release of 5-fluorouracil) ²⁶ |

EXPERIMENTAL

Materials

Commercial, highly expanded graphite (supplied by the Carbone Lorraine Group, France), iron(III) acetylacetone (Fe(acac)₃, Aldrich, ≥97 %; IUPAC name: tris(acetylacetonato)iron(III)), iron(II) sulfate heptahydrate (FeSO₄·7H₂O), oleic acid (90 % pure; IUPAC name: (9Z)-octadec-9-enoic acid), oleylamine (70 % pure; IUPAC name: (Z)-octa-9-decenylamine), 1,2-dodecanediol (90 % pure), 1-octadecene, hexane, toluene, *meso*-2,3-dimercaptosuccinic acid (DMSA, Sigma-Aldrich, ≈98 % pure; IUPAC name: 2,3-dimercaptobutanedioic acid), poly(acrylic acid) (PAA, 450 kDa), dimethyl sulfoxide (DMSO, Sigma-Aldrich, 99.9 % pure), triethylamine (PANREAC, 99.5 % pure), branched polyethylenimine (PEI, 25 kDa; IUPAC name: poly(iminoethylene)), 1-ethyl-3-(3-dimethylaminopropyl)carbo-



diimide (EDC; IUPAC name: 3-(ethyliminomethyleneamino)-*N,N*-dimethylpropan-1-amine)), *N*-hydroxysuccinimide (NHS, Fluka, >97 %; IUPAC name: 1-hydroxy-2,5-pyrrolidinedione), absolute ethanol, potassium nitrate (KNO_3) and sulfuric acid (H_2SO_4) were used as purchased.

Exfoliated expanded graphite (EG) flakes and its surface modified nanosheets (PEI-EG)

Commercial expanded graphite (EG, 0.2 g) in 50 ml of absolute ethanol was placed into an ultrasonic bath for 10 h. A certain amount of so obtained exfoliated EG flakes in absolute ethanol (concentration \approx 4 mg mL $^{-1}$) were mixed with branched polyethylenimine (PEI, 25 kDa), previously dissolved in a mixture of milli-Q-water and dimethyl sulfoxide (DMSO) (1:4, V/V). The mass ratio of EG flake to PEI was 10:1. The mixture was agitated for two days in a rotatory mixer at room temperature. After mixing and rinsing with water, the surface-modified EG flakes were dispersed in milli-Q-water. The suspension of EG flakes was labeled as PEI-EG *aq.* (concentration \approx 1 mg of EG per mL of H_2O). For the sake of comparison, a suspension of EG flakes in absolute ethanol was only rinsed several times with milli-Q-water and finally redispersed in water (naked EG flakes).

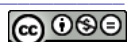
Synthesis and surface modification of iron oxide nanocrystals

Two types of iron oxide nanocrystals (IONs) were used to decorate the exfoliated expanded graphite flakes. One type of IONs was produced by thermal decomposition of iron(III) acetylacetone salt in the presence of oleic acid and oleylamine in an organic solvent.²⁸ The second type of IONs was synthesized directly through an oxidative hydrolysis method.

Synthesis of iron oxide nanocrystals (IONs) by the thermal decomposition method and its surface modification with DMSA. The iron oxide nanocrystals were synthesized by the well-studied thermal decomposition method, starting from iron(III) acetylacetone ($\text{Fe}(\text{acac})_3$).²⁸ In brief, 2.825 g of $\text{Fe}(\text{acac})_3$, 12.554 g of oleic acid, 15.286 g of oleylamine, and 8.992 g of 1,2-dedecandiol (mole ratio of 1:5:5:5) were added into in a three neck flask, previously filled with 80 mL of 1-octadecene. The solution was mechanically stirred at room temperature for 30 min under a nitrogen flow. Then, the mixture was heated to 200 °C, kept at that temperature for 2 h, further heated up to 290 °C under reflux conditions, aged at 290 °C for 30 min, and slowly cooled down to room temperature. The black precipitate was collected by a magnet and washed several times with ethanol and hexane. Finally, the precipitate was dissolved in toluene (the so-called stock solution). The concentration of IONs in the stock solution was determined by the UV-Vis spectroscopic approach²⁹ and was found to be \approx 9.53 mg mL $^{-1}$.

In the next step, iron oxide nanocrystals (from the stock solution) were subjected to a surface exchange process in which the hydrophobic oleic acid molecules were replaced by the hydrophilic *meso*-2,3-dimercaptosuccinic acid (DMSA). The exchange process occurred in dimethyl sulfoxide (DMSO). IONs (10 mg), taken from the stock solution in toluene, were added into a DMSO solution of DMSA (20 mg mL $^{-1}$). Then, 50 µl of triethylamine was added, and the mixture was stirred at 60 °C for 17 h. The obtained black precipitate was collected by a pipette, transferred into microcentrifuge tubes, redispersed in absolute ethanol and centrifuged several times at 13000 rpm for 10 min in order to remove the free oleic acid molecules. Finally, the precipitated nanoparticles were redispersed in milli-Q-water. The obtained suspension was labeled as DMSA-ION.

Synthesis of PAA-ION nanocrystals by a modified oxidative hydrolysis method. The synthesis protocol used was based on the well-known oxidative hydrolysis method that consists of the precipitation of an iron salt (FeSO_4) in basic media (NaOH) with a mild oxidant. In a



typical synthesis, a mixture of 1.364 g of KNO_3 and 0.486 g of NaOH was dissolved in 135 mL of distilled water in a three-necked flask and bubbled with N_2 . Then 15 mL of 0.01 M H_2SO_4 solution containing 0.3 g of $\text{FeSO}_4 \cdot 7\text{H}_2\text{O}$ and 0.30 g of poly(acrylic acid) (PAA, 450 kDa, previously bubbled with N_2 for 2 h) was added dropwise under constant stirring. When the precipitation was completed, nitrogen was allowed to pass through for another 5 min and the suspension with the black precipitate was held at 90 °C for 24 h under N_2 . Afterwards, the solution was cooled to room temperature with an ice bath, and the solid was separated by a magnet, washed several times with distilled water and redispersed in milli-Q-water. The obtained suspension was labeled as PAA–ION. The concentration of iron oxide nanoparticles in the suspension was found to be $\approx 0.5 \text{ mg mL}^{-1}$ (from the UV–Vis spectrum).

Preparation of iron oxide nanocrystals/expanded graphite hybrids

The four iron oxide/exfoliated expanded graphite hybrids were prepared by mixing of aqueous suspensions of exfoliated EG flakes with DMSA– and PAA–coated IONs. Exfoliated graphite flakes have been used naked (EG), or functionalized with branched polyethylenimine (PEI–EG *aq.*). The aqueous suspensions were mixed at room temperature in the presence of EDC and NHS. Details about production of the DMSA–ION/PEI–EG-2 nanohybrid structures are given below. The number at the end of sample's name represents the mass ratio between the loaded IONs and EG flakes in the sample.

Sample DMSA–ION/PEI–EG-2. 0.5 mg of graphite flakes functionalized with PEI molecules (PEI–EG *aq.*) was added into 1 mL of milli-Q-water, followed by addition of 5 mg of EDC and 5 mg of NHS. Then, 1 mg of iron oxide nanoparticles coated with DMSA and suspended in milli-Q-water (DMSA–ION), was added by dropwise into the mixture and stirred for two days at room temperature. The concentration of IONs in the solution was determined by UV–Vis spectroscopy.²⁹ The mixture was then collected, transferred into plastic tubes and washed in excess milli-Q-water three times (centrifuged at 4000 rpm for 10 min).

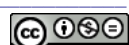
For the other three samples, EG flakes were decorated with PAA–coated IONs (PAA–ION) by the same procedure. In order to study possible influence of the PEI molecules on the attachment strength of PAA–IONs, naked EG flakes were used instead of PEI-grafted ones (sample PAA–ION/naked–EG-0.1). The mass amounts of all ingredients mixed, relative to EG, are given in Table II. The hybrids were labeled according to the type of IONs used and EG flakes, and their relative mass amounts.

Table II. The mass amount relative to exfoliated expanded graphite flakes (EG) of iron oxide nanoparticles (ION), 1-ethyl-3-(3-dimethylaminopropyl) carbodiimide (EDC), and *N*-hydroxy-succinimide (NHS) used in preparation of the hybrid structures

| Sample | ION | EDC | NHS |
|----------------------|-----|-----|-----|
| DMSA–ION/PEI–EG-2 | 2 | 10 | 10 |
| PAA–ION/PEI–EG-0.5 | 0.5 | 10 | 10 |
| PAA–ION/PEI–EG-0.1 | 0.1 | 1 | 1 |
| PAA–ION/naked–EG-0.1 | 0.1 | 1 | 1 |

Characterization and measurements

The structural features of the expanded graphite (EG) flakes were investigated by X-ray diffraction (Bruker D8 Advance diffractometer, in the glaze angle (2°) incident geometry; $\lambda = 1.5406 \text{ nm}$, $I = 30 \text{ mA}$; $V = 38 \text{ kV}$). Scanning electron microscopy (SEM, Cambridge, Stereoscan 250 Mk3) was used to observe the morphological features of EG and exfoliated



EG flakes. The hybrid structures built of naked or PEI-grafted EG flakes, and DMSA- or PAA-coated iron oxide nanoparticles were studied by transmission electron microscopy (TEM, FEI TECNAI T20, 200 kV), attenuated total reflectance infrared (ATR-FTIR, Bruker, Vertex 70) and Raman spectroscopy (Thermo Scientific DXR MicroRaman). The ATR-FTIR spectra were acquired in the 400–4000 cm⁻¹ region with a resolution of 4 cm⁻¹, by accumulating 40 scans. The Raman spectra were collected in the spectral range 60–3100 cm⁻¹ using a HeNe 532 nm gas laser with laser power 9.8 or 2 mW. The samples were previously casted onto a glass holder and dried at 40 °C for 3 h to eliminate water.

RESULTS AND DISCUSSION

The X-ray diffraction (XRD) pattern of pristine expanded graphite before sonication in ethanol revealed the presence of a diffraction peak at 26.5° which belongs to the (002) reflection of the hexagonal graphite structure (see inset in Fig. 1a). The average crystallite thickness along the (001) direction of the pristine expanded graphite, L_c , was estimated using the Scherrer Equation: $L_c = K\lambda / (\beta_{002}\cos\theta)$, and the integral width of (002) reflection, β_{002} , and it was found to be around 20 nm ($K = 0.9$). Bearing in mind that for ideal graphite, the interlayer distance along the c axis, d_{002} , is 0.335 nm, this means that the accordion-like pristine graphite (Fig. 1a and b) was built of bundles of expanded graphite sheets composed of approximately 60 graphene layers. SEM images of the exfoliated expanded graphite (EG) flakes obtained after sonication in absolute ethanol for 10 h (Fig. 1c and d) revealed that under ultrasonic treatment, thin and transparent nanosheets with high aspect ratio had been produced. The lateral dimensions of the EG flakes range from 2 to 20 μm. Based on the SEM micrographs, it could be

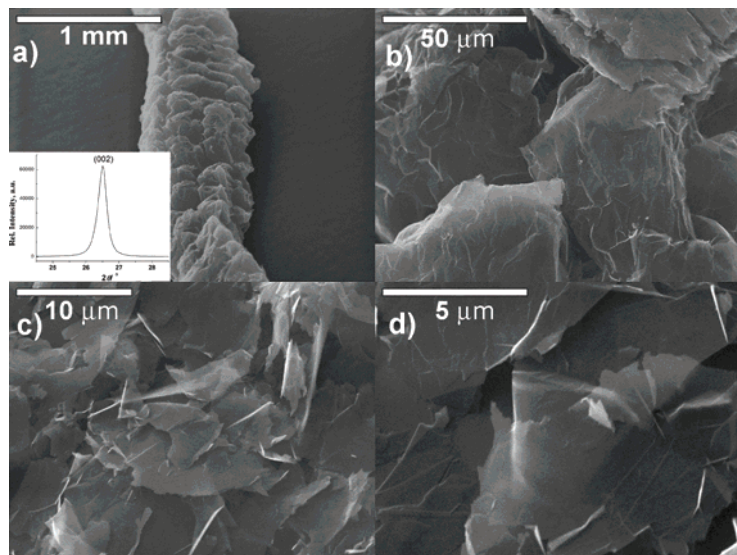


Fig. 1. SEM Images of: a) and b) expanded graphite (EG); c) and d) exfoliated EG.
Inset: the XRD profile of (002) reflection of EG.

noticed that additional cleavage of EG flakes had occurred under ultrasonic irradiation, giving rise to foliation and the production of EG flakes thinner than those found in the pristine expanded graphite. This statement was additionally corroborated by Raman spectroscopy, as follows.

The Raman spectra of pristine and exfoliated EG flakes (after ultrasonic treatment) are shown in Fig. 2a. In the Raman spectrum of pristine EG flakes, a weak D band at $\approx 1360 \text{ cm}^{-1}$, a G band at $\approx 1585 \text{ cm}^{-1}$ and an asymmetric 2D band were detected. The 2D band was deconvoluted into two Lorentzian peaks: the one at $\approx 2725 \text{ cm}^{-1}$ with a full width at half maximum, FWHM of 38 cm^{-1} , and another at $\approx 2688 \text{ cm}^{-1}$ with a FWHM of 59 cm^{-1} (Fig. 2b). A split 2D band that can be fitted by two peaks is characteristic of a 3-dimensional graphitic materials.^{27,30} The low intensity of the D band indicated to the large lateral dimension of the EG sheets. Upon sonication in ethanol for 10 h, the intensity of the D-band (at $\approx 1350 \text{ cm}^{-1}$) increased, which could be assigned to the involvement of defects and disordering in the hexagonal graphitic layers upon ultrasound treatment. Simultaneously, the G-band at $\approx 1579 \text{ cm}^{-1}$ became broader. The 2D-band of the exfoliated EG flakes was also fitted by two Lorentzian peaks with maxima at 2717 cm^{-1} (FWHM = 38 cm^{-1}) and 2685 cm^{-1} (FWHM = 75 cm^{-1} , Fig.

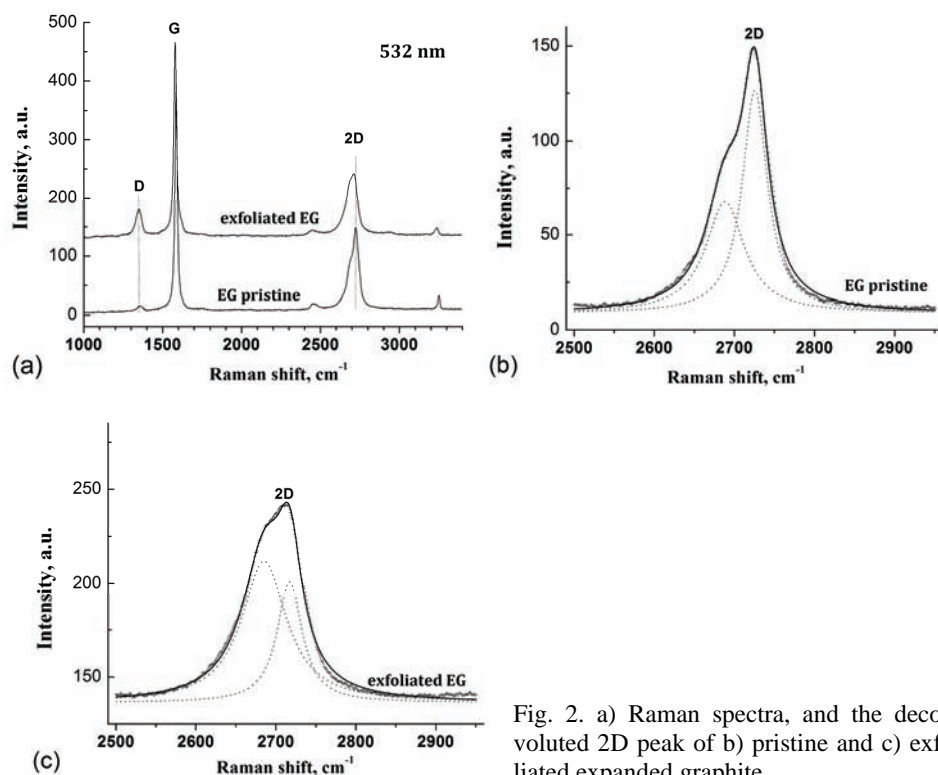


Fig. 2. a) Raman spectra, and the deconvoluted 2D peak of b) pristine and c) exfoliated expanded graphite.

2c). The relative intensities of these two Lorentzian components changed upon sonication, which indicated different degrees of stacking order along the *c* direction.³⁰

The ATR-FTIR spectra of the naked and PEI-grafted EG flakes, and the PAA-ION/PEI-EG-0.5 hybrid showed very similar, almost featureless characteristics (Fig. 3). Such behavior is probably caused by the dark gray color of the exfoliated EG flakes. Closer inspection of these spectra (inset of Fig. 3) showed the presence of a weak transmittance peaks at 870 cm^{-1} in all three samples, which could be assigned to the asymmetric ring stretching.³¹ An additional broad peak centered at *c.a.* $\approx 1100\text{ cm}^{-1}$ observed in the FTIR spectrum of the PEI-grafted EG flakes could be assigned to the C–N stretching vibration peak for primary amines³² (1130 cm^{-1}), and/or the presence of C–O groups (1060 cm^{-1}).³³ A transmittance band at *c.a.* $\approx 660\text{ cm}^{-1}$ in the FTIR spectrum of the PAA-Fe₃O₄/PEI-EG-0.5 hybrid could be attributed to Fe–O bonds. Due to nearly featureless nature of FTIR spectra, it is difficult to recognize the presence/absence of functional groups at the surface of the EG flakes. Nevertheless, the PEI-grafted EG flakes showed that better dispersion in water in comparison

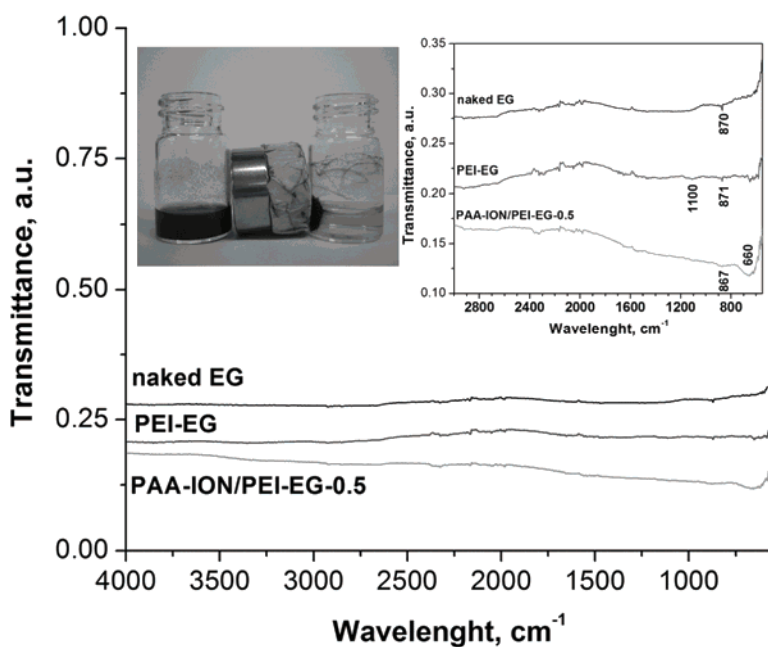


Fig. 3. ATR-FTIR spectra of exfoliated EG flakes (naked and PEI-grafted) and a selected hybrid, PAA-ION/PEI-EG-0.5. Inset (left): Response of water suspensions of pure exfoliated EG flakes and the response of the PAA-ION/PEI-EG-0.5 hybrid to the presence of a strong permanent magnet. Inset (right): Magnified ATR-FTIR spectra.

to the naked EG flakes. In addition, it was observed that if aqueous suspensions of both kinds of EG flakes were subjected to centrifugation under the same conditions, the PEI-grafted EG flakes precipitate while the naked EG flakes still float, which clearly indicates a difference in density of these two types of EG flakes. It is likely that the positively charged PEI molecules attached to the surface of the EG sheets produce surface charge changes, thus causing a weakening of hydrophobicity and an improvement in the stability of the dispersion of PEI-grafted EG flakes in water.

During the formation of hybrid structures between the PEI-grafted EG flakes and DMSA- and PAA-coated IONs, the amino groups ($-NH_2$) of the PEI molecules could react with the free carboxyl ($-COOH$) and thiol ($-SH$) groups of the DMSA molecules, as well as with the $-COOH$ groups of the PAA molecules. The role of the EDC molecules is to activate the carboxylic groups for direct conjugation to primary amines and thus facilitate the attachment of iron oxide nanoparticles onto the EG flakes. Complete integration of IONs onto the exfoliated expanded graphite flakes in the PAA-ION/PEI-EG-0.5 hybrid was verified by its attraction to a strong permanent magnet (see inset of Fig. 3), while the naked EG flakes were not attracted. The microstructure of the DMSA-ION/PEI-EG-2

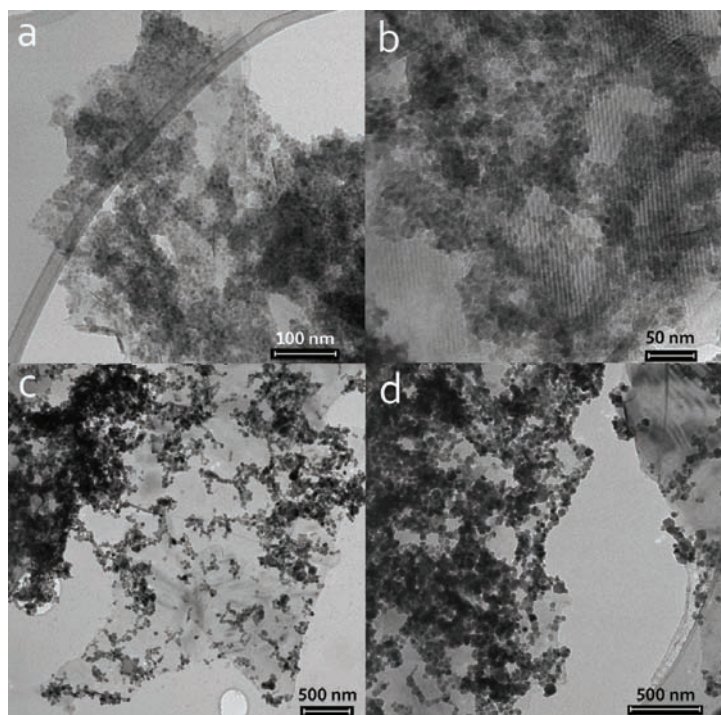


Fig. 4. TEM Images of a) and b) DMSA-ION/PEI-EG-2, and c) and d) PAA-ION/PEI-EG-0.5 hybrids.

and PAA–ION/PEI–EG-0.5 hybrids, shown in Fig. 4, indicate that the iron oxide nanoparticles are randomly distributed on the basal plane of the PEI-grafted EG flakes and they are agglomerated or form clusters of nanoparticles. Any preferential site for attachment of the IONs onto exfoliated EG sheets was not registered. On the contrary, Zhang *et al.*, achieved a preferential periphery decoration of the graphene oxide sheets by magnetic nanoparticles caused by a difference in the spatial distribution of the oxygen-containing groups attached onto GO sheets (the carboxylic groups are located on the edge, while the epoxy and hydroxyl groups are usually located on the basal plane of GO sheets).²²

To check if there were any influence of the PEI molecules on the assembly process of coated magnetic nanoparticles with EG flakes, two hybrids were introduced with the same nanoparticle loading (10 wt. % of PAA–IONs), using PEI-grafted and naked EG flakes as substrates (PAA–ION/PEI–EG-0.1 and PAA–ION/naked–EG-0.1 samples, respectively). In both cases, the integration of iron oxide nanoparticles with EG flakes was achieved. The TEM micrographs of

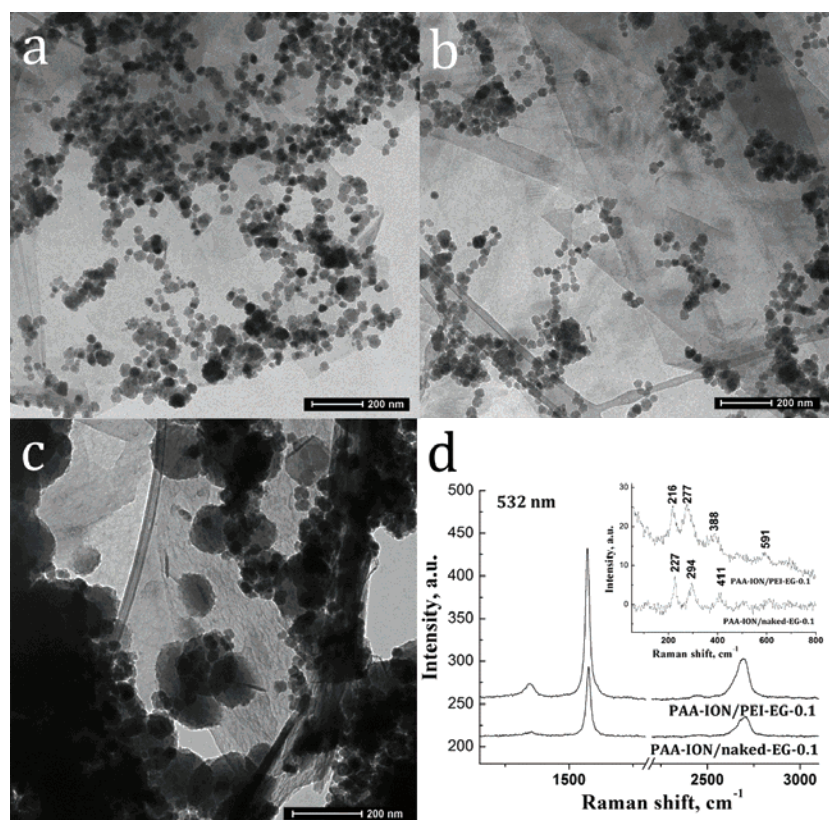


Fig. 5. TEM Micrographs of a) and b) PAA–ION/PEI–EG-0.1, c) PAA–ION/naked–EG-0.1 hybrids and d) the Raman spectra.

these two hybrids are shown in Fig. 5. Dark spots, observed only in the TEM micrograph of PAA–ION/naked–EG-0.1 hybrid, can be an indication of the presence of water droplets on a surface of the naked EG flakes. This could be explained by the difference in the macroscopic wetting behavior of water droplets on the naked and PEI-grafted EG sheets due to a difference in the binding energy (given by the Lennard–Jones potential) between a water monomer on one side and naked or PEI-grafted EG flakes on the other side.³⁴

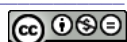
The Raman spectra of these two nanohybrids, PAA–ION/PEI–EG-0.1 and PAA–ION/naked–EG-0.1, are shown in Fig. 5c. In order to avoid degradation of PAA, the spectra were recorded with lower laser power. The intensity of the Raman bands characteristic for the exfoliated EG structure decreases. The Raman modes at 227, 294 and 411 cm⁻¹ found in the spectrum of the PAA–ION/naked–EG-0.1 sample indisputably correspond to the hematite phase (inset of Fig. 5c). In the sample PAA–ION/PEI–EG-0.1, the characteristic Raman modes for hematite are shifted to 216, 277 and 388 cm⁻¹, respectively. The appearance of the α –Fe₂O₃ (instead of the expected magnetite) phase could have resulted from the laser treatment on the IONs during collection of the Raman spectrum.

As can be seen, the IONs are attached on the surface of the exfoliated EG flakes, either naked or PEI-grafted, without any preferential sites along the EG sheets for attachment of nanoparticles. This could be an indication that either the PEI molecules are not preferentially anchored along the border of the EG flakes, or it might also be that epoxy groups or some structural defects inside the honeycomb graphene lattice serve as anchoring sites.

CONCLUSIONS

In summary, successful decoration of exfoliated expanded graphite (EG) flakes with DMSA- or PAA-coated iron oxide nanoparticles was achieved by an *ex situ* process through the mixing of aqueous suspensions of two constituents at room temperature. The integration of the EG flakes and iron oxide nanoparticles was supported by EDC and NHS molecules. The bonds between the hybrid constituents were stable for more than 12 months. No preferential spatial distribution of anchoring sites for attachment of iron oxide nanoparticles was observed, regardless of whether the employed EG flakes were naked or functionalized with PEI molecules. This can indicate that other oxygen-containing functional groups (epoxy and/or hydroxyl) or structural defects inside graphene plane might serve as anchoring sites.

Acknowledgements. This work was supported by the Ministry of Education, Science and Technological Development of the Republic of Serbia through Project No. 45015. N. J. would like to thank the Ministry of Education, Science and Technological Development of the Republic of Serbia for a Postdoctoral fellowship at the Institute of Nanoscience of Aragon, University of Zaragoza, Spain (2010/2011). We thank Dr. Danica Bajuk-Bogdanović for performing the Raman measurements.



ИЗВОД

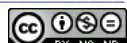
EX SITU УГРАЂИВАЊЕ НАНОЧЕСТИЦА ГВОЖЂЕ ОКСИДА НА ЛИСТИЋЕ
ЕКСПАНДИРАНОГ ГРАФИТА У ВОДЕНОЈ СУСПЕНЗИЈИНАТАША ЈОВИЋ¹, MARIA P. CALATAYUD², BEATRIZ SANZ², AMELIA MONTONE³ и GERARDO F. GOYA²¹Институут за нуклеарне науке Винча (020), Универзитет у Београду, б.п. 522, 11001 Београд,²Aragón Institute of Nanoscience and Department of Physics of Condensed Matter, University of Zaragoza, Zaragoza, Spain и ³ENEA, Technical Unit Materials Technology, Research Centre of Casaccia, Via Anguillarese 301, 00123 Rome, Italy

Хибридне наноструктуре изграђене од наночестица оксида гвожђа и листића експандираног графита добијене су *ex situ* поступком. Водене суспензије наночестица оксида гвожђа, претходно обложених молекулама мезо-2,3-димеркаптосукцинском киселином (DMSA), односно молекулама поли(акрилне киселине) (PAA), и листића експандираног графита мешане су на собној температури уз додатак 1-етил-3-(3-диметиламинопропил)карбодимида (EDC) и *N*-хирдоксисукцинимиде (NHS). Коришћени су чисти и полиетиленимином (PEI) функционализовани листићи графита. Постигнуто је комплетно сједињавање две компоненете, а разградња хибридних структура није уочена ни након годину дана. Одсуство преферентне просторне расподеле места на графитним листићима за која се каче наночестице оксида гвожђа такође није уочена, без обзира на то да ли су коришћени чисти или функционализовани листићи графита. Структурна и физичко-хемијска својства листића експандираног графита и хибридних структура испитивана су применом скенирајуће и трансмисионе електронке микроскопије и инфрацрвене и Раманове спектроскопије.

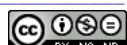
(Примљено 21. новембра 2013, ревидирано 3. марта, прихваћено 10. марта 2014)

REFERENCES

1. X. Geng, L. Niu, Z. Xing, R. Song, G. Liu, M. Sun, G. Cheng, H. Zhong, Z. Liu, Z. Zhang, L. Sun, H. Xu, L. Lu, L. Liu, *Adv. Mater.* **22** (2010) 638
2. Z. S. Wu, W. Ren, L. Wen, L. Gao, J. Zhao, Z. Chen, G. Zhou, F. Li, H. M. Cheng, *ACS Nano* **4** (2010) 3187
3. B. S. Kong, J. Geng, H. T. Jung, *Chem. Comm.* (2009) 2174
4. M. Liu, H. Zhao, S. Chen, H. Yu, X. Quan, *ACS Nano* **6** (2012) 3142
5. H. Wu, J. Wang, X. Kang, C. Wang, D. Wang, J. Liu, I. A. Aksay, Y. Lin, *Talanta* **80** (2009) 403
6. J. Zhou, H. Song, L. Ma, X. Chen, *RSC Adv.* **1** (2011) 782
7. P. Bhunia, G. Kim, C. Baik, H. Lee, *Chem. Comm.* **48** (2012) 9888
8. F. He, J. Fan, D. Ma, L. Zhang, C. Leung, H. Laiwa Chan, *Carbon* **48** (2010) 3139
9. Y. W. Liu, M. X. Guan, L. Feng, S. L. Deng, J. F. Bao, S. Y. Xie, Z. Chen, R. B. Huang, L. S. Zheng, *Nanotechnology* **24** (2013) 025604
10. J. Zhu, Z. Luo, S. Wu, N. Haldoarachchige, D. P. Young, S. Wei, Z. Guo, *J. Mater. Chem.* **22** (2012) 835
11. L. Ćirić, D. M. Djokić, J. Jaćimović, A. Sienkiewicz, A. Magrez, L. Forró, Ž. Šljivančanin, M. Lotya, J. N. Coleman, *Phys. Rev., B* **85** (2012) 205473
12. Q. Tang, Z. Zhou, Z. Chen, *Nanoscale* **5** (2013) 4541
13. W. S. Hummers Jr., R. E. Offeman, *J. Am. Chem. Soc.* **80** (1958) 1339
14. G. Chen, W. Weng, D. Wu, C. Wu, J. Lu, P. Wang, X. Chen, *Carbon* **42** (2004) 753
15. I. Zaman, H. C. Kuan, Q. Meng, A. Michelmore, N. Kawashima, T. Pitt, L. Zhang, S. Gouda, L. Luong, J. Ma, *Adv. Funct. Mater.* **22** (2012) 2735



16. J. Malig, C. Romero-Nieto, N. Jux, D. M. Guldi, *Adv. Mater.* **24** (2010) 800
17. A. Prakash, S. Chanda, D. Bahadur, *Carbon* **50** (2012) 4209
18. H. P. Cong, J. J. He, Y. Lu, S. H. Yu, *Small* **6** (2010) 169
19. D. W. P. Pang, F. W. Yuan, Y. C. Chang, G. A. Li, H. Y. Tuan, *Nanoscale* **4** (2012) 4562
20. L. Ren, S. Huang, W. Fan, T. Liu, *Appl. Surf. Sci.* **258** (2011) 1132
21. K. Zhou, Y. Zhu, X. Yang, C. Li, *New J. Chem.* **34** (2010) 2950
22. Y. Zhang, B. Chen, L. Zhang, J. Huang, F. Chen, Z. Yang, J. Yao, Z. Zhang, *Nanoscale* **3** (2011) 1446
23. T. T. Tung, J. F. Feller, T. Y. Kim, H. Kim, W. S. Yang, K. S. Suh, *J. Polym. Sci., A* **50** (2012) 927
24. X. Xia, Q. Hao, W. Lei, W. Wang, D. Sun, X. Wang, *J. Mater. Chem.* **22** (2012) 16844
25. S. Stankovich, R. D. Piner, X. Chen, N. Wu, S. T. Nguyen, R. S. Ruoff, *J. Mater. Chem.* **16** (2006) 155
26. X. Fan, G. Jiao, W. Zhao, P. Jin, X. Li, *Nanoscale* **5** (2013) 1143
27. G. Katsukis, J. Malig, C. Schulz-Drost, S. Leubner, N. Jux, D. M. Guldi, *ACS Nano* **6** (2012) 1915
28. S. Sun, H. Zeng, *J. Am. Chem. Soc.* **124** (2002) 8204
29. M. P. Calatayud, C. Riggio, V. Raffa, B. Sanz, T. E. Torres, M. R. Ibarra, C. Hoskins, A. Cuschieri, L. Wang, J. Pinkernelle, G. Keilhoff, G. F. Goya, *J. Mater. Chem., B* **1** (2013) 3607
30. M. A. Pimenta, G. Dresselhaus, M. S. Dresselhaus, L. G. Cançado, A. Jorio, R. Saito, *Phys. Chem. Chem. Phys.* **9** (2007) 1276
31. M. Lotya, Y. Hernandez, P. J. King, R. J. Smith, V. Nicolosi, L. S. Karlsson, F. M. Blighe, S. De, Z. Wang, I. T. McGovern, G. S. Duesberg, J. N. Coleman, *J. Am. Chem. Soc.* **131** (2009) 3611
32. Z. Qian, M. A. Khan, S. Mikkelsen, P. Chen, *Langmuir* **26** (2010) 2176
33. Y. Si, E. T. Samulski, *Nano Lett.* **8** (2008) 1679
34. T. Werder, J. H. Walther, R. L. Jaffe, T. Halicioglu, P. Koumoutsakos, *J. Phys. Chem., B* **107** (2003) 1345.





Actual contamination of the Danube and Sava Rivers at Belgrade (2013)

MILAN D. ANTONIJEVIĆ¹, MARIJA ARSOVIĆ², JOSEF ČÁSLAVSKÝ³, VESNA CVETKOVIĆ⁴, PREDRAG DABIĆ⁴, MLAĐEN FRANKO⁵, GORDANA ILIĆ⁶, MILENA IVANOVIĆ⁷, NEVENA IVANOVIĆ⁸, MILICA KOSOVAC⁸, DRAGANA MEDIĆ⁷, SLOBODAN NAJDANOVIC^{7#}, MILICA NIKOLIĆ⁷, JOVANA NOVAKOVIĆ⁴, TATJANA RADOVANOVIC⁵, ĐURĐINA RANIĆ⁴, BOJAN ŠAJATOVIĆ⁶, GORICA ŠPIJUNOVIC², IVANA STANKOV⁶, JELENA TOŠOVIĆ⁸, POLONCA TREBŠE⁵, OLIVERA VASILJEVIĆ² and JAN SCHWARZBAUER^{9*}

¹School of Science, University of Greenwich, England, UK, ²High Business-Technical School, Užice, Serbia, ³Faculty of Chemistry, Brno University of Technology, Czech Republic,

⁴Faculty of Technology and Metallurgy, Faculty of Chemistry, Faculty of Mining and Geology, Technical Faculty in Bor, University of Belgrade, Serbia, ⁵Laboratory for Environmental Research, University of Nova Gorica, Slovenia, ⁶Faculty of Science, University of Novi Sad, Serbia, ⁷Faculty of Science and Mathematics, University of Niš, Serbia, ⁸Faculty of Science and Mathematics, University of Kragujevac, Serbia and ⁹Institute of Geology and Geochemistry of Petroleum and Coal, RWTH Aachen University, Germany

(Received 5 November 2013, revised 14 February, accepted 23 February 2013)

Abstract: This study was focussed on a comprehensive investigation on the state of pollution of the Danube and Sava Rivers in the region of Belgrade. Different complementary analytical approaches were employed covering both *i*) organic contaminants in the river water by target analyses of hormones and neonicotinoids as well as non-target screening analyses and *ii*) heavy metals in the sediments. Finally, some common water quality parameters were analysed. The overall state of pollution is on a moderate level. Bulk parameters did not reveal any unusual observations. Moreover, quantification of preselected organic contaminants did not indicate to elevated pollution. More significant contaminations were registered for chromium, nickel, zinc and partially copper in sediments with values above the target values according to Serbian regulations. Lastly, non-target screening analysis revealed a wider spectrum of organic contaminants comprising pharmaceuticals, technical additives, personal care products and pesticides. The study presented a comprehensive view on the state of pollution of the Sava and Danube Rivers and is the base for setting up further monitoring programs. As a superior outcome, it was illustrated how different chemical analyses can result in different assessments of the river quality. A

* Corresponding author. E-mail: jan.schwarzbauer@emr.rwth-aachen.de

Serbian Chemical Society member.

doi: 10.2298/JSC131105014A

comparison of target and non-target analyses pointed to potential misinterpretation of the real state of pollution.

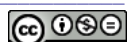
Keywords: river systems; state of pollution; organic pollutants; heavy metals; screening analyses; non-target screening.

INTRODUCTION

Large rivers are severely contaminated water bodies in aquatic ecosystems, which have become increasing serious problems for decades. Riverine contaminants are derived from both anthropogenic and biogenic sources.^{1–4} Anthropogenic inorganic, organic and organometallic pollutants are emitted into rivers by for example runoffs and leaching from agricultural fields, direct discharge of waste water, by atmospheric deposition and shipping activities. In more detail, the contamination is caused by heavy metals, nutrients and many low-molecular weight organic compounds, such as pesticides, plasticizers, pharmaceuticals, ingredients of personal care products, *etc.* Many of them are known to have, or are suspected to have, toxic, ecotoxic or endocrinic effects at trace levels. Note-worthy, surface water is becoming more and more relevant as a source of drinking water. Therefore, an appropriate water quality control is needed as a base for a sustainable usage of river water.

Pollution of the aquatic environment caused by inorganic chemicals is considered a major threat to aquatic organisms including fish. The most common anthropogenic sources of metals are industrial plants, petroleum contamination, waste water treatment plants and sewage disposal.⁵ Metal ions can be incorporated into the food chains and concentrated in aquatic organisms to a level that affects their physiological state. Trace metals such as Zn, Cu and Fe play a biochemical role in the life processes of all aquatic plants and animals; therefore, they are essential in the aquatic environment in trace amounts.⁶ One of the major problems that heavy metals cause with respect to their effects on aquatic organisms is their long biological half-life. Therefore, they are among the most frequently monitored micropollutants, and reliable techniques have been established for their extraction and quantification, since sediment contamination by heavy metals in rivers and estuaries has become an issue of increasing environmental concern.^{7–10} However, in most cases only total amounts are determined instead of the more relevant bioavailable fractions.

River sediments act as a fundamental environmental compartment and hold many functions, *e.g.*, providing foodstuff for living organisms. They also serve as a sink and reservoir for a variety of environmental contaminants in accumulation or deposition areas. It has been recognized that aquatic sediments accumulate persistent and toxic chemicals.¹¹ In the past years, tremendous efforts have been made to characterize the fate, loading and distribution of heavy metals in sediments.¹²

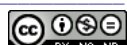


The River Danube is the second longest river in Europe with a length of about 2 800 km.¹³ Its catchment area covers 801 500 km², with approximately 81 million inhabitants in 19 countries.¹⁴ The Danube flows through four capitals (Vienna, Budapest, Bratislava and Belgrade) with 0.5 million to 2.5 million inhabitants contributing to extensive water use and pollution.

Many organic compounds have been identified in the Danube River, *i.e.*, to date: hydrophobic alkylphenolic, lipid series (*n*-alkanoic acids, *n*-alkanes, *n*-alkanols and sterols), pharmaceuticals (such as ibuprofen, diclofenac, sulphamethoxazole and carbamazepine), pesticides and their degradation products (*e.g.*, benthiazole, 2,4-D, mecoprop, atrazine, terbutylazine and desethylterbutylazine), perfluorinated acids, and endocrine disrupting compounds (nonylphenol, NPE1C, bisphenol A and estrone).^{15–17} Polychlorinated biphenyls (PCBs), polybrominated diphenyl ethers (PBDEs) and organochlorine pesticides (OCPs), such as dichlorodiphenyltrichloroethane (DDT) and analogues, hexachlorocyclohexanes (HCHs) and hexachlorobenzene (HCB), were measured in sediments and biota.¹⁸ Lipids, amino acids and carbohydrates are reported to be present in particulate and dissolved organic matter as constituents of the organic matrix.¹⁶

The Sava River represents the largest tributary of the River Danube. It is 945 km long and it flows through Slovenia, Croatia, Bosnia and Herzegovina and Serbia. The Sava River Basin covers a catchment area of 95 719 km², which is approximately 40 % of the countries' combined total surface area and it is the source of more than 80 % of the total available freshwater in the area. Only a few publications have considered contamination of the Sava River water. The following persistent organic pollutants were investigated: polycyclic aromatic hydrocarbons (PAH), polychlorinated biphenyls (PCB), selected chlorinated pesticides and organo-tin compounds.¹⁹ It has been reported that many organic compounds were found in Sava groundwaters: hydrocarbons, petroleum hydrocarbons, aromatic hydrocarbons, PAHs, fatty acids, phenolic compounds, alkylsulphides, indoles, benzophenone, detergent-derived organic compounds, biodegradation products of nonylphenol polyethoxylates surfactants and EDTA.²⁰ On the other hand, dissolved metals were observed in grab water samples - Fe, Mn, Zn, Ni, Cu, Cr, Co, Pb and Cd. Inorganic pollutants were investigated in sediments as well - Cd, Pb, Ni, Hg, Cu, Zn, Cr, As and P were determined.²¹

The present study focused on a comprehensive investigation on the state of pollution of the Danube and Sava Rivers in the area of their confluence, the Belgrade region. For these purposes, different complementary analytical approaches were used at different laboratories in Europe (Czech Republic, Slovenia, United Kingdom and Germany). The analytical approaches covered on the one hand organic contaminants in the river water by target analyses of hormones and neonicotinoids as well as non-target screening analyses. On the other hand inorganic contaminants were investigated in sediments, particularly heavy metals.



Furthermore, some common water quality parameters were analysed, including Total Organic Carbon (TOC), Total Nitrogen (*TN*) and major ions.

The overall goal of this case study was to illustrate how complex and complementary can be a more comprehensive analytical view on an aquatic system. To the best of our knowledge this approach has been ignored as far as possible in environmental geochemical studies in the Danube Basin catchment area.

EXPERIMENTAL

Sampling

Water samples. River water samples were taken during two different sampling campaigns in January and February 2013 at five sampling locations along the Danube and the Sava Rivers in Serbia (Fig. 1, Table I). Water samples of 2.5 L were taken from approximately 20 cm below the water surface nearby the river bank and bottled in pre-cleaned flasks. The sample material was stored in the dark at a temperature of approximately 4 °C. Before extraction and *TOC* determination, all water samples were filtered through pre-cleaned Whatman GF/F filters (0.45 mm) in order to remove suspended particulate matter from the aqueous phase.

Sediment samples. Surface sediment samples were taken at the same five sampling locations along the Danube and the Sava Rivers in Serbia (see Table S-I, of the Supplementary material to this paper). Sediment samples from the first two locations on the Sava River (Zabran and Makiš) were taken by means of a Van Veen grab from a depth of 1.20 m and at the third location (Kapetanija), from a depth of 3.50 m. Sediment samples from the two locations on the Danube River were taken from depths of 0.90 m (Batajnica) and 1.20 m (Vinča). The samples were kept in pre-cleaned vessels and stored at a temperature of approximately 4 °C.

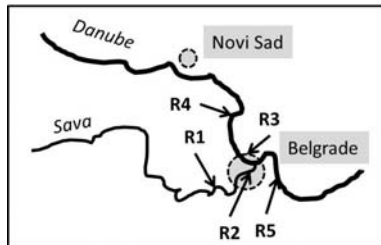


Fig. 1. Map of the sampling locations on the Danube and Sava Rivers.

Water quality parameters

TOC analyses. Total non-purgeable organic carbon (*TOC*) concentration were analyzed by a TOC Analytik Jena AG multi N/C 3100 instrument, calibrated with potassium hydrogen phthalate. Prior to the measurements, the samples were acidified to pH 2–3 with hydrochloric acid.

Major ion analysis by ion chromatography

The anions were determined on a Dionex IonPac AS4A separation column (250 mm×4 mm) using a Shimadzu LC-10Ai liquid chromatograph with a CDD-6A conductivity detector. A mixture of sodium carbonate and sodium bicarbonate in water (1.8:1.7 mole ratio) was used as the mobile phase at a flow rate of 1.5 mL min⁻¹. The injection volume was 100 µL. For

quantification purposes, linear calibration curves were prepared and the r^2 values of the regression lines were around 0.99.

The cations were determined on a Shimatzu LC 10Ai ion Chromatograph using a DIONEX ION PAC SCS1 separation column (250 mm×4 mm). As a mobile phase 3 mM sulphuric acid was used at a flow rate of 1.0 mL min⁻¹. The injection volume was 50 µL.

Determination of ammonium

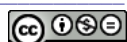
Aliquots of 2 mL of ammonium standard solutions or water samples were separately mixed with 200 µL manganese sulphate solution (2.5 mM), 0.5 mL sodium salicylate solution (1.5 M), 0.5 mL potassium sodium tartrate solution (30 mg mL⁻¹), 0.5 mL 5 % aqueous hypochlorite solution and 0.5 mL sodium hydroxide solution (0.5 M). The mixture was incubated 10 min for Indophenol Blue formation. After 10 min, the samples were diluted by adding a mixture of acetonitrile:water (1:1, V/V) to obtain a final volume of 10 mL. The mixtures were sonicated in an ultrasonic bath for 20 s before 3 mL of the mixture was introduced into a 10 mm optical path length quartz cell. All analyses were performed on the same day and each sample was analyzed in triplicate.

Ammonium determinations based on the formation of Indophenol Blue and thermal lens spectrometric (TLS) detection were performed on a dual beam, mode mismatched TLS spectrometer using the TLS experimental setup consisting of a krypton laser (Coherent, Innova 300C, Santa Clara, CA, USA) with excitation beam source tuned at 647 nm providing 100 mW power. An He–Ne laser (Melles Griot, Uniphase, model 1103P, Carlsbad, CA, USA) provided the probe beam at 632.8 nm with 2 mW of power.

Non-target screening

Extraction. Sequential liquid/liquid extraction was preformed on approximately 2000 mL aliquots of the water samples with two kinds of solvents – *n*-pentane and dichloromethane.²² Three extraction steps were performed in a separating funnel with 50 mL of the solvent. The first one with *n*-pentane, the second one with dichloromethane and the third one with dichloromethane after addition of 2 mL of concentrated hydrochloric acid that was pre-cleaned by intense extraction with *n*-hexane. Subsequently, the organic layers were separately dried by filtration over approximately 1 g of anhydrous granulated sodium sulphate (Merck, Germany) and 50 µL of an internal standard solution containing d₃₄ *n*-hexadecane, fluoroacetophenone and decafluorobenzophenone in *n*-hexane (the concentrations were 6.0, 7.2 and 6.9 ng µL⁻¹, respectively) was added to the first and second extracts. Acidic compounds in the third extract were methylated by addition of a diazomethane solution. The methylated extract was purified by fractionation with dichloromethane and methanol (50:50, V/V) through silica-gel in order to remove high polar derivatisation artefacts. In addition, 50 µL of the same internal standard was added to the third fraction as well. Before injection into the gas chromatograph (GC), all of the extracts were reduced to a volume of 50 µL at room temperature. For the gas chromatographic–mass spectrometric (GC–MS) analyses, the extracts were reduced to a volume of 20 µL at room temperature.

GC–MS analyses. GC–MS analysis was performed on a Finnigan Trace MS, ThermoQuest (Egelsbach, Germany) linked to a Carlo Erba, HRGC 5160 gas chromatograph equipped with a 25 m×0.22 mm ID×0.25 µm film BPX5 (SGE, Germany). The GC oven heating programme was 3 min hold at 60 °C, 60 °C to 300 °C at a rate of 3 °C min⁻¹ and a 20 min hold at 300 °C. The injection was performed via a split/splitless injector at 270 °C; the splitless time was 60 s. The carrier gas was helium at a velocity was 2 cm s⁻¹ and a source temperature of 200 °C. The



MS was operated in the electron impact ionization mode (EI^+ , 70 eV) scanning from 35 to 500 Da at a rate of 1 s dec^{-1} and an inter-scan time of 0.1 s.

Identification of the organic compounds. The EI^+ -mass spectra were compared with spectra of reference compounds from mass spectral databases (NIST/EPA/NIH Mass Spectral Library NIST05, Wiley/NBS Registry of Mass Spectral Data, 7th electronic version) and gas chromatographic retention times. The retention times of the internal standard compound were used for correction of inaccuracies in the injection time.

Hormone analyses

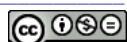
Extraction. The target compounds were isolated from the river water using SPE. SUPELCLEAN ENVI-18 SPE Tubes (6 mL, 1 g) that had been conditioned with 5 mL of *n*-hexane, 5 mL of ethyl acetate and 5 mL of methanol and washed with 10 mL of Milli-Q water. Then 400 mL of river water was loaded under moderate flow (3 mL min⁻¹). SPE cartridge was subsequently dried under vacuum for 20 min and then the hormones were eluted with 6 mL of a mixture of ethyl acetate and methanol (5:1). Extract was evaporated to dryness under gentle stream of nitrogen and reconstituted in small volume (100 μL) of methanol. This solution was filtered using LUT Syringe Filters PTFE, 13 mm, 0.45 μm and transferred to low-volume autosampler vials.

HPLC-ESI-MS analyses. An Agilent 1100 HPLC system with an Agilent 6320 spherical ion trap mass spectrometer and electrospray ionization was used. The hormones were separated on a Phenomenex Kinetex C₁₈ column, 100 Å, 150×3 mm, 2.6 μm particle size (Core-shell type) at a temperature of 25 °C using an acetonitrile (ACN)/water mixture at a flow of 0.25 mL min⁻¹ (t_0 : 40 % of ACN, t_{20} : 90 % of ACN). Nitrogen was used as the nebulising gas at a pressure of 25 psi, drying gas (N_2) temperature and flow were 350 °C and 10 L min⁻¹, respectively. The ion trap scanning range was set from 50 to 800 u. Estradiol (α - and β -), estriol, estrone, diethylstilbestrol and ethinyl estradiol were detected in the negative ESI-mode, and norethindrone and progesterone in the positive ESI-mode. The limit of quantification (*LOQ*) ranged from 0.03 to 0.5 ng L⁻¹ and the limit of detection (*LOD*) was between 0.01 and 0.15 ng L⁻¹. The recoveries obtained for all target compounds, evaluated by using spiked real samples, were higher than 70 %.

Neonicotinoid pesticides analyses

Extraction. Water samples of 1 L in volume were divided into two replicates and extracted using Strata C18-E columns polymeric sorbent (200 mg, 6 mL). Prior to extraction, the cartridges were activated with 5 mL of methanol and 5 mL of distilled water. After extraction, the samples were eluted with 5 mL of methanol. After evaporation of the solvent, the samples were dissolved in 0.5 mL of mobile phase and analyzed using HPLC-DAD.

HPLC-DAD analysis. Neonicotinoids were analyzed by HPLC-DAD (UV-Vis) consisting of a Hewlett Packard 1100 Series chromatograph coupled with a DAD detector operating in the UV-Vis range. The separation was achieved using a C8 column (250 mm×4.6 mm) with Chromasil 100 (5 μm) as the stationary phase. The column thermostat was maintained at 25 °C. The injection volume was 75 μL . The eluents consisted of 30 % acetonitrile and 70 % acetic acid; the flow rate was 1 mL min⁻¹ and the wavelength for thiamethoxam was 247 nm, for imidacloprid 250 nm and for clothianidin 260 nm. The retention time for thiamethoxam was 5.7 min, for imidacloprid 8.5 min and for clothianidin 7.4 min. For quantification purposes, calibration curves in the range from 0.1 to 100 mg L⁻¹ were prepared. The *LOD* value for all the analysed neonicotinoids was 0.5 mg L⁻¹ mg.



Ecotoxicological tests

The ecotoxicity of samples was assessed using liquid-dried luminescent bacteria *Vibrio fischeri* NRRL B-11177 with system LUMISTox, Dr. Lange. The toxicity endpoint was determined as the reduced luminescence emission after incubation in the presence of selected chemicals or mixtures. Before analyzing the samples, the pH was adjusted to 7 ± 0.2 with hydrochloric acid or sodium hydroxide and sodium chloride salt was added to obtain a 2 % concentration in order to avoid possible adverse effects due to an incorrect pH value or an inappropriate sodium chloride concentration. The liquid-dried luminescent bacteria were reactivated before the test was started. An aliquot containing *V. fischeri* was added to each vial in two parallels and luminescence was measured immediately. Afterwards the selected sample was added to the vial with bacteria and thermostated to 15 ± 1 °C for 30 min. Luminescence was measured with a photomultiplier LUMISTox 300 luminometer and thermostated at 15 ± 1 °C. The luminescence of the bacteria within the sample was again measured after 30 min of exposure and the inhibition of luminescence with 95 % confidence limits, according to ISO 11348-2, was calculated, using a model supported by computer software. The whole process was completed in accurate time intervals provided by machine and computer signalization. The blank test was performed with 2 % sodium chloride solution.

Heavy metal determination in sediments

Prior to heavy metal analysis, the sediment samples were dried at 110 °C for 24 h. After drying, the sediments were subjected to mechanical homogenization by grounding to a powder. Then, aliquots of 0.5 g of dry sediments were digested in 10 mL of concentrated nitric acid and the mixture was heated to 190 °C in a microwave oven at 400 W until total dissolution. The solution was filtered through a Whatman No 41 filter, diluted with water to 100 mL and analysed for heavy metal concentration using inductively coupled plasma optical emission spectrometry (ICP-OES). A Perkin Elmer, Optima 4300 DV spectrometer equipped with an AS-93 plus autosampler was used with a sample flow 1.5 mL min⁻¹ and a wet plasma aerosol.

RESULTS AND DISCUSSION

Since a major aim of this study was to provide a comprehensive view on the state of pollution of the Danube and Sava Rivers in the region of Belgrade, an extensive analytical investigation was performed. In the following, results from bulk parameter analysis, heavy metal determination as well as target and non-target screening analyses on organic compounds are presented and discussed in detail.

General characterisation of the water quality

The water samples investigated in this study were first characterized by some general parameters in order to reflect the general state of the water quality.

As a relevant parameter, the TOC was determined and the data are given in Table S-I. For a preliminary assessment, a comparison with literature data is useful. The average TOC values for natural water systems were reported as follows: in common ground waters – around 0.7 mg L⁻¹; in ground waters with high amounts of humic substances – 6 to 15 mg L⁻¹; in sea water – around 2 mg L⁻¹; and in rivers and lakes – up to 10 mg L⁻¹. The data for Save and Danube

River water ranged from 2 to 4 mg L⁻¹ and hence none exceeded those registered under natural conditions.²³

Quite similar and low ammonium concentrations (0.12–0.14 mg L⁻¹) were found in waters from three locations, while for the Sava at Zabran and the Danube at Vinča, the values were below the limit of detection (*LOD* = 0.1 mg L⁻¹, Table S-II). These concentrations comply with the reference values for the highest quality class of surface waters according to the Water Framework Directive (European Environment Agency, 1975, Council Directive 75/440/EEC).

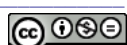
Furthermore, the results of ion chromatography pointed dominantly to the environmentally relevant presence of nitrate and sulphate, with the highest values at the Dunav Batajnica sampling point. However, all the concentrations in samples were below 1 mg L⁻¹ (Table S-II) and hence the quantities of the ions were not harmful for freshwater organisms.

Lastly, a brief ecotoxicity screening performed with *V. fischeri* showed none of the river water samples had a toxic effect on this kind of bacteria.

Non-target screening analyses of river water

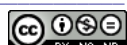
Non-target screening analyses based on GC/MS techniques were applied to all five water samples. The overall aim of this part of investigation was to identify specific organic contaminants in the two rivers and to obtain an overview on the emission sources affecting the river systems. All compounds indentified in the Danube and Sava Rivers are presented in Table S-III. They are grouped according to their technical application, unless they occur naturally in the environment (group: Natural products). Abbreviations are given for certain compounds.

The majority of the identified contaminants were of anthropogenic origin and many of them have been reported formerly as river pollutants. This is the case for, *e.g.*, of carbamazepine, which is frequently used as an antiepileptic drug.²⁴ It was identified in both samples from the Danube, but only in one from the Sava (the one closest to the confluence – location Kapetanija). A higher diversity as compared to the pharmaceuticals was evident for personal care products with their several subgroups, such as: fragrances, washing agents, or ingredients in cosmetics. Some of them may have both anthropogenic and natural origins; therefore, it is partially not possible to determine their source accurately. However, galaxolide (4,6,6,7,8,8-hexamethyl-1,3,4,6,7,8-hexahydrocyclopenta-[g]isochromene) and tonalide (1-(3,5,5,6,8,8-hexamethyl-6,7-dihydronaphthalen-2-yl)ethanone) are known synthetic fragrances and have been frequently detected in the environment, since they are emitted from domestic sewage.²⁵ These two compounds were detected in large quantities in all five samples. Direct exposure to these compounds in fragrances or indirect exposure from their presence in the environment pose no significant risk to human health, but if they



diffuse through the skin from alcoholic solutions, they can be stored in human fat tissues and human milk because of their lipophilicity.²² In addition lilial (butyl-phenylmethylpropanal) and methyl dihydrojasmonate frequently appear in fragrances. They were detected in both rivers, but methyl dihydrojasmonate was more abundant than lilial, particularly in the Danube. *N,N,N',N'-Tetraacetyl-ethylenediamine* (TAED) is used as bleaching activator in laundry detergents.²⁴ Its presence was significant in all of the samples. 4-Methoxy-2-ethylhexylcinamate is a constituent of sunscreens where it acts as a UV-protector.²⁶ It was identified in small quantities in all samples. Selected personal care products are presented in Fig. 2.

A further group of specific contaminants comprises the technical additives. [2,2,4-Trimethyl-3-(2-methylpropanoyloxy)pentyl]-2-methylpropanoate (TXIB) is added as a plasticiser to polymers such as poly(vinyl chloride), which is used in drinking water pipes, and hence TXIB, albeit of low solubility (1–2 mg L⁻¹), can be liberated into the water. No information on the environmental fate and occurrence of TXIB is available, but it is reported to have low toxicity.²⁴ Both Rivers contained large quantities of this compound. Tri-*n*-butylphosphate (TBP) is used in the manufacture of dyestuffs, lacquers, resins and plasticizers. It has moderate toxicity for aquatic organisms.²⁷ TBP was found in small amounts in all samples, except in the sample from near Vinča where higher concentrations were detected. Tris(2-chloroethyl)phosphate (TCEP) and tris(2-chloro-*iso*-propyl)-phosphate (TCPP) are flame retardants and weak plasticizers that are frequently used as plastic additives as well as flame inhibitors in carpets, and casings of electric devices. They are well known contaminants in river water, sewage effluents and river sediments.^{28,29} It was reported that the industrial usage of TCEP ceased some years ago.^{24,27} Nevertheless, both TCEP and TCPP were found in the samples, except in the sample from the location nearby Obrenovac. TMDD (2,4,7,9-tetramethyl-5-decyne-4,7-diol) is used as a dispersing additive in pigment paints and as a surfactant in printing inks.²⁴ Its occurrence in the aquatic environment is rarely reported, but it has recently been discussed in detail as river water contaminant.^{25,26} This compound is found in both the Sava and Danube Rivers, with the concentrations being higher in the Danube than in the Sava. Benzothiazole is the major leachate compound of rubber, but is also directly used as a flavouring agent and as an additive in fungicides.³⁰ It could be associated with the residues of automobile tires. Therefore, its occurrence may be partially attributed to street runoff or rubber waste discharge from the national road of the area.³¹ Quantities of this contaminant are larger in the Danube than in the Sava. Irgacure 184 (1-hydroxycyclohexyl phenyl ketone) is used as a UV photoinitiator in coatings, inks and adhesives. It may be harmful to human organism by inhalation, ingestion or skin absorption.³² Large quantities of Irgacure 184 were found in both rivers. *N*-Butylbenzenesulphonamide (NBBS) is a known neurotoxic



pollutant of, *e.g.*, surface water, groundwater, wastewater and also landfill leachates.^{33–36} 2,6-Di-*tert*-butyl-1,4-benzoquinone acts as an antioxidant and was present in significant quantities in both river waters.³⁷ Uvazols are used as UV stabilizer for polyolefines, polyester resins and coatings.³⁷ Large quantities of Uvazol 236 (2-(5-chloro-2*H*-benzotriazole-2-yl)-6-(1,1-dimethylethyl)-4-methylphenol) was found in the samples from the Sava River. Selected technical additives found in the water sample are presented in Fig. 2.

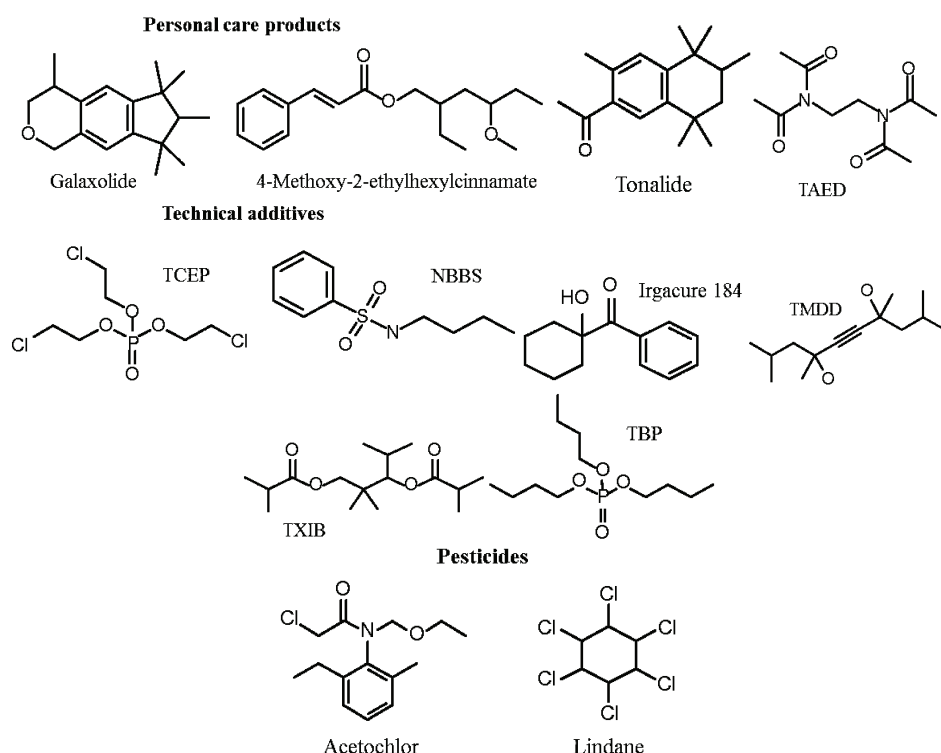


Fig. 2. Chemical structures of selected compounds identified in the waters of the Danube and Sava Rivers.

A very well known group of water pollutants are pesticides. Acetochlor (2-chloro-*N*-(ethoxymethyl)-*N*-(2-ethyl-6-methylphenyl)-acetamide) is a constituent of a variety of commercial herbicides (*e.g.*, TripleFlex®), but its use is restricted because of its high toxicity.^{39,40} In the US, acetochlor is the third most frequently detected herbicide in natural waters.⁴¹ Acute toxicology data submitted to the EPA place technical acetochlor in the toxicity category II for eye irritation and toxicity category III for acute oral, acute dermal, and acute inhalation.^{39,42} Acetochlor can accelerate metamorphosis in amphibians and can also affect the grow rate of fish.⁴³ This compound was detected in small amounts in

three samples (the Sava – Makiš, the Sava – near confluence and the Danube – Vinča). Lindane (the γ -isomer of 1,2,3,4,5,6-hexachlorocyclohexane) was produced industrially until the late 1980s when it was banned, but it can still be detected in the environment, as was case of one of the samples from the Danube River. Besides being found dissolved in water, it can also be associated with particulate matter.⁴⁴ It poses a threat to human health because of its suspected carcinogenicity.⁴⁴ The chemical structures of lindane and acetochlor are given in Fig. 2.

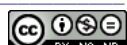
Furthermore, one food constituent has been detected. Caffeine is a component of several medicines and beverages. It is frequent component of sewage effluents, therefore, its higher concentrations are not unusual. It is found in all five samples.²⁴

Finally, dipropyldisulphide and dipropyltrisulphide are known to be formed by blue-green algae (*microcystis flos aquae*) in fresh waters and their industrial applications are unknown.²⁴ Hence, they likely represent natural products. Both compounds were detected in all of the samples.

Quantitative target screening analyses of river water

Quantitative target analyses were applied to all water samples on the pre-selected substance classes of hormones and neonicotinoids. The HPLC measurements revealed no occurrence of the selected neonicotinoid insecticides clothianidin, thiacloprid, imidacloprid and tiametoxam in any of the samples. Hence, a contamination with this type of emerging pollutants seemed to present no environmental problem for the Danube and Sava Rivers in this region in spite of the fact that this group of insecticides is becoming increasingly more important in agricultural practice. It should be stressed as well that neonicotinoid insecticides are applied in much lower concentrations than organophosphorus or other insecticides were in the past and are used in a different way (e.g., seed treatment instead of spraying).

On the other hand, quantitative analyses showed the presence of all eight hormones in the Sava River. Ethinyl estradiol was found only in the Makiš sample (0.16 ng L⁻¹) while estrone, estriol, progesterone and norethindrone were detected in concentration ranges of 0.15–0.19, 0.37–0.57, 0.02–0.03 and 0.05–0.13 ng L⁻¹, respectively. A lower level of contamination was determined in the samples from the Danube River. The compounds β -estradiol, diethylstilbestrol, and estriol were not detected in the Danube River samples. Norethindrone was only detected in the Vinča sample at low concentration of 0.08 ng L⁻¹, while ethinyl estradiol was only present in the Batajnica sample. α -Estradiol, estrone and progesterone were determined in the concentration ranges of 0.11–0.23, 0.10–0.20 and 0.03–0.06 ng L⁻¹, respectively. The levels of α -estradiol showed increasing tendency downstream of the rivers, while the levels of estrone and



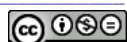
progesterone were more or less stable. This observation points to an increasing introduction of estradiol along the river course and persistence of estrone and progesterone. The levels of hormones found in the water of the Danube River water were quite similar to those found in German rivers, where estrone, 17α -estradiol, 17β -estradiol and 17α -ethinylestradiol were determined at the 20–200 pg L⁻¹ level.⁴⁶

Heavy metals in the sediments

To exemplify the distribution and levels of sediment contamination by heavy metals in the Sava and Danube Rivers, the metals As, Cd, Cr, Cu, V, Pb, Ni and Zn were selected for analyses due to their abundance and toxic effects in the environment of highly industrialized and urbanized areas. The determination of total content of heavy metals in sediments is particularly useful to collect information on the genesis of the soil and on the level of contamination. The trace metal levels in the examined sediments are presented in Table S-IV. For a preliminary risk assessment, the contents of metals were compared with Dutch recommendations and Serbian regulations of limit values of pollutant substances in surface, groundwater and sediment (Official Gazette of RS, 50/2012, in Serbian). These indicative levels for serious soil contamination and the accompanying target values for soil/sediment are also presented in Table S-IV. The given concentrations are in a standard type of sediment with 10 % organic matter and 25 % clay. Since the TOC and clay content of the investigated sediments may vary and differ significantly, the employment of these values is partially restricted. The soil remediation intervention values indicate when the functional properties of a soil for humans, plant and animal life are seriously impaired or threatened. They are representative of the level of contamination above which there is a serious case of soil contamination. The Dutch system has disadvantages being based on the total concentrations of contaminants, and in spite of a correction, the estimated risk often exceeds the actual risk.

In more details, the content of Cd was below detection limit in all samples. Furthermore, the levels of sediment contamination by As and Pb were below the target values, indicating a low risk level. The same was the case for the contents of Cr and Ni in the sediments of the Danube River at the location Batajnica, where the data were below the target values indicating low or no risk. At all other locations, the content of Cr did not exceed the intervention value but were above the target values and indicated contamination. Hence, a risk for the aquatic environment has to be assumed, but an intervention is not required.

With respect to the Cu content, the Danube sediments at the location Vinča and the Sava sediments at the location Kapetanija slightly exceeded the target values (36 mg kg⁻¹), but all other locations were characterized by insignificant contamination. Zn was detected below target values in the river sediments at the



sampling locations Batajnica and Makiš but with higher concentrations above the target values, however, not exceeding the intervention values. Hence, similar to Cr an environmental risk has to be stated, but intervention is not suggested.

In summary, a low to moderate contamination level with some location exceeding target values was evident. Noteworthy, the lowest level of contamination with all heavy metal concentrations below the target values was observed at the location Batajnica in the Danube River.

CONCLUSIONS

Water and sediment samples from the Danube and Sava Rivers in the area of Belgrade were investigated with complementary analytical approaches. Bulk parameters, such as the TOC values, and the concentrations of major ions did not reveal any unusual observation. Moreover, quantification of preselected organic contaminants (neonicotinoid pesticides and hormones) did not indicate to elevated pollution of the river waters. A more significant contamination was measured for the heavy metal contents in the sediments. For chromium, nickel, zinc and partially copper, values above the target values according to Serbian regulations were measured, but in no case did they reach Intervention Values in. Hence, an environmental risk was evidenced but intervention is not suggested for the investigated areas. Lastly, non-target screening analysis revealed a high diversity in chemical composition and a wide spectrum of organic contaminants comprising pharmaceuticals, technical additives, personal care products and pesticides. Some of the identified compounds are known pollutants whereas some other substances are so far unregistered contaminants, particularly in Serbian rivers. Although it was reported that the application of some of the identified compounds has been banned or restricted (*e.g.*, TCEP, TCPP, lindane and acetochlor), this investigation showed that they can still be found in the environment.

First, in general, it could be claimed that the overall state of pollution of the Sava and Danube Rivers in the area of Belgrade is on a moderate level. Secondly, this study presented not only a comprehensive view on the state of pollution but might also act as a base for further well adapted monitoring measures for the Sava and Danube Rivers. However, as a more relevant and superior outcome, it has been illustrated how different chemical analyses for preselected pollutants could lead to totally different assessments of the quality of a river. In particular, the confrontation of target and non-target analyses indicates to potential misinterpretation of the real state of pollution by restricted analytical approaches.

SUPPLEMENTARY MATERIAL

Tables S-I–S-IV are available electronically from <http://www.shd.org.rs/JSCS/>, or from the corresponding author on request.

Acknowledgement. This publication is the outcome of the TEMPUS project “Modernisation of Postgraduate Studies in Chemistry and Chemistry related Programmes”



(www.tempus-mchem.ac.rs). This project was funded with support from the European Commission. This publication reflects the views only of the authors, and the Commission cannot be held responsible for any use which may be made of the information contained herein.

И З В О Д

ТРЕНУТНА ЗАГАЂЕНОСТ ДУНАВА И САВЕ КОД БЕОГРАДА (2013. Г.)

МИЛАН Д. АНТОНИЈЕВИЋ¹, МАРИЈА АРСОВИЋ², ЈОСЕФ ČÁSLAVSKÝ³, ВЕСНА ЦВЕТКОВИЋ⁴, ПРЕДРАГ ДАБИЋ⁴, MLADEN FRANKO⁵, ГОРДАНА ИЛИЋ⁶, МИЛЕНА ИВАНОВИЋ⁷, НЕВЕНА ИВАНОВИЋ⁸, МИЛИЦА КОСОВАЦ⁸, ДРАГАНА МЕДИЋ⁷, СЛОБОДАН НАЈДАНОВИЋ⁷, МИЛИЦА НИКОЛИЋ⁷, ЈОВАНА НОВАКОВИЋ⁴, ТАТЈАНА РАДОВАНОВИЋ⁵, ЂУРЂИНА РАНИЋ⁴, БОЈАН ШАЈАТОВИЋ⁶, ГОРИЦА ШПИЈУНОВИЋ², ИВАНА СТАНКОВ⁶, ЈЕЛЕНА ТОШОВИЋ⁸, POLONCA TREBŠE⁵, ОЛИВЕРА ВАСИЉЕВИЋ² и JAN SCHWARZBAUER⁹

¹School of Science, University of Greenwich, England, UK, ²Висока јословно-техничка школа, Ужице,

³Faculty of Chemistry, Brno University of Technology, Czech Republic, ⁴Технолошко-металуршки

факултет, Хемијски факултет, Рударско-геолошки факултет, Технички факултет у Бору,

Универзитет у Београду, Beoograd, ⁵Laboratory for Environmental Research, University of Nova Gorica,

Slovenia, ⁶Природно-математички факултет, Универзитет у Новом Саду, Novi Sad, ⁷Природно-

-математички факултет, Универзитет у Нишу, Niš, ⁸ Природно-математички факултет,

Универзитет у Краљеву, Kraljevo, ⁹Institute of Geology and Geochemistry of Petroleum and Coal,

RWTH Aachen University, Germany

Ова студија је усмерена на свеобухватно испитивање стања загађености Дунава и Саве у пределу Београда. Различити комплементарни аналитички приступи су употребљени за испитивање: *i)* органских загађујућих материја у речној води циљаном анализом хормона и неоникотиноида, као и скрининг анализом и *ii)* тешких метала у седиментима. Коначно, анализирани су и неки уобичајени параметри квалитета воде. Укупно стање загађености је на осредњем нивоу. Укупни параметри нису открили било шта неубичајено. Ни квантификација унапред одабраних органских загађујућих материја није указала на повишено загађење. Нешто значајнија загађеност је измерена за хром, никл, цинк и делимично бакар у седиментима, са вредностима изнад циљаних вредности према српским законима. На крају, скрининг анализа је открила шире спектар органских загађујућих материја као што су фармацеутски производи, технички адитиви, средства за личну хигијену и пестициди. Студија даје широки поглед на стање загађености Саве и Дунава и представља основу за постављање даљих програма мониторинга. Значајан резултат је да је илустровано како различите хемијске анализе могу да укажу на различите оцене квалитета речне воде. Поређење циљане и нециљане анализе указало је на потенцијално погрешно тумачење стварног стања загађености.

(Примљено 5. новембра 2013, ревидирано 14. фебруара, прихваћено 23. фебруара 2014)

REFERENCES

1. R. A. Hites, *J. Chromatogr. Sci.* **11** (1973) 570
2. J. Rivera, F. Ventura, J. Caixach, M. De Torres, A. Figueras, J. Guardiola, *Int. J. Environ. Anal. Chem.* **29** (1987) 15
3. A. Puig, N. Cebríñ, J. Sarasa, M. C. Martínez, M. P. Ormad, M. S. Mutuberria, J. L. Ovelloiro, *Water Res.* **27** (1993) 1167
4. L. Guzzella, A. Gronda, *Acqua Aria* **6** (1995) 641
5. I. R. Santos, E. V. Silva-Filho, C. E. Schaefer, M. R. Albuquerque-Filho, L. S. Campos, *Mar. Pollut. Bull.* **50** (2005) 85
6. C. F. Mason, *Biology of freshwater pollution*, 4th ed., Essex University, Colchester, 2002, p. 387



7. M. Chem, L. Q. Ma, *Soil. Sci. Soc. Am. J.* **65** (2001) 491
8. C. Ianni, N. Ruggieri, P. Rivaro, R. Frache, *Anal. Sci.* **17** (2001) 1273
9. S. J. Hill, T. A. Arowolo, O. T. Butler, S. R. N. Chinery, J. M. Cook, M. S. Cresser, D. L. Miles, *J. Anal. At. Spectrom.* **17** (2002) 284
10. V. Sandroni, M. M. C. Smith, A. Donovan, *Talanta* **60** (2003) 715
11. S. T. Casper, A. Mehra, M. E. Farago, R. A. Gill, *Environ. Geochem. Hlth.* **26** (2004) 59
12. G. P. Glasby, P. Szefer, J. Geldon, J. Warzocha, *Sci. Total Environ.* **330** (2004) 249
13. P. Literathy, F. Laszlo, *Water Sci. Technol.* **32** (1995) 125
14. A. K. T. Kirschner, G. Kavka, B. Velimirov, R. Mach, R. Sommer, A. H. Farnleitner, *Water Res.* **43** (2009) 3673
15. V. Micic, T. Hofmann, *Environ. Pollut.* **157** (2009) 2759
16. A. Saliot, C. C. Parrish, N. Sadouni, I. Boulobassi, J. Filliaux, G. Cauwet, *Mar. Chem.* **79** (2002) 243
17. R. Loos, G. Locoro, S. Contini, *Water Res.* **44** (2010) 2325
18. A. Covaci, A. Gheorghe, O. Hulea, P. Schepens, *Environ. Pollut.* **140** (2006) 136
19. E. Heath, J. Ščančar, T. Zuliani, R. Milačić, *Environ. Monit. Assess.* **163** (2010) 277
20. M. Ahel, *Bull. Environ. Contam. Toxicol.* **47** (1991) 586
21. Z. Dragun, V. Roje, N. Mikac, B. Raspor, *Environ. Monit. Assess.* **159** (2009) 99
22. L. Dzikowitzky, J. Schwarzbauer, R. Littke, *Org. Geochem.* **33** (2002) 1747
23. W. Stumm, J. J. Morgan, *Aquatic chemistry: an introduction emphasizing chemical equilibria in natural waters*, 2nd ed., Wiley, New York, 1981, p. 780
24. L. Dzikowitzky, J. Schwarzbauer, A. Kronimus, R. Littke, *Chemosphere* **57** (2004) 1275
25. J. Schwarzbauer, M. Ricking, *Environ. Sci. Pollut. Res.* **17** (2010) 934
26. J. Schwarzbauer, S. Heim, *Water Res.* **39** (2005) 4735
27. O. Botalova, J. Schwarzbauer, T. Frauenrath, L. Dzikowitzky, *Water Res.* **43** (2009) 3797
28. J. W. Metzger, E. Möhle, *Flammschutzmittel in Oberflächengewässern, Grundwässern und Abwässern – Eintragspfade und Gehalte*. Forschungsbericht, Institut für Siedlungswasserbau, Wassergüte und Abfallwirtschaft, University of Stuttgart, Stuttgart, 2001
29. J. Andersen, K. Bester, *Water Res.* **40** (2006) 621
30. C. Suwanchaichinda, L. B. Brattsten, *Arch. . Insect Biochem. Physiol.* **49** (2002) 71
31. A. Grigoriadou, J. Schwarzbauer, A. Georgakopoulos, *Environ. Pollut.* **151** (2008) 231
32. M. Ash, I. Ash, *Handbook of Green Chemicals*, 2nd ed., Synapse Information Resources, New York, 2004
33. L. S. Sheldon, R. A. Hites, *Environ. Sci. Technol.* **13** (1979) 574
34. J. Guardiola, F. Ventura, J. Rivera, *Water Supp.* **7** (1989) 11
35. N. Huppert, M. Würtele, H. H. Hahn, *Fresenius J. Anal. Chem.* **362** (1998) 529
36. J. Albaiges, F. Casado, F. Ventura, *Water Res.* **20** (1986) 1153
37. D. Kolpin, E. Furlong, M. Meyer, E. M. Thurman, S. Zaugg, L. Barber, H. Buxton, *Pharmaceuticals, Hormones, and Other Organic Wastewater Contaminants in U.S. Streams, 1999–2000: A National Reconnaissance*. USGS Staff – Published Research, Paper 68, University of Nebraska – Lincoln, Kearney, NE, 2002
38. G. W. A. Milne, *Gardner's Commercially Important Chemicals: Synonyms, Trade Names, and Properties*. Wiley, Hoboken, NJ, 2005
39. W. T. Thomson, *Agricultural Chemicals: Herbicides*, Book II, Thomson Publications, Fresno, CA, 1993
40. R. T. Meister, *Farm Chemicals Handbook '95*, Meister Publishing Co., Willoughby, OH 1995
41. M. Foley, V. Sigler, C. Gruden, *ISME J.* **2** (2008) 56



42. U.S. Environmental Protection Agency, *Federal Register* **59** No. 56 (1994)
43. W. Li, J. Zha, Z. Li, L. Yang, Z. Wang, *Aquat. Toxicol.* **94** (2009) 87
44. K. Frische, J. Schwarzbauer, M. Ricking, *Chemosphere* **81** (2010) 500
45. C. Yrieix, C. Gonzalez, J. M. Deroux, C. Lacoste, J. Leybros, *Water Res.* **30** (1996) 1791
46. H. M. Kuch, K. Ballschmiter *Environ. Sci. Technol.* **35** (2001) 3201.





SUPPLEMENTARY MATERIAL TO
Actual contamination of the Danube and Sava Rivers at Belgrade (2013)

MILAN D. ANTONIJEVIĆ¹, MARIJA ARSOVIĆ², JOSEF ČÁSLAVSKÝ³, VESNA CVETKOVIĆ⁴, PREDRAG DABIĆ⁴, MLAĐEN FRANKO⁵, GORDANA ILIĆ⁶, MILENA IVANOVIĆ⁷, NEVENA IVANOVIĆ⁸, MILICA KOSOVAC⁸, DRAGANA MEDIĆ⁷, SLOBODAN NAJDANOVIC^{7#}, MILICA NIKOLIĆ⁷, JOVANA NOVAKOVIĆ⁴, TATJANA RADOVANOVIC⁵, ĐURĐINA RANIĆ⁴, BOJAN ŠAJATOVIĆ⁶, GORICA ŠPIJUNOVIĆ², IVANA STANKOV⁶, JELENA TOŠOVIĆ⁸, POLONCA TREBŠE⁵, OLIVERA VASILJEVIĆ² and JAN SCHWARZBAUER^{9*}

¹School of Science, University of Greenwich, England, UK, ²High Business-Technical School, Užice, Serbia, ³Faculty of Chemistry, Brno University of Technology, Czech Republic,

⁴Faculty of Technology and Metallurgy, Faculty of Chemistry, Faculty of Mining and Geology, Technical Faculty in Bor, University of Belgrade, Serbia, ⁵Laboratory for Environmental Research, University of Nova Gorica, Slovenia, ⁶Faculty of Science,

University of Novi Sad, Serbia, ⁷Faculty of Science and Mathematics, University of Niš, Serbia, ⁸Faculty of Science and Mathematics, University of Kragujevac, Serbia and ⁹Institute of Geology and Geochemistry of Petroleum and Coal, RWTH Aachen University, Germany

J. Serb. Chem. Soc. 79 (9) (2014) 1169–1184

TABLE S-I. Locations and parameters measured during sampling as well as the TOC values of the five water samples

| Sample No. | Location | GPS Coordinates | Water temp., °C | Transparency m | pH | O ₂ content mg L ⁻¹ | O ₂ saturation % | Conductivity μS cm ⁻¹ | TOC mg L ⁻¹ |
|------------|--------------------------|------------------------------|-----------------|----------------|-----|-------------------------------------------|-----------------------------|----------------------------------|------------------------|
| R1 | Sava River – Zabran | N 44°40'06.0" E 020°14'40.0" | 6.7 | 0.50 | 8.3 | 11.7 | 96 | 393 | 2.5 |
| R2 | Sava River – Makiš | N 44°45'58.0" E 020°21'24.0" | 6.5 | 0.40 | 8.2 | 11.3 | 92 | 374 | 2.8 |
| R3 | Sava River – Kapetanija | N 44°49'59.4" E 020°26'72.0" | 7.3 | 0.45 | 8.3 | 10.6 | 88 | 379 | 3.0 |
| R4 | Danube River – Batajnica | N 44°55'21.0" E 020°19'23.0" | 5.5 | 0.65 | 7.8 | 11.8 | 94 | 431 | 4.1 |
| R5 | Danube River – Vinča | N 44°46'09.0" E 020°37'30.0" | 7.3 | 0.55 | 8.3 | 10.9 | 91 | 387 | 3.2 |

*Corresponding author. E-mail: jan.schwarzauer@emr.rwth-aachen.de



TABLE S-II. Concentrations of the major ions (in mg L⁻¹) in the surface water samples

| Sample No. | Location | Ammonium | Sodium | Magnesium | Fluoride | Chloride | Nitrate | Sulphate |
|------------|--------------------------|----------|--------|-----------|----------|----------|---------|----------|
| R1 | Sava River - Zabran | < 0.1 | 20.9 | 511 | 1.7 | 18.0 | 13.8 | 34.3 |
| R2 | Sava River - Makiš | 0.14 | 25.3 | 534 | 2.3 | 19.8 | 14.4 | 24.6 |
| R3 | Sava River - Kapetanija | 0.13 | 27.1 | 568 | 1.6 | 21.9 | 16.0 | 36.6 |
| R4 | Danube River - Batajnica | 0.12 | 81.2 | 613 | 2.4 | 54.8 | 32.5 | 73.3 |
| R5 | Danube River - Vinča | < 0.1 | 20.1 | 612 | 2.9 | 33.2 | 19.6 | 47.5 |

Table S-III. Organic contaminants identified in the surface water samples of the Danube and Sava Rivers (+ present in low amounts, ++ present in high amounts)

| Compound | R1 | R2 | R3 | R4 | R5 |
|----------------------------------------------------|----|----|----|----|----|
| Pharmaceuticals | | | | | |
| Carbamazepine | - | - | + | + | + |
| Personal care products | | | | | |
| Methylbenzophenone | + | + | ++ | ++ | ++ |
| 4-Methoxy-2-ethylhexylcinnamate | + | + | + | + | + |
| <i>N,N,N',N'</i> -Tetraacetylene diamine, TAED | + | ++ | ++ | ++ | ++ |
| Galaxolide | ++ | ++ | ++ | ++ | ++ |
| Tonalide | ++ | ++ | ++ | ++ | ++ |
| Methyl dihydrojasmonate | + | + | ++ | ++ | ++ |
| α-Cadinol | + | + | + | + | + |
| Lilial | + | + | + | + | + |
| Technical additives, plasticizers | | | | | |
| 2,6-Di- <i>tert</i> -butylhydroxytoluene | ++ | ++ | + | ++ | - |
| 2,6-Di- <i>tert</i> -butyl-1,4-benzoquinone | ++ | ++ | ++ | ++ | + |
| 2,2,4-Trimethyl-1,3-pentandioliisobutyrate, TXIB | ++ | ++ | ++ | ++ | ++ |
| 2-Ethylhexylbenzoate | + | + | + | + | + |
| 1-Hydroxycyclohexyl phenyl ketone, Irgacure 184 | ++ | + | ++ | ++ | + |
| <i>N</i> -Butylbenzenesulphonamide, NBBS | + | + | + | ++ | + |
| Benzothiazol | - | + | + | ++ | ++ |
| Diacetin | + | ++ | ++ | ++ | ++ |
| <i>N,N</i> -Dibutylformamide | + | + | + | + | ++ |
| 2,4,7,9-Tetramethyl-5-decyne-4,7-diol, TMDD | + | + | + | ++ | ++ |
| Tris(2-chloroethyl)phosphate, TCEP | - | + | + | ++ | + |
| Tris(2-chloro- <i>iso</i> -propyl)-phosphate, TCPP | - | + | + | ++ | + |
| Tri- <i>n</i> -butylphosphate, TBP | + | + | + | + | ++ |
| Dimethylphthalate | + | + | ++ | ++ | ++ |
| Diethylphthalate | ++ | ++ | ++ | ++ | ++ |



| | | | | | |
|----------------------------------------------------------------------|----|----|----|----|----|
| Diisobutylphthalate | ++ | ++ | ++ | ++ | ++ |
| 2-Ethylhexylmethylphthalate | - | + | - | + | - |
| Benzylbutylphthalate | + | + | + | + | + |
| Bis(2-ethylhexyl)phthalate, DEHP | ++ | ++ | - | ++ | ++ |
| Pesticides | | | | | |
| Acetochlor | - | - | - | - | - |
| Uvazol 236 | - | + | + | + | + |
| Desethylterbutylazine | ++ | ++ | + | + | - |
| Lindane, HCH | - | - | - | + | - |
| Food constituents | | | | | |
| Caffeine | + | ++ | ++ | ++ | ++ |
| Vitamin E | + | + | + | + | + |
| Natural products | | | | | |
| Dipropyl disulphide, 1-(<i>n</i> -Propyldisulphanyl)propane | ++ | + | ++ | + | + |
| Dipropyl trisulphide, 1-(<i>n</i> -Propylsulfanyldisulfanylpropane) | + | + | + | + | + |
| Non-specific (unknown application) | | | | | |
| 2-Nitro-4-methylphenol | - | + | - | + | + |
| 2-Nitrophenol | + | + | + | + | + |
| 2-Phenoxyethanol | - | + | + | + | ++ |
| 2,6-Di- <i>tert</i> -butyl-4-nitrophenol | - | + | + | + | + |
| N-Benzylformamide | + | + | + | + | ++ |
| 3-Chloroacetophenone | + | - | ++ | + | - |
| Fluorenone | - | + | - | + | + |
| Antraquinone | + | + | - | + | - |

TABLE S-IV. Content of heavy metals (mg kg^{-1}) in the sediments of the Danube and Sava Rivers compared with Target and Intervention Values (n.d. = not detected; n.v. = no values)

| Sample No. | Location | As | Cd | Cr | Cu | Ni | Pb | V | Zn |
|---------------------|-----------------------------|------|------|------|------|------|------|------|------|
| R1 | Sava River – Zabran | 9.8 | n.d. | 116 | 25.6 | 121 | 46.0 | 56.8 | 185 |
| R2 | Sava River – Makiš | 4.8 | n.d. | 111 | 12.3 | 72.0 | 23.2 | 41.9 | 105 |
| R3 | Sava River – Kapetanija | 11.2 | n.d. | 124 | 38.8 | 107 | 70.6 | 67.4 | 241 |
| R4 | Danube River – Batajnica | n.d. | n.d. | 38.1 | 8.0 | 17.3 | 12.8 | 28.3 | 84.7 |
| R5 | Danube River – Vinča | 10.4 | n.d. | 112 | 37.1 | 83.6 | 47.9 | 74.2 | 218 |
| Target values | – | 29 | 0.8 | 100 | 36 | 35 | 85 | n.v. | 140 |
| Intervention values | – | 55 | 12 | 380 | 190 | 210 | 530 | n.v. | 720 |





Dynamics of soil chemistry in different serpentine habitats of Serbia

DRAŽEN D. VICIĆ^{1*}, MILOVAN M. STOILJKOVIĆ^{2#}, JORDANA M. NINKOV³,
NENAD Ć. BOJAT⁴, MARKO S. SABOVLJEVIĆ⁵ and BRANKA M. STEVANOVIĆ⁵

¹Faculty of Ecology and Environmental Protection, Union – “Nikola Tesla” University, Cara Dušana 62–64, 11000 Belgrade, Serbia, ²University of Belgrade, “Vinča” Institute of Nuclear Sciences, Department of Physical Chemistry, P. O. Box 522, 11001 Belgrade, Serbia,

³Institute of Field and Vegetable Crops, Maksima Gorkog 30, 21000 Novi Sad, Serbia,

⁴Faculty of Economics and Engineering Management, Cvećarska 2, 21000 Novi Sad, Serbia and ⁵Institute of Botany and Botanical Gardens, Faculty of Biology, University of Belgrade, Takovska 43, 11000 Belgrade, Serbia

(Received 17 September 2013, revised 24 March, accepted 28 March 2014)

Abstract: To enhance understanding of edaphic conditions in serpentine habitats, a thorough investigation of the chemical and mechanical properties of three soils from disjunct ultramafic outcrops in the central Balkans was undertaken. Soil from a nearby chemically contrasting limestone habitat was also analyzed. Three plant species differently associated with serpentine habitats (*Halacsya sendtneri*, *Cheilanthes marantae* and *Seseli rigidum*) were references for site and soil selection. Twenty elements were determined, and fourteen were measured in seven sequentially extracted soil fractions. The quantified soil properties included pH, levels of free CaCO₃, organic matter, P₂O₅, K₂O, N, C, S, cation exchange capacity, total organic carbon, field capacity and soil mechanical composition. The usual harsh components for plant growth in serpentine soil, such as elevated Mg:Ca ratios, high levels of Ni, Cr or Co, were significantly lower in the available fractions. There was a significant positive correlation of organic matter and field capacity, with most available Ca (70–80 %) found in the mobile, rather than the organically bound fraction.

Keywords: ultramafic; serpentine soil; sequential extraction; metal availability; Mg:Ca ratio.

INTRODUCTION

Serpentine soils form on hydrothermally altered ultramafic rocks which cover a little less than 1 % of the exposed surface of the Earth.¹ The elemental composition and physical properties of the parent rock make serpentine soils

* Corresponding author. E-mail: vicicdra@gmail.com

Serbian Chemical Society member.

doi: 10.2298/JSC130917028V

different from the majority of those formed over other bedrocks found on the continental crust.² Uncommon chemical/physical soil qualities generate a complex edaphic factor. The distinctive style of plant life on serpentine is most often easily noticeable by the barren landscape, different vegetation composition, and specific plant growth habits. Together with disjunct parent rock distribution, adverse edaphic conditions strongly force adaptation in plant populations.^{3,4} The disadvantages of serpentine soils also become apparent in agriculture, where they are known to inhibit crop yields. The specific plant community affiliated to serpentine is defined as low-productive, and comprises a high number of endemics.^{1,5,6}

Even though soils derived from ultramafic rocks are diverse in profile and composition, they generally display several similar features that define their hostility towards plant life.⁷ Typically shallow and rocky, serpentine habitats are often extremely xeric, and prone to high temperatures and erosion.⁸ The usual soil chemical restraints responsible for generating a “serpentine syndrome” response in plants are: unfavorable Mg:Ca quotient, toxic Mg levels, variously elevated contents of Ni, Cr, Co and other trace metals, and typically low levels of Ca, N, P and/or K.^{6,9–11} Being physically present in the soil, does not necessarily make an element available for plant uptake, as interdependent soil qualities often impact their mobility in soil–plant systems.^{12,13} Despite the potential redistribution of elements between the newly-emptied phases,¹⁴ sequential extraction of soil metals still gives a detailed insight into elemental availability and can provide estimates of mobility, reactivity and toxicity.^{13,15–17} Evaluating the strength of metal adsorption bonds is important in health hazard surveying and monitoring, and in understanding the ecology of serpentine outcrops.^{18,19} Serpentine habitats are relatively abundant on the Balkan Peninsula and have been reviewed a number of times with focus on different components of plant life inhabiting them.^{20–27} Furthermore, the Balkan’s ultramafics are a spot of refugia and speciation, and host a significant number of endemic plant species.²² The uniqueness of the biota in the serpentine emphasizes the need for its inclusion in the overall plans for biodiversity conservation.²⁶

For elucidating the role of individual chemical components of soil in the evolution of a serpentine habitat, metal availability was investigated *via* a seven-stage sequential extraction and the soil was scanned for 20 elements within each fraction. The dynamic changes of these soil characteristics could play a significant role in shaping the edaphic conditions in serpentine habitats. The aim of the study was to compare these soil properties among three differently vegetated serpentine habitats in central/western Serbia (Brđani Gorge – grassland, Ravnik – conifer forest, and Đetinja River Gorge – sparsely vegetated talus). The plan was to identify components of the edaphic factor that are of greater importance for the development of serpentine habitats. The determined features were compared with



a limestone-derived soil (Ovčar Banja), which was regarded as “contrasting” with respect to several factors that are important for plant physiology and adaptation. Some plant species find both these habitats suitable for growth. These species, namely *Halacsya sendtneri*, *Cheilanthes marantae* and *Seseli rigidum*, were selected as reference species for site and soil comparisons.

EXPERIMENTAL

Sampling locations

All four sampling habitats were located in central/western Serbia – Fig. 1 and Table I. The reference plant species, upon the presence of which the sites were selected, were *Halacsya sendtneri* (Boiss.) Dörfel. (Boraginaceae) – a strict serpentine endemic, *Cheilanthes marantae* (L.) Domin. (Pteridiaceae) – a preferential serpentinophyte/strong serpentine indicator, and *Seseli rigidum* Waldst. et Kit. (Apiaceae) – bodenvag, found on and off serpentine. Brđani Gorge hosted all three species, while another population of *H. sendtneri* was found in Ravnik, of *C. marantae* in Đetinja River Gorge, and of *S. rigidum* in Ovčar Banja limestone habitat. In each locality, three soil samples were taken from near the roots of the reference species, from a depth of 0 to 10 cm.

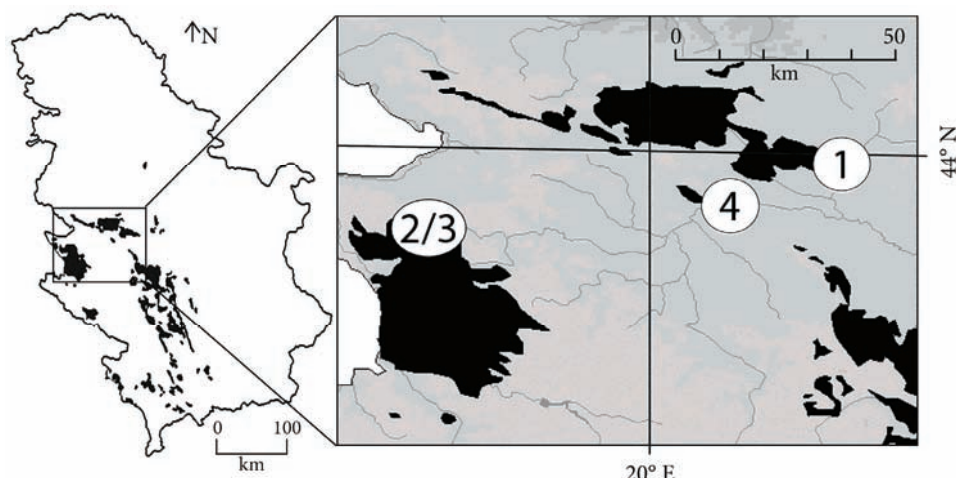


Fig. 1. Left: distribution of serpentine areas in Serbia (black). Right: close-up and position of researched habitats – see Table I for details.

Table I. Collection location substrate, location coordinates, altitude, aspect and slope

| No. | Collection location | Substrate | Location coordinate | | Altitude m | Aspect | |
|-----|--------------------------|------------|---------------------|-------------|---------------|-----------|----------|
| | | | Latitude | Longitude | | Direction | Slope, ° |
| 1 | Brđani Gorge (BR) | Serpentine | 43°59'22.1" | 20°25'34.2" | 383 | SW | 45 |
| 2 | Ravnik (RA) | Serpentine | 43°51'39.5" | 19°35'4.7" | 616 | S-SW | 30 |
| 3 | Đetinja River Gorge (DJ) | Serpentine | 43°51'22.9" | 19°35'40.1" | 600 | E-SE | 65 |
| 4 | Ovčar Banja (OB) | Limestone | 43°54'0.8" | 20°11'47.6" | 294 | NW | 70 |

Physical and chemical analysis of soils

To survey soil morphological characteristics, soil samples were air-dried and milled to <2 mm, in accordance with ISO 11464:2006.²⁸ The particle size distribution was then determined by the pipette method. The size fractions were defined as coarse sand (200–2000 µm), fine sand (20–200 µm), silt (<20 µm) and clay (<2 µm). The soil form was determined according to the ISSS (International Society of Soil Science) soil texture classification.²⁹ The field capacity was calculated as the mass percent water retention of dry soil. The pH value was determined in a 1:5 (V/V) suspension of soil in 1 M KCl using a glass electrode by the ISO 10390:1994 method.³⁰ The organic matter content was measured by the ISO 14235:1998 sulfochromic oxidation method.³¹ The free CaCO₃ content was determined by the ISO 10693:1995 volumetric method.³² The available phosphorus (P₂O₅) and available potassium (K₂O) were determined by ammonium lactate extraction,³³ followed by spectrophotometry and flame photometry detection, respectively. The total N, S, and C were determined according to the AOAC 972.43:2000 method,³⁴ and the total organic carbon (TOC) according to ISO 10694:1995,³⁵ all by elemental analysis on a CHNS analyzer Vario EL III (Elementar, Germany). The cation exchange capacity (CEC) was measured using the ISO 11260:1994 method.³⁶

Total and sequential extraction of metals

The soil pseudo-total (hereinafter: total) elemental content was gained by hotplate *aqua regia* digestion.³⁷ The samples were dried to constant mass at 105 °C, then well mixed and weighed to 0.5 g (± 0.0001). The digestion was performed in 12 mL of *aqua regia* on a hot-plate at 110 °C for 3 h. After evaporation to near dryness, the samples were diluted with 20 mL of 2 % HNO₃ (*p.a.*, Carlo Erba), then filtered and brought to 100 mL with double-distilled water.

Procedure for the sequential extraction is given in the Supplementary material to this paper.

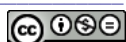
Data analysis

Linear correlations were determined using the two-tailed Pearson correlation, with the appropriate level of significance indicated in each case. All significance tests were performed by One-Way ANOVA, followed by the Post-hoc Tukey HSD test. Principal components analysis (PCA) was performed and the scores for different soil collection locations and loadings for each variable included in the calculation were plotted. The original variables found to be the most plant-relevant for the edaphic factor were included in the PCA. These were TOC, organic matter, CEC, S, K₂O, C:N, P₂O₅, field capacity, CaCO₃, pH-KCl, sums of available Ca, Cr, Cu, Mg, Ni and Zn. Eigenvalues were extracted from the correlation matrix. All statistical analyses were performed with IBM SPSS software.⁴¹

RESULTS AND DISCUSSION

Mg:Ca ratio

High Mg:Ca ratios (>> 1.0) are typical of serpentine soils, but are not usually encountered in non-serpentine habitats.² Being competitive for uptake into root,⁴² the Ca and Mg contents and their balance are some of the most important factors behind the harshness of serpentine to plant life.¹ Both elements are macronutrients, but plants need higher amounts of Ca than of Mg for proper functioning.⁴² Such a requirement is primarily due to the role of Ca in maintaining the structural integrity of the cell walls. This is especially true for dicot-



yledonous plants and their pectin-rich Type I cell wall that has a high Ca requirement. The Type II wall of commelinoid monocotyledonous, and Type III wall of Pteridophytes have somewhat different structures and, consequently, lower Ca requirements and higher tolerances towards extreme Mg:Ca ratios.^{43,44} These pre-adaptations lead towards specific and low-productive vegetation patterns in serpentine.

In serpentine soils of sites RA and BR, the Mg:Ca ratio fell under 1 only slightly (0.9–0.7) in the final plant-available fraction (F4), while in DJ soil, 2.8 was the lowest detected ratio. Subsequent available fractions differed only moderately in their ratios in each serpentine soil. The difference was however very large when the available fractions were compared with the ratio of total contents, which ranged from 28 to 206 (Fig. 2). The available amounts of metals in soil were therefore more relevant, and considerably less harsh for plant growth than their total contents. This is an important consideration regarding reasons for low productivity on these soils.

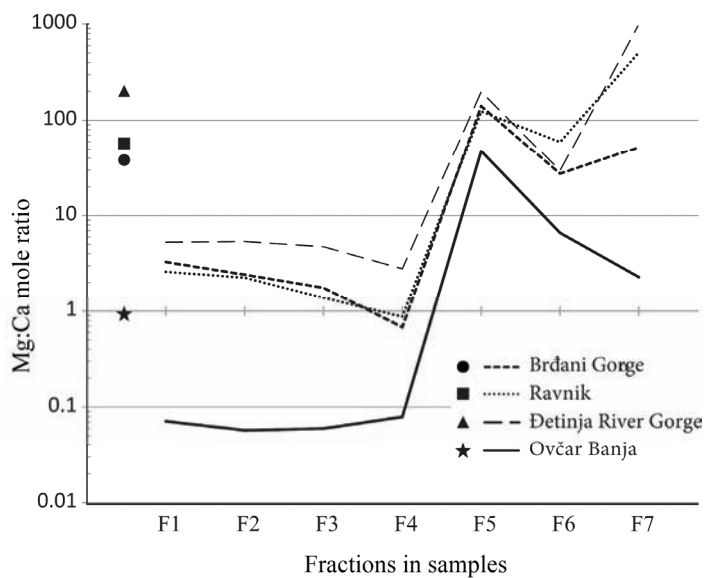


Fig. 2. Mean Mg:Ca mole ratio in *aqua regia* extract (filled shapes), and in each fraction (lines).

In the serpentine soils studied herein, the Mg:Ca ratios showed similar trends of fractional distribution (Fig. 2). However, among habitats, the ratios were most noticeably different in the available fractions, as well as in the residual fraction. While the ratio in the residual fraction reflects the specific rock mineralogy, the difference is also governed by other factors in the available fractions. The amounts of available Ca could increase due to organic matter accumulation,⁴⁵

thus decreasing the available ratio with Mg. A decreasing trend was confirmed here for serpentine soils where the Mg:Ca ratio of available fractions was negatively correlated with level of organic matter ($R = -0.832$; $p = 0.005$). Soil from the RA site contained the most organic matter (8.98 %) and the lowest Mg:Ca ratio (2.4), site DJ had the least organic matter (3.71 %) and the highest ratio (5.2). Soil from the BR site had values between the other two serpentine soils. The Mg:Ca ratio in the available fractions was also negatively correlated with TOC, C, N and K₂O ($R = -0.799$, -0.803 , -0.844 and -0.889 , respectively, $p < 0.01$) and S and P₂O₅ ($R = -0.765$ and -0.717 , respectively, $p < 0.05$). The bulk of available Ca that contributed to the trend in the ratio, however, did not originate from the organically bound fraction (F4) but from the water-soluble and exchangeable fraction (F1), containing 70 to 80 % of the bioavailable Ca. The significant positive correlation of organic matter with field capacity ($R = 0.802$, $p = 0.09$) showed that perhaps the field capacity played an important role, not only in drought relief, but also in enabling higher Ca availability and preventing its leaching. The results imply that a harsh Mg and Ca balance is strongly influenced and alleviated by the increased presence of organic debris originating from native vegetation. Although not necessarily bound in organic matter, Ca could be held in the water-soluble phase because of increasing the soil water holding capacity. The change towards a more favorable Mg:Ca regime, however, is not easily achieved in serpentine habitats as a low ratio is actually identified as one of the main reasons for low-productivity and scarce vegetation.¹

Metal load and fertility

The elemental distribution in the available fractions (Fig. 3) was very similar among the serpentine soils, despite differences in soil development level, vegetation type/structure, and variation in some chemical properties (Tables II and III). Statistically significant differences were observed only in contents of Co in the F3 and F4 fractions, and of Ca in the F7 fractions ($F = 6.881$, 9.302 and 8.081 , respectively, $p < 0.05$). Among the three serpentine habitats, the total Co, Fe, and Sc contents were significantly lower in soil from the RA site ($F = 7.627$, 8.521 and 7.620 , respectively, $p < 0.05$). In the available pools (sum of F1 to F4), the soil from the RA site was significantly lower in Co ($F = 11.325$, $p < 0.05$), and higher in Mg and Zn ($F = 5.850$ and 5.457 , respectively; $p < 0.05$) than the others. Other discrepancies included significantly lower available Al in the soil from the DJ than in the soil from the BR site ($F = 16.959$; $p < 0.05$), and the available Cr that was significantly lower in the soil from the DJ than in the soil from the RA site ($F = 13.353$; $p < 0.05$). No detectable amounts of Ag, B, Be, Cd, Mo or Pb were found in any of the examined soil samples (including the limestone soil). The total Ni content was negatively correlated with the organic matter, C, CEC, N, C, S, TOC, K₂O and P₂O₅ ($R = -0.928$, -0.956 , -0.850 , -0.940 ,



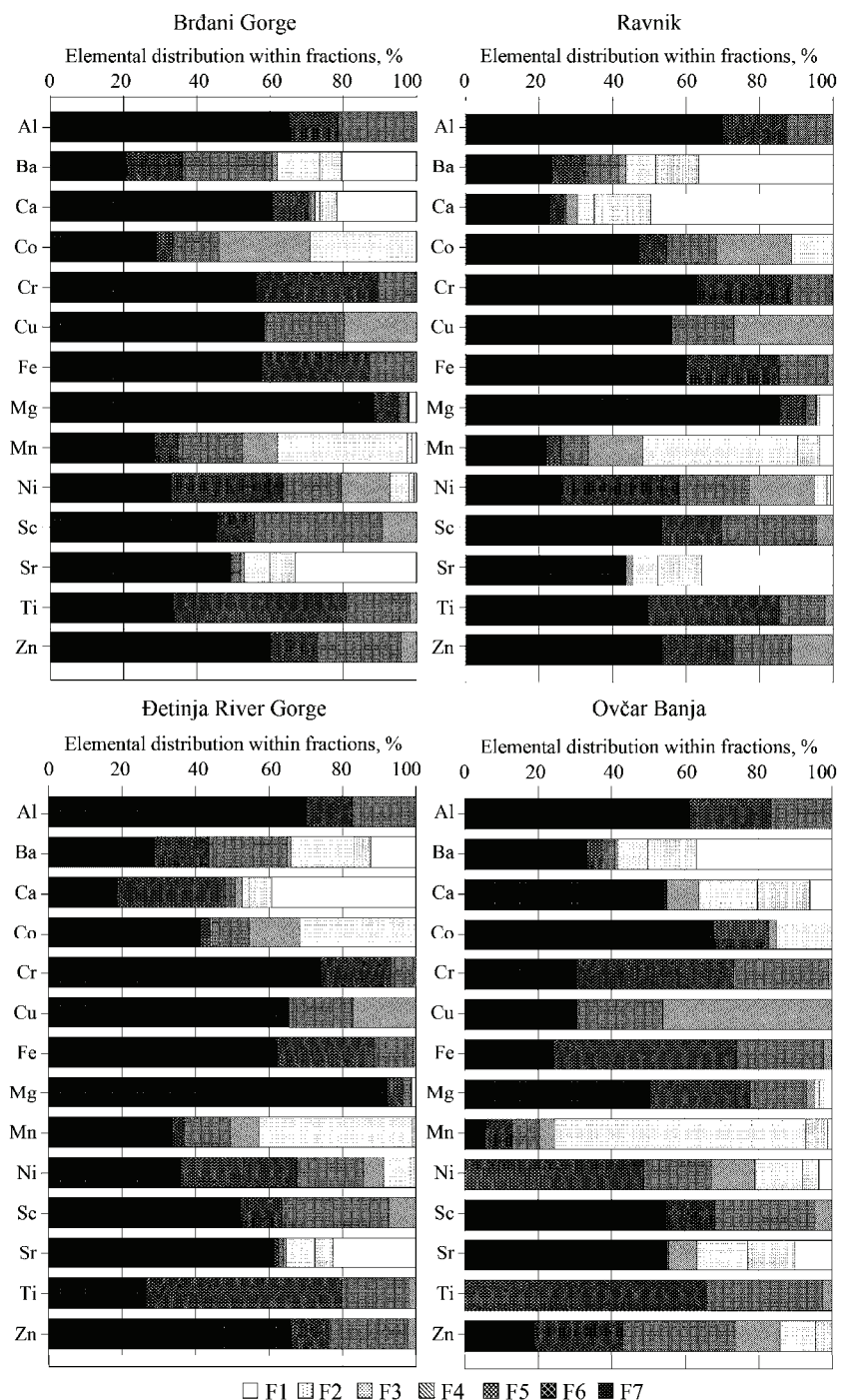


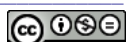
Fig. 3. Distribution of 14 elements in seven sequentially extracted soils fractions, %.

-0.956 , -0.919 , -0.955 , -0.846 and -0.806 , respectively, $p < 0.01$). Curiously, no relation of the sum of the available Ni was found with these chemical properties of soil, or with the total Ni content. However, there were positive correlations of the available Zn with organic matter, C, TOC, K₂O and P₂O₅ ($R = 0.909$, 0.963 , 0.964 , 0.800 and 0.863 , respectively, $p < 0.01$). The positive correlation with the amount of organic matter is a reasonable finding since soil organic matter is expected to increase Zn accumulation in the surface horizons of most soils.¹³

TABLE II. Chemical and morphological properties of soil; mean \pm SE

| Property/locality | Brdani Gorge | Ravnik | Detinja River Gorge | Ovčar Banja |
|-------------------------------------------------------|----------------|----------------|---------------------|----------------|
| pH-KCl | 6.2 \pm 0.2 | 6.2 \pm 0.3 | 6.5 \pm 0.1 | 7.2 \pm 0.2 |
| CaCO ₃ / % | 0.57 | 0.48 | 0.51 | 14.66 |
| Organic matter, % | 7.38 | 8.98 | 3.71 | 5.00 |
| P ₂ O ₅ / mg 100g ⁻¹ | 2.5 \pm 0.4 | 4.2 \pm 1.5 | 2.0 \pm 0.3 | 3.2 \pm 0.3 |
| K ₂ O / mg 100g ⁻¹ | 17.1 \pm 2.7 | 17.4 \pm 2.8 | 6.8 \pm 0.4 | 13.2 \pm 2.1 |
| CEC / cmol+ kg ⁻¹ | 6.1 \pm 1.6 | 8.2 \pm 1.7 | 4.0 \pm 0.6 | 4.4 \pm 0.7 |
| N / % | 0.53 | 0.54 | 0.22 | 0.34 |
| C / % | 5.31 | 12.63 | 1.92 | 6.00 |
| TOC / % | 5.16 | 12.55 | 1.87 | 3.00 |
| S / % | 0.09 | 0.15 | 0.07 | 0.09 |
| C:N | 9.70 | 20.85 | 9.03 | 15.58 |
| Clay, % | 7.8 | 9.9 | 5.3 | 7.1 |
| Silt, % | 21.8 | 10.9 | 17.8 | 26.6 |
| Fine sand, % | 33.1 | 21.9 | 29.7 | 41.5 |
| Coarse sand, % | 37.4 | 57.4 | 47.2 | 24.8 |
| Field capacity, % | 93 | 108 | 70 | 71 |
| Total mass Mg:Ca | 16.8 | 32.8 | 125.1 | 0.6 |
| Total molar Mg:Ca | 27.7 | 54.1 | 206.3 | 0.9 |

The K₂O levels of soil from the DJ site were found to be significantly lower than those in the other two serpentine sites ($F = 7.127$, $p < 0.05$), which places the DJ samples in the poor class of soil, while in other habitats, the soils were classified as optimal with regards to their K₂O levels. According to the classification of agricultural soils, all four soils were in the class of very poor soils in terms of the available P₂O₅ (< 5 mg 100 g⁻¹).⁴⁶ Contrary to this, all the examined soils were considered to be well supplied with total N (> 0.2 %).⁴⁷ In addition, a significantly lower field capacity was found for the soil from DJ site ($F = 11.734$, $p < 0.01$). Significantly elevated C:N ratios in soils occur through a low rate of organic matter decomposition and/or low N level.⁴⁸ In the soil from the RA habitat especially, it was clearly the high level of organic matter that caused the high C:N ratio ($F = 7.651$, $p < 0.05$). In the soils from the DJ and BR sites, the C:N ratios were comparable although their organic matter was considerably different. This confirms the hypothesis that serpentine soils can exhibit both higher



and lower C:N ratios compared with similar non-serpentine soils,^{2,49} even if the organic matter levels are dissimilar.

TABLE III. Eigenvalues, percentage and cumulative percentage of variance explained by the first two components, and factor loadings of the variables

| Parameter | PC 1 | PC 2 |
|-------------------------------|--------|--------|
| Eigenvalue | 7.381 | 5.243 |
| Variance, % | 46.1 | 32.8 |
| Cumulative var., % | 46.1 | 78.9 |
| <i>TOC</i> | 0.951 | -0.370 |
| organic matter | 0.933 | 0.026 |
| <i>CEC</i> | 0.924 | -0.121 |
| S | 0.914 | 0.085 |
| K ₂ O | 0.870 | 0.154 |
| C:N | 0.851 | 0.505 |
| P ₂ O ₅ | 0.799 | 0.202 |
| available Mg | 0.751 | -0.517 |
| available Cr | 0.620 | -0.250 |
| Field capacity | 0.401 | -0.168 |
| available Zn | 0.165 | 0.986 |
| available Ca | 0.144 | 0.969 |
| available Cu | 0.035 | 0.965 |
| CaCO ₃ | 0.064 | 0.963 |
| available Ni | 0.244 | -0.744 |
| pH-KCl | -0.486 | 0.735 |

Consistently and significantly lower amounts of soil organic matter, K₂O, P₂O₅, field capacity, and high Mg:Ca ratio promoted the infertility of the DJ soil. Similar causes of infertility were also identified in attempts at re-vegetating the low water-holding capacity and low nutrient roadcuts on serpentine.⁵⁰ However, the availability of potentially toxic metals typical of serpentine was also found to be lower in the DJ soil as the pH remained high, and *CEC* remained low compared with the other investigated sites. This implies that vegetation scarcity in this serpentine site is primarily due to low soil fertility and unfavorable Mg and Ca contents, rather than toxic contents of micronutrients (Ni and Zn) or other non-essential metals (Al, Co and Cr). The availability of elements (Al, Ba, Ca, Cr, Cu, Mg, Ni and Zn) was shown to be increased in the more developed grassland (BR) and forest (RA), as were the factors of fertility, including improvement in the Mg:Ca ratio.

Limestone vs. serpentine contrast

As expected, the limestone soil from Ovčar Banja differed from the three serpentine soils in many characteristics. A slightly alkaline pH was found in limestone (7.2), and mildly acidic pH in serpentine (6.2–6.5). Free CaCO₃ reached



far higher concentrations in limestone, with significantly more fine sand and less coarse sand (Table II). This classifies limestone soil as loam, in contrast to the sandy loams in serpentine. The only two elements without significant differences in total extracts from the contrasting soils were Ti and Sc, both physiologically rather irrelevant. The available Mg:Ca mole ratio in limestone averaged in the Ovčar Banja soil at 0.06, and around 1.0 in the total extraction. The available pools of Co, Mg, and Ni were significantly lower ($F = 11.057$, 11.064 and 15.441, respectively, $p < 0.01$), and Ba, Ca, Cu, Sr, Ti and Zn significantly higher ($F = 39.215$, 10.120, 70.117, 11.632, 25.755 and 16.726; respectively, $p < 0.01$) in the limestone soil compared with the serpentine soils. The results suggest that the core differences between the limestone and serpentine soils surveyed in this study were in the expected disproportional properties (pH, Mg:Ca and metal load), but did not necessarily include the fertility factors (N, P₂O₅, K₂O).

Nickel and titanium in the Ovčar Banja limestone samples, as well as Mn in one sample from the locality, were higher in the summed six sequential fractions than in the *aqua regia* extract. Therefore, their content in the seventh (residual) fraction could be considered zero, leading to the conclusion that the actual total contents in Ovčar Banja soil were at least 25 % higher for Ti, and about 30 % higher for Ni.

Principal components analysis

Percentage eigenvalues, scores plot and factor loadings on the axes are given in Table III and shown in Figs. 4 and 5. The first two principal components accounted for 78.9 % of the variance in the 16 original variables. The first axis

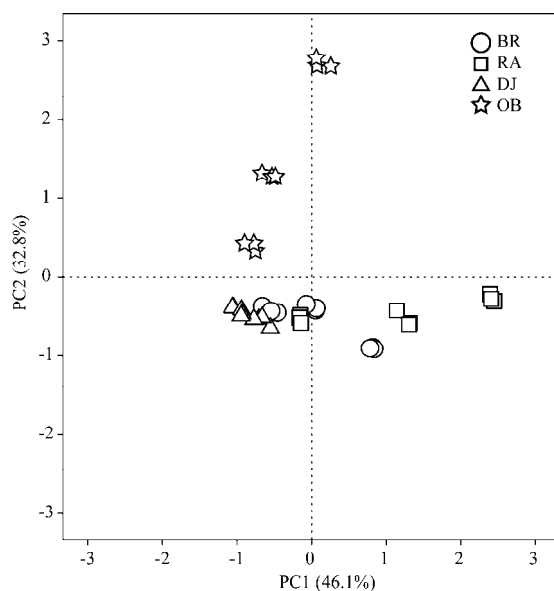


Fig. 4. Principal components analysis – scores plot of soils from the four sampled locations. The first two axes accounted for 78.9 % of the total variance.

explained 46.1 % of the variance and described the sites characterized by soil fertility markers (the fertility axis: P₂O₅, K₂O, S, N, organic matter, TOC and CEC). The second axis explained 32.8 % of the variance and was determined by other micro- and macronutrients that were elevated in limestone (Ca, Cu and Zn).

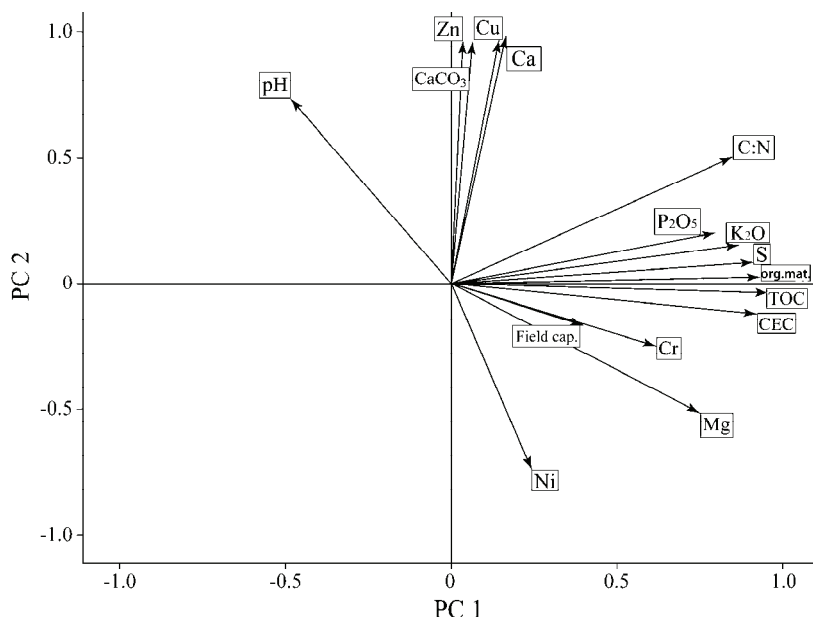


Fig. 5. Principal components analysis – loadings of the original variables on the axes.

The PCA confirmed that the prime differences among the serpentine habitats lay mostly in the fertility factors, which were explained by the fertility axis. These factors are dependent upon the richness and productivity of the vegetation, which gives rise to soil organic matter, and consequently to increased N, P and K levels. The soil from the BR habitat (Fig. 4; circles) was placed between the other two serpentine sites (DJ and RA), which may contribute to explaining the reason this habitat was able to host all three reference plant species. The Brđani Gorge habitat may therefore represent a midway condition in a plant habitat selection gradient.

CONCLUSIONS

The complexity of the edaphic factor in these surveyed serpentine ecosystems was the result of a fine balance of causally linked properties. The chemical composition of serpentine bedrock and soil, combined with different environmental factors, results in a variable vegetation composition, even in habitats physically similar to one another. A combination of these soil components con-

tinues to be an unconquerable obstacle for the majority of plants, which enables specific serpentine communities to sustain and develop.

It is clear from the present findings that some of the usual reasons for the harshness of serpentine environments, such as high levels of Ni, Cr or Co were not so intense in the bioavailable fractions of these metals. The task of identifying components with more importance becomes complicated when low-fertility components (N, P and K) and physical harshness (low field capacity, erosion and high temperatures) are included and combined with metal load. The low-fertility soil of Đetinja River Gorge maintained a low metal load through a lower CEC and higher pH. Simultaneously, its low productivity gave less organic matter, consequently leading to lower field capacity. This indicates a mechanism that prevents the Mg:Ca ratio from becoming more favorable. Conversely, the higher amount of organic matter in Brđani Gorge and Ravnik lowered Mg:Ca ratios and raised field capacity, while increasing the availability of certain metals (Al, Ba, Ca, Cr, Cu, Mg, Ni and Zn), thus increasing the metal load. Despite the more xeric conditions and higher metal availabilities, Brđani Gorge and Ravnik soils were actually less hostile with regard to the soil Mg and Ca availabilities, and consequently they hosted richer vegetation types. When comparing the soil from serpentine with the limestone soil, the differences in metal content and distribution of availabilities were large, but much smaller for other chemical and physical properties related to fertility.

The evolution of edaphic conditions in serpentine habitats is a slow and complex process. Once disturbed, they are not easily restored. The proportion of endemics determined in the serpentine flora of the Balkans is very high, and the area underlain by ultramafics is significant. In view of the fragility and value of serpentine habitats, we call for intensified research of the biota in this natural resource and protection of serpentine habitats as hotspots of diversity and endemism on the Balkan Peninsula.

ИЗВОД

ДИНАМИКА ХЕМИЈСКИХ ОДЛИКА ЗЕМЉИШТА РАЗЛИЧИТИХ СЕРПЕНТИНИТСКИХ СТАНИШТА У СРБИЈИ

ДРАЖЕН Д. ВИЦИЋ¹, МИЛОВАН М. СТОИЉКОВИЋ², ЈОРДАНА М. НИНКОВ³, НЕНАД Ч. БОЈАТ⁴,
МАРКО С. САБОВЉЕВИЋ⁵ и БРАНКА М. СТЕВАНОВИЋ⁵

¹Факултет за еколођу и заштиту животиње средине, Универзитет Унион – „Никола Тесла“, Цара Душана 62–64, 11000 Београд, ²Универзитет у Београду, Институт за нуклеарне науке „Винча“, Лабораторија за физичку хемију, Ј. Ђр. 522, 11001 Београд, ³Институт за ратарство и пољарство, Максима Горког 30, 21000 Нови Сад, ⁴Факултет за економију и инжењерски менаџмент, Цвјетарска 2, 21000 Нови Сад и ⁵Институт за ботанику и ботаничка башта, Биолошки факултет, Универзитет у Београду, Таковска 43, 11000 Београд

Ова студија бавила се стањем и развојем едафских услова у серпентинитским стаништима. Детаљно су проучене хемијске и механичке одлике три земљишта са дисјунктно дистрибуираних, али честих серпентинитских станишта централног Балкана. Компаративном анализом обухваћено је и једно просторно близко, али хемијски и биолошки

контрастно кречњачко земљиште. Узорковање је обављено на локалитетима одабраним према присуности референтних серпентинофилних биљака – *Halacsya sendtneri*, *Cheilanthes marantae* и *Seseli rigidum*. Утврђивано је ддвадесет, а квантификовано четрнаест метала у свакој од седам секвенцијално екстрахованих фракција земљишта. Поред тога, одређени су и: pH земљишта, ниво слободног CaCO_3 , количине органске материје, P_2O_5 , K_2O , N, C, S, капацитет размене катјона, укупни органски угљеник, капацитет задржавања воде, као и механички састав земљишта. Утврђено је да су типичне стресне карактеристике земљишта попут високог односа Mg:Ca, високих нивоа никла, хрома или кобалта, у значајној мери убажене у биодоступним фракцијама. Утврђена је висока корелација између нивоа органске материје и капацитета задржавања воде, као и то да се највећи део (70–80 %) доступног Ca налази у мобилној, а не органски-везаној фракцији земљишта.

(Примљено 17. септембра 2013, ревидирано 24. марта, прихваћено 28. марта 2014)

REFERENCES

1. E. Kazakou, P. G. Dimitrakopoulos, A. J. M. Baker, R. D. Reeves, A. Y. Troumbis, *Biol. Rev.* **83** (2008) 495
2. E. B. Alexander, R. G. Coleman, T. Keeler-Wolf, S. Harrison, *Serpentine Geocology of Western North America: Geology, Soils, and Vegetation*, Oxford University Press, New York, USA, 2007, p. 417
3. B. L. Anacker, J. B. Whittall, E. E. Goldberg, S. P. Harrison, *Evolution* **65** (2010) 365
4. B. Anacker, in: *Serpentine: Evolution and ecology of a model system*, S. P. Harrison, N. Rajakaruna, Eds., University of California Press, Berkeley, CA, 2011, p. 49
5. R. H. Whittaker, *Ecology* **35** (1954) 258
6. K. U. Brady, A. R. Kruckeberg, H. D. Bradshaw Jr., *Annu. Rev. Ecol. Evol. Syst.* **36** (2005) 243
7. I. Tsiripidis, A. Papaioannou, V. Sapounidis, E. Bergmeier, *Plant Soil* **329** (2010) 35
8. J. Proctor, *Trends Ecol. Evol.* **14** (1999) 334
9. R. Kruckeberg, *California serpentines: flora, vegetation, geology, soils, and management problems*, University of California Press, Berkeley, CA, 1984, p. 24
10. R. Kruckeberg, *Am. Midl. Nat.* **116** (1986) 403
11. P. Doubková, J. Suda, R. Sudová, *Soil Biol. Biochem.* **44** (2012) 56
12. M. Pansu, J. Gautheyrou, *Handbook of Soil Analysis – Mineralogical, Organic and Inorganic Methods*, Springer, Berlin, 2006, p. 895
13. A. Kabata-Pendias, *Trace Elements in Soils and Plants*, 4th ed., CRC Press, Boca Raton, FL, 2011, p. 93
14. J. Kierczak, C. Neel, U. Aleksander-Kwaterczak, E. Helios-Rybicka, H. Bril, J. Puzyewicz, *Chemosphere* **73** (2008) 776
15. H. Al-Najar, R. Schulz, V. Römhild, *Plant Soil* **249** (2003) 97
16. A. J. Zimmerman, D. C. Weindorf, *Int. J. Anal. Chem.* doi:10.1155/2010/387803
17. M. Kaupenjohann, W. Wilcke, *Soil Sci. Soc. Am. J.* **59** (1995) 1027
18. S. K. Gupta, M. K. Vollmer, R. Krebs, *Sci. Total Environ.* **178** (1996) 11
19. D. Jianu, V. Iordache, B. Soare, L. Petrescu, A. Neagoe, C. Iacob, R. Orza, in: *Bio-Geo Interactions in Metal-Contaminated Soils*, E. Kothe, A. Varma, Eds., Springer, Berlin, 2012, p. 35
20. B. Tatić, V. Veljović, in: *The ecology of areas with serpentinized rocks, a world view*, B. A. Roberts, J. Proctor, Eds., Kluwer, Dordrecht, 1992, p. 199
21. P. D. Marin, B. Tatić, *Bocconeia* **13** (2001) 145



22. V. Stevanović, K. Tan, G. Iatrou, *Plant Syst. Evol.* **242** (2003) 149
23. B. Dudić, T. Rakić, J. Šinžar-Sekulić, V. Atanacković, B. Stevanović, *Arch. Biol. Sci.* **59** (2007) 341
24. A. Bani, D. Pavlova, G. Echevarria, A. Mullaj, R. D. Reeves, J. L. Morel, S. Sulçe, *Bot. Serb.* **34** (2010) 3
25. K. Jakovljević, D. Lakušić, S. Vukojičić, G. Tomović, J. Šinžar-Sekulić, V. Stevanović, *Cent. Eur. J. Biol.* **6** (2011) 260
26. D. D. Vicić, N. Č. Bojat, B. M. Stevanović, in Proceedings of the Second international symposium on natural resources management, Zaječar, Serbia, 2012, p. 192
27. D. Vicić, K. Jakovljević, N. Kuzmanović, V. Batanjski, B. Stevanović, V. Stevanović, in Proceedings of 7th International Conference on serpentine ecology, Coimbra, Portugal, Book of abstracts, 2011, p. 136
28. ISO 11464, *Soil quality - Pretreatment of samples for physico-chemical analysis*, 2006
29. W. Verheyen, J. Ameryckx, *Pedologie* **2** (1984) 215
30. ISO 10390, *Soil quality - Determination of pH*, 1994
31. ISO 14235, *Soil quality - Determination of organic carbon by sulfochromic oxidation*, 1998
32. ISO 10693, *Soil quality - Determination of carbonate content - Volumetric method*, 1995
33. H. Egner, H. Riehm, in *Die Untersuchung von Böden*, R. Thun, R. Herrmann, E. Knickmann, Eds., Neumann Verlag, Berlin, 1955, p. 110
34. AOAC 972.43, *Microchemical Determination of Carbon, Hydrogen, and Nitrogen, Automated Method*, 2000
35. ISO 10694, *Soil quality - Determination of organic and total carbon after dry combustion (elementary analysis)*, 1995
36. ISO 11260, *Soil quality - Determination of effective cation exchange capacity and base saturation level using barium chloride solution*, 1994
37. M. Chen, L. Q. Ma, *Soil Sci. Soc. Am. J.* **65** (2001) 491
38. H. Zeien, G. W. Brümmer, *Mitt. Dtsch. Bodenkdl. Ges.* **59** (1989) 505
39. A. Grawunder, M. Lonschinski, D. Merten, G. Büchel, *Chem. Erde* **69** (2009) 5
40. T. Ratuzny, Z. Gong, B.-M. Wilke, *Environ. Monit. Assess.* **156** (2009) 171
41. IBM Corp. Released 2010. *IBM SPSS Statistics for Windows*, Version 19.0. Armonk, NY: IBM Corp.
42. H. Marschner, *Mineral nutrition of higher plants*, Academic Press, San Diego, CA, 2002, p. 172
43. G. B. Silva, M. Ionashiro, T. B. Carrara, A. C. Crivellari, M. A. S. Tine, J. Prado, N. C. Carpita, M. S. Buckeridge, *Phytochemistry* **72** (2011) 2352
44. J. Vogel, *Curr. Opin. Plant Biol.* **11** (2008) 301
45. M. E. D'Amico, F. Previtali, *Plant Soil*, **351** (2011) 73
46. S. Milić, J. Vasin, J. Ninkov, T. Zeremski, B. Brunet, P. Sekulić, *Field Veg. Crop Res.* **48** (2011) 359
47. R. Kastori, *Nitrogen. Agrochemical, agrotechnical, physiological and ecological aspects*, Institute of Field and Vegetable Crops, Novi Sad, 2005, p. 161 (in Serbian)
48. R. Burt, M. Fillmore, M. A. Wilson, E. R. Gross, R. W. Langridge, D. A. Lambers, *Commun. Soil Sci. Plant Anal.* **32** (2001) 2145
49. S. Effendi, S. Miura, N. Tanaka, S. Ohta, in *Rainforest Ecosystems of East Kalimantan*, E. Guhardja, M. Fatawi, M. Sutisna, T. Mori, S.Ohta, Eds., Springer, Tokyo, 2000, p. 79
50. M. J. Curtis, V. P. Claassen, *Restor. Ecol.* **17** (2007) 24
51. D. D. Vicić, M. M. Stoiljković, N. Č. Bojat, M. S. Sabovljević, B. M. Stevanović, *Revue d'Ecologie (Terre et Vie)* **69** (2014) 185.



SUPPLEMENTARY MATERIAL TO
**Dynamics of soil chemistry in different serpentine habitats
of Serbia**

DRAŽEN D. VICIĆ^{1*}, MILOVAN M. STOILJKOVIĆ², JORDANA M. NINKOV³,
NENAD Č. BOJAT⁴, MARKO S. SABOVLJEVIĆ⁵ and BRANKA M. STEVANOVIĆ⁵

¹Faculty of Ecology and Environmental Protection, Union – “Nikola Tesla” University, cara Dušana 62–64, 11000 Belgrade, Serbia, ²University of Belgrade, “Vinča” Institute of Nuclear Sciences, Department of Physical Chemistry, P. O. Box 522, 11001 Belgrade, Serbia,

³Institute of Field and Vegetable Crops, Maksima Gorkog 30, 21000 Novi Sad, Serbia,
⁴Faculty of Economics and Engineering Management, Cvećarska 2, 21000 Novi Sad, Serbia
and ⁵Institute of Botany and Botanical Gardens, Faculty of Biology, University of Belgrade,
Takovska 43, 11000 Belgrade, Serbia

J. Serb. Chem. Soc. 79 (9) (2014) 1185–1198

EXPERIMENTAL DETAILS

I. Brđani Gorge (BR) is a steppe-like serpentine rocky ground with rich vegetation cover, exceptions being frequent barren exposures of large ultramafic boulders. The site has a pronounced xeric character, as it is a SW oriented steep hill near the ridge top, almost entirely exposed to sunlight during the day. In that locality, *H. sendtneri* grows in a very dense tufted form, and shares the habitat with *C. marantae* and *S. rigidum*. Detinja River Gorge (DJ) is a steep E–SE exposed hill with a mobile crushed serpentine rock substratum, which hosts impoverished vegetation only. The River Detinja that runs about 20 meters below ensures that the air is constantly moist. There, *C. marantae* grows in dense, but dispersed tufts. Ravnik (RA) sampling locality is a S–SW exposed terrain, not directly above a river or a stream. The shallow surface of soil is abundant with organic matter, pine needles primarily. In this Scots Pine forest, the sunlight exposure on the ground floor is in part decreased by adult trees reaching above. Less dense *H. sendtneri* tufts of a more evenly dispersed population are found on the fully vegetated forest ground floor. A vertical cliff on one side and a busy road on the other border the limestone habitat of Ovčar Banja (OB). It is very steep, with scarce vegetation but with *S. rigidum* growing scattered at the bottom of the cliff.

II. Sequential extraction into seven fractions was performed according to Zeien and Brümmer (1989).^{15,17,38–40} Air-dried samples finer than 2 mm were weighed to 1 g (± 0.0001) and transferred to acid-washed 50 mL PP tubes. To obtain the F1 fraction, 25 mL of 1 M NH₄NO₃ (*p.a.*, Acros Organic) were added to the soil and the acute-angled tubes shaken for 24 h on a horizontal shaker. The mixture was then centrifuged at 2500 rpm for 15 min and supernatant filtered through a 0.45 µm cellulose acetate syringe filter (hereinafter centrifuging and filtering was done identically throughout the extraction). To stabilize the solution, 0.25

*Corresponding author. E-mail: vicicdra@gmail.com

mL of 65 % HNO₃ (*p.a.*, Carlo Erba) was added. For the extraction of the F2 fraction, 25 mL of 1 M CH₃COONH₄ (*p.a.*, Fisher Scientific; pH 6 adjusted with conc. acetic acid) were added to the remaining soil and shaken for another 24 h, centrifuged, filtered, and the solution stabilized with 0.25 mL of 65 % HNO₃ (*p.a.*, Carlo Erba). Another 12.5 mL of 1 M NH₄NO₃ were added to the remaining soil and shaken for 10 min, centrifuged, filtered and added to the first part of the F2 extract. The F3 fraction was gained first by adding 25 mL of 0. 1M NH₂OH-HCl (*p.a.*, Acros Organic) + 1 M CH₃COONH₄ (pH 6 adjusted with 37 % HCl) to the remaining solid phase. After 30 min of shaking, the mixture was centrifuged, filtered and the solution stabilized with 0.25 mL 37 % HCl (*p.a.*, VWR Prolabo). Next, 12.5 mL of 1 M CH₃COONH₄ was added and shaken for 10 min with the residual soil, then centrifuged and filtered into the first part of the F3 extract. This step was repeated once more. To obtain the fourth (F4) fraction, 25 mL of 0.025 M NH₄-EDTA (*p.a.*, Fisher Scientific; pH 4.6 adjusted with 28 % NH₄OH, *p.a.*, J. T. Baker) was added to the soil from the previous fraction and shaken for 90 min, centrifuged and filtered. Another 12.5 mL of 1 M CH₃COONH₄ was added to the soil residue, shaken for 10 min, then centrifuged, filtered and added to the first part of the extract. The fifth fraction (F5) was extracted with 25 mL of 0.2 M NH₄ oxalate buffer (consisting of 28.422 g L⁻¹ ammonium oxalate, *p.a.*, Fisher Scientific; 25.214 g L⁻¹ oxalic acid dehydrate, *p.a.*, Fisher Scientific; pH 3.25 adjusted with 28 % NH₄OH) by shaking for 4 h in the dark. After the content had been centrifuged and filtered, the previous step was repeated with 12.5 mL of the same solution and 10 min of shaking in the dark. Fraction F6 was extracted with 25 mL of 0.1 M ascorbic acid + 0.2 M NH₄-oxalate buffer (all: *p.a.*, Fisher Scientific; pH 3.25 adjusted with 28 % NH₄OH), which was added to the remaining solid phase and digested for 30 min in a water bath at 96 °C, then centrifuged and filtered. Another 12.5 mL of 0.2 M NH₄-oxalate buffer was added to the remaining soil and shaken for 10 min in the dark, then centrifuged, filtered and added to the first part of the F6 extract. The seventh fraction (F7) was the difference after the sum of first six fractions (F1 to F6) had been subtracted from the total amounts determined in hotplate *aqua regia* extraction.

The first fraction represented mobile metals – water soluble and exchangeable, and easily soluble organic complexes. The second fraction incorporated easily soluble, specifically adsorbed metals, metal bound to carbonates, and organo–metal complexes. The third fraction contained easily reducible metals bound to Mn-oxides. The fourth was the final plant-available fraction, and represented EDTA-extractable metals bound to organic matter. Fractions F5, F6 and F7 were unavailable for plants: F5 representing a moderately reducible fraction bound to amorphous and poorly crystalline Fe-oxides, and F6 a strongly reducible fraction bound to crystalline Fe-oxides. Solutions of hotplate-digested soil and sequential extracts were processed with an Inductively-Coupled Plasma Optical Emission Spectrometer (Spectroflame P, 27.12 MHz, 2.5 kW) for the following elements: Ag, Al, B, Ba, Be, Ca, Cd, Co, Cr, Cu, Fe, Mg, Mn, Mo, Ni, Pb, Sc, Sr, Ti and Zn.

